



Partnership for AiR Transportation  
Noise and Emissions Reduction  
An FAA/NASA/Transport Canada-  
sponsored Center of Excellence



# **Environmental Design Space Assessment of Continuous Lower Energy Emissions and Noise (CLEEN) Technologies**

**PARTNER Project 36 Final Report**

prepared by  
Dimitri Mavris, Jimmy C. Tai, Christopher Perullo

March 2016

REPORT NO. PARTNER-COE-2016-001

# **Environmental Design Space Assessment of Continuous Lower Energy Emissions and Noise (CLEEN) Technologies**

Project 36 Final Report

Dimitri Mavris (PI), Professor, School of Aerospace Engineering, Georgia  
Institute of Technology

Jimmy C. Tai (Co-PI), Senior Research Engineer, School of Aerospace  
Engineering, Georgia Institute of Technology

Christopher Perullo, Research Engineer II, Georgia Institute of Technology

---

PARTNER-COE-2016-001

March 2016

Any opinions, findings, and conclusions or recommendations expressed in this material are those of the authors and do not necessarily reflect the views of the FAA, NASA or Transport Canada.

The Partnership for AiR Transportation Noise and Emissions Reduction — PARTNER — is a cooperative aviation research organization, and an FAA/NASA/Transport Canada-sponsored Center of Excellence. PARTNER fosters breakthrough technological, operational, policy, and workforce advances for the betterment of mobility, economy, national security, and the environment. The organization's operational headquarters is at the Massachusetts Institute of Technology.

**The Partnership for AiR Transportation Noise and Emissions Reduction  
Massachusetts Institute of Technology, 77 Massachusetts Avenue, 37-395  
Cambridge, MA 02139 USA  
<http://partner.mit.edu>**

## **Project 36 Final Report**

Environmental Design Space Assessment of Continuous Lower Energy Emissions and Noise (CLEEN) Technologies

### **Georgia Institute of Technology**

---

#### **Project Lead Investigator**

Dimitri Mavris (PI)  
Professor, School of Aerospace Engineering  
Georgia Institute of Technology  
Mail Stop 0150  
Atlanta, GA 30332-0150  
Phone: 404-894-1557  
Fax: 404-894-6596  
Email: [dimitri.mavris@ae.gatech.edu](mailto:dimitri.mavris@ae.gatech.edu)

Jimmy C. Tai (Co-PI)  
Senior Research Engineer  
School of Aerospace Engineering  
Georgia Institute of Technology  
Mail Stop 0150  
Atlanta, GA 30332-0150  
Phone: 404-894-0197  
Fax: 404-894-6596  
Email: [jimmy.tai@aerospace.gatech.edu](mailto:jimmy.tai@aerospace.gatech.edu)

Christopher Perullo  
Research Engineer II  
Phone: 404-894-5404  
Email: [chris.perullo@ae.gatech.edu](mailto:chris.perullo@ae.gatech.edu)

#### **University Participant(s)**

*Georgia Institute of Technology*

- P.I.: Dimitri Mavris, Co-P.I.: Jimmy Tai
- FAA Award Number: 09-C-NE-GIT-001, Amendment Nos. 002
- Period of Performance: April 1, 2010 – May 31, 2014

# Table of Contents

1 Executive Summary .....	1
1.1 Investigation Team.....	2
1.2 Objectives .....	2
1.3 Summary of Major Accomplishments .....	3
2 Phase I - Public Domain Aircraft Technology Modeling .....	5
2.1 Fuel Burn Technologies.....	5
2.1.1 Retrofit alternate non-planar wingtips .....	5
2.1.2 Natural Laminar Flow Control.....	7
2.1.3 Open Rotor.....	9
2.1.4 Geared Turbofan (GF) .....	9
2.1.5 Active Cooling .....	12
2.1.6 Highly Loaded Compressor .....	14
2.1.7 Highly Loaded Turbine.....	15
2.1.8 Ceramic Matrix Composites .....	15
2.1.9 Adaptive Trailing Edge.....	16
2.1.10 Flight Management System (FMS) Technologies .....	16
2.1.11 End Wall Contouring.....	16
2.2 Noise Technologies.....	18
2.2.1 Landing Gear Fairings .....	18
2.2.2 Flap Fences / Flaplets.....	19
2.2.3 Fixed Geometry Chevrons .....	20
2.2.4 Core Exhaust Nozzle Liner .....	21
2.2.5 Variable Area Nozzle.....	22
2.2.6 Fan Stator Sweep and Lean.....	24
2.2.7 Soft Vane .....	25
2.2.8 Aft Cowl Liners .....	25
2.2.9 Zero Splice Inlet.....	27
2.2.10 Nose Lip Liner .....	27
2.3 Emissions Technologies.....	28
2.4 Conclusions.....	28
3 Phase II – CLEEN Technology Modeling with Proprietary Data .....	29
3.1 CLEEN Technology Modeling Approach .....	29
3.2 Addition of New EDS Turbine Cooling Model.....	30
3.2.1 Motivation.....	30
3.2.2 Assumptions.....	31
3.2.3 Inputs and EDS Supplied Values .....	32
3.2.4 Heat Transfer Analysis .....	33
3.2.5 Other Considerations .....	36
3.2.6 Description of Algorithm.....	38
3.2.7 Results.....	40
3.3 Addition of Centrifugal Compressor Map Generation Process .....	41
3.3.1 Motivation.....	41
3.3.2 Inputs, EDS Variables, and Assumed Values.....	42
3.3.3 Main Calculation Method .....	44
3.3.4 Matching Design Stall Margin.....	47

3.3.5 Summary and Results .....	49
3.4 Conclusions .....	50
4 Fleet Level Aircraft Technology Benefits Assessment .....	51
4.1 Fleet Assessment Process and Assumptions .....	51
4.2 Fleet Growth Assumptions .....	51
4.3 Fleet Retirement Assumptions .....	52
4.4 Fleet Replacement Assumptions .....	52
4.5 Technology Scenarios and Packages .....	53
4.6 Vehicle Level Results .....	56
4.7 Fleet-Level Results .....	56
5 Technology Dashboard .....	61
5.1 Technology Dashboard Development .....	62
5.1.1 Motivation and Objectives .....	62
5.1.2 Approach .....	62
5.1.3 Technology Selection .....	71
5.1.4 Technology Compatibility Matrix .....	73
5.2 Technology Checks .....	74
5.3 Calculator Functionalities .....	74
5.3.1 Parametric Cycle Parameters and Cycle Sweeps .....	74
5.3.2 Multi-Attribute Decision Making (MADM) .....	78
6 Conclusions .....	82
Appendix A Preliminary EDS Geared Turbofan Comparison Study .....	83
Appendix A.A Motivation .....	83
Appendix A.B 2011 NASA Study .....	84
Appendix A.C Approach/Assumptions .....	86
Appendix A.D Study Analysis .....	94
Appendix B Historical Technology Trends .....	102
Appendix B.A Motivation .....	102
Appendix B.B Approach .....	102
Appendix B.C High Level Trends .....	102
Appendix B.D Low Level Trends .....	143

## Listing of Figures and Tables

Figure 1: Relationship Between Wingtip Size, Weight, And Benefit .....	7
Figure 2: EDS Laminar flow transition model .....	8
Figure 3: Comparison Between GF and Direct Drive .....	10
Figure 4: Smith Chart.....	11
Figure 5: NEWAC Active Core Concept [].....	12
Figure 6: Correlation Between Compressor Loading and Efficiency.....	14
Figure 7: EDS Cooling Flow Setup .....	16
Figure 8: Description of Endwall Location .....	17
Figure 9: Example of Separation Near the Endwall .....	17
Figure 10: Example of Endwall Contouring.....	17
Figure 11: Example of Landing Gear Fairings .....	18
Figure 12: Flap Fences.....	19
Figure 13: Chevron Description.....	20
Figure 14: EDS-ANOPP Chevron Configuration Sensitivity Study .....	21
Figure 15: Combustor Liner Concept .....	22
Figure 16: Core Exhaust Liner Noise Reduction.....	22
Figure 17: Variable Area Nozzle.....	23
Figure 18: Stator Sweep.....	24
Figure 19: Stator Lean .....	24
Figure 20: Aft Cowl Liner .....	26
Figure 21: Nose Lip Liner.....	27
Figure 22: Timeline of EDS CLEEN Modeling Activities.....	29
Figure 23: Current EDS Cooling Model.....	31
Figure 24: New EDS Cooling Model.....	31
Figure 25: Flow of Information within the Cooling Model.....	33
Figure 26: Simplified Cooling Flow Model.....	34
Figure 27: Typical Radial Temperature Profile of Flow Exiting Combustor.....	37
Figure 28: Cooling Algorithm Flowchart .....	39
Figure 29: Parametric Sweep of Internal Cooling Efficiency.....	40
Figure 30: Parametric Sweep of Film Cooling Effectiveness.....	41
Figure 31: Tip Speed vs. Pressure Ratio Regression used to Size Compressor .....	43
Figure 32: Flow of Information .....	44
Figure 33: Regression of Peak Flow Coefficient vs. Tip Mach Number.....	45
Figure 34: Regression of Peak Efficiency vs. Tip Mach Number .....	46
Figure 35: Algorithm to Match Design Stall Margin.....	49
Figure 36: Flowchart of Map Generation Algorithm.....	50
Figure 37: Retirement Curve Comparison.....	52
Figure 38: CLEEN Fleet Replacement Assumptions .....	53
Figure 39: Fleet-Level Fuel Burn Impact .....	57
Figure 40: Potential Fuel Burn Savings Provided By CLEEN Technologies Modeled in This Study .....	59
Figure 41: Fleet-Level LTO NO <sub>x</sub> Impact.....	60
Figure 42: Technology Dashboard.....	61
Figure 43: Technology Dashboard Development Process.....	63
Figure 44: Single Aisle Technology Impact Matrix Excerpt.....	64

Figure 45: EDS Assessment Flowchart .....	66
Figure 46: SA ADD 500 test case Subset Scatterplot Matrix .....	67
Figure 47: Typical Artificial Neuron .....	68
Figure 48: Neural Network Conceptual Diagram .....	69
Figure 49: Checking for Goodness of Fit .....	71
Figure 50: Technology Selection Capability .....	72
Figure 51: Sample Percent Change Graph for CLEEN Fuel Burn Metric .....	73
Figure 52: Partial LSA TCM .....	74
Figure 53: Front End Incompatibility Example .....	74
Figure 54: Parametric Cycle Parameters and Cycle Sweep Functionality .....	75
Figure 55: Technology Selection for Cycle Sweep .....	76
Figure 56: Technologies Selected in Cycle Sweep .....	76
Figure 57: Sensitivity Sweep Parameters Ranges and Step Size Inputs .....	76
Figure 58: Partial Output of a Sensitivity Sweep .....	77
Figure 59: Cycle Sweep Fuel Burn Results with Varied FPR and HPCPR .....	77
Figure 60: Cycle Sweep Fuel Burn Results with Varied FPR and LPCPR .....	78
Figure 61: Areas of TOPSIS Functionality on the Dashboard Front End .....	79
Figure 62: Scatter Plot of Generated Data .....	80
Figure 63: Radar Plot of Generated Data .....	81
Figure 64: Flow of Information for the 2011 NASA Study .....	84
Figure 65: Variation in Fan efficiency with Pressure Ratio at ADP (TOC) Conditions .....	94
Figure 66: Top-of-Climb Bypass Ratio (BPR) vs. FPR Comparison .....	96
Figure 67: Thrust Specific Fuel Consumption (TSFC) vs. FPR Comparison .....	97
Figure 68: Fan Diameter vs. FPR Comparison .....	97
Figure 69: Nacelle Diameter vs. FPR Comparison .....	98
Figure 70: Engine + Nacelle Weight [lb] vs. FPR Comparison .....	98
Figure 71: Thrust-to-Weight Ratio vs. FPR Comparison .....	99
Figure 72: Operating Engine Weight vs. FPR Comparison .....	99
Figure 73: Ramp Weight vs. FPR Comparison .....	100
Figure 74: Fuel Burn vs. FPR Comparison with Step Cruise On .....	100
Figure 75: Fuel Burn vs. FPR Comparison with Step Cruise Off .....	101
Figure 76: NO <sub>x</sub> per unit Thrust [kg/kN] vs. FPR Comparison .....	101
Figure 77: L/D vs. Certification Year for LQ .....	103
Figure 78: L/D vs. Certification Year for LTA .....	104
Figure 79: L/D vs. Certification Year for STA .....	104
Figure 80: L/D vs. Certification Year for SA .....	105
Figure 81: L/D vs. Certification Year for RJ .....	105
Figure 82: L/Dmax vs. Certification Year .....	106
Figure 83: Fuel Burn/(Payload * Range) for R1 vs. Certification Year for LQ .....	107
Figure 84: Fuel Burn/(Payload * Range) for R1 vs. Certification Year for LTA .....	107
Figure 85: Fuel Burn/(Payload * Range) for R1 vs. Certification Year for STA .....	108
Figure 86: Fuel Burn/(Payload * Range) for R1 vs. Certification Year for SA .....	108
Figure 87: Fuel Burn/(Payload * Range) for R1 vs. Certification Year for RJ .....	109
Figure 88: Fuel Burn/(Payload * Range) for R2 vs. Certification Year for LQ .....	109
Figure 89: Fuel Burn/(Payload * Range) for R2 vs. Certification Year for LTA .....	110
Figure 90: Fuel Burn/(Payload * Range) for R2 vs. Certification Year for STA .....	110

Figure 91: Fuel Burn/(Payload * Range) for R2 vs. Certification Year for SA .....	111
Figure 92: Fuel Burn/(Payload * Range) for R2 vs. Certification Year for RJ .....	111
Figure 93: MTOW vs. Certification Year for LQ.....	112
Figure 94: MTOW vs. Certification Year for LTA .....	112
Figure 95: MTOW vs. Certification Year for STA.....	113
Figure 96: MTOW vs. Certification Year for SA.....	113
Figure 97: MTOW vs. Certification Year for RJ.....	114
Figure 98: MTOW vs. Certification Year.....	114
Figure 99: OEW/MTOW vs. Certification Year for LQ.....	115
Figure 100: OEW/MTOW vs. Certification Year for LTA .....	116
Figure 101: OEW/MTOW vs. Certification Year for STA .....	116
Figure 102: OEW/MTOW vs. Certification Year for SA.....	117
Figure 103: OEW/MTOW vs. Certification Year for RJ.....	117
Figure 104: OEW/MTOW vs. Year of Introduction.....	118
Figure 105: OEW/Max Payload vs. Certification Year for LQ.....	118
Figure 106: OEW/Max Payload vs. Certification Year for LTA.....	119
Figure 107: OEW/Max Payload vs. Certification Year for STA.....	119
Figure 108: OEW/Max Payload vs. Certification Year for SA .....	120
Figure 109: OEW/Max Payload vs. Certification Year for RJ.....	120
Figure 110: Rated Output vs. Certification Year for LQ.....	121
Figure 111: Rated Output vs. Certification Year for LTA.....	121
Figure 112: Rated Output vs. Certification Year for STA.....	122
Figure 113: Rated Output vs. Certification Year for SA .....	122
Figure 114: Rated Output vs. Certification Year for RJ.....	123
Figure 115: Engine W/T vs. Certification Year for LQ.....	124
Figure 116: Engine W/T vs. Certification Year for LTA .....	124
Figure 117: Engine W/T vs. Certification Year for STA.....	125
Figure 118: Engine W/T vs. Certification Year for SA .....	125
Figure 119: Engine W/T vs. Certification Year for RJ.....	126
Figure 120: SFC vs. Certification Year for LQ .....	127
Figure 121: SFC vs. Certification Year for LTA.....	127
Figure 122: SFC vs. Certification Year for STA .....	128
Figure 123: SFC vs. Certification Year for SA.....	128
Figure 124: SFC vs. Certification Year for RJ .....	129
Figure 125: Uninstalled Cruise SFC vs. Certification Year .....	129
Figure 126: Cruise TSFC vs. Certification Date.....	130
Figure 127: BPR vs. Certification Year for LQ.....	131
Figure 128: BPR vs. Certification Year for LTA .....	131
Figure 129: BPR vs. Certification Year for STA.....	132
Figure 130: BPR vs. Certification Year for SA .....	132
Figure 131: BPR vs. Certification Year for RJ.....	133
Figure 132: OPR vs. Certification Year for LQ.....	134
Figure 133: OPR vs. Certification Year for LTA .....	134
Figure 134: OPR vs. Certification Year for STA .....	135
Figure 135: OPR vs. Certification Year for SA.....	135
Figure 136: OPR vs. Certification Year for RJ.....	136

Figure 137: Cumulative Noise (EPNdB) vs. Certification Year for LQ.....	137
Figure 138: Cumulative Noise (EPNdB) vs. Certification Year for LTA .....	137
Figure 139: Cumulative Noise (EPNdB) vs. Certification Year for STA .....	138
Figure 140: Cumulative Noise (EPNdB) vs. Certification Year for SA.....	138
Figure 141: Cumulative Noise (EPNdB) vs. Certification Year for RJ.....	139
Figure 142: Cumulative Noise (EPNdB) vs. Year of Introduction.....	139
Figure 143: Noise Margin Relative to Chapter 4 (EPNdB) vs. Certification Year for LQ .....	140
Figure 144: Noise Margin Relative to Chapter 4 (EPNdB) vs. Certification Year for LTA .....	140
Figure 145: Noise Margin Relative to Chapter 4 (EPNdB) vs. Certification Year for STA .....	141
Figure 146: Noise Margin Relative to Chapter 4 (EPNdB) vs. Certification Year for SA.....	141
Figure 147: Noise Margin Relative to Chapter 4 (EPNdB) vs. Certification Year for RJ .....	142
Figure 148: Cumulative Noise Margin relative to Chapter 3 vs. Certification Year .....	142
Figure 149: Compressor Pressure Ratio vs. Certification year.....	144
Figure 150: Improvements in Compressor Pressure Ratio and Stage Loading .....	145
Figure 151: Metal Temperature Capability vs. Engine Availability Date .....	146
Figure 152: Average Metal Temperature Capability vs. Year.....	146
Figure 153: Turbine Inlet Temperature vs. Year .....	147
Figure 154: Rotor Inlet Gas Temperature (T4) vs. Cooling Effectiveness.....	148
Figure 155: Core Engine Power vs. Turbine Rotor Inlet Temperature.....	149
Figure 156: Combustor Exit Temperature vs. Relative Life .....	150
Figure 157: Burner Outlet Temperature vs. Year by Types of Engines .....	150
Figure 158: Engine Thermal Efficiency vs. Propulsive Efficiency .....	151
Figure 159: Surface Area of Composites vs. Year of Introduction .....	152
Figure 160: Percentage of Composites vs. Year of Introduction.....	153
Figure 161: Percentage of Airframe Material vs. Year.....	153
Table 1: Cooling Algorithm Inputs.....	32
Table 2: Non-Dimensional Parameters Used In Centrifugal Map Algorithm .....	42
Table 3: List of Centrifugal Map Algorithm Inputs.....	43
Table 4: Technology Package Definition .....	55
Table 5: Fleet Fuel Burn Reductions .....	58
Table 6: Sample Partial Technology Impact Matrix for Two Technologies .....	64
Table 7: TIM Ranges for a Sample of EDS Inputs for SA GF .....	65
Table 8: Desired Outputs to Train in Neural Network .....	69
Table 9: EDS Vehicle Baselines.....	72
Table 10: Cycle Parameters for each Vehicle and Class .....	75
Table 11: Revised Engine Design Ground Rules and Assumptions.....	85
Table 12: N+1 goals.....	85
Table 13: NASA TM 2011 Technologies .....	85
Table 14: Engine Trade Space .....	86
Table 15: Engine Noise Technologies .....	88
Table 16: Advanced Engine Material Assumptions .....	89
Table 17: Vehicle Design Mission.....	90
Table 18: Vehicle Assumptions.....	91
Table 19: Engine Thrust Sizing .....	92
Table 20: Bypass duct Pressure Loss as a Function of FPR.....	93

Table 21: NASA Study LPC, HPC, and LPT Stage Count ..... 95  
Table 22: High Level Metrics for Historical Trend Research ..... 102  
Table 23: Percent Change per Year for Each Metric and Vehicle Class ..... 143  
Table 24: Low Level Metrics for Historical Trend Research ..... 143

## 1 Executive Summary

The Federal Aviation Administration is pursuing the development of Continuous Lower Energy, Emissions and Noise (CLEEN) technologies for civil subsonic jet airplanes to help achieve the Next Generation Air Transportation System (NextGen) goals. These goals are to reduce significant community noise and air quality emissions impacts in absolute terms and limit the impact of aircraft CO<sub>2</sub> emissions on the global climate by achieving carbon neutral growth by 2020 compared to 2005, thereby allowing sustained aviation growth. The focus of the CLEEN Program is to: (1) mature previously conceived noise, emissions and fuel burn reduction technologies from Technology Readiness Levels (TRLs) of 3-4 to TRLs of 6-7 to enable industry to expedite introduction of these technologies into current and future aircraft and engines, and (2) assess the benefits and advance the development and introduction of alternative “drop in”<sup>1</sup> fuels for aviation with particular focus on renewable options, including blends. Additional information on the CLEEN Program can be found at: [www.faa.gov/go/cleem](http://www.faa.gov/go/cleem).

Under PARTNER Project 36, the Environmental Design Space (EDS) tool developed under PARTNER Project 14 and ongoing NASA funding have been used to provide an independent assessment of technologies funded under the CLEEN Program. This work has been performed in two phases – a public domain and a proprietary phase. In Phase I, EDS was used to assess a set of representative engine and airframe technologies, model the technologies, and assess them at the vehicle and fleet levels on five notional vehicle classes. The representative technologies were modeled using publically available, non-sensitive information. Phase II was similar in nature; however, detailed contractor modeling data and technologies were incorporated into the process. Proprietary technology data from Boeing, General Electric (GE), Honeywell, Pratt & Whitney, and Rolls-Royce has been integrated into vehicle and fleet-level benefits analyses. Note that the assessment work of some CLEEN technologies is not included here and will be conducted as a part of the follow-on Aviation Sustainability Center (ASCENT) Project 10 – Technology Modeling and Assessment. These omitted elements include GE technologies (open rotor engine, engine control/flight management system integration and flight management system/air traffic management integration efforts), and the noise reduction effects of Boeing’s ceramic matrix composite nozzle. As such, this report does not represent the full benefits of CLEEN technologies. Fleet-level analysis using these models has shown that the modeled CLEEN technologies could provide a 2% reduction in fleet fuel burn from 2025 through 2050. This translates to an additional cumulative savings of approximately 22 billion gallons of jet fuel by 2050. Additionally, CLEEN NO<sub>x</sub>-reduction technologies were shown to help maintain fleet landing and takeoff NO<sub>x</sub> levels close to 2006, in spite of the projected increase in number of operations. Fleet-level noise impacts were not assessed under PARTNER Project 36. These are also being assessed as a part of the aforementioned follow-on ASCENT project effort.

These CLEEN technologies combine with other technologies likely to enter the fleet to demonstrate the large potential aircraft technology development has on reducing aviation’s environmental footprint. The CLEEN technologies, when assessed in combination with other technologies likely to enter the fleet by 2030, showed 7 to 9% fleet fuel burn reduction by 2025,

---

<sup>1</sup> A drop in fuel is one that can be used without modification to engine or aircraft system or hardware with no significant change in emissions or performance.

growing to 21 to 28% reduction by 2050 for conservative and optimistic scenarios, respectively. It is important to note that these reductions only represent a subset of all technology improvements that are likely to enter the fleet by 2050. For example, CLEEN II technologies that are being considered at the writing of this report would not be included.

In addition to providing fleet-level assessments, the PARTNER Project 36 team completed a number of related efforts. This included development of a technology dashboard within Excel. This tool is capable of analyzing various technologies at the vehicle level and it is capable of suggesting technology packages that could meet user-defined vehicle and fleet-level scenarios. The technology dashboard is capable of calculating both vehicle level impacts of technologies and provides output compatible with the Global and Regional Environmental Aviation Trade-off (GREAT) rapid fleet analysis tool developed under PARTNER Project 14. This tool suite allows for rapid exploration of technology packages to gain understanding of the interactions between technology types, design variables, and fleet-level assumptions.

### 1.1 Investigation Team

**Georgia Institute of Technology:** Dimitri Mavris (Principal Investigator), Jimmy Tai (Co-Principal Investigator), Christopher Perullo, Russell Denney, Holger Pfaender  
Students: Kayla Aloyo, Alex Carrere, Marcus Bakke, Addison Dunn, Patrick Smith, Vincent Zamaoya, Benjamin Bitoun

**FAA:** Levent Ileri, James Skalecky, Arthur Orton, Aniel Jardines, and Rhett Jefferies (currently with Penn State University)

**NASA:** Casey Burley, Jeff Berton, Bill Haller, Mark Guynn

**Booz Allen Hamilton:** Elena De la Rosa Blanco

### 1.2 Objectives

The objectives of this project leverage the research conducted under the EDS development program (PARTNER Project 14) and NASA, to use EDS to independently model and assess the benefits of the technologies being developed under the CLEEN Program. EDS has been jointly developed by NASA and the FAA and has been used to assess a wide variety of both conventional and advanced technology configurations. The project focused on six primary elements:

- 1) Public domain aircraft technology modeling (Phase I)
- 2) Proprietary CLEEN aircraft technology modeling (Phase II)
- 3) Vehicle level assessments of fuel burn, noise, and NO<sub>x</sub> incorporating these technologies
- 4) Fleet-level assessments of fuel burn and NO<sub>x</sub> using vehicles with these technologies
- 5) Development of an Excel-based technology dashboard for use at the FAA
- 6) Examining historical trends in aircraft technology

The most significant outcome of this work was vehicle and fleet-level benefit assessments of the CLEEN aircraft technologies with regards to fuel burn, NO<sub>x</sub> emissions, and noise. Additionally, the Excel-based dashboard that was developed provides FAA with an in-house capability beyond the conclusion of this project to quickly assess combinations of these technologies and their benefits.

### 1.3 Summary of Major Accomplishments

The following were the major tasks completed under PARTNER Project 36:

#### 1. Public domain aircraft technology modeling (Phase I)

A number of technologies were identified and modeled based on public domain data sources. These models provided a basis for assessment early in the project before proprietary data was available, as well as supplementing the CLEEN technologies with other technologies expected to enter the fleet in a similar timeframe.

#### 2. Proprietary CLEEN aircraft technology modeling (Phase II)

Proprietary technology data from Boeing, General Electric (GE), Honeywell, Pratt & Whitney, and Rolls-Royce has been integrated into vehicle and fleet-level benefits analyses. Note that the assessment work of some CLEEN technologies is not included here and will be conducted as a part of the follow-on Aviation Sustainability Center (ASCENT) Project 10 – Technology Modeling and Assessment. These omitted elements include GE technologies (i.e., open rotor engine, engine control/flight management system integration and flight management system/air traffic management integration efforts), and the noise reduction effects of Boeing’s ceramic matrix composite nozzle. As such, this report does not represent the full benefits of CLEEN technologies. This activity included agreements on modeling approach, in some cases enhancements to model structure in EDS, data exchange, implementation, and validation. The majority of the CLEEN technologies were modeled. Those that were not captured are being addressed in work under the Aviation Sustainability Center (ASCENT) Project 10 – Technology Modeling and Assessment. More information of ASCENT Project 10 is available here: <https://ascent.aero/project/aircraft-technology-modeling-and-assessment/>

#### 3. Vehicle level assessments of fuel burn, noise, and NO<sub>x</sub> incorporating these technologies

The modeled public domain and CLEEN technologies were applied to five representative vehicle size classes in EDS to assess the vehicle level impacts of technologies, including benefits enabled by the technologies with redesign of engine or aircraft features. Benefits assessed included block fuel burn, NO<sub>x</sub> emissions, and certification noise levels. Results of this assessment are proprietary in nature and not shown in this report because the effects of individual proprietary technologies could possibly be discerned from the results.

#### 4. Fleet-level assessments of fuel burn and NO<sub>x</sub> using vehicles with these technologies

The vehicles defined using public domain and CLEEN technologies were then used in the Global and Regional Environmental Aviation Tradeoff (GREAT) tool for a variety of scenarios to capture the fleet-level benefits of these technologies on fuel burn and NO<sub>x</sub> emissions. Scenarios included conservative and optimistic introduction rates of technology, as well as a scenario that removed all CLEEN technologies in order to show the benefits of the modeled program technologies. Results of this assessment are included in this report. At this aggregated fleet level, effects of individual proprietary technologies cannot be discerned, making it suitable for public release.

**5. Development of an Excel-based technology dashboard for use at the FAA**

A technology dashboard tool was created for the FAA to have in-house capability to rapidly assess vehicle level impacts of combinations of the modeled technologies. The technology dashboard is a Microsoft Excel based tool that embeds surrogate models of the EDS technology impacts. This enables the FAA to exercise EDS's capabilities without having to run the full EDS tool suite.

**6. Examining historical trends in aircraft technology**

A historical trend literature review was conducted to provide insight into what technology levels might be expected to be seen in the future, as well as how any proposed technology ideas for future development fit into technology trends. The goal was to uncover if any innovations had broken trends in the past and determine if that is a possibility for the future. This work serves to inform ongoing work in ASCENT Project 10 looking at the potential of technology to meet environmental goals under various possible scenarios. This work is covered in Appendix B.

These accomplishments are addressed in greater depth in the following sections.

## 2 Phase I - Public Domain Aircraft Technology Modeling

The following is a description of the technologies modeled for Phase I of PARTNER Project 36. These technologies were identified and modeled based on public domain data sources. These models provided a basis for assessment early in the project before proprietary data on the CLEEN technologies was available. These models also served to supplement the CLEEN technologies modeled later in the project, representing other technologies expected to enter the fleet through 2050. This section describes the modeling work for the public domain aircraft technologies, including discussion of the technologies themselves, their relevance to CLEEN, how they are modeled in EDS, and the assumptions and limitations of the Phase I EDS models. In addition to public domain technologies modeled under this project, public domain, EDS technology models developed under NASA Environmentally Responsible Aviation (ERA) and NASA Fixed Wing (FW) sponsorships were also used in the PARTNER Project 36 fleet-level analysis. Descriptions of technology models completed under NASA funding are expected to be released as NASA contractor reports at a later date. The table below lists the public domain technologies modeled under PARTNER Project 36 with public domain information. Technologies are grouped by area of primary impact: fuel burn, noise, and emissions. In a number of cases, technologies provide large benefits to multiple areas, as explained in the documentation below.

**TABLE 1: TECHNOLOGIES MODELLED UNDER PHASE I**

Fuel Burn	Noise	Emissions
Retro-fit Alternate non-planar wings tips	Landing Gear Fairings	Advanced Low-NO <sub>x</sub> combustors
Natural Laminar Flow Control	Flap fences / flaplets	
Open Rotor	Fixed Geometry Chevrons	
Geared Turbofan	Combustor Liner	
Active Cooling	Variable Area Nozzle	
Highly Loaded Compressor	Stator Sweep and Lean	
Highly Loaded Turbine	Soft Vane	
Ceramic Matrix Composites	Aft Cowl Liners	
Adaptive Trailing Edge	Zero Splice Inlet	
FMS Controlled Flight Trajectories	Nose Lip Liner	
End Wall Contouring		

### 2.1 Fuel Burn Technologies

#### 2.1.1 Retrofit alternate non-planar wingtips

##### *Description*

Winglets (or wing-tip devices in general) are extensions to the tips of aircraft wings, which can be retrofitted or included in the production wing design. These devices come in various shapes and sizes, even though they provide the same essential function of induced drag reduction. In terms of application, winglets are often used in settings where the wingspan is constrained. A

vertical winglet has the effect of increasing effective span, though not as much as a direct horizontal span extension of the same length.

Contrary to popular belief, a winglet does not work by physically blocking the upwards curling wingtip vortex, but instead reshapes the global lift-distribution to a flatter shape that reduces the amount of downwash (and hence the wing vortices). Consequently, wingtip devices have to be properly loaded in order to minimize induced drag. A bad design may not achieve significant induced drag reduction, while incurring increased zero-lift drag, resulting in worse performance. Since these devices add to the wing's structure, any induced drag benefit has to be balanced against degrading zero-lift drag, increasing overall weight, flutter issues, and costs.

### ***Major Assumptions***

There are three major impacts of wingtips that must be modeled to assess the total effect of wingtips. Namely these are the reduction in induced drag provided by the installation of the winglet, the increase in profile drag caused by the increased wing wetted surface area, and the increase in weight. Each of these is estimated as described herein.

- 1) A relationship between winglet weight for varying winglet designs and sizes is reproduced in Figure 1. [1] The cruise drag reduction is applied to the vehicles profile drag estimated in the absence of wingtips. The cruise gross weight increase is actually the increase in the wing weight and is applied as such for a specific type of winglet. For the CLEEN Phase I assessments a vertical wingtip type was assumed. The size of the winglet is specified as winglet span as a percentage of the wing span. For the CLEEN Phase I assessment 15% sized wingtips were used on the regional jet (RJ) and single aisle (SA) aircraft, 12% on the small twin aisle (STA) aircraft, 7% on the large twin aisle (LTA) aircraft, and 6% on the very large aircraft (VLA). In an actual design trades between costs, ease of integration with the wing structure, structural considerations, considerations with flutter / fatigue requirements, and other factors must be considered. Another primary assumption used is that the penalties applicable to the 737NG, shown in Figure 1, are applicable to all aircraft classes. The data shown is the most complete parametric data set found thus far.

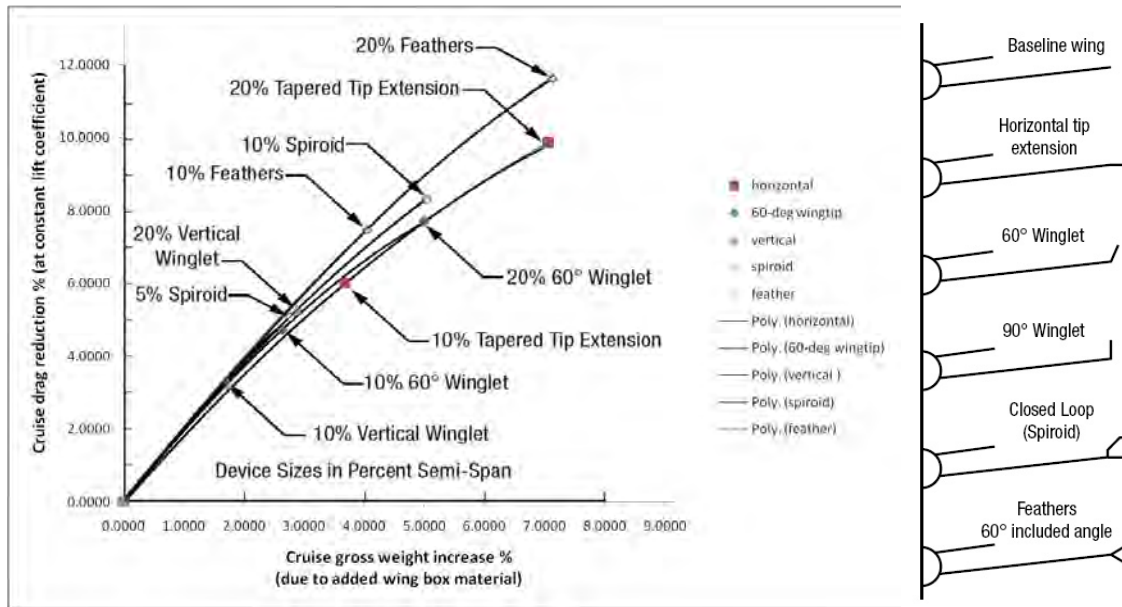


**FIGURE 1: RELATIONSHIP BETWEEN WINGTIP SIZE, WEIGHT, AND BENEFIT**

- 2) To estimate the increase in profile drag caused by the increase in wing wetted area the correlations in [1] were used, assuming that the average thickness to chord of the wingtip is half that of the tip of the main wing of the airframe. The additional wetted area is added to the total wing wetted area and the internal Flight Optimization System (FLOPS) aerodynamic predictions within EDS estimate the corresponding change in profile drag. [3]

### ***Limitations of the Current Model***

- 1) Correlations are based on the 737NG and are applied to other aircraft classes without further modification.
- 2) Additional structural considerations such as flutter and aerodynamic loading constraints are not taken into account.
- 3) A detailed study considering all of the wingtip types was not conducted. Rather a consistent wingtip type was applied to each vehicle.

### ***2.1.2 Natural Laminar Flow Control***

#### ***Description***

Laminar flow control is assumed to be a passive system in which the shape of the wing and airfoil is uniquely tailored in order to delay the boundary layer transition from a laminar to turbulent. Since laminar boundary layers exert less skin friction drag on the aircraft this reduces the drag, and thereby fuel burn required. The exact design of the airfoil and wing is not considered in this assessment; rather, past results from various laminar flow control programs were used to correlate the achievable laminar flow with aircraft geometry and flight conditions.

## Major Assumptions

- 1) Natural laminar flow (NLF) technology is simulated within EDS by predicting the transition Reynolds number at every Mach number and altitude throughout the flight using the data shown in Figure 2, as adopted from [2]. It was assumed that laminar flow technology is capable of maintaining 50% laminar flow over the mean chord (e.g., flow is laminar from the leading edge up to 50% of the chord length, depending on Reynolds number and sweep).

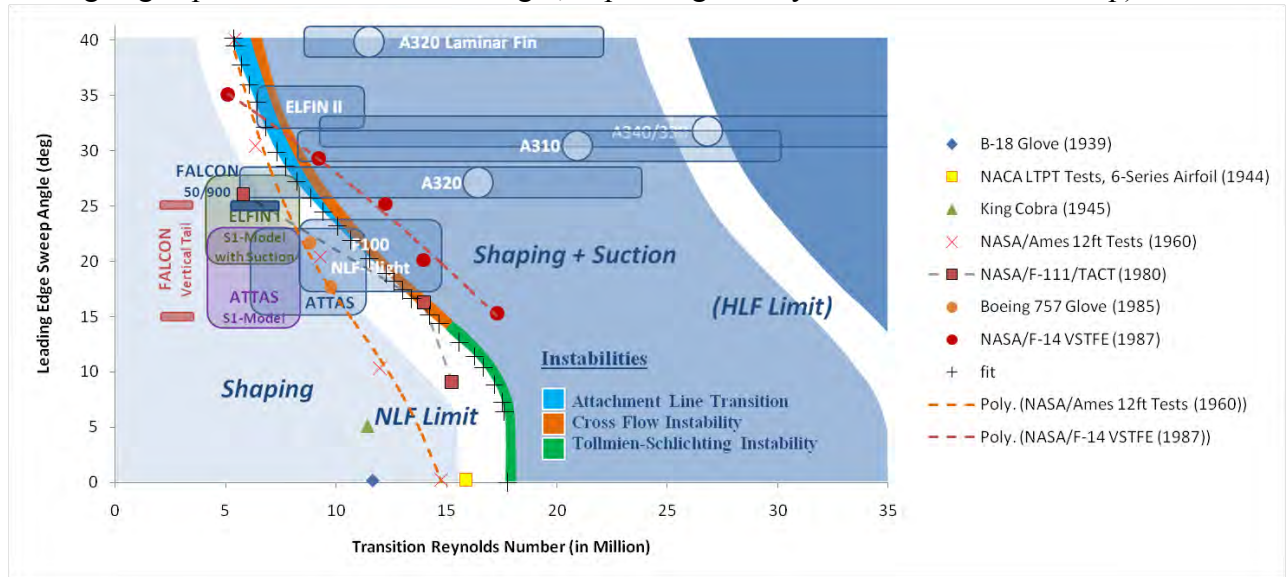


**FIGURE 2: EDS LAMINAR FLOW TRANSITION MODEL**

- 2) The process for estimating the laminar flow drag reduction is as follows:
  - a) For a given aircraft flight condition (Mach and altitude) the Reynolds number is calculated based sweep angle as provided in Figure 2, using the line marked *NLF limit*.
  - b) The transition Reynolds number is then used to calculate the location along the wing's chord at which transition from laminar to turbulent flow occurs. This yields the “percent laminar flow” at a given flight condition.
  - c) This “percent laminar flow” is fed into the FLOPS aerodynamic drag calculations which are based on [3].
    - i) By default FLOPS assumes a minimum of 8.5% laminar flow. Should the EDS NLF model predict less than 8.5%, 8.5% is used as a minimum estimate.
- 3) This process is repeated for each and every aircraft flight condition.
- 4) NLF was assumed on the wing, vertical tail, and horizontal tail surfaces
- 5) The vehicle is not resized in response to the application of NLF; in other words, reserves are kept in order to ensure that the aircraft could fly the entire mission should NLF fail in flight.
- 6) The wing sweep of the baseline aircraft was not modified to increase the potential of NLF since change in cruise speeds were not considered in this study.

## Limitations of the Current Model

- 1) Because of the manner in which EDS handles low speed aerodynamic performance prediction the NLF modifications only apply to the climb, cruise, and descent calculations. Takeoff is not considered.

- 2) Interactions between changes of the airfoil and the control surfaces in terms of performance and noise are not captured since this is beyond the fidelity of EDS.
- 3) Wing structural implications are not captured.

### ***2.1.3 Open Rotor***

#### ***Description***

An open rotor is an evolution of the commercial turbofan engine in which the ducted fan is replaced with two external, counter-rotating propellers designed for high speed operation. Removing the heavy fan cowl and using counter-rotation recover many of the efficiency and weight penalties associated with traditional ducted ultra-high bypass ratio engines. The EDS open rotor modeling methods were developed under NASA funding and are described in detail in [4,5]. The open rotor was not assessed under PARTNER Project 36, but will be examined under future work in ASCENT Project 10.

### ***2.1.4 Geared Turbofan (GF)***

#### ***Description***

A conventional turbofan engine contains two to three shafts. In both configurations, the fan is mechanically connected to the low pressure turbine (LPT) via the low pressure shaft. If a low pressure compressor is present it is connected to the low pressure shaft too. The high pressure compressor is mechanically connected to the high pressure turbine (HPT) on the high pressure shaft. This configuration causes a disconnect between the desire for compact light weight engines and those with high bypass ratios (BPR) as both metrics must be achieved simultaneously to maintain ever increasing fuel burn reductions. To increase engine propulsive efficiency, higher bypass ratios are required. With higher bypass ratios lower fan pressure ratios are required to achieve the optimum propulsive efficiency for a given bypass ratio. Lower fan pressure ratios usually require lower fan speeds. This is where the disconnect between the mechanical coupling and thermodynamic coupling of components arises. As the bypass ratio increases the fan mass flow increases and more power is required from the LPT. More power equates to more LPT stages, leading to a heavier engine. This effect is compounded by the fact that the fan needs to rotate more slowly to provide peak propulsive efficiency and the LPT would like to rotate quickly to keep the stage count down and provide more efficient operation. An exhaustive examination of these trades is well documented in [6]. By placing a gearbox between the fan and the LPT each component can rotate at their own optimal speeds, as shown in Figure 3. [6] This technology has large potential for both fuel burn and noise reduction. In addition to the brief description here, Georgia Tech conducted an extensive validation against NASA models; the results are detailed in Appendix A.

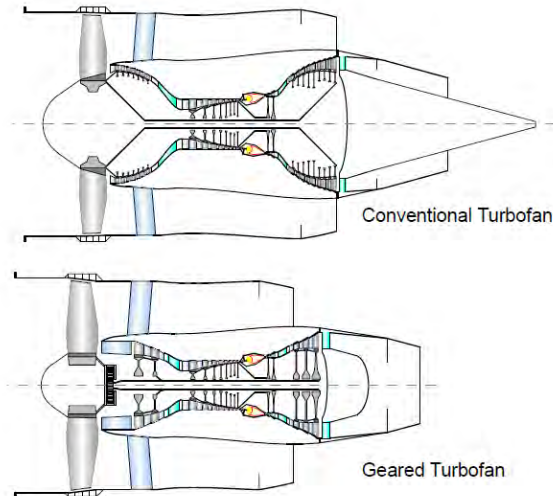


Figure 11: Common core conventional and geared turbofans with BPR=10

### FIGURE 3: COMPARISON BETWEEN GF AND DIRECT DRIVE

Several modifications were made to a standard EDS direct drive model in order to capture all of the effects associated with a geared turbofan (GF).

- 1) The additional gearbox weight must be estimated.
- 2) The LPT efficiency is related to the turbine loading as a function of the power required and the rotational speed, set by the bypass ratio and gearbox respectively.
- 3) The LPT loading must be adjusted. Since the LPT is now spinning more quickly it is designed more like an HPT than an LPT.
- 4) The new engine cycle must be set.
- 5) Weight reduction technologies must be applied to the fan exit guide vanes, nacelle, and engine installation.

#### *Major Assumptions*

The following assumptions describe the methods used to address each one of the modifications just discussed.

- 1) The gearbox weight is fundamentally a function of the torque, gear ratio, and material used to design the gear box. There are several methods available for estimating the gear box weight and many rely on correlations of existing gearboxes. [7] Unfortunately, most of these sources do not differentiate between different gearbox types. In an effort to overcome this, a more standard method was used. A star epicyclical design was assumed with a gear ratio of 3. This gear ratio was estimated by examining cutaways of the PW1000G provided on Pratt and Whitney's website. The gearbox weight is estimated using the design method in [8], using the materials associated with lightweight aircraft design. The weight estimation method is designed to estimate the lightest weight gear design for a given gear type and gear ratio. It does not provide a detailed design of the gearbox itself.
- 2) The LPT efficiency is predicted using a Smith chart as reproduced in Figure 4 from [9]. The chart relates zero-clearance turbine efficiency to turbine loading and flow coefficient. For the

EDS analysis, this relationship was converted into a map that changes the design point efficiency of the LPT as the stage work coefficient, or loading, is changed. This provides a secondary benefit of gearing the LPT by increasing the stage adiabatic efficiency. Because the Smith chart is for a single stage, it is assumed that each LPT stage has equal loading and equal polytropic efficiency. This is then used to calculate the overall LPT efficiency.

PERFORMANCE ANALYSIS RESULTS

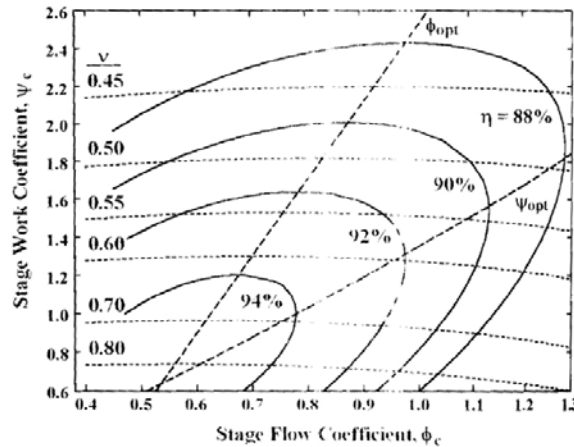


**FIGURE 4: SMITH CHART**

- 3) The LPT loading is reduced in order to set the desired LPT stage count that yields the optimum tradeoff between weight and efficiency. In the case of the RJ and SA for the CLEEN Phase I assessments the turbine loading was set to match the published stage count of the PW1000G.
- 4) In order to set the GF cycle this general process is followed:
  - a) The gear ratio is either pre-defined or optimized along with fan pressure ratio and bypass ratio depending on the needs of the study.
  - b) The fan pressure ratio is then run through a series of sweeps from while maintaining a specified overall pressure ratio (OPR).
  - c) For each fan pressure ratio, the bypass ratio is adjusted to provide the minimum vehicle fuel burn. Note that the minimum vehicle fuel burn and minimum TSFC are not at the same point.
  - d) The LPT  $AN^2$  value is constrained as outlined in [6].
  - e) This process is repeated until an optimum engine cycle for a specified gear ratio is found. During the entire process the weight of the gearbox and efficiency of the turbine vary parametrically in accordance with their respective models.

### ***Limitations of the Current Model***

- 1) In order to fully estimate the gearbox weight a more detailed design is required.
- 2) The change in LPT efficiency relies upon the accuracy of the Smith chart.
- 3) The engine cycle that results does not take into account cost, complexity, or other factors that influence cycle design. It is based on thermodynamics and is loosely based on project engines entering service in the latter part of this decade.

- 4) The weight implications of the higher bypass ratio fan rely on the assumptions built into WATE++. [40] WATE++ is a NASA based engine weight and geometry estimation code integrated into the EDS environment.
- 5) Rotor stator spacing, fan cowl length, and fan aerodynamic design play a key role in noise production. These factors are not all adjusted and detailed analysis may be beyond the capability of NASA's Aircraft Noise Prediction Program (ANOPP). [10]. ANOPP is integrated into EDS to provide vehicle level certification noise information in addition to noise data needed to generate fleet-level noise such as sound exposure level (SEL) information.

Additional information on verification of EDS's geared turbofan model against NASA studies is contained in Appendix A.

### ***2.1.5 Active Cooling***

#### ***Description***

For Phase I, the EDS team assumed active cooling to be similar to the cooling flow setup in the new aero engine core concept (NEWAC), as shown in Figure 5. The air from the compressor, which is used to cool the turbine, is cooled using air from the fan bypass duct. Since the cooling air has a lower temperature in this configuration, less of it is needed to achieve the same cooling effectiveness. This is a different form of advanced cooling than is present in the CLEEN funded technologies, which address far more specific components of the hot gas path.

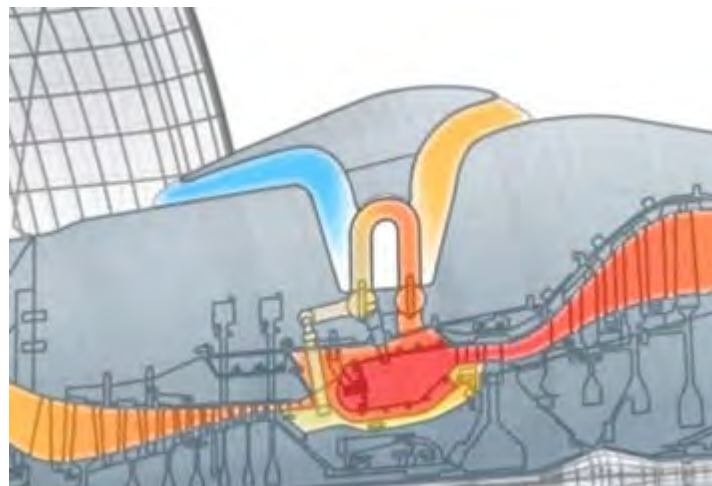


**FIGURE 5: NEWAC ACTIVE CORE CONCEPT [11]**

#### ***Major Assumptions***

Since cooling effectiveness, as defined in Equation 1, is a function of  $T_3$ , or the compressor exit temperature, cooling this air before entering the turbine will reduce the required cooling effectiveness. This in turn will reduce the required cooling flow and increase cycle thermodynamic efficiency.

$$\phi = \frac{(T_{4.1,Max} + \Delta Deterioration) - T_{metal}}{T_{4.1,Max} - T_{3,Max}}$$

where

$T_{4.1,Max}$  = Maximum power management limited turbine inlet temperature

$T_{metal}$  = Maximum turbine blade or vane metal temperature

$T_{3,max}$  = Maximum compressor exit temperature that occurs during normal operation

### EQUATION 1: COOLING EFFECTIVENESS

In addition to reducing the required cooling flow, the technology carries with it an associated weight penalty. This penalty is accounted for in the EDS CLEEN assessments and was scaled to data presented in [12]. The general process for sizing the heat exchanger is as follows:

- 1) The heat exchanger sizing model is set up to size the heat exchanger for the takeoff condition. This is done because the engine usually experiences the highest compressor and combustor exit temperatures at this point.
- 2) The user input into the heat exchanger model is the percentage of the fan bypass air that will flow through the heat exchanger. This is effectively the free design variable in the process.
- 3) The weight of the heat exchanger is estimated by relating heat exchanger weight to the required heat transfer area and correcting for the assumption that a single pass shell and tube design is used. [13] The overall heat exchanger area is estimated by calculating the heat transfer from the compressor cooling flow to the fan bypass flow and assuming an overall heat transfer coefficient of 13.3 BTU / (lbm F) as documented in [14] for compact air to air heat exchangers.
- 4) The overall weight is assumed to be directly proportional to the heat exchanger area and is calibrated to the weight given in [12].
- 5) The heat exchanger weight is added to the engine weight.
- 6) Only HPT chargeable cooling air is cooled.

Using the parametric correlation for heat exchanger weight allows the tradeoff between increased weight and increased thermodynamic efficiency to be performed. Internal studies showed that using approximately 10% of the fan bypass air to cool the turbine cooling air provided an optimum benefit. Increased cooling air fraction beyond 10% yielded diminishing returns.

#### *Limitations of the Current Model*

- 1) The current heat exchanger model uses conceptual design techniques to estimate the heat exchanger weight. In an actual design the detailed geometry of the heat exchanger would need to be calculated. This would include estimating the exact dimensions, number of tubes required and pressure drop associated with the design.

## 2.1.6 Highly Loaded Compressor

### Description

Future aerodynamic designs, processes, and tools will enable higher loading in each stage of the compression system of gas turbine engines. This may be accomplished either through advanced three-dimensional aerodynamic design or through the addition of counter-rotation between the fan, booster, and high pressure compressor. A general increase in compressor loading of 38% per stage is assumed per [15]. It was also assumed that increasing the compressor stage loading carries with it an inherent performance penalty as shown in Figure 6 for a given technology level. [16] In other words, new aerodynamic design techniques will shift the contour shown in Figure 6. For this reason it is assumed that the highly loaded compressor is always applied along with the End Wall Contouring technology described on page 16. The end wall contouring is used to counter the decrease in efficiency associated with higher loading.

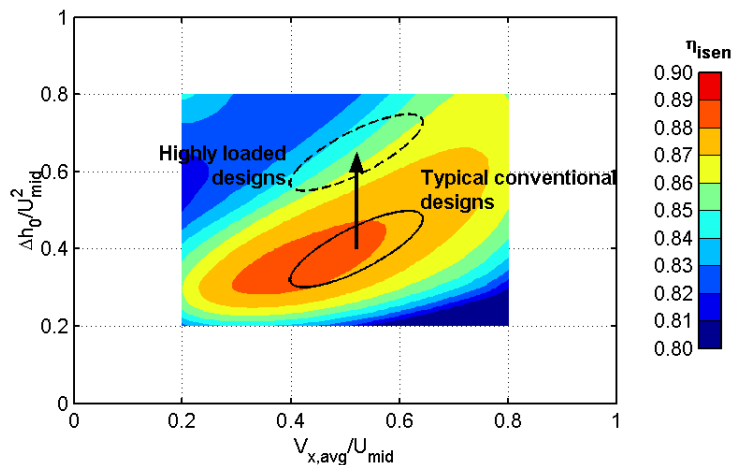


FIGURE 6: CORRELATION BETWEEN COMPRESSOR LOADING AND EFFICIENCY

### Major Assumptions

- 1) The increase in loading is simulated in EDS by increasing the allowable stage pressure ratio of the compressor such that the loading is increased by 38%. EDS then assumes that there is equal loading per stage and this is used to estimate the compressor stage count, which in turn influences compressor weight.

### Limitations of the Current Model

- 1) Highly loaded compressor technology is very design specific to an engine and is hard to simulate at an intermediate level of fidelity without delving into specific details of an actual engine design. This is the reason an increase in loading is used to simulate the technology.
- 2) Changes in weight due to any necessary compressor structural changes are not accounted for. Again this would need detailed geometry information. Weight changes due to changes in stage count or flow path are accounted for.

### ***2.1.7 Highly Loaded Turbine***

#### ***Description***

Highly loaded turbines are similar to highly loaded compressors in that they rely on the next generation of aerodynamic and structural design to increase the amount of work done per stage and thereby reduce the number of required stages. As is the case for the compressor, the turbine efficiency is a function of the loading for a given technology level. Therefore increases in aerodynamic design capability, such as end wall contouring, will enable highly loaded designs with a minimal performance penalty.

#### ***Major Assumptions***

EDS uses the turbine loading to set the turbine stage count based on the overall work the turbine must provide to drive the compressor along with the rotational speed of the connected shaft. The speed is also set by the compressor requirements. Therefore, the loading is directly proportional to the number of stages required. It was assumed that advanced technologies will increase the loading 20% for the high pressure turbine without any change in efficiency. The low pressure turbine was not modified. This was done to reduce the conflict necessary between the differing requirements for the GF. A GF actually requires the loading in the low pressure turbine (LPT) to be reduced to account for the higher rotational speeds resulting from the geared design.

#### ***Limitations of the Current Model***

- 1) Highly loaded turbine technology is very design specific to an engine and is hard to simulate at an intermediate level of fidelity without delving into specific details of an actual engine design. This is the reason an increase in loading is used to simulate the technology.
- 2) Changes in weight due to any necessary turbine structural changes are not accounted for. Again this would need detailed geometry information. Weight changes due to changes in stage count or flowpath are accounted for.

### ***2.1.8 Ceramic Matrix Composites***

#### ***Description***

Ceramic Matrix Composite (CMC) is a material technology that improves the heat resistance and reduces weight for several applicable engine components in the hot gas path. Because of their high temperature capability, the need for cooling air is reduced which increases cycle thermodynamic efficiency and leads to reduced fuel burn.

#### ***Major Assumptions***

- 1) The current EDS cooling model is broken up into chargeable and non-chargeable cooling as shown in Figure 7. Conceptually, this means that cooling flow needed for the rotors and stators is calculated and used to estimate the cooling flows delivered to the entrance and exit of a turbine. While work is ongoing to apply CMC technology throughout the hot gas path, this study assumed that CMCs would be applied only to the turbine stators, shrouds, and

static structures in the N+1 timeframe. Further applications to the HPT and LPT blades were assumed possible in N+2 applications.

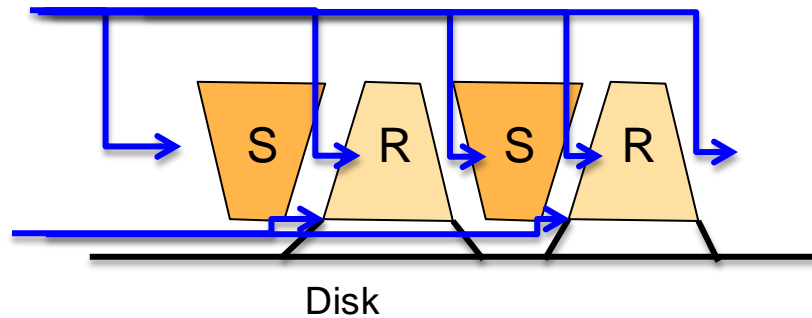


**FIGURE 7: EDS COOLING FLOW SETUP**

- 2) CMC LPT stators were simulated within EDS by increasing the allowable “metal” temperature within the CoolIt prediction module from the baseline of 2000 degree F to 2500 degree F. The density of the LPT turbine stators was also reduced to 0.093 lbm / in<sup>3</sup> which is appropriate for a SiC/SiC composite. These material properties were taken from the Cambridge Materials Selector database. [17]

### ***2.1.9 Adaptive Trailing Edge***

A rough public domain model of a wing adaptive trailing edge was developed in phase I of the project. This was later replaced with in-depth work with proprietary data to model the Boeing CLEEN adaptive trailing edge. It should be noted that this technology benefits both fuel burn and noise.

### ***2.1.10 Flight Management System (FMS) Technologies***

Modeling of flight management system technologies were deferred given the strengths of the modeling environment. These technologies are being worked under ASCENT Project 10 – Technology Modeling and Assessment. It should be noted that this technology benefits both fuel burn and noise.

### ***2.1.11 End Wall Contouring***

#### ***Description***

Endwall contouring takes advantage of advanced 3D aerodynamic computational fluid dynamics (CFD) codes to purposely shape the endwalls of the turbomachinery to improve performance. The locations of the endwalls are detailed in Figure 8.

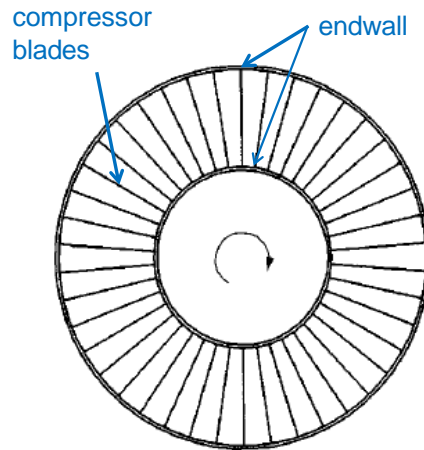


**FIGURE 8: DESCRIPTION OF ENDWALL LOCATION**

In typical designs the endwalls are smooth and ‘flat’. However, localized areas of separation may occur near the endwalls as shown in Figure 9. This can be overcome by “pushing” the endwall into the location of the stall to prevent it from occurring as shown in Figure 10. The end effect is increased efficiency.

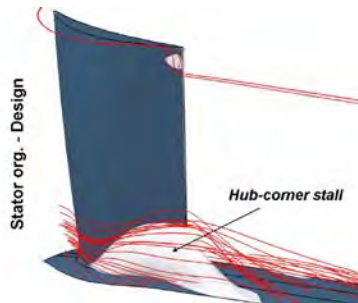


**FIGURE 9: EXAMPLE OF SEPARATION NEAR THE ENDWALL**

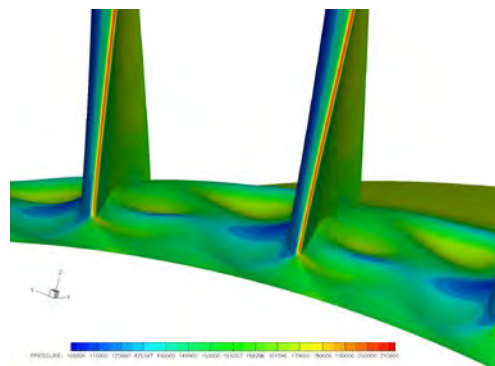


**FIGURE 10: EXAMPLE OF ENDWALL CONTOURING**

A literature review revealed that the effect of endwall contouring can increase efficiency between 0.35 and 2.5% depending on the application. Since the prediction and control of endwall stall is an unsteady, 3D phenomenon, the effects of contouring are extremely configuration

dependent; therefore, it was assumed endwall contouring would be an enabling technology for the highly loaded compressor and turbine technologies. [18][19][20][21][22][23]

### ***Limitations of the Current Model***

- 1) A broad assumption that endwall contouring is grouped with highly loaded compressors and turbines and maintains a base level of efficiency as the compressor or turbine loading increases is made.

## **2.2 Noise Technologies**

A number of noise technologies were captured in Phase I public domain modeling efforts. All noise technologies are modeled within EDS in a manner consistent with NASA-based studies. NASA's ANOPP tool is used to predict the source noise associated with the major engine and airframe components such as the fan, jet, landing gear, and flaps, in addition to several others. [24] (Noise reductions stated in this section are source noise unless otherwise noted.) The noise of all of the components is then propagated from the aircraft to the observer to calculate certification metrics or information to generate noise contours. When possible, direct inputs to ANOPP (e.g., liner area, blade count) are used to model technologies; however, in many cases it is necessary to suppress source noise. Since the suppression factor is an input rather than a computed value it must be obtained from test data or higher fidelity analysis. In the case of the Phase I EDS modeling, the suppression factor is obtained from open source literature. Unless otherwise noted all noise technology noise reductions are applied across all frequencies and directions.

### ***2.2.1 Landing Gear Fairings***

#### ***Description***

Landing gear fairings are used to reduce the turbulent flow around landing gear with the end goal of reducing landing gear noise. Figure 11 shows an example of landing gear fairings as tested on the main gear of the A340. [25]

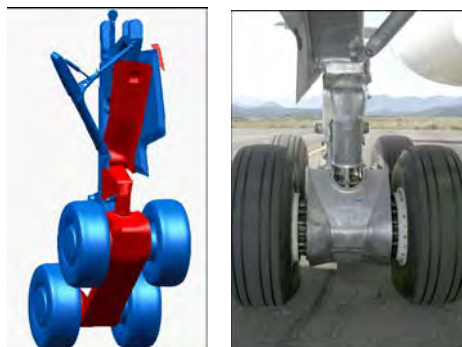


**FIGURE 11: EXAMPLE OF LANDING GEAR FAIRINGS**

### ***Major Assumptions***

- 1) Data from the A340 landing gear test was used to estimate the reduction in landing gear source noise as approximately 2.4 dB. This reduction is applied to the ANOPP internally predicted landing gear source noise within EDS. [26]
- 2) A one percent landing gear weight penalty was assumed.

### ***Limitations of the Current Model***

- 1) As is the case with several other technologies, the exact benefits of this technology may be configuration dependent and error may be introduced through the one fits all approach.
- 2) Without more detailed high fidelity analysis or test data it is difficult to predict exactly how the technology will scale to other systems.

## **2.2.2 Flap Fences / Flaplets**

### ***Description***

Flap fences, or flaplets, are similar to winglets in that they are small devices applied to the outboard section of the flap airfoil and are designed to reduce tip edge vortices, as shown in Figure 12. Reducing the vortex helps to reduce flap noise.

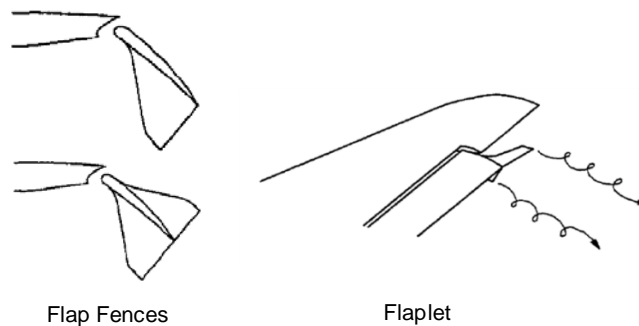


**FIGURE 12: FLAP FENCES**

### ***Major Assumptions***

- 1) Since the flaplets are a small control surface on the edge of the flap it was assumed that the weight penalty is within the margin of error of the prediction capability of the EDS aircraft performance and sizing tool, FLOPS.
- 2) There are differing results of the noise reduction capability of flaplets, but a general overview of available public domain data shows that an average reduction of 5 dB is achievable. [27][28]

### ***Limitations of the Current Model***

- 1) There may be additional interactions that are not captured in the model, such as small changes to the lift-to-drag (L/D) ratio of the flaps which may affect the low speed

aerodynamic performance of the aircraft. This may influence the climb rate of the aircraft which would have a secondary impact on aircraft noise at approach and cutback as it would increase the distance between the source and observer.

- 2) The exact reductions are configuration dependent and would require detailed testing or CFD to get more accurate results.

### 2.2.3 Fixed Geometry Chevrons

#### *Description*

Chevrons are small devices placed at the jet engine nozzle exit plane that modify the jets shear layer in a manner that reduces jet noise. As shown in Figure 13, chevrons may be applied to the core nozzle, fan nozzle, or both. [29] Most in-service aircraft with chevrons only have them on the core nozzle. Chevrons on the fan nozzle are usually present to control cabin noise at altitude.

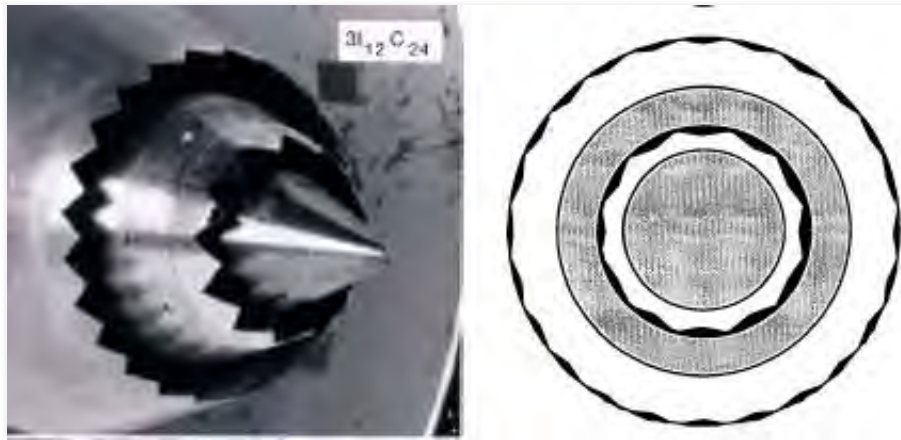


**FIGURE 13: CHEVRON DESCRIPTION**

As indicated in [29], there may be a small thrust loss associated with the presence of chevrons ranging from zero to one percent.

#### *Major Assumptions*

Unlike the other noise technologies simulated for this project which require suppression factors to be applied to engine or aircraft source noises, ANOPP provides specific inputs to model the presence of chevrons on both the fan and core nozzles. The assumption was made to apply chevrons only to the core nozzle. A sensitivity study was performed for the five different vehicle classes within EDS and the results are shown in Figure 14. Differences in level of suppression are caused by different bypass ratios (5-9) for the different engine types.

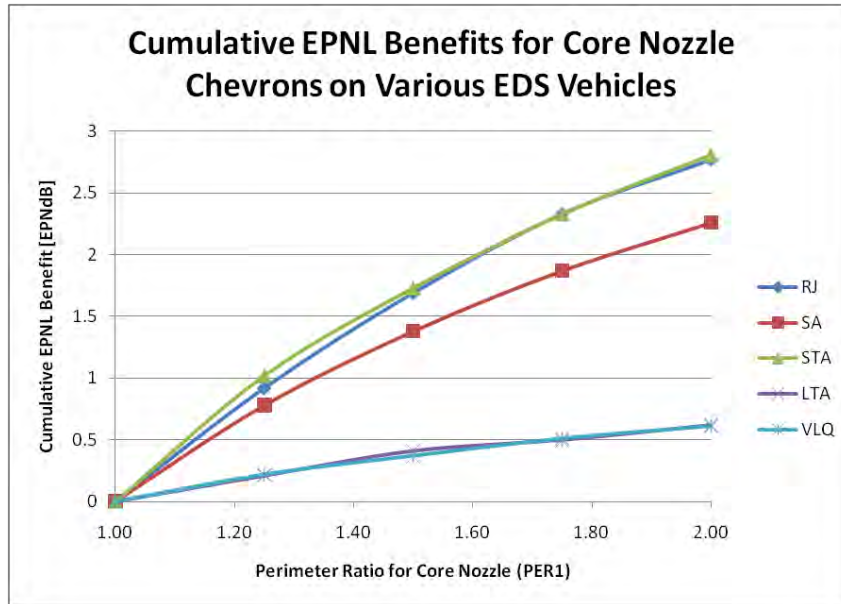


**FIGURE 14: EDS-ANOPP CHEVRON CONFIGURATION SENSITIVITY STUDY**

The parameter PER1 in Figure 14 is the ANOPP variable that controls the presence of chevrons with 1.0 indicated the absence of chevrons and 2.0 indicating maximum chevron coverage. From the results of the sensitivity study it was decided to choose a PER1 value of 1.6 which corresponds to approximately a 0.5 EPNdB reduction on large wide body, high bypass ratio engines and approximately 1.6 EPNdB on the narrow body, lower bypass ratio aircraft. By using the built in ANOPP capability the suppression of jet noise varies parametrically with jet velocity, temperature, and bypass ratio.

Due to feedback at multiple PARTNER meetings, and from industry and NASA sponsors, no thrust penalty was assumed for chevrons. That being said, multiple reports indicate that there may be a penalty associated with chevrons. Most recently the Airbus A321 noise insertion program (NIP) added chevrons which had a small thrust penalty associated with them. [30]

### ***Limitations of the Current Model***

- 1) Any interaction between performance and noise is not accounted for.
- 2) Relies upon ANOPP to correctly predict chevrons' effect on jet noise.

### ***2.2.4 Core Exhaust Nozzle Liner***

#### ***Description***

Core exhaust liners are noise reduction liners commonly placed at the core exit nozzle. They are tuned to combustion core and LPT noise which can be dominant on approach depending on the exact engine configuration. An example is shown in Figure 15. [31]

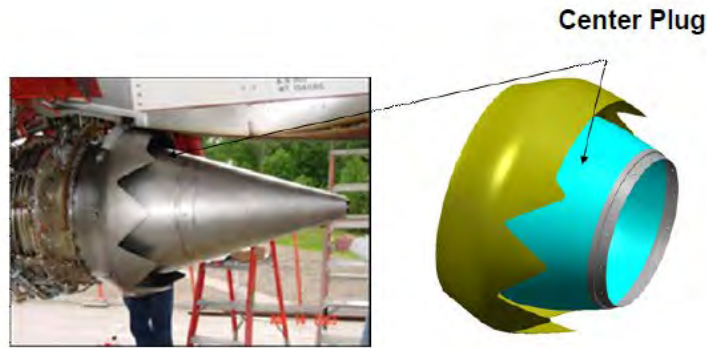


**FIGURE 15: COMBUSTOR LINER CONCEPT**

**Major Assumptions**

- 1) Because the cavity acoustic liner contains a hollow Helmholtz resonator it may not contribute much to the weight of the engine, and that impact may be minimized in new aircraft, optimized designs. Combined with the fact that public domain weight information was not available, no weight impact is assumed.
- 2) The noise reduction is taken as 5 dB source noise for the peak frequencies shown in Figure 16 as taken from [31].

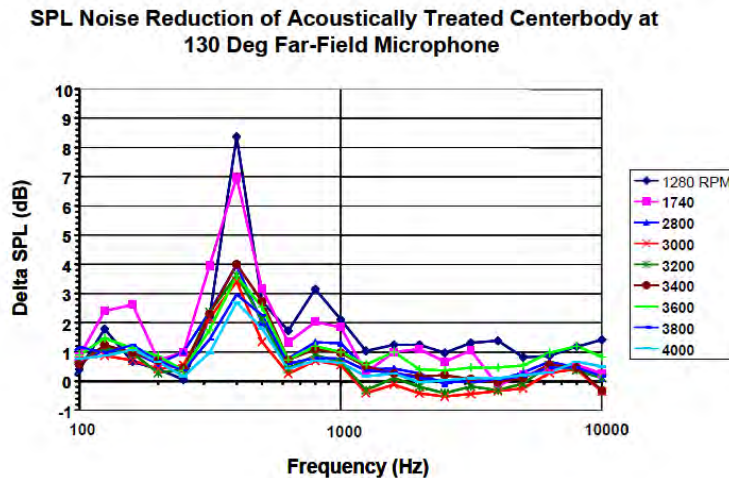


**FIGURE 16: CORE EXHAUST LINER NOISE REDUCTION**

**2.2.5 Variable Area Nozzle**

**Description**

The variable area fan nozzle has several benefits. Increasing the nozzle area during takeoff allows for the jet velocity to be reduced while maintaining thrust. It also allows the fan performance to be optimized throughout the flight envelope. In the case of a GF, it can be used to

maintain fan stall margin, which may be an issue for low pressure ratio fans. There is a weight penalty associated with the variable area nozzle. An example of a shape memory alloy (SMA) actuated nozzle is shown in Figure 17. [32]

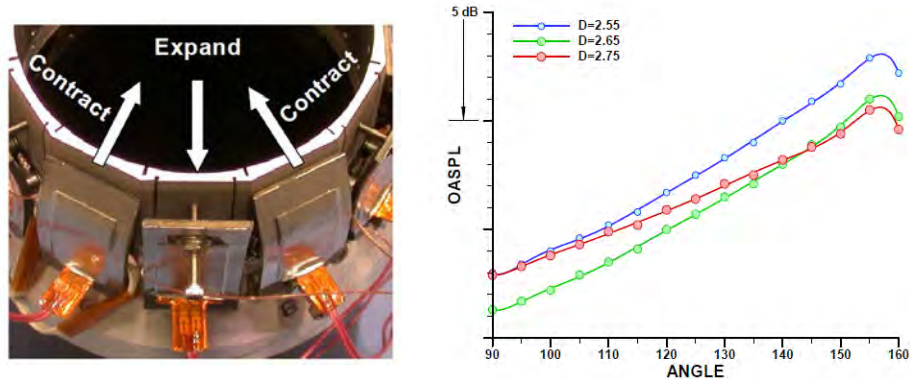


**FIGURE 17: VARIABLE AREA NOZZLE**

### ***Major Assumptions***

- 1) A 10 % weight penalty is applied to the fan nozzle corresponding to [33]
- 2) The fan nozzle has two modes of operation:
  - a) Below Mach 0.2 the nozzle area is opened to some fixed, user specified percentage of the nozzle design area. The nozzle design area is set at cruise conditions.
  - b) Above Mach 0.2 the nozzle area is varied to maintain the optimum fan efficiency possible at a given Mach, altitude, and power setting combination.
  - c) The nozzle area is constrained to open and close by 20-50% of the design area depending on the range of fan pressure ratio being investigated
- 3) When the GF is present on the system a variable area nozzle is always included to maintain a minimum fan stall margin.

Several trade studies were run to determine the best Mach number and nozzle takeoff area ratio to use. It was determined that Mach 0.2 and a takeoff area ratio of 120% of the design value provided the best combination of benefits between fuel burn and noise.

### ***Limitations of the Current Model***

- 1) The weight penalty is based on a NASA study assuming that shape memory alloys (SMA) are used and an additional 10% penalty is applied to the regularly estimated nozzle weight. [33] In reality the exact penalty will greatly depend on the exact actuation mechanism used, stresses on the bypass nozzle, potential interactions with the thrust reverser, and variability in nozzle area. These require a more detailed analysis; however aircraft with large maximum takeoff weight (MTOW) will show less sensitivity to the weight penalty than lighter, shorter range aircraft.

## 2.2.6 Fan Stator Sweep and Lean

### Description

Fan stators can be swept or leaned in order to reduce fan noise created when the rotor wake interacts with the leading edge of the stator. Specifically, the angle and phase of the wake with respect to the stator can be controlled to reduce noise and this method has been found to be more effective than simply increasing the axial spacing between the rotor and stator. [34] An example of sweep and lean is shown in Figure 18 and Figure 19. [35] Several configurations have been tested that sought to determine of sweep in addition to the combined effect. Generally, swept and leaned blades reduced blade passage frequency (BPF) tones for fan frequencies between zero to eight thousand hertz. [34] The effect on efficiency is more uncertain. Some reports indicate that swept only configurations may reduce efficiency and swept and leaned configurations may increase efficiency. [36]

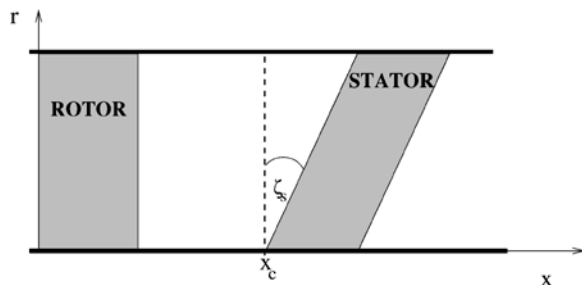


FIGURE 18: STATOR SWEEP

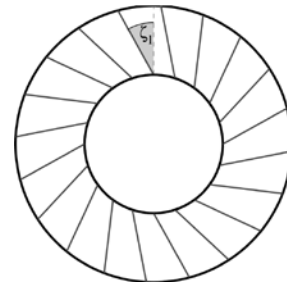


FIGURE 19: STATOR LEAN

### Major Assumptions

- 1) The information in [37] was used to estimate the noise reduction associated with 30 degrees of sweep and 30 degrees of lean, corresponding to the configuration tested in [34]. The noise reduction is assumed to be a 3 dB of aft fan broadband and tonal noise across all frequencies. A 2dB reduction was applied to forward fan noise.
- 2) No aerodynamic efficiency penalty is assumed due to conflicting results and limited test data. In reality it may be a positive or negative impact with effects of up to one percent adiabatic fan efficiency.
- 3) No weight or structural penalty is assumed, although there may be aerodynamic implications as altering sweep and lean changes the unsteady aerodynamic loading on the stators.

### Limitations of the Current Model

- 1) The exact reduction in noise is dependent upon the exact fan design including fan pressure ratio, fan design speed, rotor stator axial spacing, and many other factors; however, high fidelity analysis or test data and configuration specific designs would be required.
- 2) Structural implications are neglected as calculating the change in unsteady loading requires higher fidelity tools.

### **2.2.7 Soft Vane**

#### ***Description***

A “soft” vane concept has been developed that reduces the unsteady pressure response on the stator surface and absorbs energy that would eventually become sound radiating from the stator. This is achieved by placing a hollow, compliant material with a special structure inside the stator. It is possible to tailor the design for specific frequency ranges. [38]

#### ***Major Assumptions***

- 1) A 1.5 dB reduction of fan inlet and exit noise during takeoff, cutback, and approach was assumed. This reduction is applied across all frequencies and directions.
- 2) No weight increase is assumed.
- 3) Some documents have indicated a potential performance penalty; however, there was not any substantial documented test data to warrant applying a weight penalty for this technology.

#### ***Limitations of the Current Model***

- 1) As with many of the noise technologies, the exact reductions will be dependent upon the exact fan design, engine design, and vehicle operating conditions.
- 2) Directivity of the noise reduction and the exact frequency it is tuned for may be a function of the specific engine design being modified. A higher fidelity analysis would be necessary to capture more accurate effects.

### **2.2.8 Aft Cowl Liners**

#### ***Description***

Conventionally the inner and outer portions of the aft fan cowl are acoustically lined to help reduce engine noise. Aft cowl liners extend the liner onto the outer surface of the core nozzle as shown in Figure 20. [39] These liners may have an aerodynamic performance penalty associated with the scrubbing drag. They may also carry a structural integrity penalty.

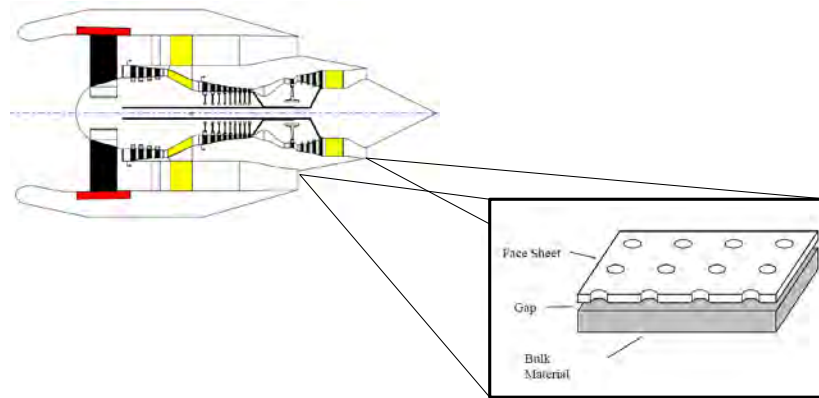


**FIGURE 20: AFT COWL LINER**

### ***Major Assumptions***

- 1) Rather than apply a fixed suppression regardless of aircraft and engine size, ANOPP's built in capabilities were used to predict the noise reduction associated with lining the aft cowl external to the fan casing. The results from WATE++, the NASA code within EDS which predicts engine weight and dimensions, are used to calculate the additional surface area present on the aft cowl. [40] This additional available liner area is added to the liner area input within ANOPP for the aft fan liner. In this manner ANOPP can predict how much the additional liner will reduce noise dependent upon the engine geometry.
- 2) Estimating the aerodynamic performance penalty requires estimating two things. First, the scrubbing drag, or the drag that occurs as the fan nozzle exit jet interacts with the outer surface of the core cowl, is not explicitly accounted for within EDS, but must be accounted for. Secondly the friction of an acoustic liner relative to a hard wall should be assessed.
  - a) An estimation of the scrubbing drag was obtained by using a model from [41]. The model takes into account several pieces of information including dynamic pressure of the fan exit flow, wetted area of the aft cowl, fan exit velocity, axial length of the aft cowl and viscosity of the fan exit flow. The scrubbing drag was then added to the EDS model.
  - b) To estimate the additional scrubbing drag that may occur in the presence of an acoustic liner, test data from [39] was used to increase the skin friction coefficient (i.e., the drag) associated with scrubbing drag by a factor of 1.6
  - c) The rolled up penalty was assessed and was found to be less than 30 lbm of block fuel for the 777 sized aircraft class. On the 737 aircraft class the effect was found to be less than 10 lbm block fuel. Therefore, it was determined that the aerodynamic penalty is negligible.

### ***Limitations of the Current Model***

- 1) The negligible performance penalty predicted for the possible additional scrubbing drag is based on a model that is more than forty years old; however a more appropriate conceptual design level model could not be found. [41] This does not preclude a more accurate model being included in the future.
- 2) The performance penalty also relies on the data set used to predict the increase in skin friction caused by an acoustic liner. [39]

### 2.2.9 Zero Splice Inlet

#### *Description*

Traditional inlet construction techniques build the forward inlet liner in two to three sections. This causes gaps in the joints between the liner sections which can cause noise due to acoustic scattering. Tests on the Trent 900 have shown a 4 – 7 dB reduction at takeoff and a 2 dB reduction at approach for a zero splice inlet liner. [42][43]

#### *Major Assumptions*

- 1) A 5 dB reduction to forward inlet noise on takeoff and a 2 dB on approach is assumed. The exact value is configuration dependent and as mention in [42] is greatly dependent on the ability to maintain a ‘zero’ splice of less than 20 mm.

#### *Limitations of the Current Model*

- 1) Exact results may depend on engine size, fan design, and several other influencing factors.

### 2.2.10 Nose Lip Liner

#### *Description*

Just like several of the other noise technologies, the nose lip liner aims to reduce forward fan noise by increasing the acoustically lined area in the inlet. This is shown in Figure 21. [42] This type of an arrangement may cause integration issues with the anti-icing system.

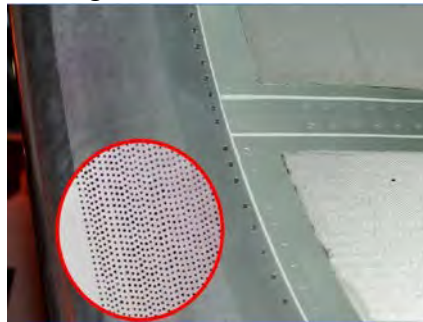


**FIGURE 21: NOSE LIP LINER**

#### *Major Assumptions*

- 1) A 2 dB reduction to forward inlet noise on takeoff and a 1 dB on approach is assumed.
- 2) A conservative assumption was applied to estimate a performance penalty by assuming the additional liner increased the skin friction drag relative to a conventional hardwall configuration. [39]

#### *Limitations of the Current Model*

- 1) Aerodynamic performance penalties may not be accurate and will depend on the exact configuration.

2) Exact results may depend on engine size, fan design, and several other influencing factors.

### 2.3 Emissions Technologies

All of the emissions technologies considered under CLEEN were modeled in the same manner using a consistent data set. The TAPS I is the first generation GE lean burn combustor and is being used in wide-body aircraft. This is not a CLEEN funded technology, but is considered as applicable to large engine, wide body aircraft for the purposes of the CLEEN Phase I analysis. The TAPS II, funded under CLEEN, is a scaled down version of the TAPS designed for smaller engines that are used on narrow-body aircraft. The TALON X, a Pratt and Whitney combustor concept, is considered applicable to narrow body aircraft. Since proprietary information was not available during Phase I of the project, Georgia Tech used publicly available information to evaluate the advanced combustors, referred to as TAPS-like and TALON X-like. **All of the combustor assessments were performed by applying a public domain emissions prediction model developed at Georgia Tech and documented in [1].**

### 2.4 Conclusions

The technology modeling completed in Phase I provided a strong foundation for initial assessments of the potential of technology to meet environmental goals, as well as supplementing the CLEEN technologies modeled under Phase II by representing other technologies expected to enter the fleet through 2050.

### 3 Phase II – CLEEN Technology Modeling with Proprietary Data

In Phase II of PARTNER Project 36, Georgia Tech worked with the CLEEN Program contractor companies to exchange proprietary data and incorporate this data into detailed models of the funded CLEEN technologies. Much of this CLEEN technology modeling work cannot be discussed in this public report due to the proprietary nature of the data and intellectual property involved. For the same reason, no vehicle level analysis results are shown, as individual proprietary technologies’ benefits could be extracted from the results.

However, the general approach followed to develop and validate the CLEEN technology models is described below. Additionally, modifications made to EDS in order to accurately represent the funded CLEEN technologies are documented, including the addition of a new turbine cooling model and an axial-centrifugal compressor map generation capability.

#### 3.1 CLEEN Technology Modeling Approach

Georgia Tech worked with each CLEEN company through a similar process to model the CLEEN technologies. A brief history of the modeling activities is shown in Figure 22.

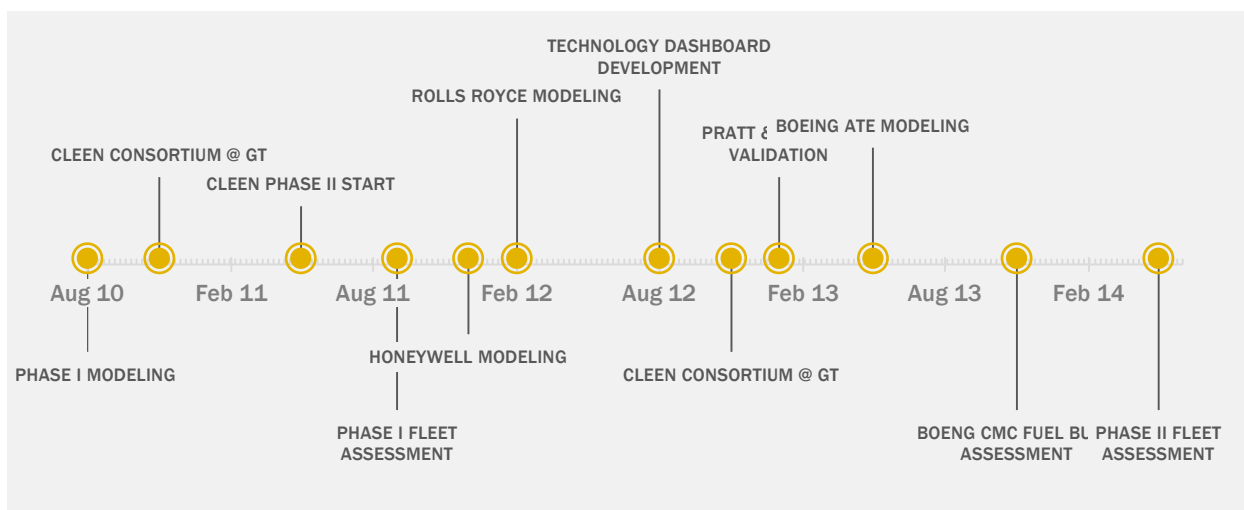


**FIGURE 22: TIMELINE OF EDS CLEEN MODELING ACTIVITIES**

First, Georgia Tech and the company would work to come to consensus about how the technology would be captured in EDS in a physics-based manner. This would often require familiarization with EDS and in some cases, dedicated runs of EDS to demonstrate to the company the fidelity and flexibility of the tool. In some cases, this effort revealed modeling structural enhancements needed in EDS, which were addressed as part of this project. Two such enhancements (addition of a new EDS turbine cooling model and the addition of a centrifugal compressor map generation capability) are documented in the sections that follow.

Once the modeling structure was identified and the approach solidified, an exchange of proprietary data on the technology’s performance and impact was exchanged under a properly executed non-disclosure agreement(s). Georgia Tech then incorporated the data into the

modeling structure in an agreed-upon manner and exercised EDS and the newly constructed models to validate the effects of the technology on the modeled engine and aircraft performance. Once concurrence was reached that the trends and effects of the technology were being appropriately captured, the technology model was ready for use in vehicle and fleet-level assessments.

Through work with Boeing, GE, Honeywell, Pratt & Whitney, and Rolls-Royce, the following technologies were modeled under Project 36:

- Boeing: adaptive trailing edge, ceramic matrix composite (CMC) exhaust nozzle
- GE: TAPS II combustor  $\text{NO}_x$  benefits captured via public domain model
- Honeywell: turbine cooling technologies
- Pratt & Whitney: ultra high-bypass geared turbofan
- Rolls-Royce: dual wall turbine cooling, ceramic matrix blade tracks

Details of the validation of EDS's geared turbofan model (no proprietary data involved) against public domain NASA analyses are shown in Appendix A.

A number of technologies were not modeled under Project 36, but are being addressed under Aviation Sustainability Center (ASCENT) Project 10, including GE's flight management system / air traffic management integration and engine control technologies and open rotor, as well as the acoustic impacts of Boeing's CMC nozzle.

### **3.2 Addition of New EDS Turbine Cooling Model**

#### **3.2.1 Motivation**

Both Honeywell and Rolls-Royce are funded under the CLEEN Program to develop technologies specifically aimed at reducing the amount of flow required to cool turbine stages and/or increasing turbine temperature capability. These technologies include improvements in blade cooling and low-conductivity thermal barrier coatings (TBC). The effects of each of these improvements need to be modeled individually for an accurate assessment of the technology benefits. These technologies may be implemented on a specific stage or blade row of the turbine; therefore, the cooling model needs to have the ability to differentiate between specific sections.

The previous EDS cooling model is based on the NASA CoolIt algorithm [44]. This algorithm uses a single regression, developed decades ago from empirical data. The only input to this regression is a normalized differential between the hot gas temperature and allowable bulk metal temperature. The metal temperature is therefore the only physical input which reflects cooling technology level. The amount of cooling required for a modern engine is then adjusted simply by a multiplier on the predicted physical cooling flow. This multiplier is calibrated for each engine individually and then left constant. It should also be noted that although the regression is calculated for each blade row, the multiplier remains fixed, making the result a 'bulk average' required cooling flow. This flow is then divided into two stations, the 'non-chargeable' flow, which performs useful work on the turbine, and the 'chargeable', which does not.

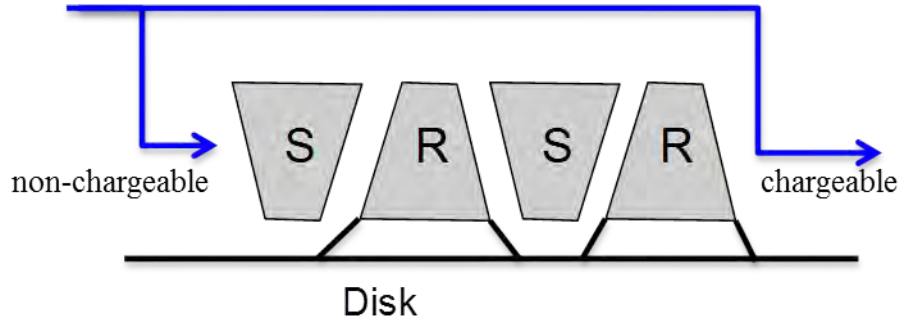


**FIGURE 23: CURRENT EDS COOLING MODEL**

While the CoolIt method has been effective in capturing the effects of cooling flows thus far, it does not have the fidelity to accurately and precisely model the combined effects of the proposed Honeywell and Rolls-Royce technologies. A new model was needed which would accept technology factors as direct inputs, and model the improvements from a physics-based approach, rather than the current historical basis. This new model must also allow for the implementation of technologies on to individual rotor or stator stages, rather than the turbine as a whole. A literature search was performed to find an appropriate approach, resulting in the choice of a method outlined by Young and Wilcock [45]. This straight-forward method satisfies all the mentioned requirements and relies on far less empirical data. The few empirical inputs used are tied to physical parameters, often material properties. The same paper also develops a method for calculating the change in turbine efficiency due to cooling flows, which may be the source of future work.

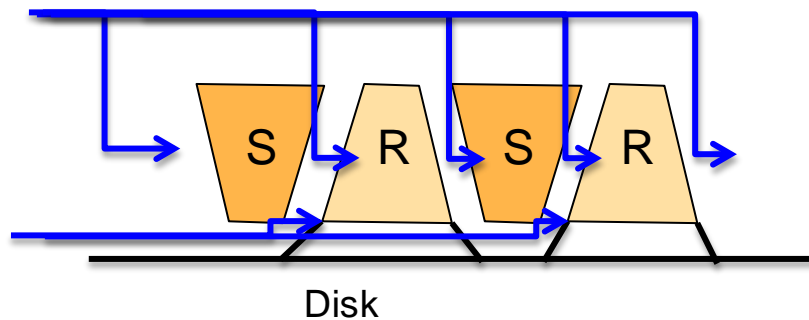


**FIGURE 24: NEW EDS COOLING MODEL**

### 3.2.2 Assumptions

A few basic assumptions are made to simplify the analysis. These assumptions are in line with the method described in [45]. The first is that the cooling flow exiting each blade is completely mixed with the main flow at the end of each rotor/stator blade row, giving the flow uniform thermodynamic properties going into the next row. Along the same lines, the internal and external metal temperatures are assumed uniform across the entire blade width.

In reality, neither of these assumptions is entirely accurate because cooling flows are distributed in discrete places throughout the stage. However, fully capturing the detailed temperature profiles of the flow and turbines would require a higher-fidelity 2-D or 3-D simulation which is

beyond the needs of a conceptual design tool such as EDS. These types of simulations take longer to run and many more hours to implement. It would also require the detailed geometry of the flow path, which in most cases will not be provided or defined in this stage of design. Given that EDS as a whole is designed to predict system level metrics, and not analyze detailed designs, knowing such information is not necessary. The averaged flow assumptions therefore bring the cooling analysis to an equal level of fidelity as the rest of the EDS components and can be modeled quickly and generically.

The total work output of the turbine is assumed to be generated equally by each rotor stage, so that the decrease in total enthalpy across each stage is also equal. This is consistent with the assumptions made by WATE++, EDS's engine weight and flowpath prediction tool [46]. Similarly, the total temperature decreases linearly across each stage. It is also assumed that there is no total pressure drop across the stator for the purposes of thermodynamic mixing calculations between stages. Lastly, the degree of reaction of each stage is assumed to be 0.5, i.e. the gas is expanded equally in both the rotor and stator, and static pressure increases are equal. Most turbines have a degree of reaction close to this or lower; this assumption is needed to avoid the need to input blade angles and geometry. It also results in a constant axial velocity, which will further simplify some of the analysis. The model has been set up in such a way that these assumptions can be changed should the user desire to enter more detailed design information; however, the assessments performed in this work assume a minimum level of blade geometry is available, as described in Table 1.

### 3.2.3 Inputs and EDS Supplied Values

A full list of the inputs required by the new EDS cooling algorithm is given below in Table 1. These inputs can be divided into three main categories: geometry (used to calculate cooled surface area), gas properties, and technology parameters. The geometry of each rotor or stator row is automatically generated within EDS by a program called WATE++ [46], and the gas properties by NPSS. This makes the technology parameters the only needed user input. These parameters are what will represent the new technologies being developed under CLEEN, and they can be easily adjusted on each individual rotor or stator row as needed. The gas flow properties are updated by NPSS at the exit of each blade row using the new average enthalpy and pressure. A flowchart depicting the process with which all of these variables are updated is given by Figure 25.

**TABLE 1: COOLING ALGORITHM INPUTS**

Technology Parameters	Source
$\lambda_{tbc}$ (thermal conductivity of TBC)	Material property
$t_{tbc}$ (thickness of TBC)	Design value
$Bi_m$ (Biot number of metal)	Empirical table
$T_{m,ext}$ (Allowable bulk metal temperature)	Empirical blade stress chart
$\eta_{c,int}$ (internal cooling efficiency)	Empirical data/technology assumption
$\epsilon_f$ (film cooling effectiveness)	Empirical data/technology assumption
$K_{comb}$ (combustor pattern factor)	Empirical chart
$K_{disk}$ (disk cooling factor)	Technology assumption
WATE++ Geometry	Source
$c_{blade}$ (blade chord)	WATE++ engine sizing

AR (aspect ratio)	WATE++ engine sizing
TOC (avg. thickness over chord)	WATE++ engine sizing
$n_{blade}$ (# of buckets / nozzles)	WATE++ engine sizing
$r_{hub}$ (radius of the hub)	WATE++ engine sizing
$r_{tip}$ (radius of the tip)	WATE++ engine sizing
$l_{stage}$ (stage length)	WATE++ engine sizing
<b>NPSS Flow Properties</b>	<b>Source</b>
$T_{0c,i}$ (cooling flow total temperature)	Compressor discharge temperature
$\rho_{0g}$ (hot gas density)	Combustor or previous stage flowpath conditions
$T_{0g}$ (hot gas total temperature)	Combustor or previous stage flowpath conditions
$p_{0g}$ (hot gas total pressure)	Combustor or previous stage flowpath conditions
$c_{p,g}$ (hot gas specific heat)	Combustor or previous stage flowpath conditions
$\mu_g$ (hot gas viscosity)	Combustor or previous stage flowpath conditions
$m_g$ (hot gas mass flow)	Combustor or previous stage flowpath conditions
$V_{axial}$ (hot gas axial velocity)	Combustor or previous stage flowpath conditions
$N_{shaft}$ (shaft RPM)	WATE++ engine sizing

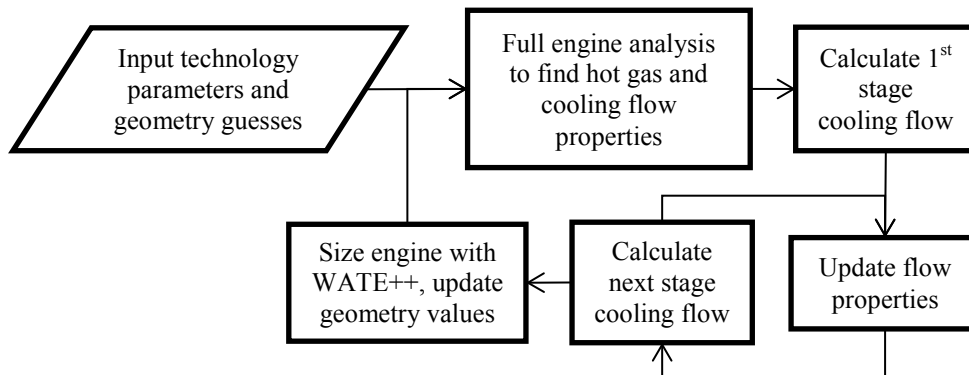


**FIGURE 25: FLOW OF INFORMATION WITHIN THE COOLING MODEL**

### 3.2.4 Heat Transfer Analysis

The underlying theory for this analysis is a simple heat transfer balance for the following:

- across the blade metal
- across the TBC
- the heat transfer associated with film cooling
- the heat transferred to the cooling flow from its initial state at the cooling passage entrance to its state after the film cooling takes place

The equations representing each of these heat transfer balance are shown below with a diagram showing the location of each temperature (aside from the adiabatic wall temperature  $T_{aw}$ , which represents the wall temperature in the absence of film cooling). In order for the system to be at steady-state, each of these values of ‘Q’ must be equal, providing a basic system of equations to be solved for the various temperatures, and ultimately the required cooling flow rate.

$$Q = m_c c_{pc} (T_{oc,x} - T_{oc,i})$$

**EQUATION 2**

$$Q = \alpha_g A_{surf} (T_{aw} - T_w)$$

**EQUATION 3**

$$Q = \frac{\lambda_{tbc}}{t_{tbc}} A_{surf} (T_w - T_{m,ext})$$

**EQUATION 4**

$$Q = \frac{\lambda_m}{t_m} A_{surf} (T_{m,ext} - T_{m,int})$$

**EQUATION 5**

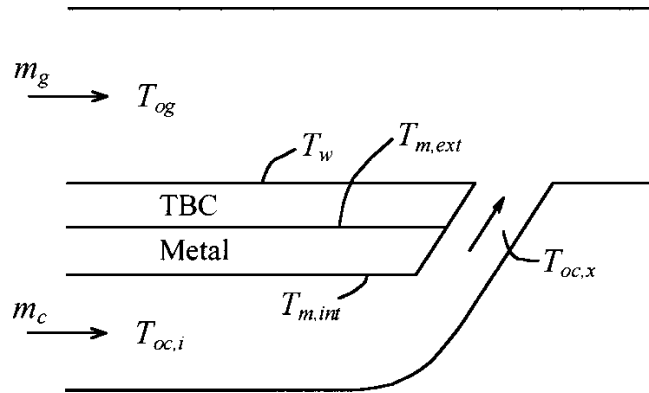


**FIGURE 26: SIMPLIFIED COOLING FLOW MODEL [45]**

The above set of equations will not be solved directly to find the cooling flow but rather used to derive a set of non-dimensional parameters which relate directly to the technologies being modeled (and match the set of inputs listed in Table 1). These four parameters are the metal Biot number, TBC Biot number, film cooling effectiveness, and internal cooling efficiency, and they are defined by Equation 6-Equation 9. The Biot number represents the ratio of the heat transfer resistances inside of and at the surface of the material. Although the average thickness and thermal conductivity of the metal/TBC is an input, the external heat transfer coefficient  $\alpha_g$  must still be calculated before proceeding with solving the system. This is calculated using Equation 10-Equation 14, and relies on an empirical correlation for finding Nusselt number.

$$Bi_m = \frac{\alpha_g t_m}{\lambda_m} = \frac{T_{m,ext} - T_{m,int}}{T_{aw} - T_w}$$

**EQUATION 6**

$$Bi_{tbc} = \frac{\alpha_g t_{tbc}}{\lambda_{tbc}} = \frac{T_w - T_{m,ext}}{T_{aw} - T_w}$$

**EQUATION 7**

$$\varepsilon_f = \frac{T_{0g} - T_{aw}}{T_{0g} - T_{0c,x}}$$

**EQUATION 8**

$$\eta_{c,int} = \frac{T_{0c,x} - T_{0c,i}}{T_{m,int} - T_{0c,i}}$$

**EQUATION 9**

$$Re = \frac{\rho_{0g} l_{blade} V_{axial}}{\mu_g}$$

**EQUATION 10**

$$y = 0.14 \left( \frac{Re}{200000} \right)^{-0.4}$$

**EQUATION 11**

$$Nu = 450 \left( \frac{Re}{200000} \right)^{0.7} \left( \frac{T_{0g}}{T_{m,ext}} \right)^y$$

**EQUATION 12**

$$St = \frac{Nu}{p_{0g} Re}$$

**EQUATION 13**

$$\alpha_g = \frac{c_{p,g} m_g St}{A_{cs}}$$

**EQUATION 14**

All needed information is now known to simultaneously solve Equation 6-Equation 9. The cooling inlet temperature ( $T_{0c,i}$ ) is set by the compressor from which it is bled, and the exterior metal temperature ( $T_{m,ext}$ ) is set to the maximum allowable metal temperature, an input ( $T_{m,max}$ ) based on the turbine blade or vane material. This setup results in a system of four linear equations and four unknowns ( $T_{aw}$ ,  $T_w$ ,  $T_{m,int}$ ,  $T_{0c,x}$ ), which can be solved algebraically. This algebraic manipulation was accomplished using the program Mathematica, and the final forms of the equations used in the algorithm are given by Equation 15-Equation 20.

$$B = 1 + Bi_{tbc}$$

**EQUATION 15**

$$D = B + Bi_m \varepsilon_f \eta_{c,int}$$

**EQUATION 16**

$$T_{aw} = \{T_{0g} B - \varepsilon_f [B(\eta_{c,int} - 1) T_{0c,i} + T_{0g} B - (B + Bi_m) \eta_{c,int} T_{m,ext}]\} / D$$

**EQUATION 17**

$$T_w = \{T_{m,ext}(1 + Bi_m \varepsilon_f \eta_{c,int}) + Bi_{tbc}[T_{0g} + \varepsilon_f(T_{0c,i}(1 - \eta_{c,int}) - T_{0g} + \eta_{c,int}T_{m,ext})]\}/D$$

**EQUATION 18**

$$T_{m,int} = \{T_{m,ext}B + Bi_m [\varepsilon_f ((\eta_{c,int} - 1)T_{0c,i} + T_{0g}) + T_{m,ext} - T_{0g}]\}/D$$

**EQUATION 19**

$$T_{0c,x} = \{\eta_{c,int} [T_{m,ext}B + Bi_m ((\varepsilon_f - 1)T_{0g} + T_{m,ext})] - B(\eta_{c,int} - 1)T_{0c,i}\}/D$$

**EQUATION 20**

Finally, the temperatures found can be used to calculate the required cooling mass flow. This is done using an intermediate non-dimensional cooling flow ( $m_{c+}$ ). Converting this into an absolute number requires the total surface being cooled, including the blades and endwalls. The full set of equations used for these calculations are given by Equation 21-Equation 25.

$$m_{c+} = \frac{T_{aw} - T_w}{T_{0c,x} - T_{0c,i}}$$

**EQUATION 21**

$$A_{blade} = c_{blade}^2 AR$$

**EQUATION 22**

$$A_{cs,blade} = c_{blade}^2 TOC$$

**EQUATION 23**

$$A_{surf} = 2n_{blade}(A_{blade} - A_{cs,blade}) + 2\pi(r_{hub} - r_{tip})l_{stage}$$

**EQUATION 24**

$$m_c = \frac{m_{c+} \alpha_g A_{surf}}{c_{p,g}}$$

**EQUATION 25**

### 3.2.5 Other Considerations

A few other factors need to be taken into account. The first deals with the assumption that the inlet conditions to each stage are an uniform, average value. The temperature profile of the gas a few stages into the turbine is relatively uniform, to the point where this assumption is valid. However, the flow coming out of the combustor is usually not uniform, typically having a peak of high temperatures near the centerline (Figure 27, [47]). These local temperature peaks wear the blades more quickly, and additional cooling must be added to combat this effect. The model takes this into account simply through multipliers on the total temperature, combustion pattern factors ( $K_{comb}$ ), which can take a different value on each stage. Once the total temperature is multiplied by  $K_{comb}$ , the calculations proceed normally. This is a similar method as was used in CoolIt and correlations for estimating the pattern factor have been used from [47].

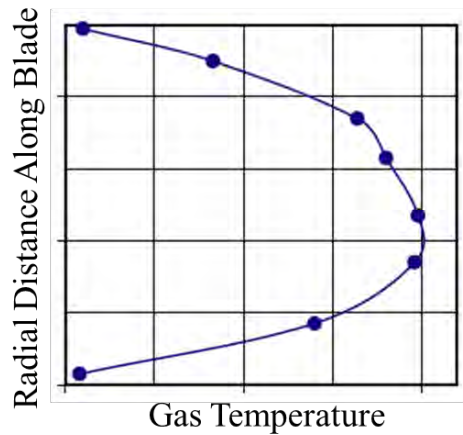


**FIGURE 27: TYPICAL RADIAL TEMPERATURE PROFILE OF FLOW EXITING COMBUSTOR [47]**

$$T_{0g,effective} = K_{comb}T_{0g,actual}$$

**EQUATION 26**

There are no fundamental differences between a rotor or stator stage in the heat transfer analysis method described so far. The difference in the stagnation properties of the gas flow due to the rotation of the rotor does need to be accounted. The total temperature relative to the rotor is calculated using the meanline speed, and the assumption that each stage has a 0.5 degree of reaction (Equation 27-Equation 29). Referring back to Table 1 it can be seen that the inputs to Equation 27 are generated by WATE++ and are updated dynamically each time the cooling model is run. The last difference between rotor and stator is that the relative velocity calculated in Equation 30 is used in the Reynolds number calculation of Equation 10.

$$U_{mean} = N_{shaft}(r_{hub} + \frac{l_{blade}}{2})$$

**EQUATION 27**

$$V_{tangential} = \frac{\Delta H_{stage}}{2m_g U_{mean}} + \frac{U_{mean}}{2}$$

**EQUATION 28**

$$T_{0g,rel} = T_{0g} + \frac{U_{mean}^2}{2c_{p,g}} \left(1 - \frac{2V_{tangential}}{U_{mean}}\right)$$

**EQUATION 29**

$$V_{rel} = \sqrt{(V_{tangential} - U_{mean})^2}$$

**EQUATION 30**

### 3.2.6 Description of Algorithm

Now that the details have been explained, the step-by-step order of the algorithm is summarized in Figure 28. The method starts with inputs of all the geometry and technology parameters, along with the gas flow properties at the entrance to the turbine, and the cooling flow properties at the entrance of the blade cooling passages. The thermodynamic properties of the gas flow need to be updated after each rotor or stator stage using Equation 31-Equation 34. The enthalpy is averaged with that of the cooling flow, per the averaged flow properties assumption. The rotor stages extract work out of the flow, and this is accounted for by the  $\Delta h$  term in Equation 32. The total pressure also drops across a rotor, and this is accounted for by Equation 33. Both of these deltas are found by dividing the total work of the turbine and pressure ratio by the number of stages.

$$h_{0g} = \frac{m_g h_{0g} + m_c h_{0c}}{m_g + m_c}$$

**EQUATION 31**

$$h_{0g} = \frac{m_g (h_{0g} - \Delta h_{stage}) + m_c h_{0c}}{m_g + m_c}$$

**EQUATION 32**

$$p_{0g} = p_{0g} - \Delta p_{stage}$$

**EQUATION 33**

$$m_g = m_g + m_c$$

**EQUATION 34**

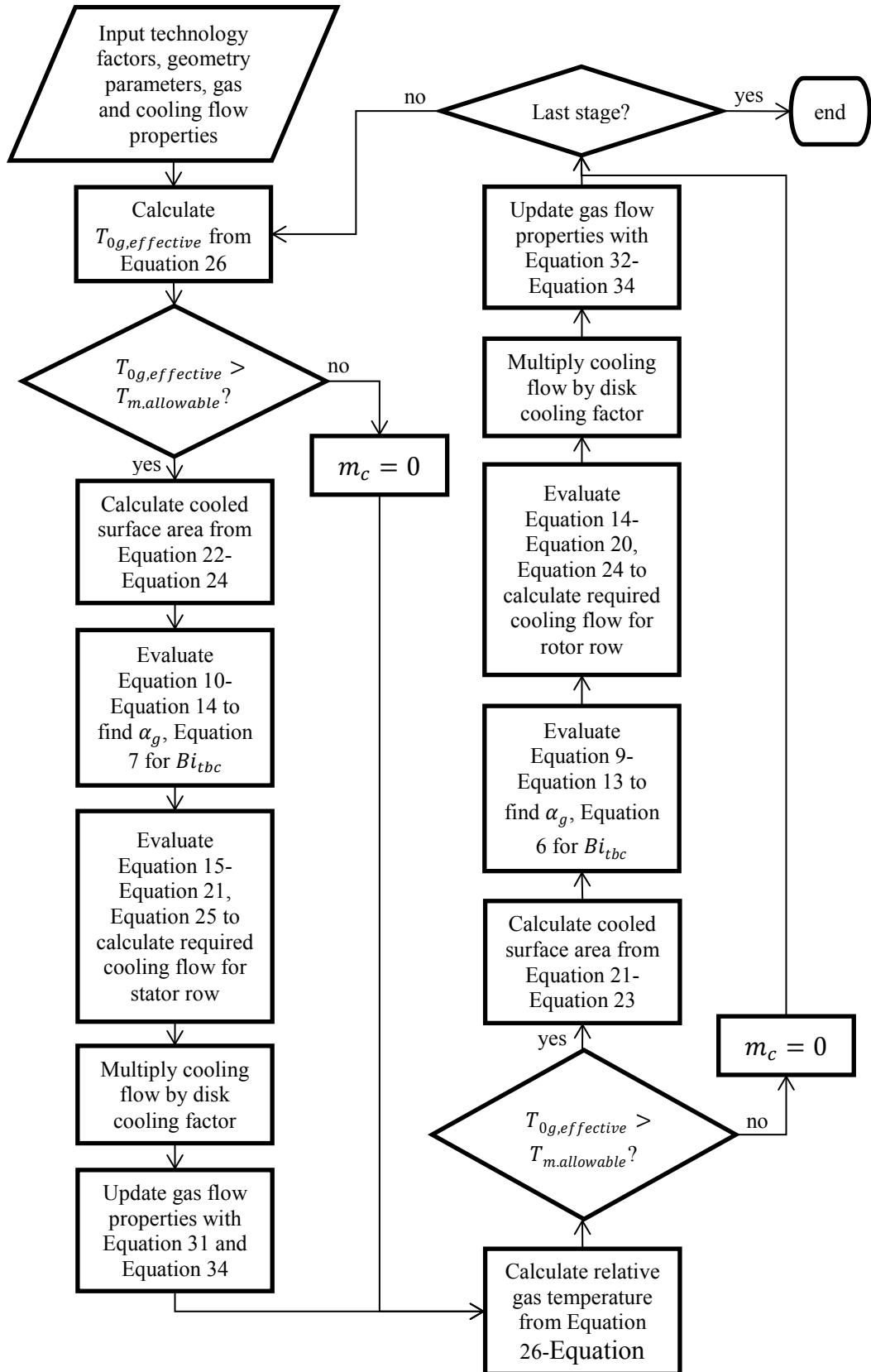


FIGURE 28: COOLING ALGORITHM FLOWCHART

### 3.2.7 Results

For verification that the algorithm was correctly capturing the required cooling flows, a parametric study was completed comparing the new model with the old algorithm, CoolIt. Two different parametric sweeps were performed, as shown in Figure 29 and Figure 30. The new method should overlap with the old one in terms of predictive capability.

The first figure varies the internal cooling efficiency while keeping film cooling constant, and the second the reverse. Both of these plots show cooling flow as a fraction of the main gas flow, and the temperature differential in terms of a variable  $\phi$ , as defined in Equation 35. These sweeps are compared with the underlying equations of CoolIt. The intent of this comparison is to make sure that the new method covers the same design space as the original CoolIt implementation. The difference between the two methods is that the CoolIt curves are all generated by applying a single scalar to a baseline empirical curve. The new implementation curves are generated by varying the inputs that represent physical quantities. There is not a one-to-one comparison to be made in Figure 29, but it is clear that the new method is backwards compatible with CoolIt. The curves generated by the new algorithm are slightly steeper than the CoolIt curves, but overall follow the same trend. The main takeaway is that the design space is covered. The curves could be matched even more closely with further adjustment of the technology inputs.

$$\phi = \frac{T_{0g} - T_{m,ext}}{|T_{0g} - T_{0c,i}|}$$

EQUATION 35

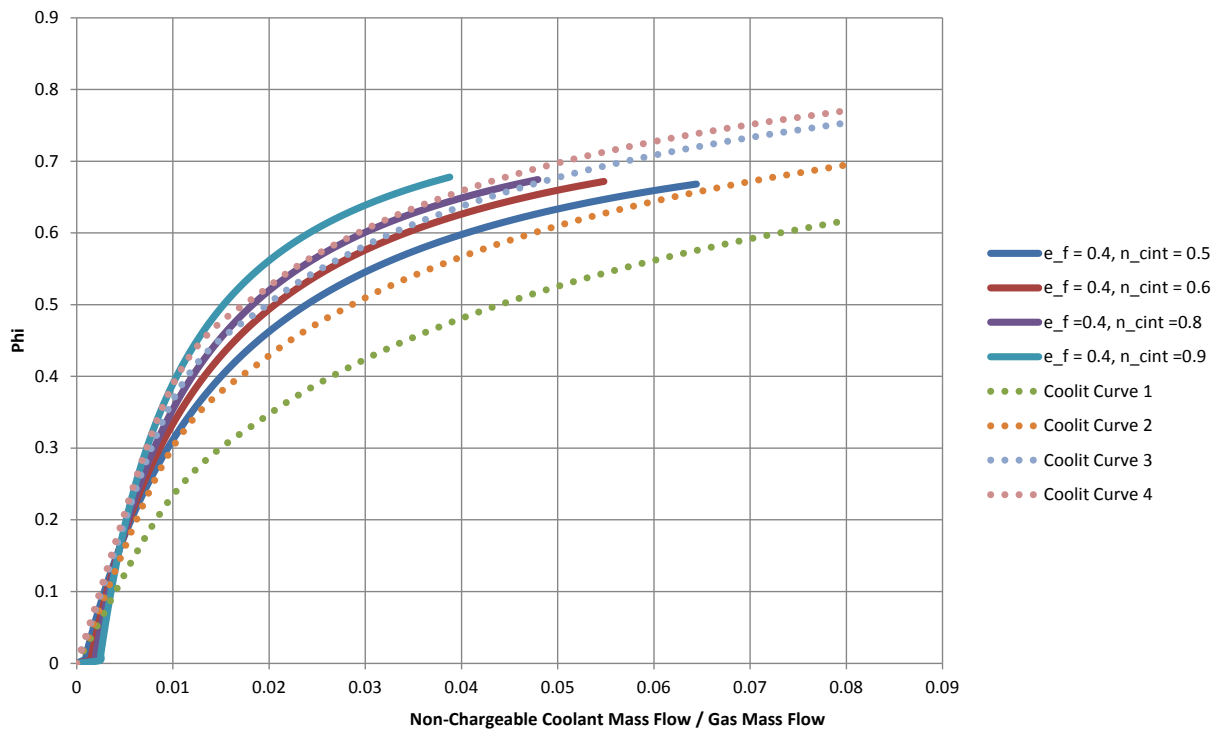
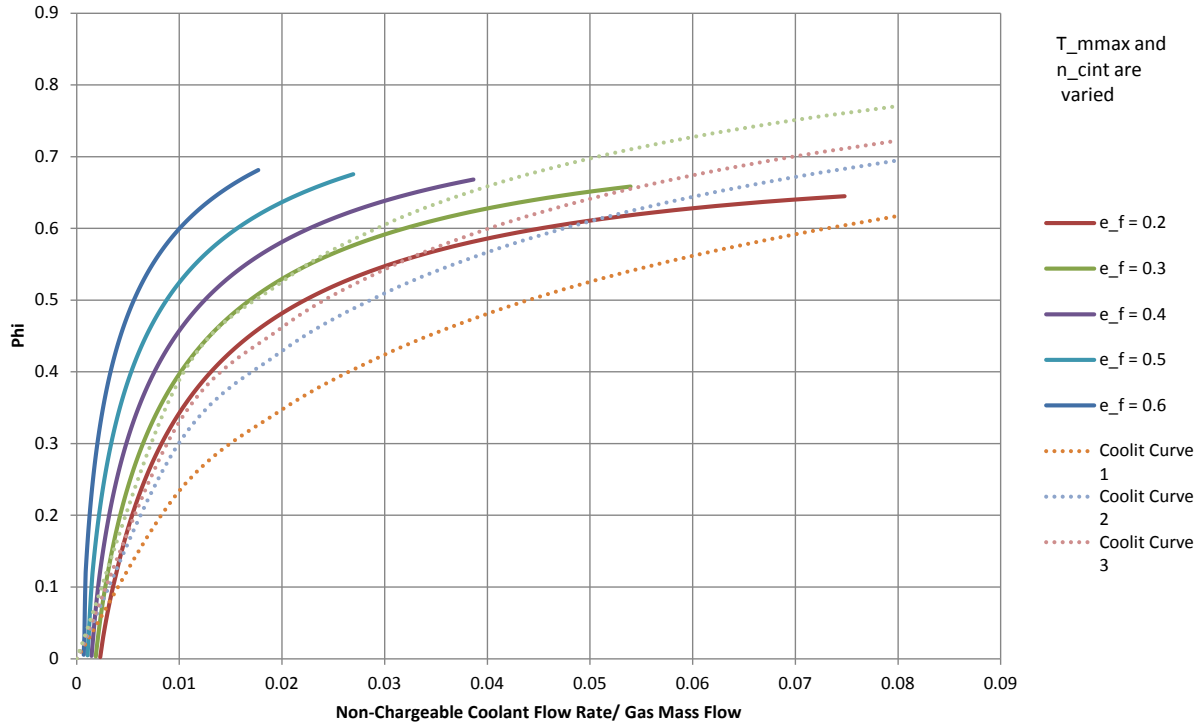


FIGURE 29: PARAMETRIC SWEEP OF INTERNAL COOLING EFFICIENCY



**FIGURE 30: PARAMETRIC SWEEP OF FILM COOLING EFFECTIVENESS**

### 3.3 Addition of Centrifugal Compressor Map Generation Process

#### 3.3.1 Motivation

Prior to PARTNER Project 36, EDS did not have the ability to generate performance maps for centrifugal compressor stages. Centrifugal compressors are typically only used on very small turbofan and turboprop engines, and all engines which have previously been analyzed by EDS solely use axial stages. However, Honeywell is funded under CLEEN to develop technologies for one of its next generation business jet engines, which uses a centrifugal compression stage. It should also be noted that future, ultra-high OPR cores may rely on centrifugal compressor technology as cores grow smaller and more efficient.

A literature search was undertaken to find the most appropriate method for generating a centrifugal compressor map. This included looking at existing codes, most notably the NASA-developed MODFAN. However, it was quickly realized that the maps generated from this algorithm have a very fixed shape, and it would be difficult to adapt it to the problem at hand. A method was needed which could be parametrically ‘tuned’ to fit any map. This method also needed minimum required knowledge of the compressor geometry. For these reasons, a method developed by Casey and Robinson [48] was chosen.

Although this method uses several fixed empirically-derived regressions, the overall behavior of the map can be changed through tuning several constants. The method was actually developed

with turbochargers in mind; however, these are quite similar to aircraft compressors and the constants can be adjusted to make up the difference as needed. Through the use of these regressions, and four non-dimensional parameters as the main variables (see Table 2 and Equation 36, Equation 37), the algorithm avoids requiring specific blade geometry. These four parameters can easily be adapted into the variables of a typical compressor map which EDS employs.

**TABLE 2: NON-DIMENSIONAL PARAMETERS USED IN CENTRIFUGAL MAP ALGORITHM**

Variable	Symbol
Flow coefficient	$\phi$
Work Coefficient	$\lambda$
Tip-speed Mach Number	M
Polytropic Efficiency	$\eta$

$$\phi = \frac{\dot{V}}{u_2 D_2^2}$$

**EQUATION 36: FLOW COEFFICIENT**

$$\lambda = \frac{\Delta h}{u_2^2}$$

**EQUATION 37: WORK COEFFICIENT**

### 3.3.2 Inputs, EDS Variables, and Assumed Values

The major inputs into the model are simply the design point values of the map, i.e. design pressure ratio, efficiency, and stall margin. Matching the design stall margin is not discussed in the Casey and Robinson paper; this is done through a Georgia Tech developed method which will be discussed later. Note that the input efficiency is adiabatic, rather than the polytropic efficiency which is one of the four non-dimensional parameters listed earlier. EDS and most other compressor maps use adiabatic efficiencies, but the regressions used in this method are all polytropic. The values are converted using the pressure ratio, ratio of specific heats, and Equation 38.

$$\eta_{adb} = \frac{\pi^{\gamma-1/\gamma} - 1}{\pi^{\gamma-1/\eta_{poly}\gamma} - 1}$$

**EQUATION 38**

The one piece of geometry information which this method does require is the compressor tip diameter. This is not a value that will be known prior to sizing an engine, so an assumption was needed to compensate. The answer was to use an empirical regression of compressor tip speed vs. design pressure ratio for centrifugal stages of this size [49]. The design pressure ratio is already given, and the shaft speed is generated within EDS. Using this and the tip speed from the regression, the diameter can be calculated (see Equation 39, where  $N_{\text{shaft}}$  is in RPM and  $u_2$  in ft/s).

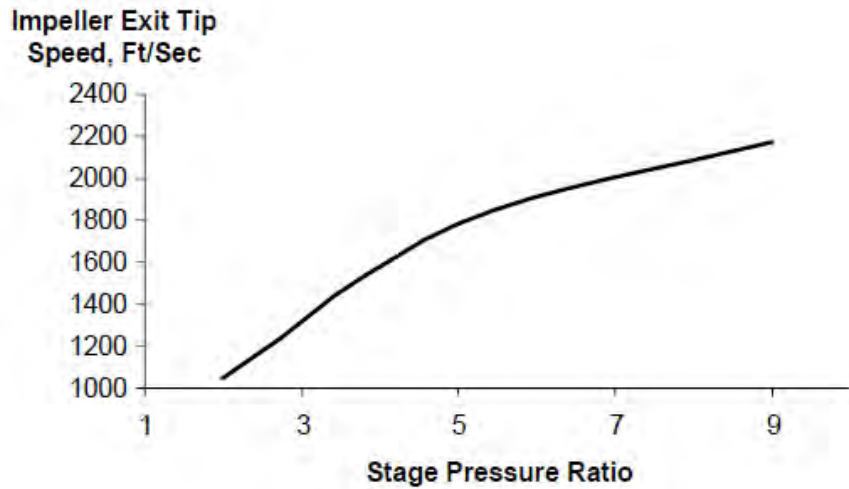


**FIGURE 31: TIP SPEED VS. PRESSURE RATIO REGRESSION USED TO SIZE COMPRESSOR [49]**

$$D_2 = \frac{60u_2}{\pi N_{shaft}}$$

**EQUATION 39**

Several other input values have assumed values, which can be altered but in most cases remain fixed. These include the degree of reaction, slip factor, and disk friction coefficient. The latter two have suggested values from the paper, and the suggested values of the empirical constants (discussed below) are made to match these values. A list of these variables and their assumed values are given in Table 3. The remaining input variables are generated by EDS and updated with each iteration of the map generation algorithm, as illustrated in Figure 32.

**TABLE 3: LIST OF CENTRIFUGAL MAP ALGORITHM INPUTS**

Variable	Assumed Value
$R$	0.5
$c_s/u_2$	0.1-0.2
$k_{df}$	0.003
$A$	0
$B$	1.2
$C$	5
$D_{LO}$	2.1
$D_{HI}$	1.7
$G_{LO}$	2
$G_{HI}$	0.3
$H_{LO}$	2
$H_{HI}$	3.5
$(\phi_p/\phi_c)_{LO}$	0.5
$(\phi_p/\phi_c)_{HI}$	0.9

Variable	Assumed Value
$(\phi_s/\phi_c)_{LO}$	0.225
$(\phi_s/\phi_c)_{HI}$	0.835
$A_s$	0
$B_s$	1.25
$C_s$	4.75
<b>Design Input</b>	
$\pi_d$	-
$\eta_{d,adb}$	-
$SMW$	-
<b>EDS Generated Input</b>	
$N_{shaft}$	-
$\gamma$	-
$\Delta h_{stage}$	-
$w_{c,d}$	-

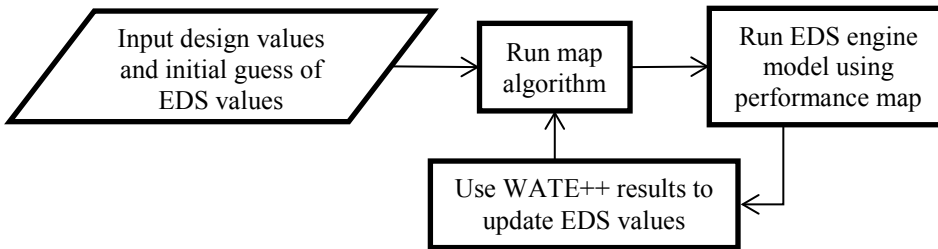


**FIGURE 32: FLOW OF INFORMATION**

### 3.3.3 Main Calculation Method

The first step is to calculate the four main variables at the design point. The design efficiency comes from Equation 38, and the Mach number from the tip speed regression and the usual definition of speed of sound. The flow and work coefficients are calculated using their definitions, and the definitions of corrected speed and mass flow, resulting in Equation 40 and Equation 41. Once again, this formula contains the conversion factor due to shaft speed having units of RPM.

$$\phi_d = \frac{60w_{c,d}}{n_{c,d}\pi D^3 \rho_{ref} g}$$

**EQUATION 40**

$$\lambda_d = \frac{\pi_d^{\gamma-1/\eta_d\gamma} - 1}{M_d^2(\gamma - 1)}$$

**EQUATION 41**

The steps required to generate the rest of the map will now be outlined in detail. Points are placed at evenly spaced intervals between stall, peak efficiency, and choke along a line of

constant corrected speed. The speeds along these lines can be chosen explicitly, however in most cases it makes to choose them as a percentage of the design speed. The tip Mach number is a constant along each of these lines, and is found simply by multiplying the chosen percentage by the design Mach number.

The first step is to find the flow coefficient at peak efficiency ( $\phi_p$ ) along each of these constant speed lines. This is accomplished using the first empirical regression from the paper, shown in Figure 33 (the turbocharger-vaneless curve is used, as it is most similar to a turbofan compressor). An equation for this regression is not given in the paper, so it was digitized and fit with a polynomial curve. Notice that the flow coefficient is normalized against an arbitrary constant  $\phi_{p0}$ . This constant can be found by assuming that the design point coincides with the peak efficiency point. The design Mach number and flow coefficient are known, so the regression sets  $\phi_{p0}$ .

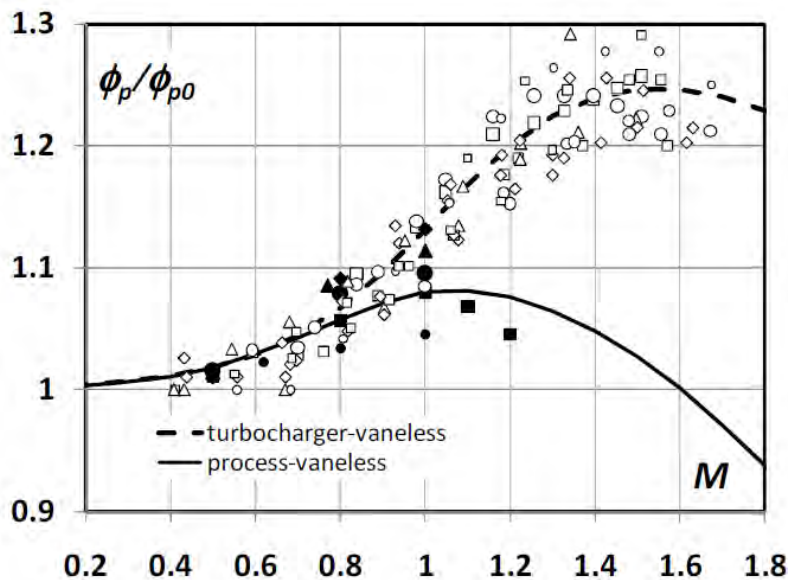


**FIGURE 33: REGRESSION OF PEAK FLOW COEFFICIENT VS. TIP MACH NUMBER [48]**

The next step is to determine the ratio of  $\phi_p$  to choke flow coefficient  $\phi_c$  along a speed line, and by extension the value of  $\phi_c$ . This is done through the first set of empirical constants. The ratio is a function of tip Mach number only, but a series of variables are calculated along the way (Equation 42-Equation 45). The same method is used to calculate the stall flow coefficient, but with different values of A, B, and C. The rest of the points on the speed line will be given flow coefficients evenly spaced between  $\phi_s$ ,  $\phi_p$ , and  $\phi_c$ .

$$t = (M - B)(AM - C)$$

**EQUATION 42**

$$P = \frac{1}{1 + e^{-t}}$$

**EQUATION 43**

$$\frac{\phi_p}{\phi_c} = (1 - P) \left( \frac{\phi_p}{\phi_c} \right)_{LO} + P \left( \frac{\phi_p}{\phi_c} \right)_{HI}$$

**EQUATION 44**

$$\frac{\phi_s}{\phi_c} = (1 - P) \left( \frac{\phi_s}{\phi_c} \right)_{LO} + P \left( \frac{\phi_s}{\phi_c} \right)_{HI}$$

**EQUATION 45**

The peak efficiency along a speed line is also found using a regression. The ‘corrected efficiency’ line in Figure 34 was used (the other represents experimental data with a measurement error). Once again, this plot was digitized and fit with a polynomial. Note that the values in this plot are normalized with respect to the design efficiency and Mach number. These will be replaced by ‘reference’ values to match the design stall margin (more on this later).

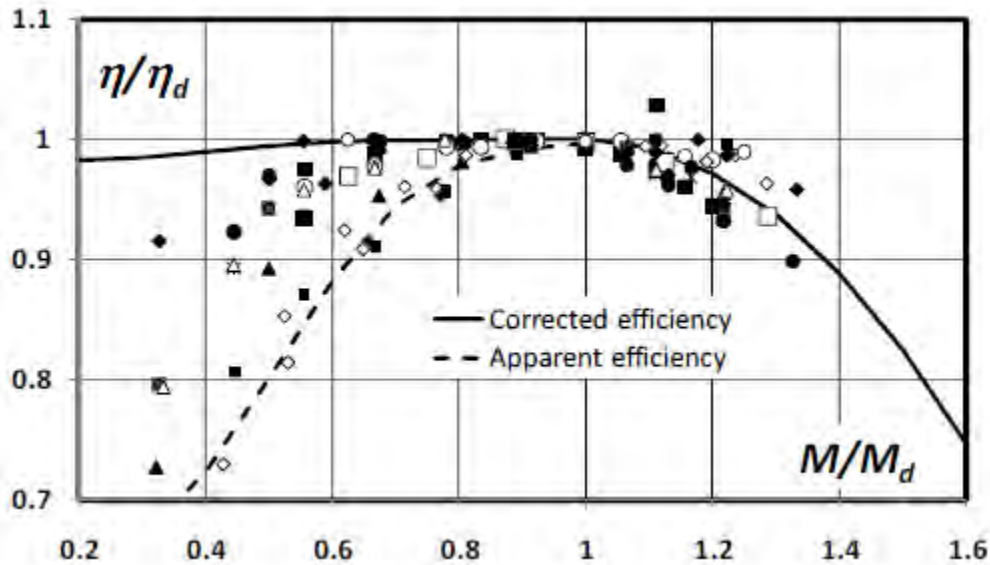


**FIGURE 34: REGRESSION OF PEAK EFFICIENCY VS. TIP MACH NUMBER [48]**

Finding the efficiencies at the non-peak points along a speed line requires an additional set of equations and empirical constants. Two equations are used, one for  $\phi > \phi_p$  and the other for  $\phi < \phi_p$ . These are a function of the flow coefficient and Mach number, given below in Equation 46 - Equation 50.

$$D = (1 - P)D_{LO} + PD_{HI}$$

**EQUATION 46**

$$G = (1 - P)G_{LO} + PG_{HI}$$

**EQUATION 47**

$$H = (1 - P)H_{LO} + PH_{HI}$$

**EQUATION 48**

$$\eta_i = \eta_p \left[ 1 - \left( 1 - \frac{\phi_i}{\phi_p} \right)^D \right]^{1/D}, \phi_i < \phi_p$$

**EQUATION 49**

$$\eta_i = \eta_p \left\{ (1 - G) + G \left[ 1 - \left( 1 - \frac{\phi_i - \phi_p}{\phi_c - \phi_p} \right)^H \right]^{1/H} \right\}, \phi_i > \phi_p$$

**EQUATION 50**

The last of the four non-dimensional parameters to be calculated is the work coefficient.

$$\lambda_{euler,d} = \frac{\lambda_d}{1 + k_{df}/\phi_d}$$

**EQUATION 51**

$$k_{\lambda,d} = \left( \lambda_{euler,d} - 1 + \frac{c_s}{u_2} \right) / \phi_d$$

**EQUATION 52**

$$k_{\lambda,i} = k_{\lambda,d} \frac{[1 + (\gamma - 1)R\lambda_d M_d^2]^{1/\gamma-1}}{[1 + (\gamma - 1)R\lambda_i M_i^2]^{1/\gamma-1}}$$

**EQUATION 53**

$$\lambda_i = \left( 1 + \frac{k_{df}}{\phi_i} \right) \left( 1 - \frac{c_s}{u_2} + \phi_i k_{\lambda,i} \right)$$

**EQUATION 54**

With all four variables known, the pressure ratio and corrected mass flow at each point along the speed line can be calculated via Equation 55 and Equation 56. At this point, the efficiency is also converted from polytropic to adiabatic by Equation 38. A final summary of the entire map generation process is shown in Figure 35.

$$w_{c,i} = \frac{\phi_i n_c \pi D^3 \rho_{ref} g}{60}$$

**EQUATION 55**

$$\pi_i = [1 + (\gamma - 1)\lambda M_i^2]^{1/\gamma-1}$$

**EQUATION 56**

### 3.3.4 Matching Design Stall Margin

As already mentioned, matching a design stall margin was not specified in the original paper outlining the rest of this method. This was added to further customize the shape of the map to a

specific compressor. Refer back to Figure 34, and notice that this regression is set up so that maximum efficiency will always occur at the design point. Although it is being assumed that the design point is at the maximum efficiency along the 100% speed line (and in practice this is generally true), it is usually not true that the design point is at the maximum efficiency of the entire map.

Both of the parameters in this regression are normalized by the design values ( $M_d$ ,  $\eta_d$ ). In order to shift the point of maximum efficiency away from the design point, these normalizing values will be replaced with reference values  $M_{ref}$  and  $\eta_{ref}$ . The stall margin taken as an input is the stall margin at constant corrected flow, as defined in Equation 57. This represents the percent difference between the pressure ratio at the design point and along the stall line at the design corrected flow.

$$SMW = 100 \left( \frac{\pi_s - \pi_d}{\pi_d} \right)$$

**EQUATION 57**

The process for finding the correct  $M_{ref}$  and  $\eta_{ref}$  takes several steps, as shown in Figure 35. The first step is to find the Mach number along the stall line corresponding to the design mass flow. This is done through an iterative loop which guesses a Mach number and compares the flow coefficient computed by Equation 45 with that of a form of the flow coefficient definition given by Equation 58.

$$\phi_s = \frac{w_{c,d} \sqrt{\rho_{ref}/p_{ref}}}{M_s D^2}$$

**EQUATION 58**

With the Mach number known at the stall point, it is now possible to calculate the pressure ratio at this point given a value for  $M_{ref}$  using the method outlined for a normal map point. The initial guess is that  $M_{ref} = M_d$ . Once a guess for  $M_{ref}$  is known,  $\eta_{ref}$  can be determined knowing that the design point ( $M_d$ ,  $\eta_d$ ) still must lie on the regression curve. If the value of  $\pi_s$  calculated from this method is greater than that from Equation 57, then  $M_{ref}$  needs to be decreased to lower the stall point efficiency with respect to the design point, therefore decreasing the stall margin. If  $\pi_s$  is too small, then  $M_{ref}$  is increased, increasing the stall efficiency and consequently the stall margin. The regression in Figure 34 has a limited range of values of  $M/M_{ref}$ . Because of this, there are limits on what stall margins can be matched. If the regression exceeds these bounds, the code will display an error message advising the user to raise or lower the input stall margin as necessary.

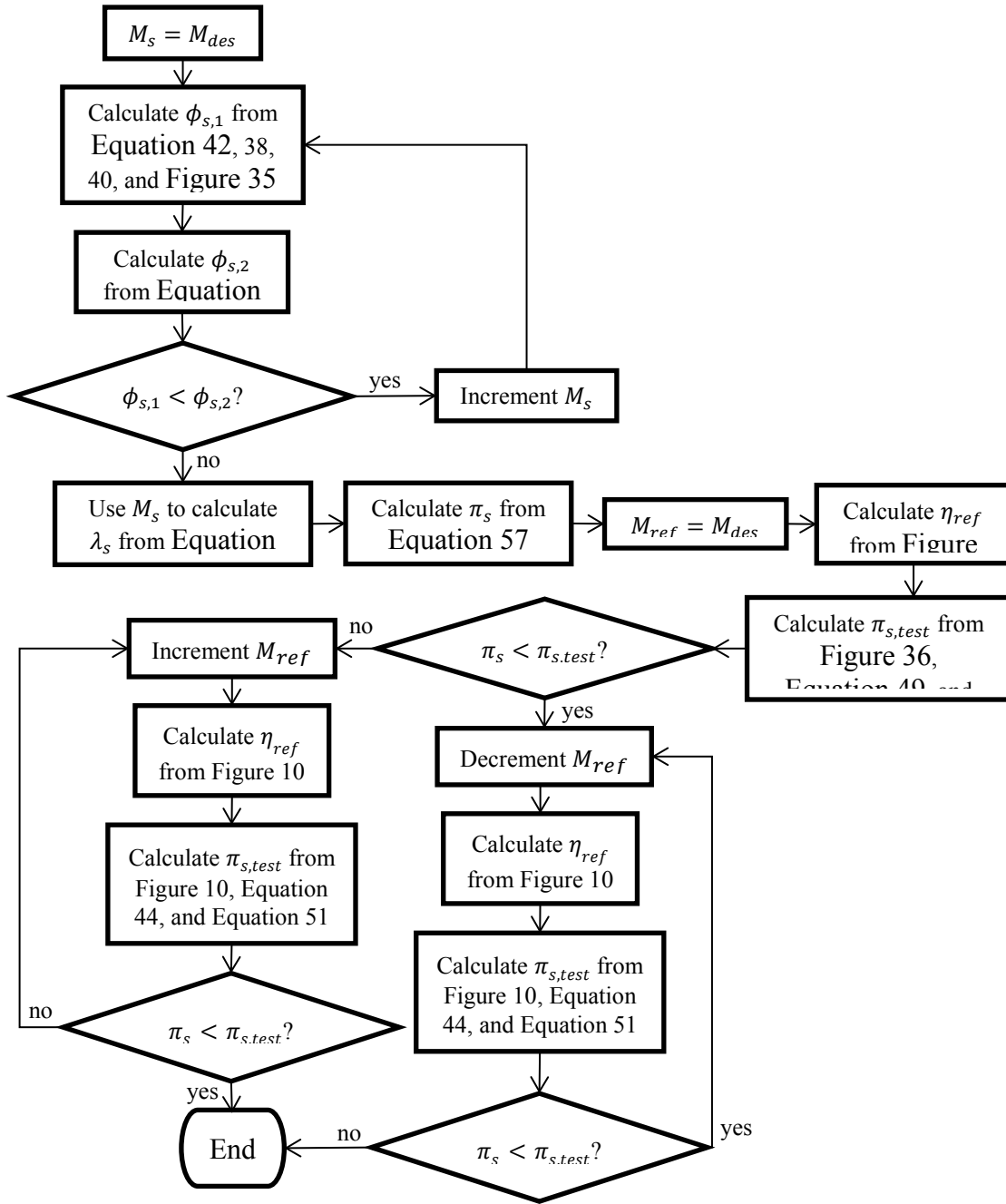
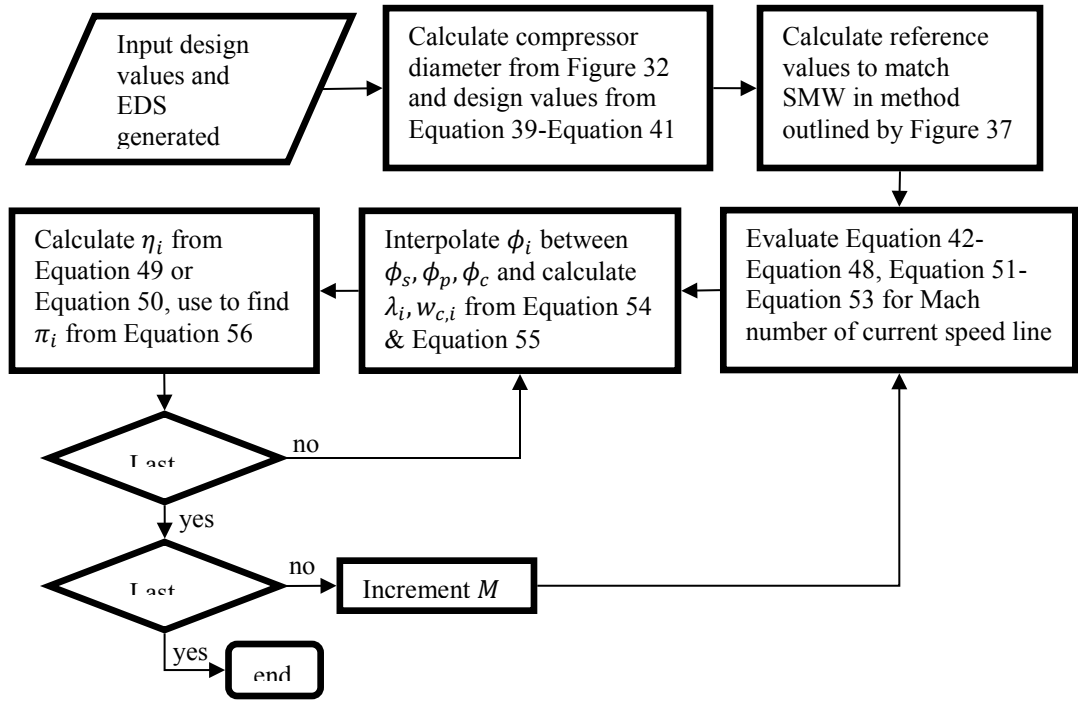


FIGURE 35: ALGORITHM TO MATCH DESIGN STALL MARGIN

### 3.3.5 Summary and Results

All of the major calculation processes have now been described in detail. A final summary of the entire map generation process is shown in Figure 36.



**FIGURE 36: FLOWCHART OF MAP GENERATION ALGORITHM**

### 3.4 Conclusions

The efforts under Phase II to model the CLEEN Program funded technologies using proprietary data were successful. Structural improvements were implemented in EDS where necessary to accurately represent the CLEEN technologies. The majority of the CLEEN Program’s funded technologies were modeled in EDS under this effort. Remaining technologies will be worked under ASCENT Project 10 – Aircraft Technology Modeling and Assessment. The models developed directly supported the fleet-level assessment described in section 4.

## 4 Fleet Level Aircraft Technology Benefits Assessment

### 4.1 Fleet Assessment Process and Assumptions

With the completion of the Phase II modeling efforts that covered the a large number of the CLEEN funded industry technologies, there was sufficient detail to complete a fleet-level assessment to identify the benefits of the modeled CLEEN Program technologies. Note that the GE open rotor, flight management system (FMS) to air traffic management integration, FMS to engine control integration, and Boeing CMC nozzle acoustic impacts are not modeled here. This analysis process was laid out in several steps. First, fleet-level growth, retirement, and replacement assumptions were identified. Replacement assumptions were based on announced upcoming product introductions and historical information on time between aircraft projects. Once fleet-level assumptions were defined, the aircraft technology packages can be generated for different scenarios and timeframes. This involves selecting technologies for each scenario based on expected availability. Finally, EDS is used to generate vehicle level results for fuel burn, NO<sub>x</sub>, and emissions in addition to the detailed mission information needed to run the GREAT rapid fleet-level assessment tool and compute fleet-level environmental impacts. A detailed discussion on GREAT, including major assumptions and validation can be found in [50].

The GREAT tool is an interactive environment that allows for infusion of new technologies and propagates the results to assess the fleet-level implications [51]. This screening tool can be used as a lower fidelity means to assess a multitude of possible scenarios.

The screening tool incorporates the Terminal Area Forecast (TAF) and CAEP/8 retirement curves to determine the future operations of the fleet. The user has the ability to introduce vehicles with new technologies to quantify the fleet-wide environmental metrics from 2006 to 2050 and compare different technology introduction scenarios [51,52]. Predictions of fuel burn, NO<sub>x</sub> emissions, and noise impact are determined for flights within the United States and leaving from the United States. GREAT did not have fleet-level noise analysis capability at the time of this analysis, although that capability is being developed under ASCENT Project 11. As a result, the analysis results presented in this report contain fleet-level fuel burn and LTO NO<sub>x</sub> results only. Further detail on the fleet prediction methods used by GREAT can be found in [51] and [52].

The three major elements that drive fleet performance are:

- Fleet Growth (How many future operations will there be?)Fleet Retirement (How many years is an aircraft in service before being replaced with a new variant?)
- Fleet Replacement (When are new aircraft available?)
- Technology Assumptions (How efficient are new aircraft to enter the fleet?)

### 4.2 Fleet Growth Assumptions

The fleet growth was predicted using the 2012 TAF forecast; however, GT used retirement curves based on [50], and summarized in section 4.3. For years beyond the extent of the TAF, a linear extrapolation of number of operations was used for this analysis. Section 4.4 discusses

fleet replacement assumptions, and section 4.5 provides technology assumptions for the aircraft used in this analysis.

### 4.3 Fleet Retirement Assumptions

In order to predict how long an aircraft is in service before being replaced by a new variant, Georgia Tech constructed parametric retirement curves, shown in Figure 37. These curves are represented for narrow and wide body aircraft. The curves represent the percent of aircraft surviving after a specified number of years in service for each size category. Further details on how these curves are implemented in GREAT can be found in [50].

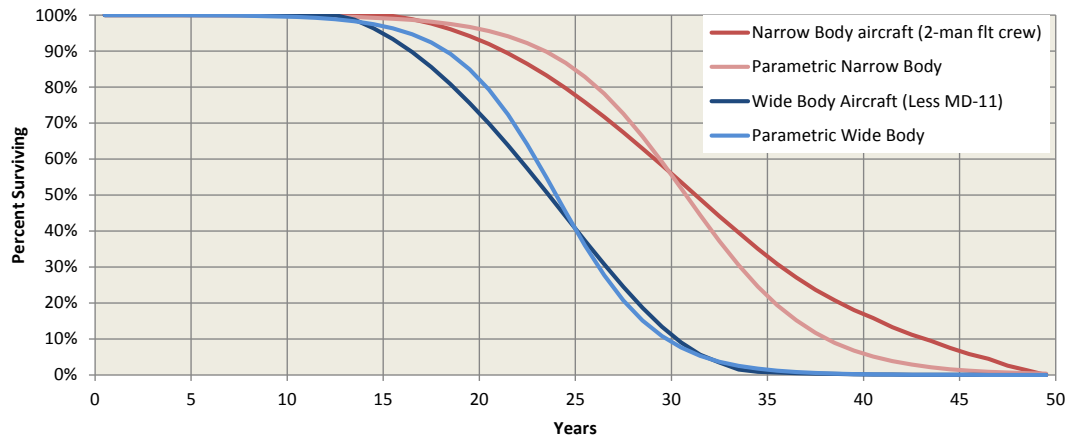


FIGURE 37: RETIREMENT CURVE COMPARISON

### 4.4 Fleet Replacement Assumptions

Fleet replacement assumptions were defined for two generations of new aircraft and the associated technology, termed N+1 and N+2. These scenarios were based on available public domain information regarding upcoming industry aircraft projects. It is important to note that this analysis considers these technologies and aircraft likely to enter the fleet through 2030. New aircraft were defined for each of the five representative aircraft size classes for each of the two technology generations. Previous work has found that using five classes, regional jet, single aisle, small twin aisle, large twin aisle, and very large aircraft, provide an appropriate balance between having to develop an EDS model for every aircraft currently in the fleet that will need to be replaced vs. accuracy by using one aircraft per size class to represent replacements from the starting year [53,54].

In order to determine the introduction rate of new technology, the percentage of new and replacement vehicles that would contain these technologies was defined. Figure 38 shows the percent of replacement vehicles that consist of new vehicles defined by EDS. For example, in 2015, 0% indicates that all of the replacements will be current, in-production aircraft. In 2018, 25% of the RJ replacements will be new technology vehicles, defined by EDS, and the remainder will be in-production. It is assumed that in the N+1 timeframe the geared fan will only be present on the single aisle and regional jet. This is consistent with industry product announcements until the end of this decade. In order to avoid specifics on orders and engine selection by airlines, it was assumed that the geared fan and direct drive engines are split evenly for a given vehicle. For

example, the RJ/N+1 in 2018 has 25% of replacements coming from future (EDS) vehicles. 50% of those future vehicles will be direct drive and 50% will be geared fans. (Meaning 12.5% of replacements will be direct drive and 12.5% will be geared fan, with the remaining 75% being current in-production aircraft). For the N+2 aircraft the geared fan was scaled to all vehicles classes. Four year linear phase-ins between generations of aircraft were assumed. This is consistent with historical data showing the transition from the 737 classic to 737NG series of airplanes.

Vehicle	Timefram	2015	2016	2017	2018	2019	2020	2021	2022	2023	2024	2025	2026	2027	2028	2029	2030	2031	2032	2033	2034	2035
RJ	N+1	0	0	0	25	50	75	100	100	100	100	100	100	100	75	50	25	0	0	0	0	0
RJ	N+2	0	0	0	0	0	0	0	0	0	0	0	0	0	25	50	75	100	100	100	100	100
SA	N+1	0	25	50	75	100	100	100	100	100	100	75	50	25	0	0	0	0	0	0	0	0
SA	N+2	0	0	0	0	0	0	0	0	0	0	25	50	75	100	100	100	100	100	100	100	100
STA	N+1	0	0	0	25	50	75	100	100	100	75	50	25	0	0	0	0	0	0	0	0	0
STA	N+2	0	0	0	0	0	0	0	0	25	50	75	100	100	100	100	100	100	100	100	100	100
LTA	N+1	0	0	0	25	50	75	100	100	100	100	100	100	100	100	100	75	50	25	0	0	0
LTA	N+2	0	0	0	0	0	0	0	0	0	0	0	0	0	0	25	50	75	100	100	100	100
VLA	N+1	0	0	0	0	0	25	50	75	100	100	100	100	75	50	25	0	0	0	0	0	0
VLA	N+2	0	0	0	0	0	0	0	0	0	0	0	0	25	50	75	100	100	100	100	100	100

**FIGURE 38: CLEEN FLEET REPLACEMENT ASSUMPTIONS**

For the regional jet class, the N+1 replacements were assumed to enter service in at 2018, consistent with the Bombardier C-series slated to enter service later this decade. A 10 year product development cycle is then assumed which results in an N+2 RJ entering service in 2028. The single aisle N+1 enters service in 2016 to represent the arrival of the 737MAX and the A320neo. Again a 10 year development cycle is assumed for the next aircraft resulting in an N+2 single aisle in 2025. For the STA, the announcement of the 787-10 formed the basis for a new N+1 aircraft in 2018. A shorter development cycle was assumed for the N+2 introduction since the 787-10 is a derivative aircraft and it is feasible for both a new product and derivative to be developed simultaneously. (Such as is the case with the 737MAX and 777X). The LTA N+1 enters service in 2018 to represent the 777X and a 10 year development cycle is used to set the LTA N+2 entry into service. Finally, 2020 was assumed to be a re-engining opportunity for the wide body large quad, resulting in a shorter timeframe to introduce a new aircraft in 2027.

#### 4.5 Technology Scenarios and Packages

Once the fleet replacement assumptions have been defined technology packages for each class and generation of aircraft can be created. For this assessment three overarching technology scenarios were defined: Evolutionary (EV), Aggressive (AG) and Aggressive without CLEEN technologies (AG-C). The Evolutionary and Aggressive scenarios represent different levels of technology available for implementation in new aircraft in more conservative and optimistic conditions, respectively. The Aggressive without CLEEN scenario was created in order to look at the delta impact of the modeled CLEEN technologies by looking at their impact when removed. For each scenario vehicles were defined for the N+1 and N+2 generations. N+1 packages are labeled as EV and AG, whereas N+2 packages have a '2' in the name (EV2, AG2). Table 4 shows the list of technologies considered and their inclusion in different generational technology packages. A blank cell in the row to the right of the technology name indicates that the technology is not included in a given package. Text in a cell in the row to the right of the

technology name indicates that the technology was included in a technology package (e.g. EV2 – evolutionary scenario N+2 aircraft).

The technology list in Table 4 contains both N+1 and N+2 public domain technologies developed in prior years, as well as modeled CLEEN funded technologies (shaded in grey). In addition to public domain technologies modeled under this project, public domain, EDS technology models developed under NASA Environmentally Responsible Aviation (ERA) and NASA Fixed Wing (FW) sponsorships were also used in the PARTNER Project 36 fleet-level analysis. Descriptions of technology models completed under NASA funding are expected to be released as NASA contractor reports at a later date.

It is important to note that this analysis represents a subset of all technology improvements that are likely to enter the fleet by 2050. For example, CLEEN II technologies that are being considered at the writing of this report are not included.

**TABLE 4: TECHNOLOGY PACKAGE DEFINITION**

		Packages					
1	Aft Cowl Liners	EV	EV2	AG	AG-C	AG2	AG2-C
2	Blisk	EV	EV2	AG	AG-C	AG2	AG2-C
3	Combustor Noise Plug Liner	EV	EV2	AG	AG-C	AG2	AG2-C
4	Composite Technologies (2010 Baseline)	EV	EV2	AG	AG-C	AG2	AG2-C
5	Excrescence Reduction	EV	EV2	AG	AG-C	AG2	AG2-C
6	Fixed Geometry Core Chevrons	EV	EV2	AG	AG-C	AG2	AG2-C
7	PMC Fan Blade with Metal Leading Edge	EV	EV2	AG	AG-C	AG2	AG2-C
8	Polymer Matrix Composites (PMC) - Bypass Duct	EV	EV2	AG	AG-C	AG2	AG2-C
9	Polymer Matrix Composites (PMC) - Fan Case	EV	EV2	AG	AG-C	AG2	AG2-C
10	Polymer Matrix Composites (PMC) - Fan Stator	EV	EV2	AG	AG-C	AG2	AG2-C
11	Polymer Matrix Composites (PMC) - Nacelles	EV	EV2	AG	AG-C	AG2	AG2-C
12	Ti-Al - LPT Aft Blades	EV	EV2	AG	AG-C	AG2	AG2-C
13	Variable Area Nozzle	EV	EV2	AG	AG-C	AG2	AG2-C
14	Zero Splice Inlet	EV	EV2	AG	AG-C	AG2	AG2-C
15	Winglet	EV	EV2	AG	AG-C	AG2	AG2-C
16	Ti-Al - LPT Vane	EV					
17	Advanced TBC Coatings - HPT Vane	EV					
18	Advanced TBC Coatings - LPT Vane	EV					
19	Boeing CMC Exhaust Core Nozzle		EV2	AG		AG2	
20	Boeing Adaptive Trailing Edge		EV2	AG		AG2	
21	Honeywell Cooling		EV2	AG		AG2	
22	Rolls-Royce Cooling		EV2	AG		AG2	
23	CLEEN Advanced Geared Turbofan		EV2	AG		AG2	
24	Advanced Powder Metallurgy Disk - HPC Last Stage Disc		EV2	AG	AG-C	AG2	AG2-C
25	Advanced Powder Metallurgy Disk - HPT Disc		EV2	AG	AG-C	AG2	AG2-C
26	Advanced Powder Metallurgy Disk - LPT First Stage Disc		EV2	AG	AG-C	AG2	AG2-C
27	Advanced Turbine Superalloys - LPT Last Stage Disc		EV2	AG	AG-C	AG2	AG2-C
28	AFC Tail		EV2	AG	AG-C	AG2	AG2-C
29	Continuous Moldline Link for Flaps		EV2	AG	AG-C	AG2	AG2-C
30	Damage Arresting stitched composites- Fuselage		EV2	AG	AG-C	AG2	AG2-C
31	Damage Arresting stitched composites- Wing		EV2	AG	AG-C	AG2	AG2-C
32	Highly Loaded Compressor					AG2	AG2-C
33	Landing Gear Integration - Main		EV2	AG	AG-C	AG2	AG2-C
34	Landing Gear Integration - Nose		EV2	AG	AG-C	AG2	AG2-C
35	Lightweight CMC Liners		EV2	AG	AG-C	AG2	AG2-C
36	Low Interference Nacelle	EV	EV2	AG	AG-C	AG2	AG2-C
37	Natural Laminar Flow - Nacelle	EV	EV2	AG	AG-C	AG2	AG2-C
38	Over the Rotor Acoustic Treatment					AG2	AG2-C
39	TAPS II	EV	EV2	AG		AG2	AG2-C
40	CMC HPT Vane + Hi Temp Erosion Coating		EV2			AG2	AG2-C
41	CMC LPT Vane + Hi Temp Erosion Coating		EV2	AG	AG-C	AG2	AG2-C
42	DRE for HLFC - Wing					AG2	AG2-C
43	Advanced TBC Coatings - HPT Blade		EV2	AG	AG-C		
44	Advanced TBC Coatings - LPT Blade		EV2	AG	AG-C		
45	Soft Vane		EV2	AG	AG-C		
46	Ti-Al - LPT Forward Blades		EV2	AG	AG-C		
47	Compound Rotor Sweep for UHB Fan					AG2	AG2-C
48	Short Nacelle Lip Liner		EV2	AG	AG-C	AG2	AG2-C
49	Riblets - Fuselage					AG2	AG2-C
50	Riblets - Wing					AG2	AG2-C
51	Active Turbine Clearance Control					AG2	AG2-C
52	Active Turbine Flow Control					AG2	AG2-C
53	Advanced Turbine Superalloys - HPT Blades					AG2	AG2-C
54	Advanced Turbine Superalloys - LPT Blade					AG2	AG2-C
55	Cooled Cooling - Turbine					AG2	AG2-C
56	Out-of-Autoclave Composite Fabrication - Fuselage					AG2	AG2-C
57	Out-of-Autoclave Composite Fabrication - Wing					AG2	AG2-C
58	Thrust Reversers - Nacelles					AG2	AG2-C
59	Active Compressor Clearance Control					AG2	AG2-C
60	N+2 Advanced TBC Coatings - HPT Blade					AG2	AG2-C
61	N+2 Advanced TBC Coatings - LPT Blade					AG2	AG2-C
62	Primary Structure Joining Methodologies - Fuselage					AG2	AG2-C
63	Primary Structure Joining Methodologies - Wing					AG2	AG2-C
64	Active Film Cooling					AG2	AG2-C
65	Highly Loaded HP Turbine					AG2	AG2-C
66	Slat Inner Surface Acoustic Liner					AG2	AG2-C
67	Solid Oxide Fuel Cell Auxiliary Power Unit					AG2	AG2-C
68	Noise Cancelling Stator (GTF)					AG2	AG2-C
69	Gust Load Alleviation					AG2	AG2-C

The technology packages identified in Table 4 were generated through significant iteration between the FAA and Georgia Tech. The EDS representation of the advanced geared turbofan engine is included in the EV and AG scenarios; however, the AG-C scenarios are constrained to current technology geared fans. It is also worth noting that the TAPS II combustor, an N+1 technology slated for entry into service in 2016, was carried into the AG2-C scenario since some form of advanced combustor technology would be required to meet CAEP emission standards due to increased OPR in the N+2 timeframe. This is discussed further in the fleet NO<sub>x</sub> results presented in Figure 41.

#### 4.6 Vehicle Level Results

Once the technology packages and engine cycles were chosen they were modeled on the five notional vehicles in different size classes in order to assess their impacts on fuel burn, noise, and emissions both on an absolute basis, and relative to the CLEEN Program goals. Extensive vehicle redesign was not performed, but the vehicle's wing and tail areas were allowed to vary to capture the effects of reduced vehicle weight potential that results from reducing the fuel that must be carried. Vehicle design capabilities did not change, in other words, the vehicle design range and payload were maintained. Wing sweep and general configuration were not altered. Fuselage size was maintained so that payload capacity would remain constant. A list of other major vehicle sizing assumptions is provided below:

- Aircraft thrust-to-weight and wing loading is held constant.
- Fuselage size is kept the same as the baseline aircraft in order to maintain payload capability.
- Design point is unchanged from baseline aircraft.
- Wing and tail areas are allowed to scale.
- Other aircraft geometries are held constant to the baseline aircraft.

Specific Vehicle Results are proprietary, and therefore not included in this report. Results include fuel burn reduction relative to a baseline aircraft in each size class, NO<sub>x</sub> reduction relative to CAEP/6, cumulative noise reduction below Stage IV, and relevant design parameters for each aircraft. For each aircraft a fan pressure ratio sweep was performed to identify the optimal cycle for each set of technologies.

#### 4.7 Fleet-Level Results

Fleet-level fuel burn results were generated using GREAT in combination with the technology assumptions from Table 4 with the replacement assumptions defined in Figure 38. The resulting fuel burn values are shown in Figure 39. Four scenarios are shown in the results. Frozen Technology (FT), is the datum line and represents the case of the current fleet technology level being fixed in perpetuity. In other words, the current in-production aircraft will be produced forever with no change in technology level. Any new aircraft introduced into the fleet to meet demand are current in-production aircraft with no further technology insertion. The Frozen Technology scenario provides the foundation for calculating percent reductions in fleet fuel burn.

The next scenario, EV or Evolutionary, represents the EV and EV2 packages from Table 4 being used for N+1 and N+2 vehicle replacement in Figure 38 respectively. Evolutionary represents a

conservative level of technology development and introduction. The EV scenario does contain all modeled CLEEN technologies. Next, the AG or Aggressive scenario is plotted, representing a more optimistic level of technology development and introduction.

Finally, the AG-C scenario is included to show the effect of removing all modeled CLEEN technologies, including the second generation geared fan, from the fleet analysis. The y-axis shows fleet fuel burn normalized to 2006 levels.

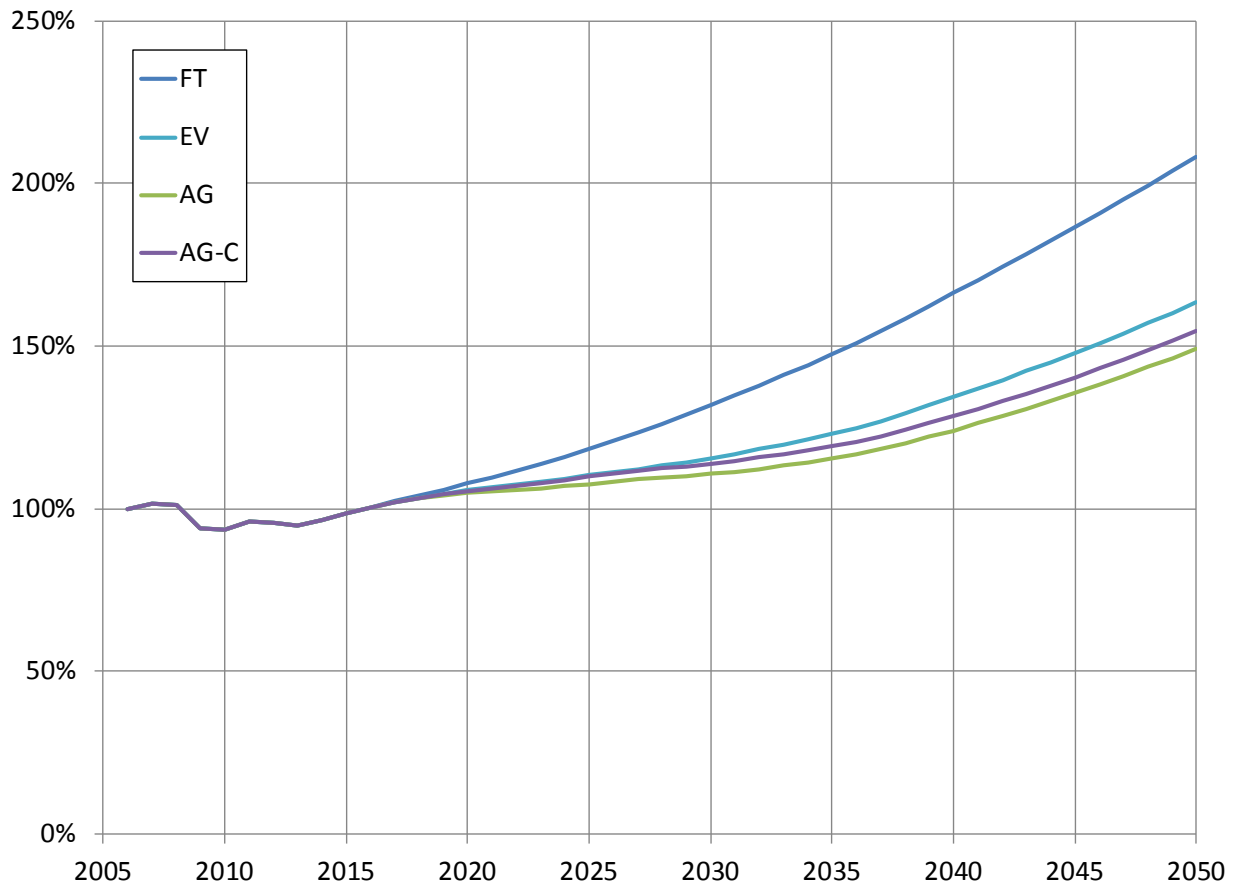


**FIGURE 39: FLEET-LEVEL FUEL BURN IMPACT**

In addition to looking at overall fuel burn trends over time, the reductions provided by each scenario relative to the Frozen Technology baseline are shown in Table 5 for different years of interest.

**TABLE 5: FLEET FUEL BURN REDUCTIONS**

Scenario	Reductions		
	EV	AG	AG-C
2020	-2%	-3%	-3%
2025	-7%	-9%	-7%
2030	-12%	-16%	-14%
2050	-21%	-28%	-26%

The evolutionary scenario reduces fuel burn by 2% over the Frozen Technology scenario by 2020, increasing to a 21% reduction by 2050. The aggressive technology scenario provides further benefit, with fuel burn reductions 1 – 7% greater than the evolutionary scenario as the fleet evolves from 2020 to 2050. This is driven by additional technologies and earlier technology introduction.

The AG-C scenario shows benefits less than the AG scenario, but greater than the EV scenario, as expected. The difference between the AG and AG-C scenarios represents the benefits of the modeled CLEEN technologies at the fleet level, with 2% lower fleet fuel burn from 2025 through 2050. As noted previously, the assessment work of some CLEEN technologies is not included here and will be conducted as a part of the follow-on Aviation Sustainability Center (ASCENT) Project 10 – Technology Modeling and Assessment. As such, this analysis not represent the full benefits of all CLEEN technologies, but does demonstrate the benefit of those modeled to date.

In order to add context to the impact of the modeled CLEEN technologies, the difference between the AG and AG-C scenarios was translated into absolute fuel burn savings using Form 41 Schedule P-12(a) for scheduled and non-scheduled domestic and international fuel burn. Fuel burn savings over year along with cumulative savings are shown in Figure 40. Between 2020 and 2050 the CLEEN technologies modeled in this study help contribute to an average of 490 million gallons of fuel saved per year. This adds up to just over 22 billion gallons of fuel saved by introduction of the modeled advanced technologies developed under the CLEEN Program. This is a significant benefit, but even still does not yet include the benefits of the GE open rotor engine, flight management system (FMS) to air traffic management integration, and FMS to engine control integration technologies being developed under CLEEN. These technologies are being investigated under ASCENT Project10 – Technology Modeling and Assessment.

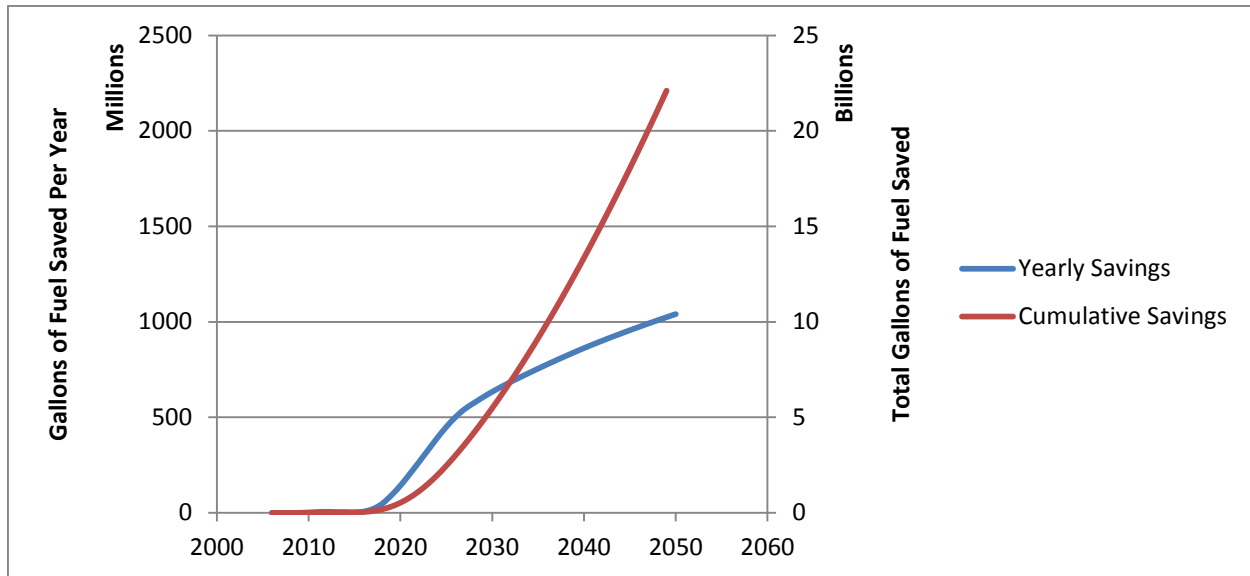


**FIGURE 40: POTENTIAL FUEL BURN SAVINGS PROVIDED BY CLEEN TECHNOLOGIES MODELED IN THIS STUDY**

It should be noted that the CLEEN technologies do not exist in isolation and will not enter the fleet in isolation. Future product aircraft will take advantage of CLEEN technologies alongside other technologies in development, such as those N+1 and N+2 public domain technologies represented in this analysis. In many cases, these technologies may have positive interaction, providing benefit in enabling engine and aircraft redesigns for greater benefit.

Similar studies were performed for  $\text{NO}_x$  and the results are shown in Figure 41. Fleet  $\text{NO}_x$  impacts were calculated by computing the ICAO landing and takeoff (LTO) cycle  $\text{NO}_x$  emissions for both the Fixed Technology, in-production aircraft and for the advanced configurations generated using EDS. Then, using the operations per vehicle class, total LTO emissions per year can be calculated. The emissions results have some trends that merit further explanation.

Even though all of the N+1 and N+2 vehicles provided large vehicle level  $\text{NO}_x$  reductions, the fleet-wide  $\text{NO}_x$  is relatively constant. This can be explained by the interrelationship between fuel efficiency and emissions. As engine overall pressure ratio is increased the engine efficiency increases; however, the combustor entry temperature also rises. As a result the flame temperature and  $\text{NO}_x$  formation also increases. This is why the CAEP/6 standard allows for more LTO  $\text{NO}_x$  as OPR increases. There is an intrinsic trade between reduced  $\text{NO}_x$  and reduced emissions. For the fleet results shown in Figure 41, the advanced combustors and TAPS II are keeping  $\text{NO}_x$  levels reduced relative to the case with no advanced combustor technology. AG-C shows the impact of not having a CLEEN advanced combustor in the N+1 timeframe. There is an increase in  $\text{NO}_x$  that parallels the increase in operations. While total  $\text{NO}_x$  is still reduced below the baseline through 2027, this effect is solely due to fuel burn reductions.

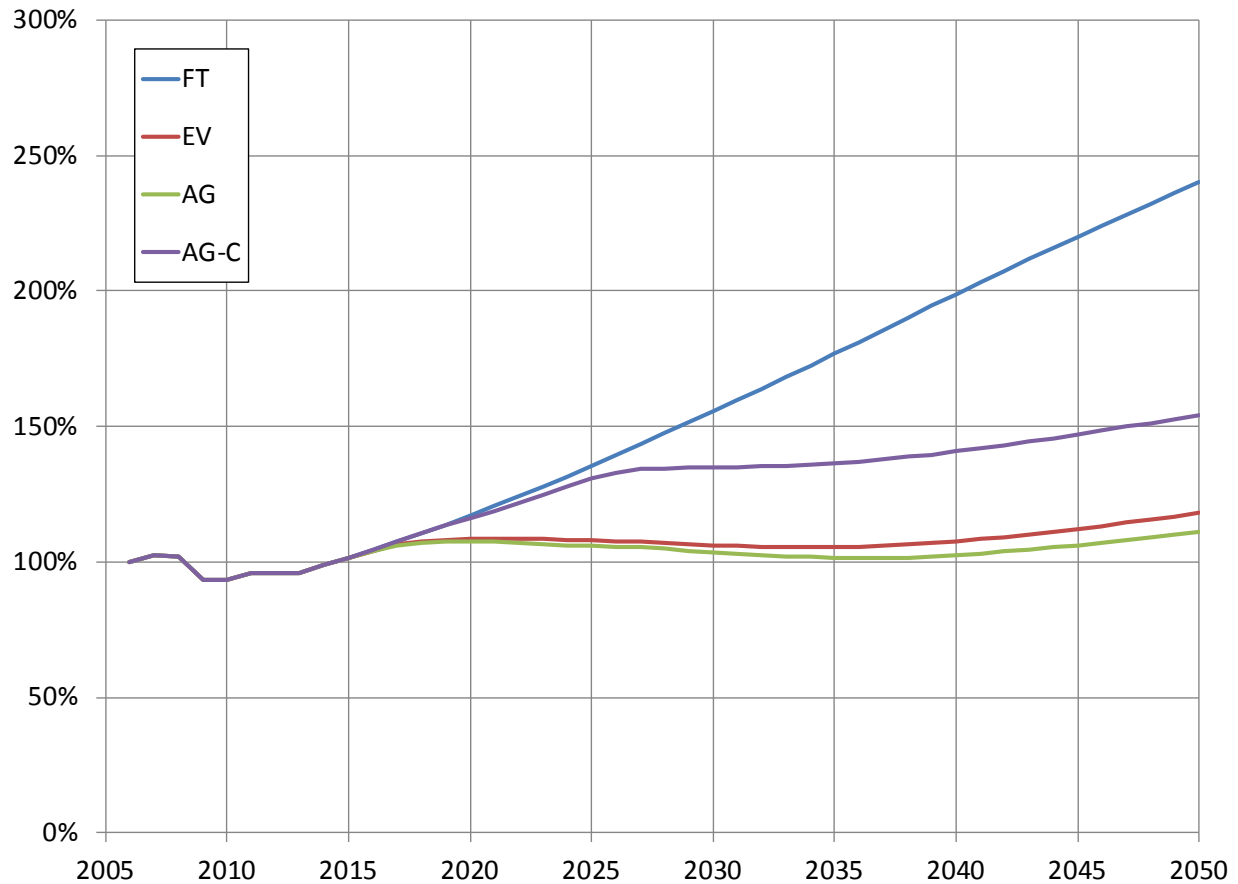


**FIGURE 41: FLEET-LEVEL LTO NO<sub>x</sub> IMPACT**

The results of this fleet-level analysis indicate the significant benefits of CLEEN funded technologies to fuel burn and LTO NO<sub>x</sub>, while also demonstrating the strong potential of aircraft technology to affect aviation’s future fleet fuel burn and NO<sub>x</sub> emissions. Additionally, the results highlight the importance of acceleration of environmentally beneficial technologies. CLEEN’s intent to accelerate maturation of these technologies results in earlier transition into service and thereby earlier realization of significant environmental benefits.

## 5 Technology Dashboard

A technology dashboard tool was developed under PARTNER Project 36 in order to provide the FAA with an in-house, vehicle level assessment capability. The dashboard is implemented in Excel with embedded EDS capabilities using surrogate models with the goal of allowing informed real-time decision making. The user is able to select technology packages from the 58 technologies modeled within the dashboard. Technology models are included from CLEEN EDS Phase I and II along with technology models for N+2 leveraged from the NASA Environmentally Responsible Aviation (ERA) program, as discussed previously. The resulting outputs are the impacts on fuel burn, emissions, and noise on the vehicle level. The included technologies can be applied to the five EDS generic vehicles: Regional Jet (RJ), Single Aisle (SA), Single Twin Aisle (STA), Large Twin Aisle (LTA) and Large Quad (LQ) for both the Advanced Direct Drive Turbofan (ADD) and the Geared Fan (GF) engine cycles. In addition, the dashboard contains multiple functionalities to perform different trade studies, for instance, multi-attribute decision making methods to assist in technology package selection, and design cycle parameter sweeps to help understand confluence of technology and design. The dashboard has been developed as a spiral process with intermediate versions delivered to the FAA. Throughout the development FAA feedback was incorporated into updates.

The technology dashboard was also expanded to include surrogate regressions of the inputs needed to use GREAT, the rapid fleet tradeoff tool developed under PARTNER Project 14. This added capability means that the dashboard can be used to trade technologies, engine and airframe design assumptions, and fleet-level assumptions rapidly to understand trades between technology impact and availability without having to resort to detailed EDS runs. Once promising scenarios are identified they can be more thoroughly investigated using EDS.

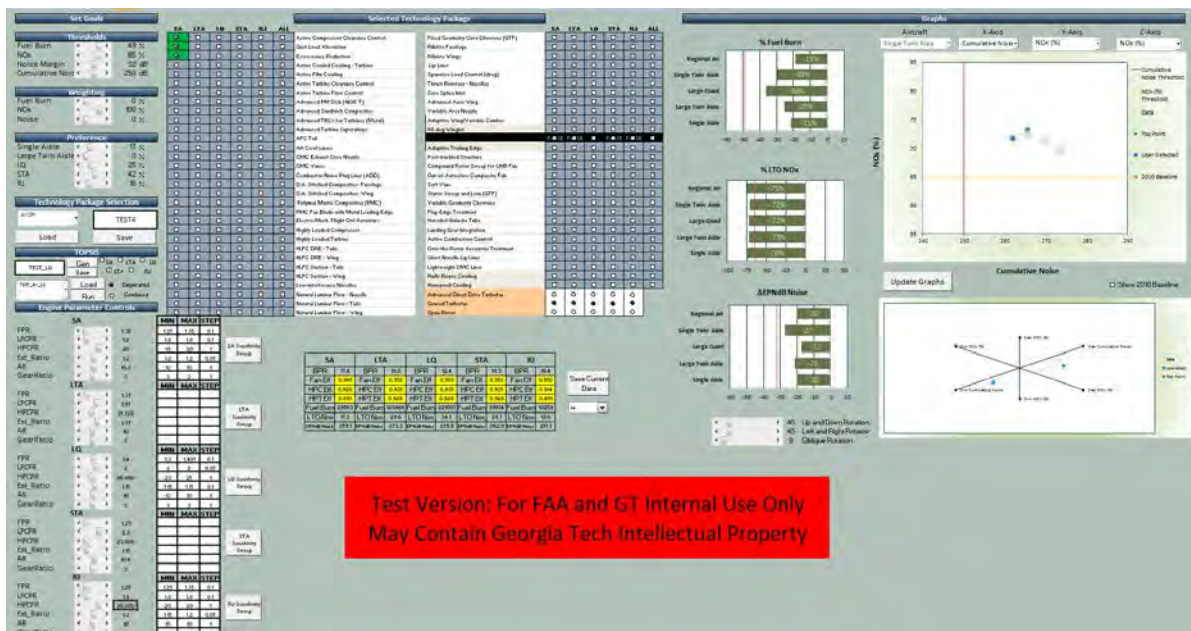


FIGURE 42: TECHNOLOGY DASHBOARD

## 5.1 Technology Dashboard Development

### 5.1.1 Motivation and Objectives

The motivation behind the creation of the technology dashboard is to allow the FAA to assess the impact of technologies on different vehicle classes without the use of EDS. EDS is a multi-disciplinary design and analysis tool which requires a team of experts to run and analyze results. By embedding EDS capabilities into a dashboard, it reduces need to run EDS for each individual technology package that needs to be analyzed. Rather, the dashboard may be used to identify combinations of interest, then EDS can be used to provide more detailed output metrics of interest such as engine weight, thrust specific fuel consumption, or wing span. The dashboard integrates these capabilities with a user-friendly interface in Excel to allow the user to conduct defined technology trade studies instantaneously. In order to evaluate specific technology packages based on top level objectives and scenarios, the user can select any technology set and will immediately receive the impacts the chosen technologies will have on the vehicle level. The objective of the dashboard is to be used as a screening tool and cases of interest can still be run through EDS for detailed or fleet-level analysis. The dashboard is also a building block to providing an integrated fleet-level analysis. This long term goal of an integrated technology and fleet analysis will allow the CLEEN Program the ability to evaluate and quantify fleet-level benefits to relevant stakeholders without disclosing proprietary data, as well as calculate system-wide environmental metrics.

In order to understand what capabilities were required within the dashboard, iterations of the tool were provided to the FAA. Once the full potential was realized, functionalities were added to answer specific questions that were identified.

### 5.1.2 Approach

The development of the dashboard for each vehicle was a five step process, as indicated by Figure 43. The process began by understanding the impact that each technology will have on the different EDS inputs for each vehicle class using a Technology Impact Matrix (TIM). A Design of Experiments (DOE) was then used to generate 10,000 cases with a range of inputs that will be assessed in EDS. Following the evaluation of the DOE in EDS, a mathematical function was produced as a surrogate, with the help of neural networks, in order to calculate the desired outputs for a specific technology input. Once the surrogate was integrated into Excel, the application of the TIM, as well as a Technology Compatibility Matrix (TCM), allows for the selection of specific, user-defined technology packages and the calculation of their impacts.

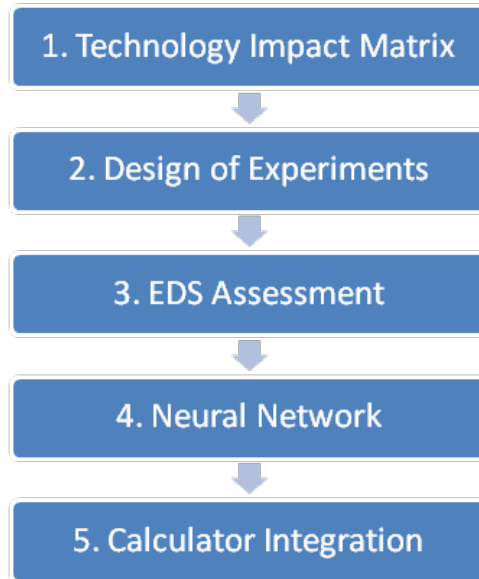


**FIGURE 43: TECHNOLOGY DASHBOARD DEVELOPMENT PROCESS**

### ***Technology Impact Matrix***

When a technology is ‘turned on’ for a specific vehicle within the dashboard, the impacts for the CLEEN vehicle level performance metrics (fuel burn, LTO NO<sub>x</sub> and certification point noise) will automatically update. In order to create such an environment, the impacts of each technology must be mapped within the calculator. The CLEEN technologies researched and modelled in Phase I, along with the public domain technologies modelled for the NASA ERA program, determined the impact on the vehicle parameters of each technology. The TIM is a matrix which stores the deterministic impact estimations for the different technologies. In this context, deterministic simply means the assumed technology impact value determined from research and expert input. The different impacts in the TIM are changes to the model’s baseline input vector which appropriately model a specific technology within the model. In other words, each technology has a corresponding impact vector which shows the change the technology has on the different system inputs to model its effect. Once a technology is “turned on”, the impact vector for that technology is added to the baseline model input vector using appropriate additive logic determined for each technology. This resulting input vector is used as an input to either EDS or the surrogate model. An example TIM is shown in Figure 44. The left column, indicated in blue, is a sample list of input variables for EDS. The top row, indicated in green, is a sample list of the technologies. For each technology, its impact, a positive or negative value, is input into the matrix, shown with the red box. If a certain technology is chosen, for instance technology X, its impact is added to the baseline value for all of the inputs to create a “baseline + technology X” configuration.



**FIGURE 44: SINGLE AISLE TECHNOLOGY IMPACT MATRIX EXCERPT**

In the technology dashboard, a TIM was implemented and populated for each of the five vehicle types. Fifty-eight technologies have been modeled as impact vectors which modify inputs into EDS. If a technology is activated on the front end of the dashboard, the impact vector for that technology is activated and then added to the baseline input vector within the TIM. An example of part of the technology impact vectors for Damage Arresting Stitched Composite Material on the Wing and Fuselage for the SA vehicle is shown in Table 6. This new calculated input vector is then inserted into the neural net surrogates once they are generated. These surrogates then map the input to the responses which are then outputted for the user to see on the front end of the dashboard.

**TABLE 6: SAMPLE PARTIAL TECHNOLOGY IMPACT MATRIX FOR TWO TECHNOLOGIES**

Variable	Units	Baseline	Damage Arresting Stitched Composites Fuselage	Damage Arresting Stitched Composites- Wing	Model Input Vector
FCDO	NONE	1	0	0	1
FCDSUB	NONE	0.985448	0	0	0.985448
FRFU	NONE	1	0	-0.1	0.9
FRHT	NONE	1	0	0	1
FRLGM	NONE	1	0	0	1
FRLGN	NONE	1	0	0	1
FRSC	NONE	1	0	0	1
FRVT	NONE	1	0	0	1
FRWI	NONE	1	-0.1	0	0.9
FRWI1	NONE	1.211	0	0	1.211
FRWI2	NONE	0.681	0	0	0.681
FRWI3	NONE	0.681	0	0	0.681

## Design of Experiments

Once the impact of each individual technology is defined and mapped to a set of EDS inputs via the TIM, a process must be defined to use that information to create surrogate models. Recall that surrogate models are accurate mathematical regressions of an underlying code or model. The first step in performing a mathematical regression is to generate the data for the training set. This is accomplished for this problem using a design of experiments. The TIM was used to define the minimum and maximum values for each of the EDS inputs. This was accomplished by turning on and off all of the technologies to find the minimum and maximum combined input value for each EDS input. Input ranges will be different for each vehicle. An example of these ranges is shown in Table 7. Each class of vehicle is different, however, on average there are 85 inputs that can be impacted by the technologies in this calculator.

**TABLE 7: TIM RANGES FOR A SAMPLE OF EDS INPUTS FOR SA GF**

Variable Name	Description	Minimum	Maximum	Units
<b>Burner_Liner_rho</b>	Burner liner material density	0.076	0.322	lbm/in <sup>3</sup>
<b>Duct15_rho</b>	Duct 15 material density	0.052	0.1	lbm/in <sup>3</sup>
<b>Fan_Blade_rho</b>	Fan Blade Material density	0.06	0.092	lbm/in <sup>3</sup>
<b>Fan_Case_rho</b>	Fan Case Material density	0.052	0.1	lbm/in <sup>3</sup>
<b>HPC_Dutip</b>	HPC tip speed delta at Aero Design Point	-326	0	ft/s
<b>SWETW</b>	Override parameter for wing wetted area	1.000	1.053	N/A
<b>VCTE</b>	Variable Camber Trailing Edge Scalar	0	1	N/A

Rather than run every single permutation of technologies within EDS to prepopulate all possible technology combination for a training dataset, which would be on the order of  $10^{20}$  data points for the CLEEN technology set, a DOE was used to reduce computational time. For this task, a space filling DOE was applied to create cases that represent changing the inputs within the ranges assigned. Furthermore, by choosing a sampling technique that samples each EDS input throughout its continuous space, rather than at discrete values specific to possible technology packages, the surrogates are embedded with the information to perform a gap analysis. In other words, the TIM maps specific inputs to the surrogates; however, there is nothing in the surrogate generation process that precludes any input value from being used within the surrogate model. This allows for future use of the dashboard as a technology goal setting device in a top-down modeling approach.

## EDS Simulation

Using the space filling DOE, a 10,000 case DOE was generated to create a series of EDS input vectors which are subsequently used to generate regression data for the surrogate models. Historical evidence has shown this size DOE will have sufficient data points in order to create a satisfactory surrogate representation with a +/-2% error. This error was estimated through interpreting the diagnostic tests, Figure 49, outputted following the surrogate generation. By

using a DOE in the EDS simulation, the technology dashboard becomes an appropriate tool for technology package and cycle selection studies.

However, running a 10,000 case DOE takes between 17 and 24 hours to complete in EDS. Due to the ‘square’ nature of the design space and the requirement of low correlation between input variables, it was necessary to run a series of test cases. In essence, a smaller subset of the full DOE, on the order of 500 cases, was run to ensure convergence at the edges of the design space. Combinations that exhibit either numerical instability or physical infeasibility (such as extremely high engine overall pressure ratio) are eliminated via a manual trimming of the design ranges. The process shown in the flowchart in Figure 45 was followed to check if the ranges generated from the TIM were sufficient.

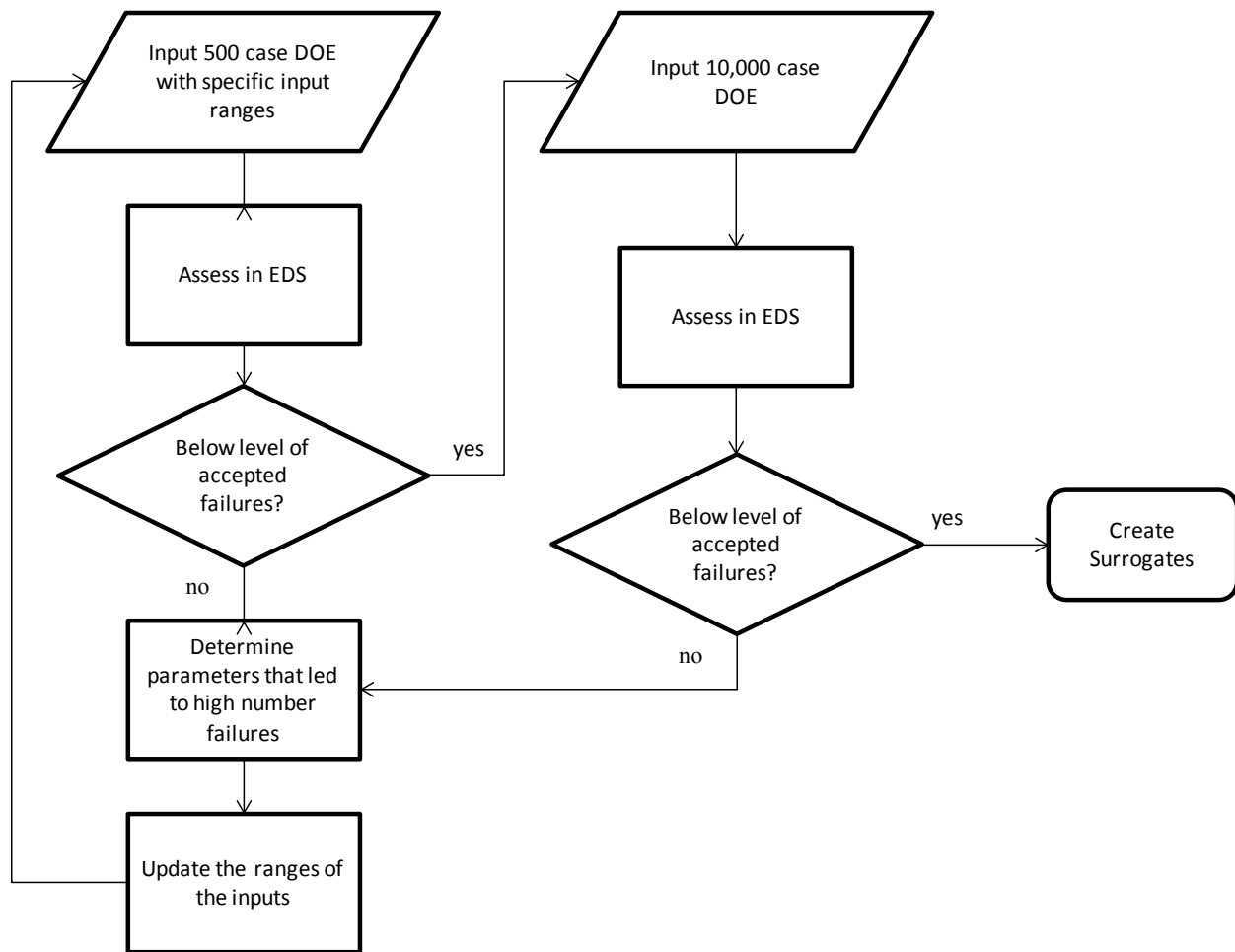


**FIGURE 45: EDS ASSESSMENT FLOWCHART**

A 500 case test DOE was generated using the space filling design and then ran through EDS for each vehicle class and engine cycle (i.e. SA GF, SA ADD, LTA GF, LTA ADD, etc). Once the cases returned, completing in less than 2 hours, the number of cases that did not converge were calculated. The level of accepted failures was determined to be fewer than 10% with the failure points of a numerical convergence in nature and randomly distributed throughout the design space. A scatterplot matrix, as shown in subset matrix Figure 46, is used to identify patterns in the cases that did not converge. Failure cases were color coded red. Successful analysis points

were colored green. This enabled the failed cases to be easily seen within a scatterplot matrix, as shown in Figure 46. The scatterplot matrix shows the input and their ranges against each other. Each dot in the matrix represents a case in the DOE. If the red dots are randomly spaced throughout a box, for instance in the box of Duct15\_rho versus Burner\_Liner\_rho indicated by the purple circle, then that parameter had minimal effect on the failure cases. On the other hand, if the box has a specific location in which there are red dots, for instance fan pressure ratio (FPR) versus any other input as shown by the blue circles, then it can be deduced that for that range of FPR cases will always fail to converge. For this specific example, it was found that the lower bound on FPR for a direct drive with the assumed technology level was not feasible. This is due to the extremely large low pressure turbine stage count needed to drive the fan.

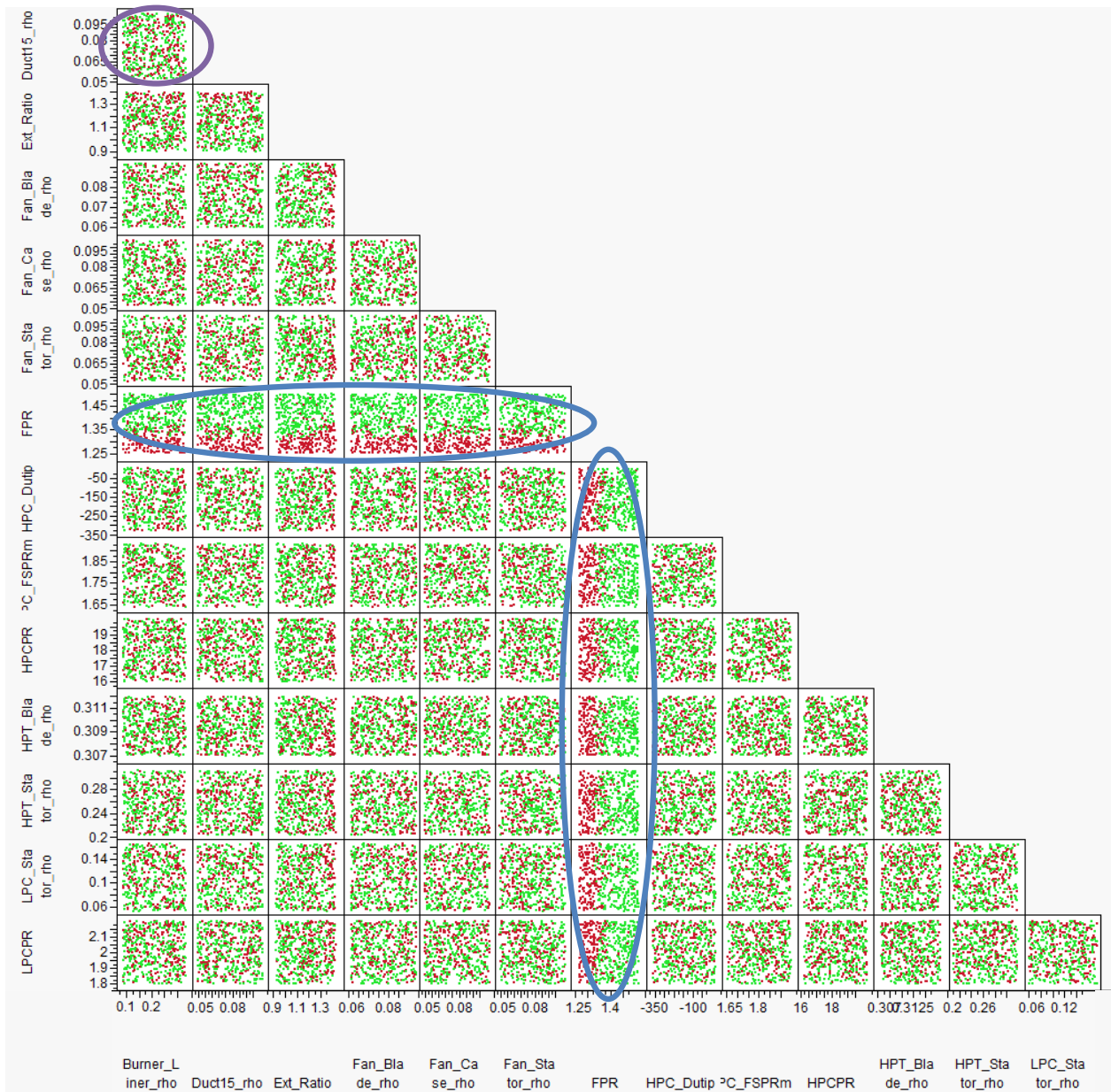


**FIGURE 46: SA ADD 500 TEST CASE SUBSET SCATTERPLOT MATRIX**

## Neural Networks

Once the 10,000 case DOE returns a number of failed outputs that are below the level of accepted failures, a Neural Network was fit to the EDS responses. The neural network surrogate model is then integrated with the TIM in the technology dashboard to predict the vehicle level metrics for a specific technology package and engine cycle. A brief description of neural networks is given below.

The neural net surrogate modeling technique was inspired by the biological nervous system. Neurons, the main cell type responsible for information processing in the brain, are used to compute by learning through example instead of by being programmed. Given the right amount of stimulation, neurons will send signals to other neurons eventually resulting in a desired action. An artificial neuron, as depicted in Figure 47, is developed in order to complete a similar task. Variables are input into the neural net and then multiplied by different weights. An activation function is used in order to produce a nonlinearly activated output of the weighted linear sum of inputs as shown by Equation 59.

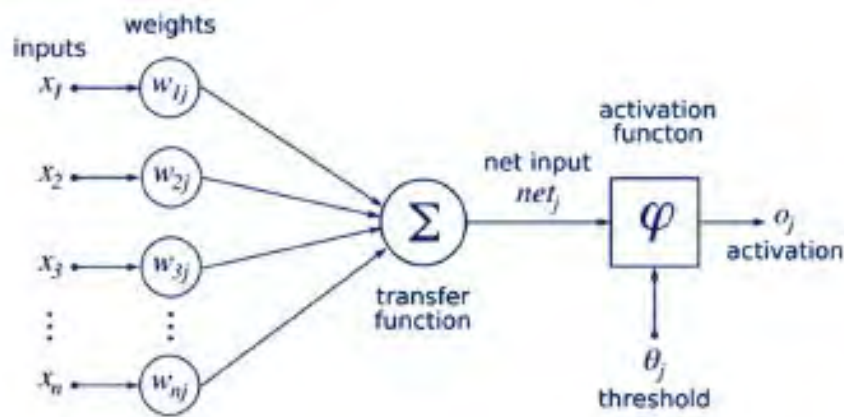


**FIGURE 47: TYPICAL ARTIFICIAL NEURON**

$$O_j = \varphi\left(\sum_{i=1}^n (w_{ij}x_i) - \theta_j\right)$$

**EQUATION 59: TYPICAL ARTIFICIAL NEURON MODEL**

The neural net associates past memory with new inputs by mapping a set of input variables to a set of responses through a set of filters, called the hidden layer. A hidden layer compares values from the input layer to a threshold value which is used to determine what sort of signal to send to the output layer. The process of training a neural net determines when and what signals are passed to the output layer. Figure 48 depicts how the hidden layer is used to compute the output.

**FIGURE 48: NEURAL NETWORK CONCEPTUAL DIAGRAM [55]**

Neural Networks have the ability to derive meaning from complicated sets of data within which trends are not obvious without thorough investigation. This surrogate modeling technique is also optimal for handling a large number of variables; however, this technique needs a large sample size to work to sufficiently calculate the output. Therefore, a large number of cases are needed to return from EDS without failing.

A Neural Network-based regression program, included with the MATLAB toolbox, is used to generate the surrogates for the dashboard. The necessary input in MATLAB is a “training set”: the compiled inputs from the 10,000 case DOE joined together with the EDS outputs from Table 8. Note that additional EDS outputs are available; however, the outputs in Table 8 are of primary importance to tracking the CLEEN goals.

**TABLE 8: DESIRED OUTPUTS TO TRAIN IN NEURAL NETWORK**

Output	Variable Name
desTOGW	Design takeoff gross weight
desBlockFuel	Design block fuel
SLS_Thrust_Uninstalled	Sea level static uninstalled thrust
dPfooNO <sub>x</sub>	LTO NO <sub>x</sub>
diamFan	Fan Diameter
Cruise_SFC_Min	Engine SFC at the bottom-of-loop
SLS_UI_OPR	SLS uninstalled overall pressure ratio
SLS_UI_BPR	SLS uninstalled bypass ratio
Cutback	Cutback EPNdB
Approach	Approach EPNdB
Sideline	Sideline EPNdB

The neural network was trained for each individual response to receive an equation based on the network coefficients.

A series of diagnostic tests were performed to see if the surrogate is a good fit for the data, as seen in Figure 49. The procedure to check the goodness of the model was completed by viewing the:

- (1)  $R^2$  value
- (2) Actual by Predicted Plot
- (3) Residual by Predicted Plot
- (4) Model Fit Error
- (5) Model Representation Error

The  $R^2$  value measures how much variability is accounted for by a model. As a rule of thumb, this value should be greater than 0.98. The Actual versus Predicted plot shows the actual values computed by EDS plotted against the predicted equation for the response. It is assumed that the regressed equation is sufficiently modeling the behavior of the data when the data points are very close to the perfect fit line. The Residual versus Predicted Plot depicts the error associated with the predicted equation. The residual is the error which represents the difference between the actual value of each observation and the value predicted by the model. The Model Fit Error (MFE) is the relative error of the model with respect to the actual values measured on the data points from EDS. Lastly, the Model Representation Error (MRE) is the relative error of the model with respect to the actual values; however, the MRE is different from the MFE because it is measured on the validation points. The surrogate can be considered a good fit if the MRE Standard deviation is less than 1.

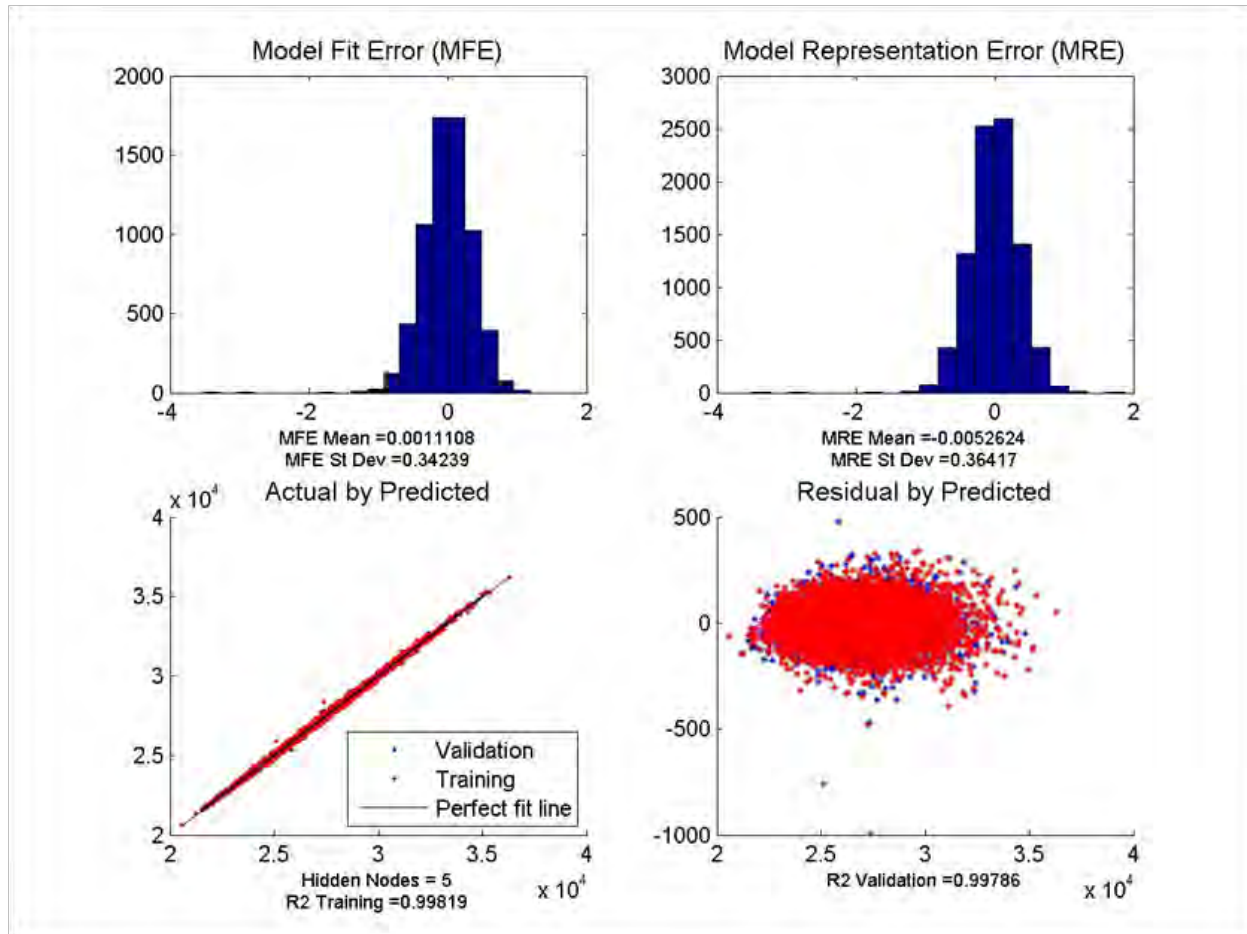


**FIGURE 49: CHECKING FOR GOODNESS OF FIT**

### ***Calculator Integration***

Once the surrogates were generated, the outputs were linked to the respective vehicle TIM. This allows for updates to the TIM to directly affect the responses. These responses can be viewed visually on the Front End of the dashboard. In essence, the TIM functionality is used to create an input vector for each surrogate model rather than EDS; however, the end result is identical (within the accuracy of the surrogate models). A more thorough description of the technology impact matrix follows in the next section.

### ***5.1.3 Technology Selection***

Fifty-eight different technologies and two engine types, the geared turbofan (GF) and advanced direct drive (ADD) have been modeled in the technology dashboard for five different vehicle classes. (Please note that the geared fan representation shown in any examples in this section does not include proprietary data.) To visualize the impact that one of these technologies or engine type has on a vehicle, the user can click on a check box which corresponds to a given technology and vehicle type. Any combination of technologies can be selected to form a technology package. Once a technology has been selected the checkbox will turn green. If the box turns red, this denotes an incompatible technology combination (discussed in the

Technology Compatibility Matrix section). Clicking on a technology or package of technologies, as well as GF or ADD, automatically updates and propagates through the models in the dashboard. These models generate the CLEEN metric outputs of interest for each vehicle type: fuel burn, landing and takeoff (LTO) NO<sub>x</sub> emissions, and EPNdB certification point noise levels. The metrics are then displayed graphically on the Front End. Fuel burn is displayed as a percent change from an EDS vehicle baseline, while LTO NO<sub>x</sub> and cumulative noise are shown as deltas from the CAEP/6 and Stage 4 standards, respectively. The EDS vehicle baseline is class-specific and is specified in Table 9. A sample plots depicting the percent changes from the baselines are shown in Figure 51.

Selected Technology Package		SA	LTA	LQ	STA	RJ	ALL
<input type="checkbox"/>	Active Compressor Clearance Control	<input type="checkbox"/>					
<input type="checkbox"/>	Gust Load Alleviation	<input type="checkbox"/>					
<input type="checkbox"/>	Excrescence Reduction	<input type="checkbox"/>					
<input type="checkbox"/>	Active Cooled Cooling - Turbine	<input type="checkbox"/>					
<input type="checkbox"/>	Active Film Cooling	<input type="checkbox"/>					
<input type="checkbox"/>	Active Turbine Clearance Control	<input type="checkbox"/>					
<input type="checkbox"/>	Active Turbine Flow Control	<input type="checkbox"/>					
<input type="checkbox"/>	Advanced PM Disk (1400 F)	<input type="checkbox"/>					
<input type="checkbox"/>	Advanced Sandwich Composites	<input type="checkbox"/>					
<input type="checkbox"/>	Advanced TBCs for Turbines (Metal)	<input type="checkbox"/>					
<input type="checkbox"/>	Advanced Turbine Superalloys	<input type="checkbox"/>					
<input type="checkbox"/>	AFC Tail	<input type="checkbox"/>					
<input type="checkbox"/>	Air Cowl Liners	<input type="checkbox"/>					
<input type="checkbox"/>	CMC Exhaust Core Nozzle	<input type="checkbox"/>					
<input type="checkbox"/>	CMC Vanes	<input type="checkbox"/>					
<input type="checkbox"/>	Combustor Noise Plug Liner (ADD)	<input type="checkbox"/>					
<input type="checkbox"/>	D.A. Stitched Composites- Fuselage	<input type="checkbox"/>					
<input type="checkbox"/>	D.A. Stitched Composites- Wing	<input type="checkbox"/>					
<input type="checkbox"/>	Polymer Matrix Composites (PMC)	<input type="checkbox"/>					
<input type="checkbox"/>	PMC Fan Blade with Metal Leading Edge	<input type="checkbox"/>					
<input type="checkbox"/>	Electro-Mech. Flight Ctrl Actuators	<input type="checkbox"/>					
<input type="checkbox"/>	Highly Loaded Compressor	<input type="checkbox"/>					
<input type="checkbox"/>	Highly Loaded Turbine	<input type="checkbox"/>					
<input type="checkbox"/>	HLFC DRE - Tails	<input type="checkbox"/>					
<input type="checkbox"/>	HLFC DRE - Wing	<input type="checkbox"/>					
<input type="checkbox"/>	HLFC Suction - Tails	<input type="checkbox"/>					
<input type="checkbox"/>	HLFC Suction - Wing	<input type="checkbox"/>					
<input type="checkbox"/>	Low-interference Nacelles	<input type="checkbox"/>					
<input type="checkbox"/>	Natural Laminar Flow - Nacelle	<input type="checkbox"/>					
<input type="checkbox"/>	Natural Laminar Flow - Tails	<input type="checkbox"/>					
<input type="checkbox"/>	Fixed Geometry Core Chevrons (GTF)	<input type="checkbox"/>					
<input type="checkbox"/>	Riblets Fuselage	<input type="checkbox"/>					
<input type="checkbox"/>	Riblets Wings	<input type="checkbox"/>					
<input type="checkbox"/>	Lip Liner	<input type="checkbox"/>					
<input type="checkbox"/>	Spanwise Load Control (drag)	<input type="checkbox"/>					
<input type="checkbox"/>	Thrust Reverser - Nacelles	<input type="checkbox"/>					
<input type="checkbox"/>	Zero Splice Inlet	<input type="checkbox"/>					
<input type="checkbox"/>	Advanced Aero Wing	<input type="checkbox"/>					
<input type="checkbox"/>	Variable Area Nozzle	<input type="checkbox"/>					
<input type="checkbox"/>	Adaptive Wing/Variable Camber	<input type="checkbox"/>					
<input type="checkbox"/>	60 deg Winglet	<input type="checkbox"/>					
<input type="checkbox"/>	Adaptive Trailing Edge	<input type="checkbox"/>					
<input type="checkbox"/>	Post-buckled Structure	<input type="checkbox"/>					
<input type="checkbox"/>	Compound Rotor Sweep for UHB Fan	<input type="checkbox"/>					
<input type="checkbox"/>	Out-of-Autoclave Composite Fab.	<input type="checkbox"/>					
<input type="checkbox"/>	Soft Vane	<input type="checkbox"/>					
<input type="checkbox"/>	Stator Sweep and Lean (GTF)	<input type="checkbox"/>					
<input type="checkbox"/>	Variable Geometry Chevrons	<input type="checkbox"/>					
<input type="checkbox"/>	Flap Edge Treatment	<input type="checkbox"/>					
<input type="checkbox"/>	Herschel-Quincke Tube	<input type="checkbox"/>					
<input type="checkbox"/>	Landing Gear Integration	<input type="checkbox"/>					
<input type="checkbox"/>	Active Combustion Control	<input type="checkbox"/>					
<input type="checkbox"/>	Over-the-Rotor Acoustic Treatment	<input type="checkbox"/>					
<input type="checkbox"/>	Short Nacelle Lip Liner	<input type="checkbox"/>					
<input type="checkbox"/>	Lightweight CMC Liner	<input type="checkbox"/>					
<input type="checkbox"/>	Rolls Royce Cooling	<input type="checkbox"/>					
<input type="checkbox"/>	Honeywell Cooling	<input type="checkbox"/>					
<input type="checkbox"/>	Advanced Direct Drive Turbofan	<input type="checkbox"/>					
<input type="checkbox"/>	Geared Turbofan	<input type="checkbox"/>					

**FIGURE 50: TECHNOLOGY SELECTION CAPABILITY**

**TABLE 9: EDS VEHICLE BASELINES**

Passenger Class	Airframe	Engine
<b>RJ</b>	CRJ900	CF34-8C5
<b>SA</b>	737-800	CFM56-7B27
<b>STA</b>	767-300ER	CF6-80C2
<b>LTA</b>	777-200ER	GE90-94B
<b>LQ</b>	747-400	PW4056

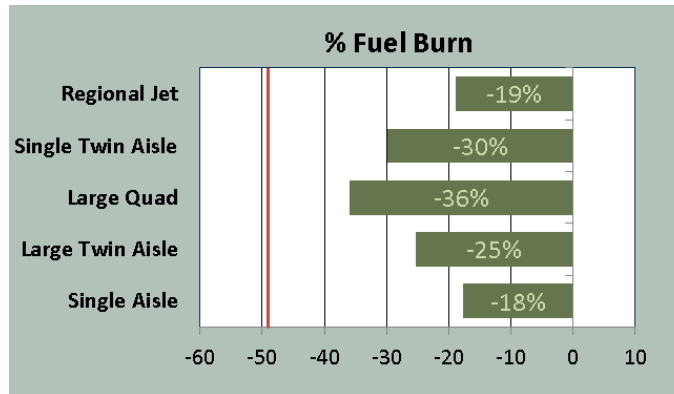


**FIGURE 51: SAMPLE PERCENT CHANGE GRAPH FOR CLEEN FUEL BURN METRIC**

### 5.1.4 Technology Compatibility Matrix

To prevent incompatible and nonsensical technology combinations from being chosen by the user, a Technology Compatibility Matrix (TCM) was implemented in the dashboard. This TCM is a symmetric matrix where the columns and rows are composed of different technologies. The cells of the matrix are then populated with “-1”s and “0”s. A “0” at the intersection of two technologies indicates that the two are compatible while a “-1” indicates they are not. Two technologies are incompatible when the technologies cannot be implemented simultaneously or when significant interaction effects may occur. This may occur for a variety of reasons such as both perform a similar function, both utilize the same physical location, or one changes the vehicle in a way which makes implementing the other impossible. A subset of one section of the TCM used for the LSA vehicle is shown in Figure 52. When multiple technologies are chosen, the TCM verifies the compatibility of these combinations by checking the number at the intersection of the two technologies. If a technology pair is found to be incompatible, the boxes for those technologies will turn red. For example if hybrid laminar flow control (HLFC) Suction – Wing is selected at the same time as Natural Laminar Flow – Wing, the dashboard will check the TCM, find the two are incompatible and color their boxes red (Figure 53). It is worth mentioning that the TCM simply alerts the user to potential incompatibilities or interactions, it does not actually prevent the TIM from being used to create a corresponding impact matrix. This is done intentionally to allow for compatibility decisions to be overruled by the user.

2	Legend	T0-ADD	T0-GTF	T1	T3.1	T3.2	T4	T6	T7	T8	T9	T10.1	T10.2	T11.1	T11.2	T11.3	T12.1	T12.2	T14	T15	T16.1	T16.2	T17	T18	T19
3	Incompatible = -1 Compatible = 0																								
4	ADD Cycle																								
5	GTF Cycle	-1																							
6	Composite Technologies (2010 Baseline) - Fuselage	0	0																						
7	Damage Arresting stitched composites- Fuselage	0	0	0																					
8	Damage Arresting stitched composites- Wing	0	0	0	0																				
9	Gust Load Alleviation	0	0	0	0	0																			
10	Electro Mechanical Flight Control Actuators	0	0	0	0	0	0																		
11	Solid Oxide Fuel Cell Auxiliary Power Unit	0	0	0	0	0	0	0																	
12	Adaptive Wing/Variable Camber	0	0	0	0	0	0	0	0																
13	Excessance Reduction	0	0	0	0	0	0	0	0	0															
14	HLFC Suction - Wing	0	0	0	0	0	0	0	0	0	0														
15	HLFC Suction - Tails	0	0	0	0	0	0	0	0	0	0	0													
16	Natural Laminar Flow - Wing	0	0	0	0	0	0	0	0	0	0	0	0	0	0	0	0	0	0	0	0	0	0	0	0
17	Natural Laminar Flow - Tails	0	0	0	0	0	0	0	0	0	0	0	0	0	0	0	0	0	0	0	0	0	0	0	0
18	Natural Laminar Flow - Nacelle	0	0	0	0	0	0	0	0	0	0	0	0	0	0	0	0	0	0	0	0	0	0	0	0
19	Riblets - Fuselage	0	0	0	0	0	0	0	0	0	0	0	0	0	0	0	0	0	0	0	0	0	0	0	0

FIGURE 52: PARTIAL LSA TCM

<input type="checkbox"/>	<input type="checkbox"/>	<input type="checkbox"/>	<input type="checkbox"/>	<input type="checkbox"/>	<input type="checkbox"/>	HLFC DRE - Tails
<input checked="" type="checkbox"/>	<input type="checkbox"/>	HLFC DRE - Wing				
<input type="checkbox"/>	<input type="checkbox"/>	<input type="checkbox"/>	<input type="checkbox"/>	<input type="checkbox"/>	<input type="checkbox"/>	HLFC Suction - Tails
<input type="checkbox"/>	<input type="checkbox"/>	<input type="checkbox"/>	<input type="checkbox"/>	<input type="checkbox"/>	<input type="checkbox"/>	HLFC Suction - Wing
<input type="checkbox"/>	<input type="checkbox"/>	<input type="checkbox"/>	<input type="checkbox"/>	<input type="checkbox"/>	<input type="checkbox"/>	Low-interference Nacelles
<input type="checkbox"/>	<input type="checkbox"/>	<input type="checkbox"/>	<input type="checkbox"/>	<input type="checkbox"/>	<input type="checkbox"/>	Natural Laminar Flow - Nacelle
<input type="checkbox"/>	<input type="checkbox"/>	<input type="checkbox"/>	<input type="checkbox"/>	<input type="checkbox"/>	<input type="checkbox"/>	Natural Laminar Flow - Tails
<input checked="" type="checkbox"/>	<input type="checkbox"/>	Natural Laminar Flow - Wing				

FIGURE 53: FRONT END INCOMPATIBILITY EXAMPLE

## 5.2 Technology Checks

Several technology checks were completed on the dashboard to verify the surrogates were accurately representing EDS’s original outputs on an individual technology basis. To perform the technology checks, a series of cases were run using the dashboard. The same TIM generated input vectors from the dashboard cases were then imported into EDS, allowing for the comparison between the dashboard surrogates and EDS outputs in terms of fuel burn, noise, and NO<sub>x</sub> emissions. Percent differences were calculated for each technology.

## 5.3 Calculator Functionalities

A number of functionalities are implemented in the calculator to enable the user to make decisions based on different factors. The functionalities for technology selection, with the use of the TIM, and technology compatibilities, through the use of the TCM have previously been discussed. This section will discuss the capabilities for parametric cycle parameters and cycle sweeps, as well as a Multi-Attribute Decision Making (MADM).

### 5.3.1 Parametric Cycle Parameters and Cycle Sweeps

Since the engine cycle has a strong interaction with the chosen technology set, cycle parameters were included on the Front End to allow the user to manually choose the cycle for each vehicle

to match a desired level of engine technology or engine design philosophy, or to better understand the impacts between cycle and technology settings. The cycle parameters, which include Fan Pressure Ratio, High and Low Pressure Compressor Pressure Ratio, Extraction Ratio, Aspect Ratio, and Gear Ratio, can be manipulated for each vehicle by using slider bars (Figure 54). The ranges for these inputs can vary depending on the vehicle and engine type, and are displayed in Table 10. These ranges were selected after iteration with FAA personnel and then refined in order to keep resulting designs feasible. The values must be kept within these bounds for the surrogate models to remain valid. The user can also input a number into the cell directly and the cell will turn red if it is outside the range.



**FIGURE 54: PARAMETRIC CYCLE PARAMETERS AND CYCLE SWEEP FUNCTIONALITY**

**TABLE 10: CYCLE PARAMETERS FOR EACH VEHICLE AND CLASS**

PAX Class	Engine Type	FPR		LPCPR		HPCPR		Extraction Ratio		Aspect Ratio		Gear Ratio	
		Max	Min	Max	Min	Max	Min	Max	Min	Max	Min	Max	Min
SA	GF	1.25	1.5	1.8	2.2	16	20	0.9	1.4	8	12	2.5	3.5
	ADD	1.37	1.625	1.76	2.1	15.6	20.4	0.85	1.45	8	12	2.5	3.5
LTA	GF	1.25	1.5	1.35	1.9	23	30	0.9	1.4	8	12	2.5	3.5
	ADD	1.3	1.6	1.35	1.9	23	30	0.9	1.4	8	12	2.5	3.5
STA	GF	1.25	1.5	1.8	2.2	23	30	0.9	1.4	8	12	2.5	3.5
	ADD	1.35	1.6	1.8	2.2	23	30	0.9	1.4	8	12	2.5	3.5
RJ	GF	1.25	1.5	1.8	2.2	16	19	0.85	1.15	8	12	2.5	3.5
	ADD	1.35	1.6	1.7	2.1	15	19	0.9	1.4	8	12	2.5	3.5
LQ	GF	1.25	1.5	1.8	2.05	23	30	0.9	1.25	8	12	2.5	3.5

The cycle sweep allows the user to iterate through the cycle parameters with a minimum, maximum, and step size in order to generate parametric performance, noise, and emissions data for a given technology package. Once generated, the data can be visualized to display the data in the form of carpet plots or other instructive figures.

To illustrate the generation of this sweep, an example cycle sweep is performed for the SA vehicle with a GF engine. (Please note that the geared fan representation shown in any examples in this section does not include proprietary data.) Any of the technologies can be applied to the vehicle (Figure 55). In this case, four cooling technologies have been applied (Figure 56).

Selected Technology Package						
SA	LTA	LQ	STA	RJ	ALL	
<input type="checkbox"/>	<input type="checkbox"/>	<input type="checkbox"/>	<input type="checkbox"/>	<input type="checkbox"/>	<input type="checkbox"/>	Active Compressor Clearance Control
<input type="checkbox"/>	<input type="checkbox"/>	<input type="checkbox"/>	<input type="checkbox"/>	<input type="checkbox"/>	<input type="checkbox"/>	Gust Load Alleviation
<input type="checkbox"/>	<input type="checkbox"/>	<input type="checkbox"/>	<input type="checkbox"/>	<input type="checkbox"/>	<input type="checkbox"/>	Exorescence Reduction
<input checked="" type="checkbox"/>	<input type="checkbox"/>	Active Cooled Cooling - Turbine				
<input checked="" type="checkbox"/>	<input type="checkbox"/>	Active Film Cooling				
<input type="checkbox"/>	<input type="checkbox"/>	<input type="checkbox"/>	<input type="checkbox"/>	<input type="checkbox"/>	<input type="checkbox"/>	Active Turbine Clearance Control
<input type="checkbox"/>	<input type="checkbox"/>	<input type="checkbox"/>	<input type="checkbox"/>	<input type="checkbox"/>	<input type="checkbox"/>	Active Turbine Flow Control
<input type="checkbox"/>	<input type="checkbox"/>	<input type="checkbox"/>	<input type="checkbox"/>	<input type="checkbox"/>	<input type="checkbox"/>	Advanced PM Disk (1400 F)
<input type="checkbox"/>	<input type="checkbox"/>	<input type="checkbox"/>	<input type="checkbox"/>	<input type="checkbox"/>	<input type="checkbox"/>	Advanced Sandwich Composites
<input checked="" type="checkbox"/>	<input type="checkbox"/>	Advanced TBCs for Turbines (Metal)				
<input checked="" type="checkbox"/>	<input type="checkbox"/>	Advanced Turbine Superalloys				
<input type="checkbox"/>	<input type="checkbox"/>	<input type="checkbox"/>	<input type="checkbox"/>	<input type="checkbox"/>	<input type="checkbox"/>	AFC Tail
<input type="checkbox"/>	<input type="checkbox"/>	<input type="checkbox"/>	<input type="checkbox"/>	<input type="checkbox"/>	<input type="checkbox"/>	Aft Cowl Liners
<input type="checkbox"/>	<input type="checkbox"/>	<input type="checkbox"/>	<input type="checkbox"/>	<input type="checkbox"/>	<input type="checkbox"/>	CMC Exhaust Core Nozzle
<input type="checkbox"/>	<input type="checkbox"/>	<input type="checkbox"/>	<input type="checkbox"/>	<input type="checkbox"/>	<input type="checkbox"/>	CMC Vanes
<input type="checkbox"/>	<input type="checkbox"/>	<input type="checkbox"/>	<input type="checkbox"/>	<input type="checkbox"/>	<input type="checkbox"/>	Combustor Noise Plug Liner (ADD)
<input type="checkbox"/>	<input type="checkbox"/>	<input type="checkbox"/>	<input type="checkbox"/>	<input type="checkbox"/>	<input type="checkbox"/>	D.A. Stitched Composites- Fuselage
<input type="checkbox"/>	<input type="checkbox"/>	<input type="checkbox"/>	<input type="checkbox"/>	<input type="checkbox"/>	<input type="checkbox"/>	D.A. Stitched Composites- Wing
<input type="checkbox"/>	<input type="checkbox"/>	<input type="checkbox"/>	<input type="checkbox"/>	<input type="checkbox"/>	<input type="checkbox"/>	Polymer Matrix Composites (PMC)
<input type="checkbox"/>	<input type="checkbox"/>	<input type="checkbox"/>	<input type="checkbox"/>	<input type="checkbox"/>	<input type="checkbox"/>	PMC Fan Blade with Metal Leading Edge
<input type="checkbox"/>	<input type="checkbox"/>	<input type="checkbox"/>	<input type="checkbox"/>	<input type="checkbox"/>	<input type="checkbox"/>	Electro-Mech. Flight Ctrl Actuators
<input type="checkbox"/>	<input type="checkbox"/>	<input type="checkbox"/>	<input type="checkbox"/>	<input type="checkbox"/>	<input type="checkbox"/>	Highly Loaded Compressor
<input type="checkbox"/>	<input type="checkbox"/>	<input type="checkbox"/>	<input type="checkbox"/>	<input type="checkbox"/>	<input type="checkbox"/>	Highly Loaded Turbine
<input type="checkbox"/>	<input type="checkbox"/>	<input type="checkbox"/>	<input type="checkbox"/>	<input type="checkbox"/>	<input type="checkbox"/>	HLFC DRE - Tails
<input type="checkbox"/>	<input type="checkbox"/>	<input type="checkbox"/>	<input type="checkbox"/>	<input type="checkbox"/>	<input type="checkbox"/>	HLFC DRE - Wing
<input type="checkbox"/>	<input type="checkbox"/>	<input type="checkbox"/>	<input type="checkbox"/>	<input type="checkbox"/>	<input type="checkbox"/>	HLFC Suction - Tails
<input type="checkbox"/>	<input type="checkbox"/>	<input type="checkbox"/>	<input type="checkbox"/>	<input type="checkbox"/>	<input type="checkbox"/>	HLFC Suction - Wing
<input type="checkbox"/>	<input type="checkbox"/>	<input type="checkbox"/>	<input type="checkbox"/>	<input type="checkbox"/>	<input type="checkbox"/>	Low-interference Nacelles
<input type="checkbox"/>	<input type="checkbox"/>	<input type="checkbox"/>	<input type="checkbox"/>	<input type="checkbox"/>	<input type="checkbox"/>	Natural Laminar Flow - Nacelle
<input type="checkbox"/>	<input type="checkbox"/>	<input type="checkbox"/>	<input type="checkbox"/>	<input type="checkbox"/>	<input type="checkbox"/>	Natural Laminar Flow - Tails
<input type="checkbox"/>	<input type="checkbox"/>	<input type="checkbox"/>	<input type="checkbox"/>	<input type="checkbox"/>	<input type="checkbox"/>	Natural Laminar Flow - Wing
<input type="checkbox"/>	<input type="checkbox"/>	<input type="checkbox"/>	<input type="checkbox"/>	<input type="checkbox"/>	<input type="checkbox"/>	Fixed Geometry Core Chevrons (GTF)
<input type="checkbox"/>	<input type="checkbox"/>	<input type="checkbox"/>	<input type="checkbox"/>	<input type="checkbox"/>	<input type="checkbox"/>	Riblets Fuselage
<input type="checkbox"/>	<input type="checkbox"/>	<input type="checkbox"/>	<input type="checkbox"/>	<input type="checkbox"/>	<input type="checkbox"/>	Riblets Wings
<input type="checkbox"/>	<input type="checkbox"/>	<input type="checkbox"/>	<input type="checkbox"/>	<input type="checkbox"/>	<input type="checkbox"/>	Lip Liner
<input type="checkbox"/>	<input type="checkbox"/>	<input type="checkbox"/>	<input type="checkbox"/>	<input type="checkbox"/>	<input type="checkbox"/>	Spanwise Load Control (drag)
<input type="checkbox"/>	<input type="checkbox"/>	<input type="checkbox"/>	<input type="checkbox"/>	<input type="checkbox"/>	<input type="checkbox"/>	Thrust Reverser - Nacelles
<input type="checkbox"/>	<input type="checkbox"/>	<input type="checkbox"/>	<input type="checkbox"/>	<input type="checkbox"/>	<input type="checkbox"/>	Zero Splice Inlet
<input type="checkbox"/>	<input type="checkbox"/>	<input type="checkbox"/>	<input type="checkbox"/>	<input type="checkbox"/>	<input type="checkbox"/>	Advanced Aero Wing
<input type="checkbox"/>	<input type="checkbox"/>	<input type="checkbox"/>	<input type="checkbox"/>	<input type="checkbox"/>	<input type="checkbox"/>	Variable Area Nozzle
<input type="checkbox"/>	<input type="checkbox"/>	<input type="checkbox"/>	<input type="checkbox"/>	<input type="checkbox"/>	<input type="checkbox"/>	Adaptive Wing/Variable Camber
<input type="checkbox"/>	<input type="checkbox"/>	<input type="checkbox"/>	<input type="checkbox"/>	<input type="checkbox"/>	<input type="checkbox"/>	60 deg winglet
<input type="checkbox"/>	<input type="checkbox"/>	<input type="checkbox"/>	<input type="checkbox"/>	<input type="checkbox"/>	<input type="checkbox"/>	Adaptive Trailing Edge
<input type="checkbox"/>	<input type="checkbox"/>	<input type="checkbox"/>	<input type="checkbox"/>	<input type="checkbox"/>	<input type="checkbox"/>	Post-buckled Structure
<input type="checkbox"/>	<input type="checkbox"/>	<input type="checkbox"/>	<input type="checkbox"/>	<input type="checkbox"/>	<input type="checkbox"/>	Compound Rotor Sweep for UHB Fan
<input type="checkbox"/>	<input type="checkbox"/>	<input type="checkbox"/>	<input type="checkbox"/>	<input type="checkbox"/>	<input type="checkbox"/>	Out-of-Autoclave Composite Fab.
<input type="checkbox"/>	<input type="checkbox"/>	<input type="checkbox"/>	<input type="checkbox"/>	<input type="checkbox"/>	<input type="checkbox"/>	Soft Vane
<input type="checkbox"/>	<input type="checkbox"/>	<input type="checkbox"/>	<input type="checkbox"/>	<input type="checkbox"/>	<input type="checkbox"/>	Stator Sweep and Lean (GTF)
<input type="checkbox"/>	<input type="checkbox"/>	<input type="checkbox"/>	<input type="checkbox"/>	<input type="checkbox"/>	<input type="checkbox"/>	Variable Geometry Chevrons
<input type="checkbox"/>	<input type="checkbox"/>	<input type="checkbox"/>	<input type="checkbox"/>	<input type="checkbox"/>	<input type="checkbox"/>	Flap Edge Treatment
<input type="checkbox"/>	<input type="checkbox"/>	<input type="checkbox"/>	<input type="checkbox"/>	<input type="checkbox"/>	<input type="checkbox"/>	Herschel-Quincke Tube
<input type="checkbox"/>	<input type="checkbox"/>	<input type="checkbox"/>	<input type="checkbox"/>	<input type="checkbox"/>	<input type="checkbox"/>	Landing Gear Integration
<input type="checkbox"/>	<input type="checkbox"/>	<input type="checkbox"/>	<input type="checkbox"/>	<input type="checkbox"/>	<input type="checkbox"/>	Active Combustion Control
<input type="checkbox"/>	<input type="checkbox"/>	<input type="checkbox"/>	<input type="checkbox"/>	<input type="checkbox"/>	<input type="checkbox"/>	Over-the-Rotor Acoustic Treatment
<input type="checkbox"/>	<input type="checkbox"/>	<input type="checkbox"/>	<input type="checkbox"/>	<input type="checkbox"/>	<input type="checkbox"/>	Short Nacelle Lip Liner
<input type="checkbox"/>	<input type="checkbox"/>	<input type="checkbox"/>	<input type="checkbox"/>	<input type="checkbox"/>	<input type="checkbox"/>	Lightweight CMC Liner
<input type="checkbox"/>	<input type="checkbox"/>	<input type="checkbox"/>	<input type="checkbox"/>	<input type="checkbox"/>	<input type="checkbox"/>	Rolls Royce Cooling
<input type="checkbox"/>	<input type="checkbox"/>	<input type="checkbox"/>	<input type="checkbox"/>	<input type="checkbox"/>	<input type="checkbox"/>	Honeywell Cooling
<input type="checkbox"/>	<input type="checkbox"/>	<input type="checkbox"/>	<input type="checkbox"/>	<input type="checkbox"/>	<input type="checkbox"/>	Advanced Direct Drive Turbofan
<input type="checkbox"/>	<input type="checkbox"/>	<input type="checkbox"/>	<input type="checkbox"/>	<input type="checkbox"/>	<input type="checkbox"/>	Geared Turbofan
<input type="checkbox"/>	<input type="checkbox"/>	<input type="checkbox"/>	<input type="checkbox"/>	<input type="checkbox"/>	<input type="checkbox"/>	Open Rotor

FIGURE 55: TECHNOLOGY SELECTION FOR CYCLE SWEEP

Cooling Technologies
Advanced TBC
Advanced Turbine Superalloys
Active Cooled Cooling - Turbine
Active Film Cooling

FIGURE 56: TECHNOLOGIES SELECTED IN CYCLE SWEEP

Once the technologies have been selected then the maximum, minimum, and step size of the cycle sweep must be input (Figure 57). Care must be taken to ensure that minimum and maximum of each cycle parameter is within the allowable ranges for that vehicle in the dashboard. Deviating from the ranges causes the surrogates to extrapolate data. This can result in large response error. The allowable ranges are given by the bounds of the slider bars for that vehicle. After setting these values, the sweep can be initiated by clicking the “Sensitivity Sweep” button.

Engine Parameter Controls			
SA	MIN	MAX	STEP
FPR	1.25	1.5001	0.0625
LPCPR	1.8	2.2	0.1
HPCPR	16	20	1
Ext_Ratio	1.2	1.2	0.125
AR	10	10	1
GearRatio	3	3	1

FIGURE 57: SENSITIVITY SWEEP PARAMETERS RANGES AND STEP SIZE INPUTS

The results of the sweep are then recorded in the “Saved Sensitivity” sheet. An example output from this sweep can be seen in Figure 58. The output includes the CLEEN metrics as well as calculated Fan, HPC and HPT efficiency, and BPR. The cycle parameters used in each run are also recorded.

19	2/22/2013	1:36:02 PM														
20	Case #	1	2	3	4	5	6	7	8	9	10	11	12			
21	VehicleType	SA	SA	SA	SA	SA	SA	SA	SA	SA	SA	SA	SA	SA	SA	SA
22	EngineType	GTF	GTF	GTF	GTF	GTF	GTF	GTF	GTF	GTF	GTF	GTF	GTF	GTF	GTF	GTF
23	BPR	20.2194409	20.14615	20.06931	19.98889	19.90487	20.1302	20.05277	19.97173	19.88705	19.7987	20.03673	19.95515	19.87351	19.79087	19.70823
24	Fan Eff	0.950416011	0.950416	0.950416	0.950416	0.950416	0.950416	0.950416	0.950416	0.950416	0.950416	0.950416	0.950416	0.950416	0.950416	0.950416
25	HPC Eff	0.914184682	0.914031	0.91389	0.913762	0.91365	0.914185	0.914031	0.91389	0.913762	0.91365	0.914185	0.914031	0.91389	0.913762	0.91365
26	HPT Eff	0.89132	0.89132	0.89132	0.89132	0.89132	0.89132	0.89132	0.89132	0.89132	0.89132	0.89132	0.89132	0.89132	0.89132	0.89132
27	Fuel Burn	32323.31202	32207.91	32090.86	31972.25	31852.17	32230.88	32117.94	32003.42	31887.41	31769.98	32133.36	32022.67	31907.15	31790.64	31674.13
28	LTO Nox	18.65365591	19.42592	20.22361	21.04737	21.89796	19.37191	20.1678	20.98971	21.83838	22.71476	20.11108	20.93101	21.76194	22.59331	23.42468
29	EPNdB Noise	258.2043277	257.9234	257.6419	257.3601	257.0782	258.0087	257.7294	257.4498	257.1699	256.8901	257.814	257.5365	257.2587	256.9809	256.7031
30	FPR	1.25	1.25	1.25	1.25	1.25	1.25	1.25	1.25	1.25	1.25	1.25	1.25	1.25	1.25	1.25
31	LPCPR	1.8	1.8	1.8	1.8	1.8	1.9	1.9	1.9	1.9	1.9	2	2	2	2	2
32	HPCPR	16	17	18	19	20	16	17	18	19	20	16	17	18	19	20
33	Ext_Ratio	1.2	1.2	1.2	1.2	1.2	1.2	1.2	1.2	1.2	1.2	1.2	1.2	1.2	1.2	1.2
34	AR	10	10	10	10	10	10	10	10	10	10	10	10	10	10	10
35	Gear Ratio	3	3	3	3	3	3	3	3	3	3	3	3	3	3	3

**FIGURE 58: PARTIAL OUTPUT OF A SENSITIVITY SWEEP**

The outputs from this sweep can then be plotted in order to produce carpet plots which show the trends and relationships between the parameters and the CLEEN metrics. Two such graphs are shown below. Both graphs show Fuel Burn against EPNdB with one varying FPR and HPCPR and the other varying FPR and LPCPR.

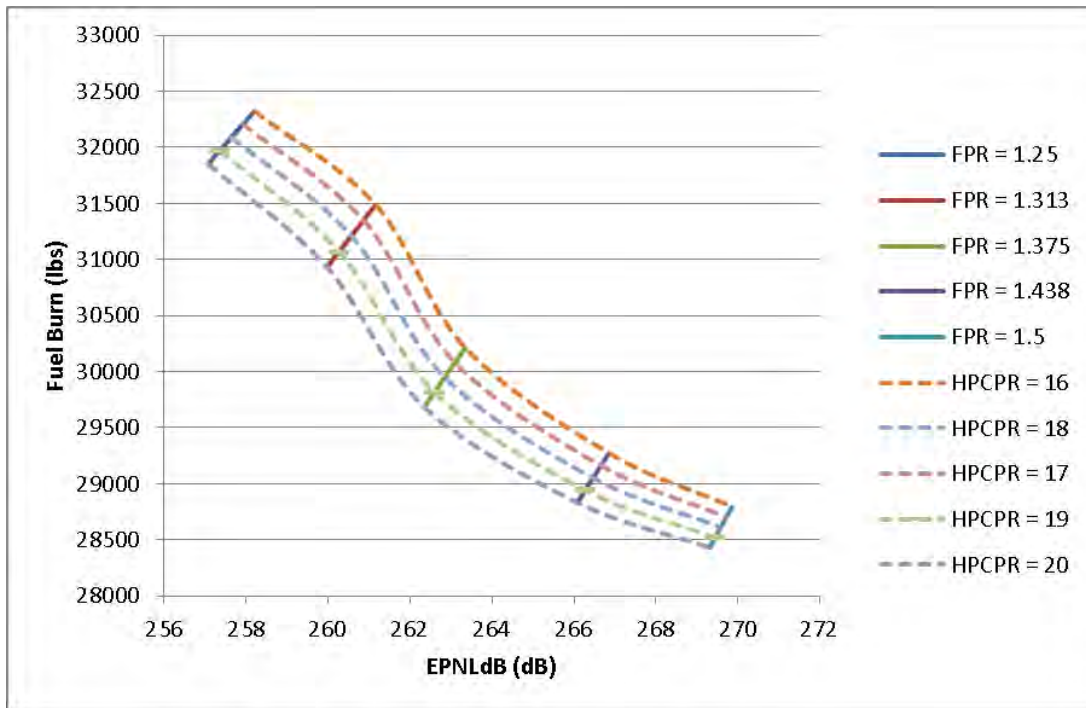


**FIGURE 59: CYCLE SWEEP FUEL BURN RESULTS WITH VARIED FPR AND HPCPR**

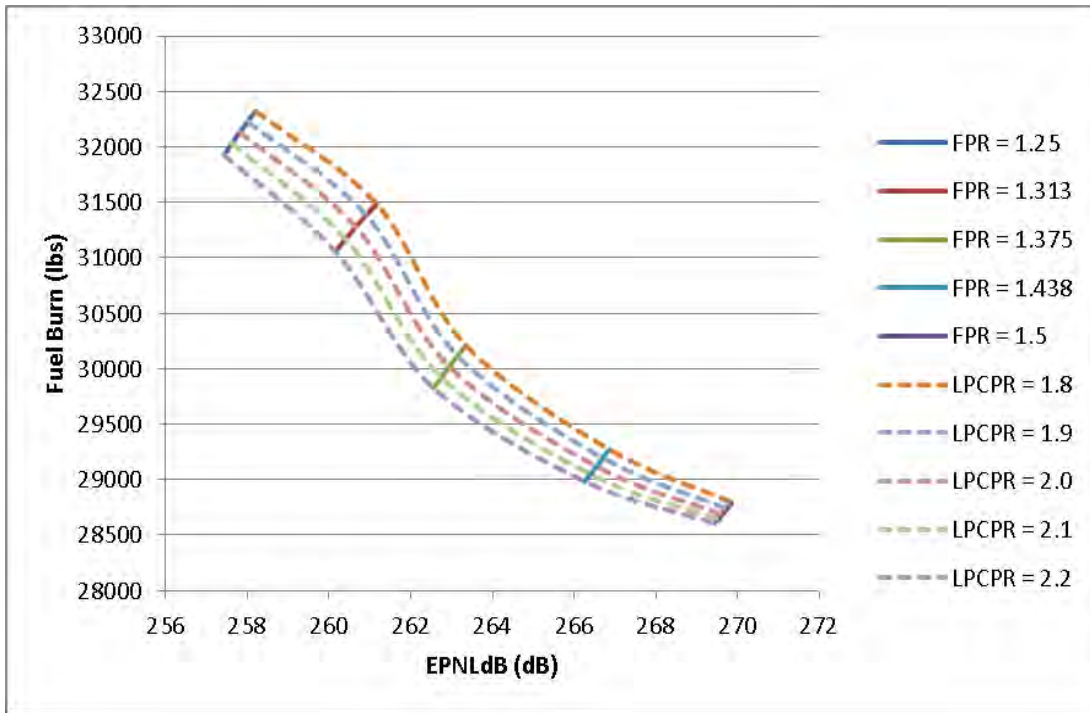


**FIGURE 60: CYCLE SWEEP FUEL BURN RESULTS WITH VARIED FPR AND LPCPR**

### 5.3.2 Multi-Attribute Decision Making (MADM)

Multi-Attribute Decision Making (MADM) techniques determine the best alternative based on a multi-attribute utility function that is closest to a hypothetical ideal solution. This is an analytic and deterministic approach for evaluating subjective, multiple criteria to aid in decision making. One such MADM technique is known as TOPSIS (Technique for Order Preference by Similarity to Ideal Solution). As the name implies, TOPSIS is a technique which ranks a set of alternatives based on their relative closeness to the ideal solution and distance from the negative ideal solution. The rankings are calculated by using preference in the form of weights for each criterion. The advantages of TOPSIS are its simplicity in terms of interface with the user as well as calculations, and its full utilization of all the data points available.

#### *TOPSIS Data Generation*

In order to perform TOPSIS, the sets of alternatives (in this case various technology combinations) and their various responses must be calculated. The dashboard can generate these sets for any group of 5, 10, 15, ..., 55, or all 58 technologies by using stored fractional factorial DOEs. These DOEs allow the dashboard to generate technology and cycle parameter combinations in order to understand the design space with fewer cases while exploring the entire design space. Once these different combinations have been generated, the dashboard calculates the responses from each different one. This data can then be saved for future use or explored immediately. To generate this data, first choose a group of technologies with 5, 10, 15, and up to 58 technologies in multiples of five. If choosing technology groups for multiple vehicles, the packages must be the same for each vehicle. It is recommended that the user saves the technology package under the “Technology Package Selection” header on the left-most side of

the Front End for records and later use (Figure 61). Enter a name for the saved package and then click the “Save” button. After this, go to the “TOPSIS” area (directly under the “Technology Package Selection”). In this area, enter a name for the data which will be generated. Next, click the different vehicles for which data will be generated. Click “Gen Data” in order to generate the TOPSIS Data (this could take several hours depending on the number of technologies selected). Finally click “Save Data” to save the data for later use. In order to visualize this generated data, first load the relevant data by choosing the name of the data set to be analyzed and viewed on the drop down menu and click the “Load” button.

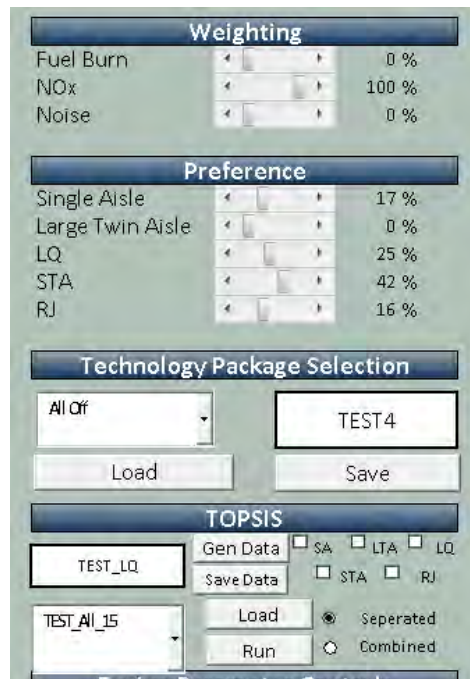


**FIGURE 61: AREAS OF TOPSIS FUNCTIONALITY ON THE DASHBOARD FRONT END**

### ***Applying TOPSIS Preferences and Visualizing Results***

Once the TOPSIS data has been generated and loaded, the user is ready to specify preferences by changing the parametric inputs in the “Weighting” and “Preference” sections (Figure 61). In these areas, the user can place a specified preference on each CLEEN metric and vehicle type. For example, a higher weighting for fuel burn will favor technology combinations which minimize fuel burn. The “Combined” or “Separated” option must be also chosen. The “Combined” option chooses the best global technology and cycle parameter combination based on the TOPSIS results and applies that combination to each vehicle class. Therefore, each vehicle class has the same technology package. The preference for certain vehicle classes is also incorporated in this section. A higher preference for a vehicle will make the technology combination which is the best for that vehicle more likely of being the best overall combination for all the vehicles. The “Separated” option finds the best combination based on the TOPSIS results for each individual vehicle. Therefore, the technology package chosen for each vehicle might be different. Finally, clicking the “Run” button finds the best package based on the preferences and options chosen and displays it by turning on each technology in the package technology selection area.

All of the different data points generated from the DOE of technology packages can be visualized using the scatterplot shown in Figure 62. This graph allows the user to visualize the technology impacts for all the generated technology package data. The data which the plot shows is customizable. The information displayed on each axis along with the vehicle type can be changed using drop down menus. The vertical (red) and horizontal (yellow) line are targets for that specific metric and are determined by the user using parametric slider bars. The best combination as determined by TOPSIS will be plotted as the “Top Point” in green on the scatterplot. The user-defined point, the current technology package in the technology selection area, shows up as blue. If the TOPSIS “Run” button has just been pressed then this blue and green point will coincide since the current technology selection will also be the top point. All other non-top combinations are displayed as grey dots to show the entire design space (Figure 62).

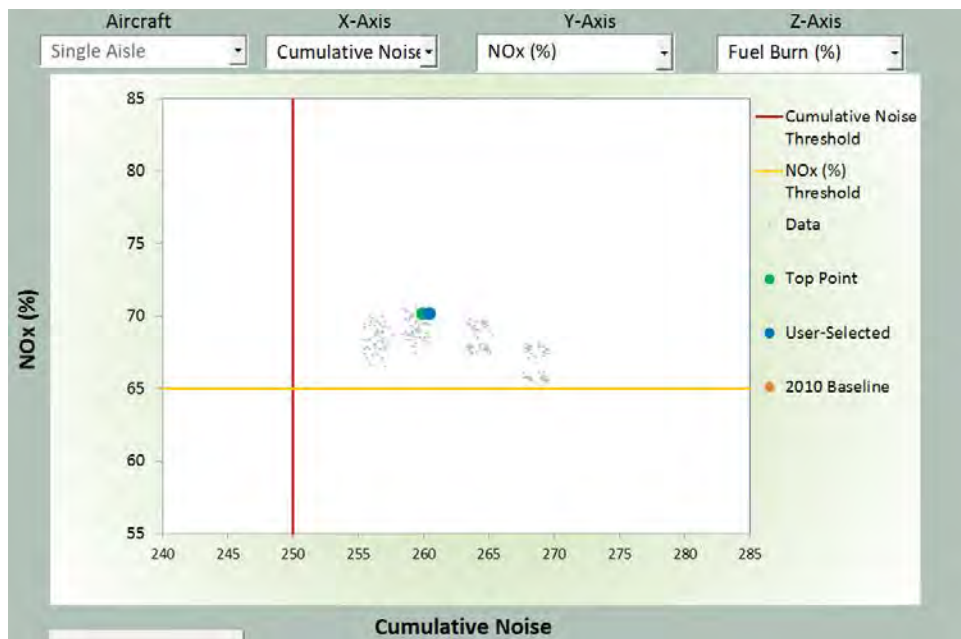


**FIGURE 62: SCATTER PLOT OF GENERATED DATA**

The scatterplot allows the visualization of two dimensional tradeoffs between the metric outputs of the dashboard. The radar plot, as seen in Figure 63, allows these same trades, but in a quasi-three dimensional plot which can display another metric (on the z-axis) chosen by the user. These axes can be rotated using slider bars positioned next to the radar plot. In this plot, the gray dots are all the generated data points while the blue and green dots which denote the user-selected and TOPSIS determined best point.

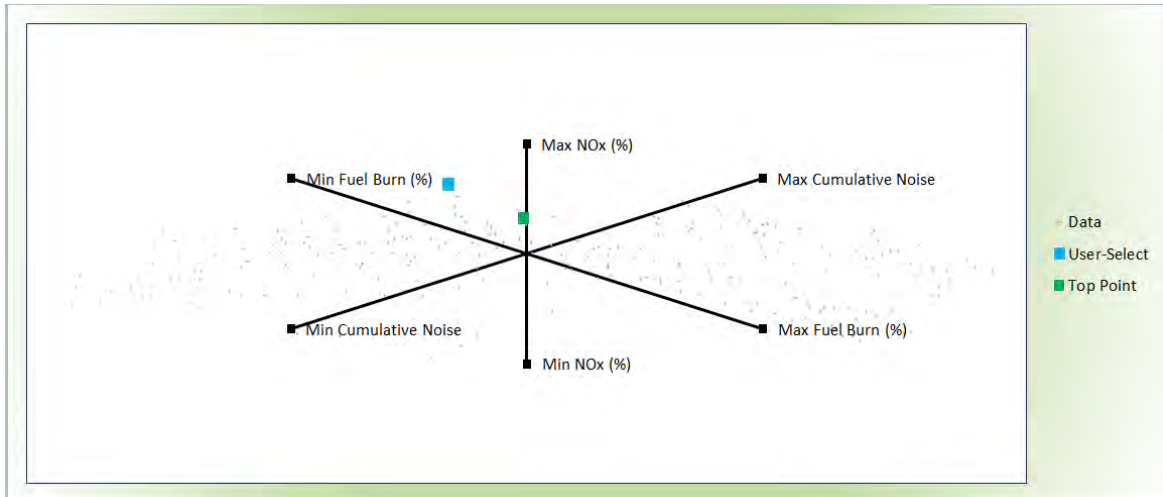


**FIGURE 63: RADAR PLOT OF GENERATED DATA**

## 6 Conclusions

PARTNER Project 36 has served as the primary vehicle for independently modeling and assessing the benefits of the CLEEN Program's aircraft technology investments. The effort modeled both public domain N+1 technologies, as well as a large number of the CLEEN funded aircraft technologies. These models formed a basis for vehicle and fleet-level assessment of the technologies' benefits. Although not all CLEEN funded technologies were captured in the modeling work conducted under this project, results indicate the modeled CLEEN technologies reduce fleet-level fuel burn by 2% from 2025 through 2050 resulting in a 22 billion gallon cumulative fuel burn savings by 2050. Additionally, the modeled CLEEN technologies help keep LTO NO<sub>x</sub> emissions close to 2006 levels, even as the number of forecast operations grows. It is expected that incorporation of operational improvements (via flight management systems / engine control technologies) and the open rotor, being developed by GE, as well as the acoustic benefits of Boeing's CMC nozzle, will show further increase in assessed benefits. However, it is important to note that these reductions only represent an incomplete set of the CLEEN technologies and a subset of all technology improvements that are likely to enter the fleet by 2050. For example, CLEEN Phase II technologies that are being considered at the writing of this report are not included and are expected to provide further benefits. These results demonstrate the strong potential of aircraft technology to affect aviation's future fleet fuel burn and NO<sub>x</sub> emissions.

The technology models developed under this effort provide an excellent basis for future aircraft technology modeling and assessment work, such as the Aviation Sustainability Center's (ASCENT) Project 10 – Technology Modeling and Assessment. This project will carry on modeling the remaining CLEEN technologies not captured under this project.

Finally, the Excel-based technology dashboard provides FAA with an in-house analysis capability for examining the impact of a large number of technologies on the five representative vehicle classes.

## Appendix A Preliminary EDS Geared Turbofan Comparison Study

### Appendix A.A Motivation

As part of the Phase II modeling work of the Pratt and Whitney (PW) Geared Turbofan, Georgia Tech was asked to validate and verify the capability of EDS to model such engine architectures. This study was completed in 2013 in order to give Pratt and Whitney confidence to move forward with further modeling of the second generation geared turbofan technologies being developed under the CLEEN Program. This comparison study focused on EDS as compared to NASA studies on geared turbofan architectures and is public domain. This study is documented below. Following completion of the comparison study and review with Pratt and Whitney, GT was able to begin modeling of PW's GF within EDS. This work is proprietary and not available for publication.

The EDS study conducted by Georgia Tech is a comparison between GT's EDS model and the GF study conducted by J. J. Berton and M.D. Guynn from NASA in 2011. The 2011 NASA study is published in the NASA Technical Memorandum (TM), TM-2011-216883, "Refined Exploration of Turbofan Design Options for an Advanced Single-Aisle Transport"[56]. Through thorough research of this TM, many of the modeling assumptions used by NASA were discovered. Some remaining discrepancies need to be resolved to bring the fan and nacelle weight prediction in line with NASA predictions. The thermodynamic cycle matching to NASA results is very good; however, there is some disagreement in the predicted fan diameter leading to overall differences in operating empty weight (OEW).

Initially, Georgia Tech was asked to look at the GF NASA study published in the 2010 AIAA conference paper and 2011 journal paper conducted by same authors of the 2011 NASA study:

- 1) "Multi-Objective Optimization of a Turbofan Design Parameters for an Advanced, Single-Aisle Transport" AIAA-2010-9168 [57]
- 2) "Multi-Objective Optimization of a Turbofan for an Advanced, Single-Aisle Transport" Journal of Aircraft Vol 48 No. 5, Sept-Oct 2011 [58]

In order to simulate the study conducted by NASA, the conference and the journal paper were examined and several more reports were utilized to fully capture the assumptions and approach:

- 1) "Engine Concept Study for an Advanced Single-Aisle Transport," NASATM-2009-215784, August 2009 [59]
- 2) "Analysis of Turbofan Design Options for an Advanced Single-Aisle Transport Aircraft," AIAA Paper 2009-6942, Sept. 2009 [60]
- 3) "An Analytical Assessment of NASA's N+1 Subsonic Fixed Wing Project Noise Goal," AIAA Paper 2009-3144, May 2009 [61]

Through these additional three reports, the majority of the assumptions used when modeling new technologies on the advanced single aisle transport were determined. However, in order to perform the exact same study, the interpretation of the assumptions and approach were discussed with the NASA authors. In the first conversation with NASA, it was discovered that modeling the EDS study after the 2010 conference paper [57] and 2011 journal paper [2] did not capture the latest revisions to the study conducted by NASA. Instead, the NASA TM2011 [56] summarized the most recent GF study performed. Once this report was examined, additional

conversations with NASA occurred to ensure the correct assumptions were applied. Many of the previous papers were still utilized in the research phase; however, any assumptions that were not explicitly explained within these reports were provided for by NASA, as depicted by Figure 64.

In order to validate and verify Georgia Tech’s model to the NASA published study, Georgia Tech’s results were compared to the magnitudes and trends of the 2011 NASA study. By applying the same vehicle and cycle parameters conducted in the NASA report, conclusions can be made about the similarity of the EDS model to NASA tools.

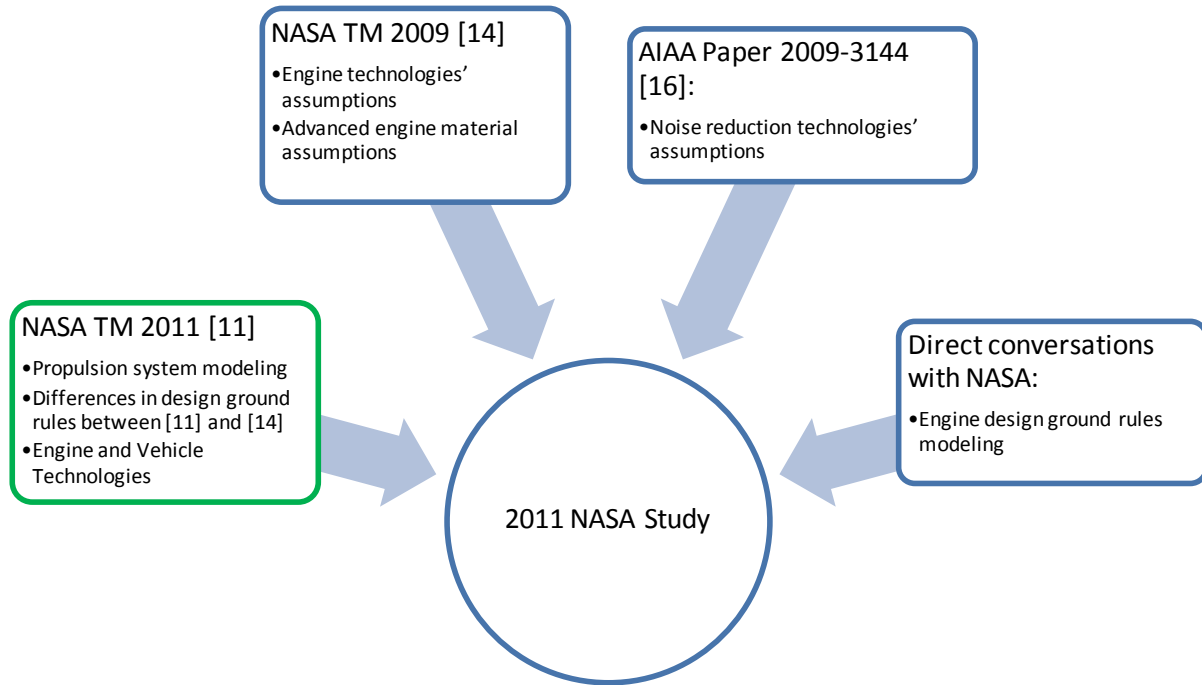


**FIGURE 64: FLOW OF INFORMATION FOR THE 2011 NASA STUDY**

### Appendix A.B 2011 NASA Study

The comparison study was based on the NASA TM report published in 2011 [3]. This report modifies the ground rules for engine design and assumptions from their prior study, “Engine Concept Study for an Advance Single-Aisle Transport”[59]. The NASA TM 2009 report is a comprehensive study of the turbofan engine design space by running 48 different engines. The NASA TM 2011 is a follow-on effort to enhance the assumptions previously used by running a subset of those original cases. Both studies explore the design space for an advanced technology single-aisle aircraft (ASAT), such as a 737/A320 class aircraft, in order to determine if the fuel consumption and noise benefits of engines having lower FPR (and high BPR) translate into overall aircraft system level benefits. The modifications between studies are summarized in Table 11.

**TABLE 11: REVISED ENGINE DESIGN GROUND RULES AND ASSUMPTIONS**

	NASA TM 2009 [4]	NASA TM 2011 [3]
<b>Engine Thrust Sizing</b>	ADP: 5,000 lb SLS: 23,000 lb	ADP: 5,000 lb SL, M=0.25; 17,500 lb
<b>Bypass Ratio</b>	Extraction Ratio of 1.25 at ADP	Jet Velocity Ratio of 1.6 at ADP
<b>Bypass Duct Losses</b>	Constant	Function of FPR
<b>Inter-Turbine Duct Losses</b>	Constant	Different assumptions for direct drive and geared fan architectures
<b>Turbine Cooling Philosophy</b>	LPT temperature limited to allow uncooled LPT	LPT cooling permitted
<b>LPT Adiabatic Efficiency</b>	Constant with constant LPT loading	Function of LPT cooling level
<b>HPT Design</b>	Single stage	Two stage

The study conducted supports the “N+1” goals from NASA [5]. An advanced single-aisle transport (ASAT) was chosen based on the technologies that provide the best opportunity to meet the goals for the next generation indicated in Table 12. These goals and technologies are applied to a Boeing 737-800 single-aisle aircraft. Improvements on the engine are also considered. The CFM56-7B, a 2-spool, separate flow turbofan, is used as the baseline system for comparison.

**TABLE 12: N+1 GOALS**

NASA Project goal metrics	N+1 goals
Fuel Burn	33% reduction
Noise	32 EPNdB under Chapter 4
Emissions	60% below CAEP/6
Ramp weight	minimize

A series of technologies for both the engine and vehicle were chosen based on a 2015 entry into service (EIS) target for the vehicle. Advanced noise reduction technologies, such as soft vane stators, or weight reduction technologies, such as composite construction, are applied to each of the 12 engines. A list of the technologies used in this study is indicated in Table 13.

**TABLE 13: NASA TM 2011 TECHNOLOGIES**

Engine Technologies	Vehicle Technologies
Variable geometry nozzle	Composite construction of primary structures
Soft vane stators	787-like improvements
Over-the-rotor foam metal treatment	Trailing edge variable camber and drag cleanup
Conventional inlet, interstage, and aft fan duct liners	Innovative slat cove designs
Geared turbofan	Flap porous tips
Advanced engine material for blades and stators	Landing gear fairings

In conjunction with the 2009 study, the 2011 study focused on varying four different cycle parameters between engine designs. The primary engine design parameters of interest were fan pressure ratio (FPR), fan drive system (direct drive versus geared turbofan) and compression system work split. FPR, which is inversely related to bypass ratio (BPR), varied from 1.4 to 1.7 for the direct drive engines and 1.3 to 1.6 for the geared turbofan engines. The compression work split maps to the pressure ratios for both the high pressure compressor (HPC) and low pressure compressor (LPC). The study considered a low and high work engine for the direct drive cases and a high work engine for the geared turbofan cases. A low work engine refers to when the LPT is producing less work than the HPT. This means that the LPC will have a relatively lower pressure rise. For the 12 runs conducted in this study a constant OPR of 42 is maintained. The engine cycle parameters vary for the 12 runs according to Table 14.

**TABLE 14: ENGINE TRADE SPACE**

	Fan Drive	Fan Nozzle	FPR	Work Split	LPCPR	HPCPR
1	Direct	Variable	1.4	Low Work	1.69	17.7
2	Direct	Fixed	1.5		1.58	17.7
3	Direct	Fixed	1.6		1.48	17.7
4	Direct	Fixed	1.7		1.39	17.7
5	Direct	Variable	1.4	High Work	2.50	12.0
6	Direct	Fixed	1.5		2.33	12.0
7	Direct	Fixed	1.6		2.19	12.0
8	Direct	Fixed	1.7		2.06	12.0
9	Geared	Variable	1.3	High Work	2.69	12.0
10	Geared	Variable	1.4		2.50	12.0
11	Geared	Fixed	1.5		2.33	12.0
12	Geared	Fixed	1.6		2.19	12.0

The study concludes with engine and vehicles comparisons between the high work direct drive engines, low work direct drive engines, and high work geared engines. Some general observations of the effect of FPR on different engine characteristics include:

1. A BPR of nearly 25 is observed with a FPR of 1.3
2. TSFC increases linearly with FPR
3. The work split or fan drive approach has no impact on the nacelle diameter
4. As FPR decreases, the fan diameter increases
5. There is a weight penalty for lower FPR
  - a) More severe penalty for direct drive due to the necessity of more LPT stages

### **Appendix A.C Approach/Assumptions**

In order to model the 12 different engines, the engine and vehicle technologies indicated within the 2011 NASA study were researched. The ground rules and assumptions were taken into account and used to adjust the EDS environment to ensure minimal differences from this study.

Prior to running these 12 cases with the technology impacts and assumptions researched, each point was discussed with NASA and updated according to their feedback.

### ***Engine Technologies***

The engine technologies, indicated in Table 13, map to specific impacts on the EDS inputs. It is important to model the technologies in the same way as the NASA study modeled them. For these technologies, the information necessary to model them were found in the NASA TM 2011 study, as well as “An Analytical Assessment of NASA’s N+1 Subsonic Fixed Wing Project Noise Goal” (Berton, Envia, 2009) and the NASA TM 2009 Study. Once the description of the impact of a specific technology was acquired, the impact was mapped to EDS. Table 15 describes the advanced noise technologies for the engine, as well as the impact of the variable area nozzle and the geared turbofan. The “Impact” column indicates the EDS input that is impacted from that specific technology. The “Refined” column shows the updated value for each technology impact based on NASA reports and feedback. Technologies 2-4 within the table are advanced noise technologies that are applied on each of the 12 cases. Variable area nozzle and the geared turbofan are switches that are varied throughout the 12 cases. Only when these technologies are “turned on” will the “Refined” value be used.

Advanced material for the engine stators and vanes were also applied to each of the 12 cases. The NASA TM 2009 study goes into detail on the material used and where the material was applied. Using this information, the corresponding EDS input variable was chosen. In order to “apply” an advanced material, the material density of that component was changed. For instance, polymer matrix composites were applied to the fan blade, fan vane, and inlet/nacelle case. Therefore, the material density of these components was changed to show that effect. The five advanced materials and their locations are indicated in Table 16. The value in the “Refined” column was directly provided by NASA to ensure that the same densities of these materials were used.

**TABLE 15: ENGINE NOISE TECHNOLOGIES**

	Technology	Impact	Input name	Baseline	Refined	Units	Description	
1	<b>Variable geometry nozzle</b> <sub>[1]</sub>	Byp_Nozz_s_Wt	Bypass Nozzle weight scalar	1	1.1		10% weight penalty relative to equivalent fixed-geometry design	
2	<b>Soft vane stators</b> <sub>[6]</sub>	DISAP	Suppression Factor on Fan Discharge Noise	0	-4	dB	System level decrement of -4 dB was applied to the freefield hardwall fan source noise predictions made by ANOPP, applied as a simple constant to the predicted fan sound pressure levels across all 1/3rd octave band frequencies, directions, and throttle settings	
		DISTO	Suppression Factor on Fan Discharge Noise	0	-4	dB		
3	<b>Over-the-rotor foam metal treatment</b> <sub>[6]</sub>	INLAP	Suppression Factor on Inlet Noise	0	-4	dB		
		INLTO	Suppression Factor on Inlet Noise	0	-4	dB		
4	<b>Conventional inlet, interstage, and aft fan duct liners</b> <sub>[4]</sub>	Apply an acoustic suppression map of 1/3rd octave band sound pressure level decrements to the hardwall fan source spectra, based on measured acoustic data of 22-in diameter fan						
5	<b>Geared Turbofan</b> <sub>[4]</sub>	GearBoxLosses	Percent Losses from Gearbox - Applied to LP shaft	0	0.01			Gearbox mechanical efficiency of 99%

**TABLE 16: ADVANCED ENGINE MATERIAL ASSUMPTIONS**

	Advanced Material	Impact	Input Name	Baseline	Refined	Units
1	Polymer Matrix Composite <sub>[3]</sub>	Inl_Nacelle_rho	Inlet Nacelle Material density	0.098	0.06	lbm/in <sup>3</sup>
		Fan_Blade_rho	Fan Blade Material density	0.092	.097	lbm/in <sup>3</sup>
		Fan_Stator_rho	Fan Stator Material Density	0.1	.06	lbm/in <sup>3</sup>
2	Polymer Matrix Composite wrapped by Zylon <sub>[3]</sub>	Fan_Case_rho	Fan Case Material density	0.1	.06	lbm/in <sup>3</sup>
3	Titanium Aluminide <sub>[3]</sub>	LPC_Blade_rho	LPC Blade Material density	0.168	.145	lbm/in <sup>3</sup>
		LPC_Stator_rho	LPC Stator Material density	0.168	.145	lbm/in <sup>3</sup>
		HPC_Blade_rho	HPC Blade Material density	0.168	.168	lbm/in <sup>3</sup>
		HPC_Stator_rho	HPC Stator Material density	0.168	.168	lbm/in <sup>3</sup>
		HPC_Blade2_rho	HPC rear Blade Material density	0.297	.145	lbm/in <sup>3</sup>
		HPC_Stator2_rho	HPC rear Stator Material density	0.297	.145	lbm/in <sup>3</sup>
4	5 <sup>th</sup> generation nickel-based alloy <sub>[3]</sub>	HPT_Blade_rho	HPT Blade Material density	0.312	.308	lbm/in <sup>3</sup>
		HPT_Stator_rho	HPT Stator Material density	0.312	.308	lbm/in <sup>3</sup>
		LPT_Blade_rho	LPT Blade Material density	0.313	.308	lbm/in <sup>3</sup>
		LPT_Stator_rho	LPT Stator Material density	0.313	.308	lbm/in <sup>3</sup>
5	Nickel-based powder metallurgy alloy <sub>[3]</sub>	HPT_Disk_rho	HPT Disk Material density	1	.299	lbm/in <sup>3</sup>
		LPT_Disk_rho	LPT Disk Material density	1	.299	lbm/in <sup>3</sup>

### **Vehicle Technologies**

The vehicle technologies in Table 18 were applied to change the baseline Boeing 737-800 into an advanced single-aisle transport vehicle. It was decided that a number of technologies used for the newer Boeing 787, produced starting in 2007, should be applied. These technologies were composite materials for primary structures, an increase in hydraulic pressure, and trailing edge variable camber and drag cleanup. It was assumed that the composites would reduce the component weights for wing, fuselage, and empennage by 15%. Therefore, the weight factor for each component was changed from the baseline value of 1 to the refined value of 0.85. The trailing edge variable camber and drag cleanup was used to assume a 1% reduction in overall drag. Finally, three noise reduction technologies were applied: innovative slat cove design, flap porous tips, and landing gear fairings. The impacts of these technologies were found in the NASA TM 2009. Each noise technology has a deduction on its source noise. For instance, the innovative slat cove design is modeled with a 4 db deduction from the leading edge slat approach noise. These technologies and their impacts, summarized in Aircraft Sizing Changes were also made to the vehicle to account for the projected performance enhancements. As previously mentioned, the cruise Mach number was increased to 0.8. To reflect the higher cruise Mach number, the wing sweep was slightly increased. Lastly, the design range was increased while maintaining the same maximum payload. These improvements in airspeed and range are considered appropriate for a future vehicle in this class.

**TABLE 17: VEHICLE DESIGN MISSION**

	<b>Assumption</b>	<b>Input</b>	<b>Baseline</b>	<b>Refined</b>	<b>Units</b>
1	Cruise Mach number <sub>[1]</sub>	ADP_Mn	0.785	0.8	
2	Wing quarter-chord sweep <sub>[1]</sub>	SWEEP	25	27	deg
3	Design range <sub>[1]</sub>	DESRNG	3060	3250	nm
4	Payload <sub>[1]</sub>		32,400	32,400	lb

**TABLE 18: VEHICLE ASSUMPTIONS**

	Technology	Impact	Input name	Baseline	Refined	Units	Description
1	<b>Composite construction of primary structures</b> <sub>[1]</sub>	FRFU	Fuselage weight factor	1	0.85		Assumed a 15% reduction in the component weights for wing, fuselage, and empennage
		FRHT	Horizontal tail weight	1	0.85		
		FRVT	Vertical tail weight	1	0.85		
		FRWI	Total wing weight	1	0.85		
2	<b>787 additional improvements</b> <sub>[2]</sub>	HYDPR	Hydraulic pressure	3000	5000	psi	
3	<b>Trailing edge variable camber and drag cleanup</b> <sub>[4]</sub>	FCDI	Lift dependent drag factor	1	0.99		1% reduction in drag
4	<b>Innovative slat cove designs</b> <sub>[4]</sub>	LESAP	Suppression Factor on Leading Edge Slats	0	-4	dB	Modeled with a -4 dB across all frequencies and directions from the freefield 1/3rd octave band sound pressure levels for flap and slat noise
5	<b>Flap porous tips</b> <sub>[4]</sub>	TEFAP	Suppression Factor on Trailing Edge Flap	0	-4	dB	
		TEFCB	Suppression Factor on Trailing Edge Flap	0	-4	dB	
6	<b>Landing gear fairings</b> <sub>[4]</sub>	MGRAP	Suppression Factor on Main Landing Gear	0	-3	dB	Modeled with -3 dB from the Fink gear method prediction for all directions but only above 250 Hz
		NGRAP	Suppression Factor on Nose Landing Gear	0	-3	dB	

### **Revised Engine Design Ground Rules and Assumptions**

A number of assumptions were also taken into consideration when modeling the 12 cases. Table 19 summarizes these assumptions. The assumptions used in the NASA TM 2011 were researched further in order to replicate. For this study, the engine was sized to two points: top-of-climb (TOC) and a rolling takeoff (TO). The Aerodynamic design point was considered to be TOC with a Mach number of 0.8, altitude of 35,000 ft and 5,000 lb thrust. The rolling TO condition is set by changing the TO thrust to 17,500 lb and the Mach number to 0.25. The 2011 NASA study uses these two points to size the engine and then receive the thrust for the sea level static (SLS) condition. In order to receive similar results, the SLS thrust was set to the 2011 NASA study output for this value, indicated in the final column of Table 19.

**TABLE 19: ENGINE THRUST SIZING**

	Fan Drive	Work Split	FPR	TOC_Thrust [lb]	TO_Thrust [lb]	SLS_Thrust [lb]
<b>1</b>	Direct	Low	1.4	5000	17,500	23813
<b>2</b>	Direct	Low	1.5	5000	17,500	23370
<b>3</b>	Direct	Low	1.6	5000	17,500	23046
<b>4</b>	Direct	Low	1.7	5000	17,500	22734
<b>5</b>	Direct	High	1.4	5000	17,500	24915
<b>6</b>	Direct	High	1.5	5000	17,500	23365
<b>7</b>	Direct	High	1.6	5000	17,500	22920
<b>8</b>	Direct	High	1.7	5000	17,500	22561
<b>9</b>	Geared	High	1.3	5000	17,500	26343
<b>10</b>	Geared	High	1.4	5000	17,500	24917
<b>11</b>	Geared	High	1.5	5000	17,500	23369
<b>12</b>	Geared	High	1.6	5000	17,500	22924

BPR, which is an output of the study, is usually set by the extraction ratio (ratio of total pressures for bypass nozzle and core nozzle). This study sets BPR by iterating until a jet velocity ratio ( $V_{core}/V_{bypass}$ ) constraint of 1.6 is met. Unlike the technology impacts and assumptions discussed thus far, this must be set by changing how the BPR is calculated within the model. Instead of extraction ratio, the velocity ratio is set as the dependent variable for BPR.

The losses created at the bypass duct are also modeled differently than the 2009 NASA study. Previously bypass duct losses were set at the same value for each of the types of engines. However, due to the large variation in geometry and flow conditions for the different engines, variation in duct losses should be expected. Therefore, these losses were modeled as a function of FPR. NASA provided the exact pressure losses used for varying FPR values (Table 20).

**TABLE 20: BYPASS DUCT PRESSURE LOSS AS A FUNCTION OF FPR**

FPR	delP
	Duct 15 pressure drop
<b>1.3</b>	0.005
<b>1.4</b>	0.010
<b>1.5</b>	0.015
<b>1.6</b>	0.020
<b>1.7</b>	0.025

Another difference accounted for in the 2011 NASA study is the consideration of varying turbine geometries between a direct drive and a geared turbofan. The direct drive engines have a larger radial variation for the turbines, which will lead to higher inter-turbine duct pressure losses. NASA used a pressure drop of 0.01 for the direct drive and a pressure drop of 0.005 for the geared engine. These numbers were also provided through conversations with NASA.

The turbine cooling philosophy was also revised. The original constraint of an uncooled LPT was removed. For the high work engines there were higher HPT exit temperatures, which made the constraint of an uncooled LPT hard to reach. Instead, a cooling analysis was performed for each engine to determine how much cooling air is needed in order to maintain acceptable temperatures for the HPT and LPT. To do this NASA provided the HPT and LPT technology inputs and blade and vane temperatures. These values are constant between all 12 engines. It was now necessary to base the LPT adiabatic efficiency on this cooling analysis. To calculate the new efficiency based on the cooling the difference between the “uncooled efficiency” and “ideal cooled efficiency” was subtracted from the baseline value of 0.94. Due to minimal amount of actual cooling, the value 0.9377 was set for all engines.

The fan, HPC, and LPC polytropic efficiencies were also set by NASA. Indicated in the 2009 TM, the fan polytropic efficiency was calculated as a function of FPR. This function was based on the Georgia Tech curves for advanced technology; however, a slight adjustment was made to reflect these advanced technology capabilities with an entry into service date of 2015. The curve that was utilized for the fan polytropic efficiency is shown in Figure 65. The efficiency was adjusted to model these changes in efficiency. The NASA TM in 2009 also specifies that the HPC and LPC polytropic efficiency was kept constant at 0.91 and 0.89, respectively. These values were verified with NASA to ensure that they were also used in the 2011 NASA Study.

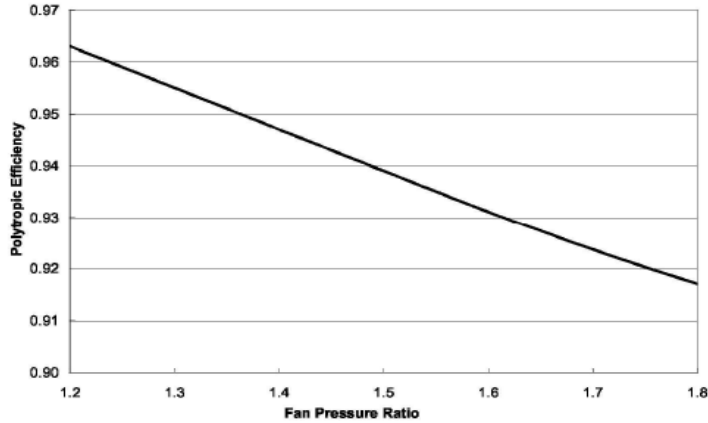


**FIGURE 65: VARIATION IN FAN EFFICIENCY WITH PRESSURE RATIO AT ADP (TOC) CONDITIONS [61]**

Lastly, an assumption was made that the HPT will have 2 stages. This was based on more likely industry design for this component.

#### **Appendix A.D Study Analysis**

Once all of the necessary modeling assumptions were understood, the same 12 case study was conducted using EDS. Preliminary results are shown in Figure 66-Figure 76. These ten metrics compared between the 2011 NASA Study, as indicated by the points, and the EDS study conducted by Georgia Tech, as indicated by the dashed lines, were chosen based on the results that were shown in the NASA TM 2011 [3]. The engines modeled are split into three sets, with varying color, in order to compare engines of the same type: direct drive with a low work split, case 1-4, direct drive with a high work split, case 5-8, and geared turbofan with a high work split, case 9-12.

The EDS study’s preliminary results compare well to the 2011 NASA study. It should be worth noting that while there are slight discrepancies in the magnitude of the EDS response, the slope is in good agreement. In order to match the engine precisely, three parameters from the 2011 NASA TM were used as inputs. The bypass ratio is set to the values presented in the 2011 NASA TM. In the 2011 NASA study, this value is varied by setting the velocity ratio to 1.6; however, this method can lead to a multi-modal answer due to the choking in the core nozzle during sizing. In the same manner, the 2011 NASA study Thrust-to-Weight ratio results were used as direct vehicle sizing inputs. Matching thrust to weight ensures consistency between vehicle sizing assumptions and thereby fuel burn.

As the engines were sized in EDS an engine weight discrepancy was discovered between the EDS and NASA results. The difference was due to LPC and LPT stage prediction for low values of FPR due to different values for allowable stage loading. At low fan (N1) RPM, low rotational speeds and constant aerodynamic loading limitations, more LPC and LPT stages are required to perform the same pressure rise or expansion. Once this weight discrepancy was discovered, the EDS study used the NASA study LPC, HPC, and LPT stage counts in order for EDS to size the

engine accordingly. These stage counts were obtained directly from NASA personnel and are summarized in Table 21.

**TABLE 21: NASA STUDY LPC, HPC, AND LPT STAGE COUNT**

	Fan Drive	Work Split	FPR	LPC Stages	HPC Stages	LPT Stages
<b>1</b>	Direct	Low	1.4	6	9	13
<b>2</b>	Direct	Low	1.5	3	9	8
<b>3</b>	Direct	Low	1.6	2	9	5
<b>4</b>	Direct	Low	1.7	2	9	4
<b>5</b>	Direct	High	1.4	14	8	15
<b>6</b>	Direct	High	1.5	9	8	12
<b>7</b>	Direct	High	1.6	5	8	8
<b>8</b>	Direct	High	1.7	4	8	6
<b>9</b>	Geared	High	1.3	3	8	3
<b>10</b>	Geared	High	1.4	3	8	3
<b>11</b>	Geared	High	1.5	3	8	3
<b>12</b>	Geared	High	1.6	3	8	3

In the remaining seven plots, slight differences in magnitudes between the 2011 NASA study and the EDS study values can be observed; however, the trends or slopes are very similar. For thrust specific fuel consumption (TSFC), Figure 67, the same linear trend is observed with a very small percent difference between the EDS study and the NASA study (~0.05%). The fan diameter, the length from the tip of one fan blade to the other, is compared in Figure 68 and the nacelle diameter, the fan diameter including the nacelle out mold line and curvature, is compared in Figure 69. The fan diameter’s slope and magnitude is consistent with the NASA study; however, the EDS study resulted in lower magnitudes for the nacelle diameter, at about a 7-9% difference from NASA’s study. The percent differences are consistent throughout all of the cases, which indicate that the EDS study results is simply an offset from the NASA study. This is due to the differences in the version of WATE between the EDS study and the NASA study.

The engine plus nacelle weight, shown in Figure 70, indicate very close results for all three engine sets. Due to the close results in engine plus nacelle weight, the trends propagate through to the operating empty weight (OEW), Figure 72, and ramp weight, Figure 73. All three weight parameters match close in magnitude and trend to NASA’s study.

Finally, the two metrics that NASA specifies in the “N+1” goals, fuel burn and NO<sub>x</sub> emissions, are compared in Figure 74 and Figure 75, respectively. This fuel burn is much lower in magnitude than the NASA study. This difference was interesting because there is little to no difference between the two studies for engine plus nacelle weight, operating engine weight, or ramp weight. Therefore, the difference must be attributed to how the mission analysis is run through FLOPS. For instance, the mission can be run at a constant altitude, contain a cruise climb or a step cruise. The mission profile used in the EDS study contains different assumptions from NASA for the climb ceiling during cruise climb. In order to test this, the EDS study ran the 12 cases again without the step cruise segment in the mission profile. All the previous parameters discussed returned with no change; however, fuel burn resulted in a higher magnitude than the

NASA study, shown in Figure 75. Although the magnitudes are higher, the slopes are more comparable to NASA's trends. Without inputting the exact mission profile, the fuel burn values will exhibit a difference compared to the NASA study. Lastly, Figure 76, expresses the landing-takeoff cycle  $\text{NO}_x$  as an engine parameter "Dp/Foo". This is the number of grams of  $\text{NO}_x$  emitted over a standard LTO cycle divided by the rated output at SLS conditions. The emissions are estimated as lower magnitudes than the NASA study, but the linear slope is still in agreement with NASA's results.

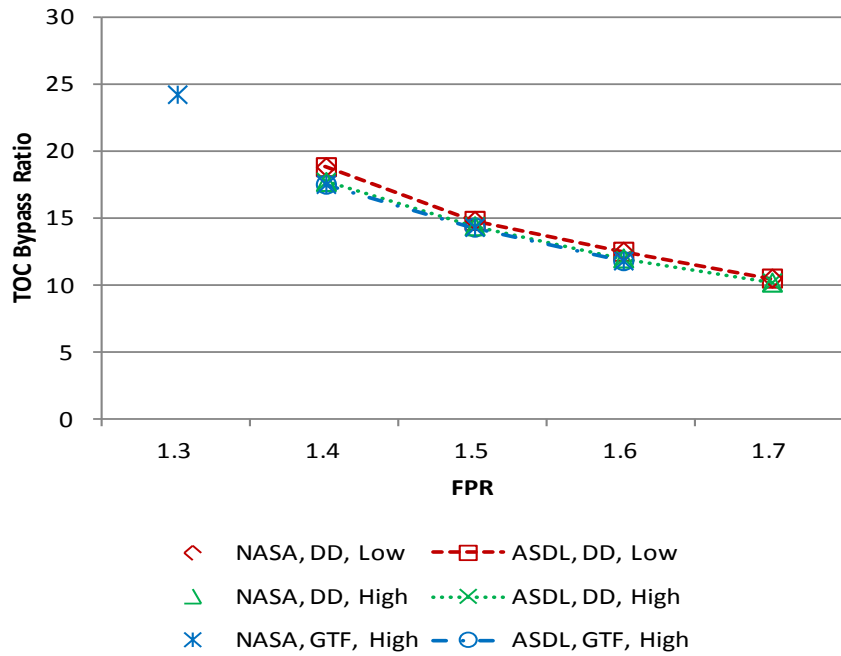


**FIGURE 66: TOP-OF-CLIMB BYPASS RATIO (BPR) VS. FPR COMPARISON**

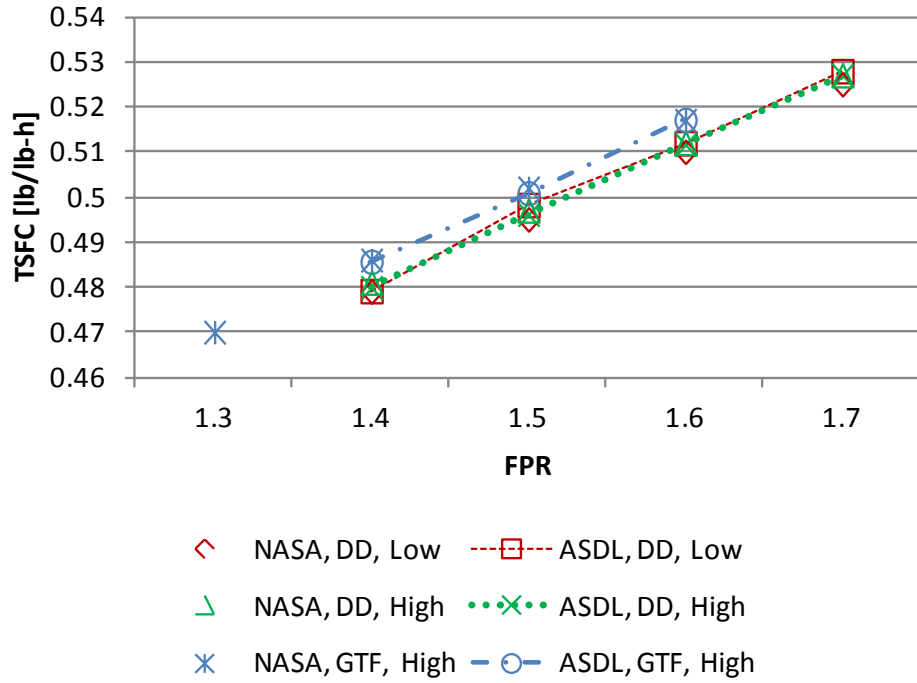


**FIGURE 67: THRUST SPECIFIC FUEL CONSUMPTION (TSFC) VS. FPR COMPARISON**

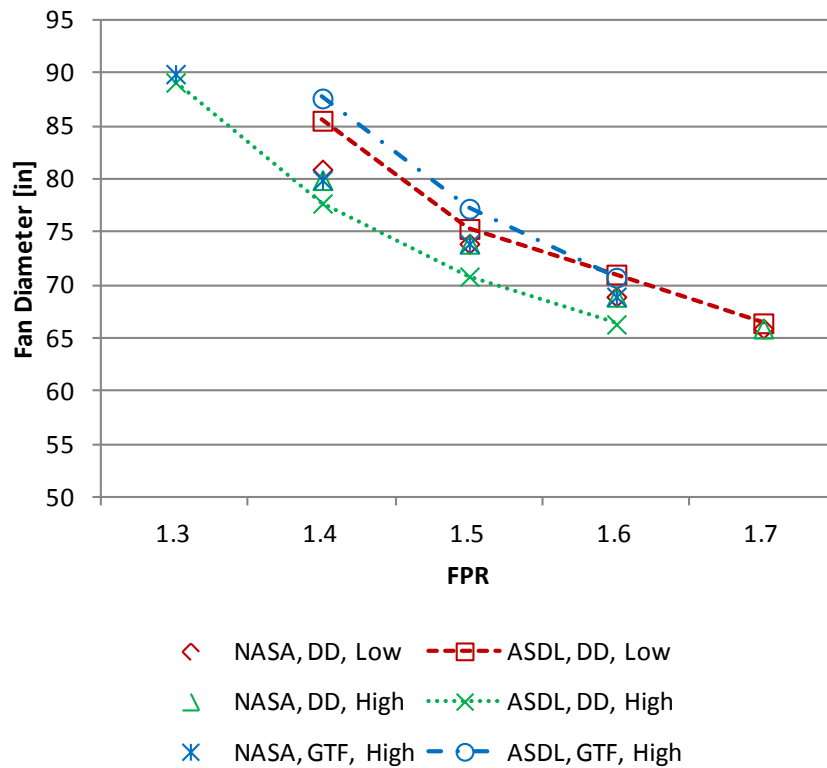


**FIGURE 68: FAN DIAMETER VS. FPR COMPARISON**

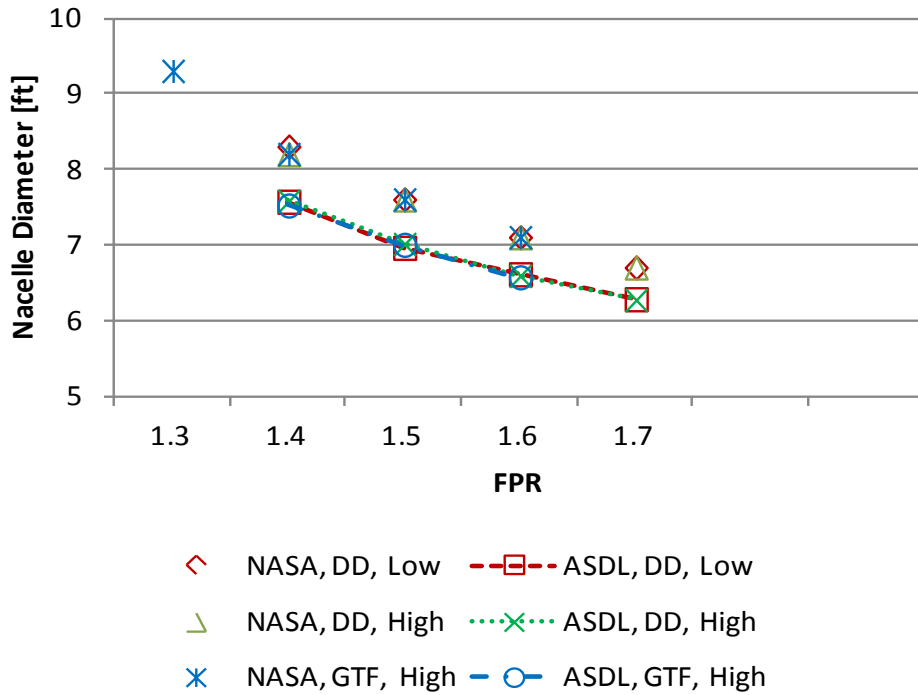


**FIGURE 69: NACELLE DIAMETER VS. FPR COMPARISON**

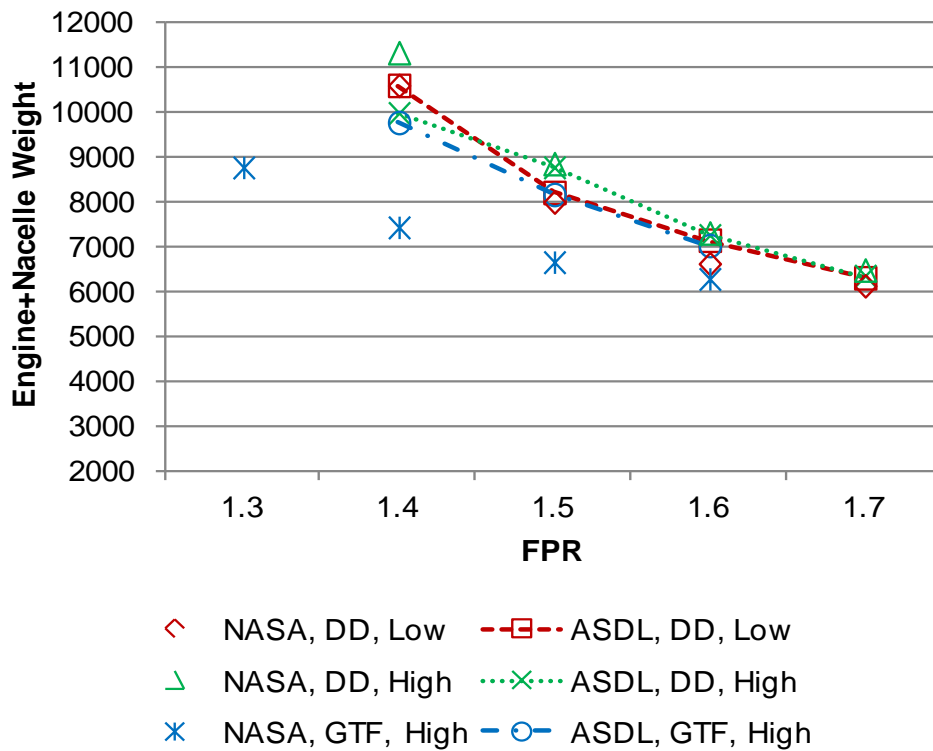


**FIGURE 70: ENGINE + NACELLE WEIGHT [LB] VS. FPR COMPARISON**

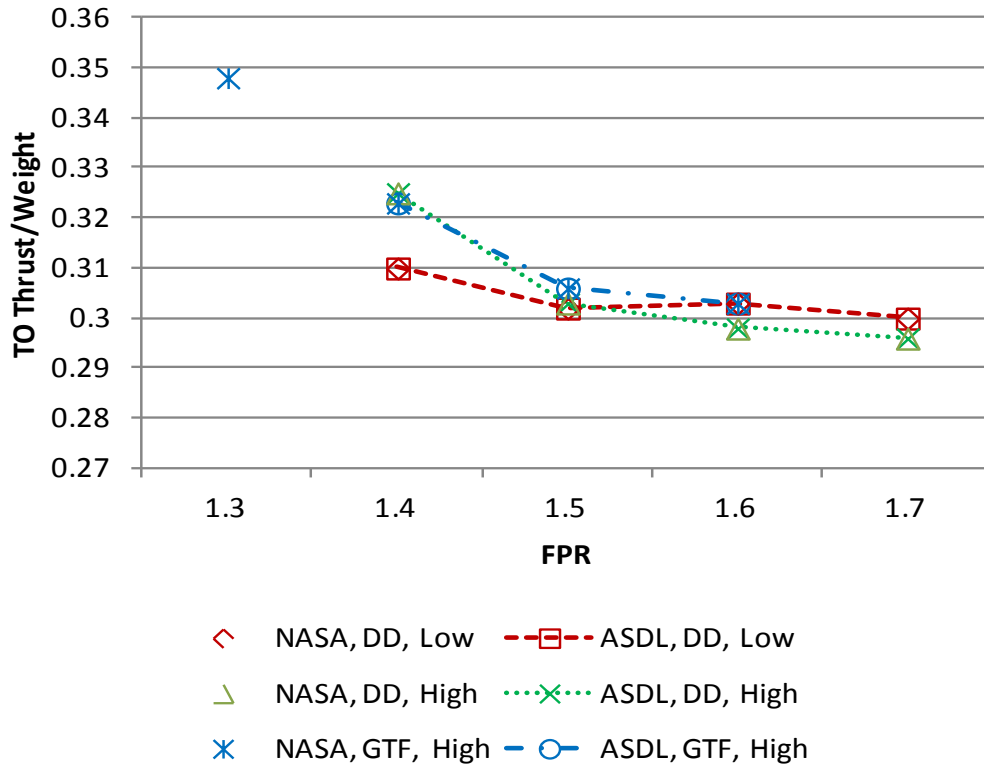


FIGURE 71: THRUST-TO-WEIGHT RATIO VS. FPR COMPARISON

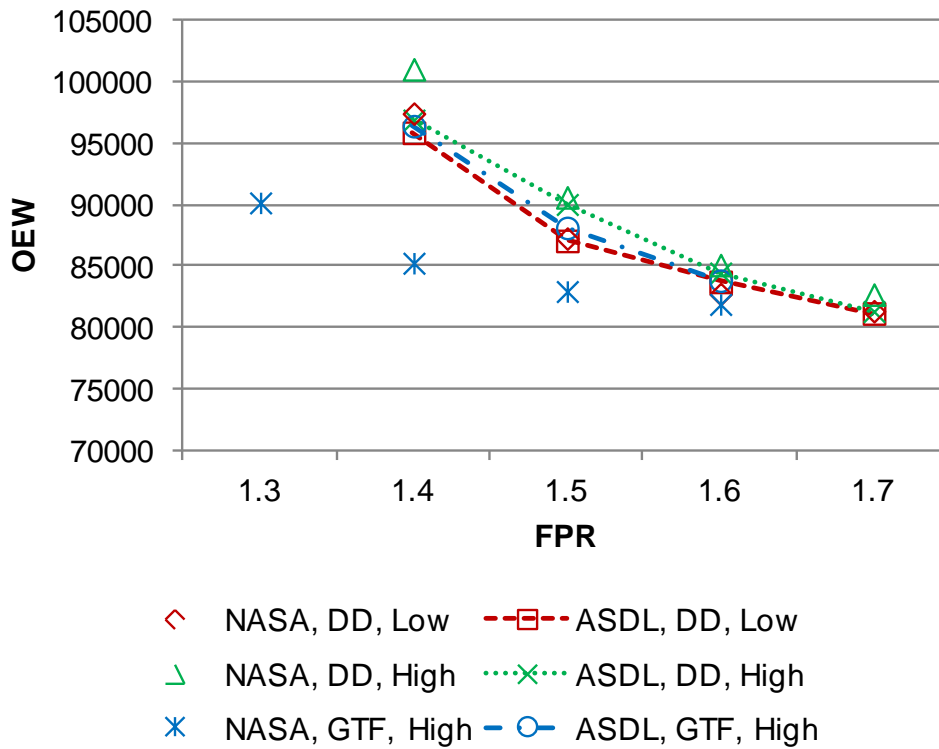
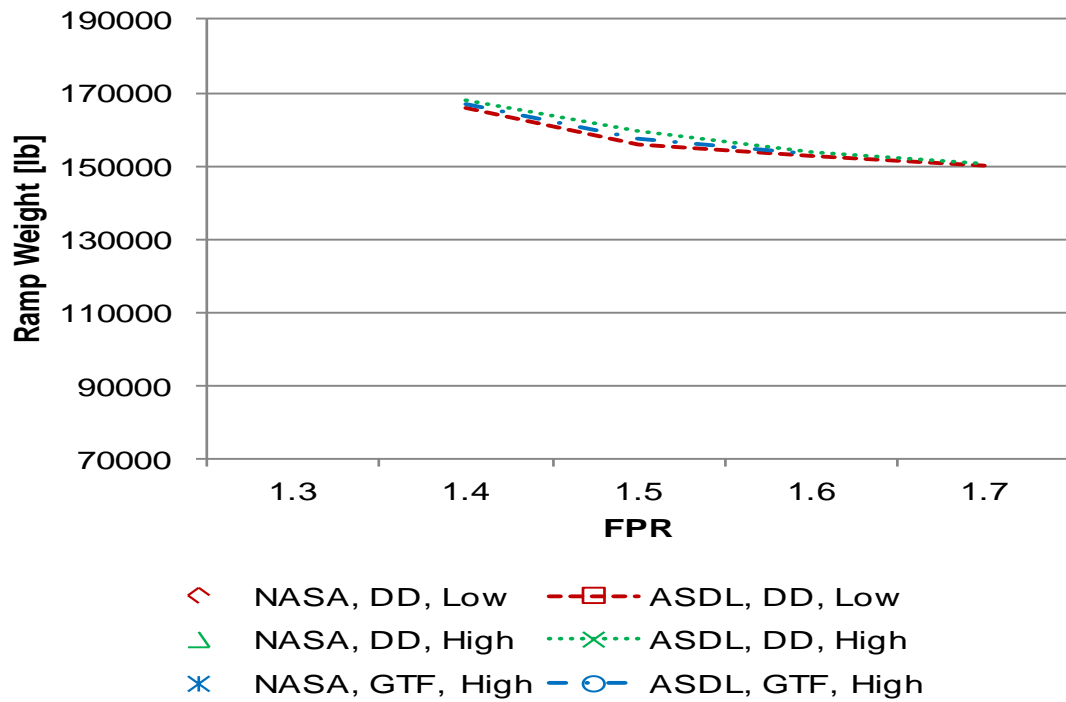
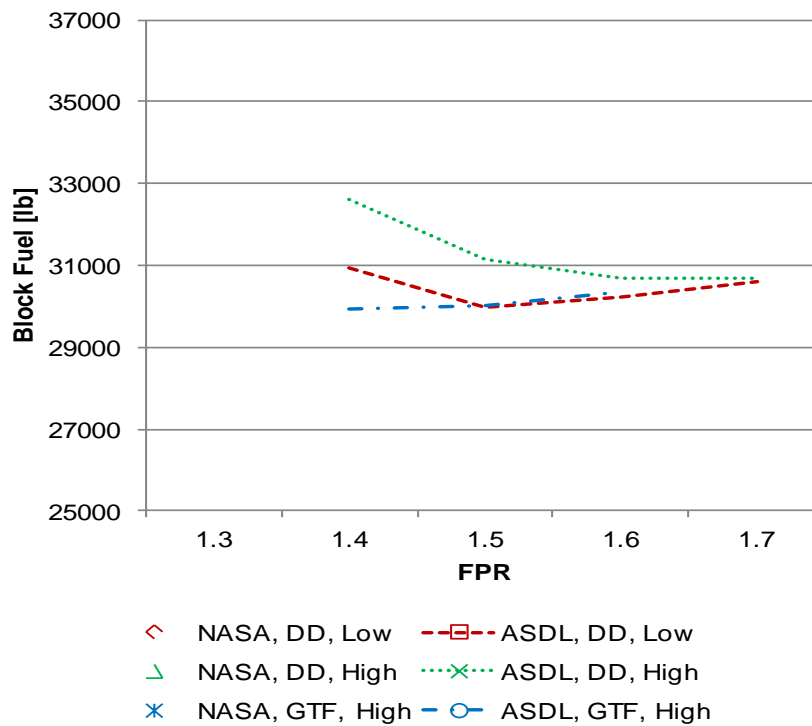


FIGURE 72: OPERATING ENGINE WEIGHT VS. FPR COMPARISON



**FIGURE 73: RAMP WEIGHT VS. FPR COMPARISON**



**FIGURE 74: FUEL BURN VS. FPR COMPARISON WITH STEP CRUISE ON**

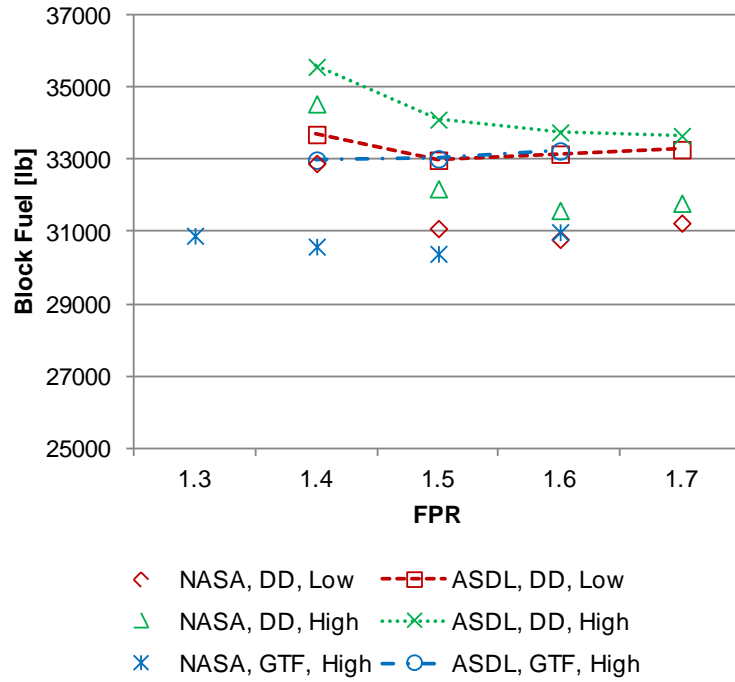


**FIGURE 75: FUEL BURN VS. FPR COMPARISON WITH STEP CRUISE OFF**

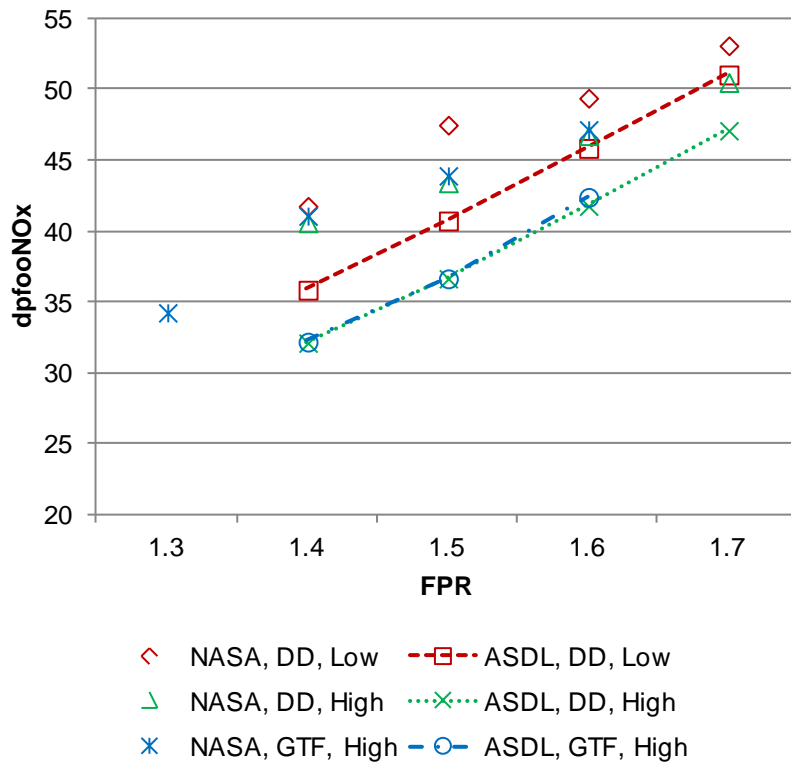


**FIGURE 76: NO<sub>x</sub> PER UNIT THRUST [KG/KN] VS. FPR COMPARISON**

## Appendix B Historical Technology Trends

### Appendix B.A Motivation

To get a better insight of what technologies might be expected to see in the future as well as how proposed ideas for CLEEN II might fit into technology trends; a historical trend literature review was conducted for a number of quantified metrics. The goal was to uncover if any innovations had broken trends in the past and determine if that is a possibility for the future.

### Appendix B.B Approach

Georgia Tech's approach to the task was to create a database of quantified trends for a set of parameters requested by the FAA. GT and the FAA iterated on a list of higher level metrics that could be found in published data and be able to depict certain technologies' effect. Table 22 lists the higher level metrics where actual numbers were able to be found within manufacturers' data, press releases, journal articles, or conference papers. With data points, the high level metrics were able to be plotted for different aircraft classes in order to see the change over time but also for different size vehicles.

**TABLE 22: HIGH LEVEL METRICS FOR HISTORICAL TREND RESEARCH**

High Level Metrics		
$\frac{\text{Fuel Burn}}{\text{Payload} * \text{Range}}$	MTOW	$\frac{\text{Empty Weight}}{\text{Gross Takeoff Weight}}$
$\frac{\text{Empty Weight}}{\text{Payload Weight}}$	$\frac{L}{D}$	Rated Output
$\frac{\text{Engine Weight}}{\text{Thrust}}$	TSFC	Cumulative Noise
OPR	BPR	Noise Margin

### Appendix B.C High Level Trends

The high level data was compiled into one database. The information came from the International Civil Aviation Organization (ICAO) Engine Emissions, Aviation Week Gas Turbine Engine Survey and Noise Certification Database. For each database the data was recorded for different aircraft. Each aircraft was then categorized by the 5 different aircraft classes: Large Quad (LQ, 400 passengers), Large Twin Aisle (LTA, 300 passengers), Small Twin Aisle (STA, 210 passengers), Single Aisle (SA, 150 passengers) and Regional Jet (RJ, 50 passengers). Prior to using these numbers to plot trends, 10% of the database was cross-checked with the manufacturers' datasheets in order to ensure its validity. The error between the database and the manufacturer's datasheets were between 0 and 4%. Five plots (one per each aircraft class) were created for each of the metrics in Table 22. A trend line was then fitted to determine the percent change per year for each vehicle class. Table 23 summarizes the percent change for each vehicle and metric.

### Lift-to-Drag Ratio

The Lift-to-Drag ratio, or L/D, is the amount of lift generated by the vehicle divided by the drag it creates. For this metric, each vehicle class increases L/D per year, as seen in Figure 77-Figure 82. A higher L/D is more favorable as delivering a required lift with lower drag leads to better fuel economy or climb performance. Each vehicle has a 0.3-0.5% increase per year, except for the SA percent change. This is because the data points are more spread out in Figure 80, leading to a lower percent change per year to be calculated. However, if the values for the B727-200A in 1968 (L/D = 14.6) is compared to the B737 in 2000 (L/D = 18.7) then the trend would be the same as the other vehicles.

To cross reference the trend, an L/D versus year plot was found in a paper written by F. I. Romli in the *International Journal of Environmental Science and Development* [62]. There are two differences between the data shown in the GT plots and the plot shown in Figure 82: 1) this plot includes military aircraft while the database data does not, 2) this plot shows L/D at maximum takeoff weight (MTOW) whereas the database data is at 85% MTOW. However, the trends are still similar for both the large aircraft (blue triangles) and the regional jets (red circles), there is a slight increase over time.

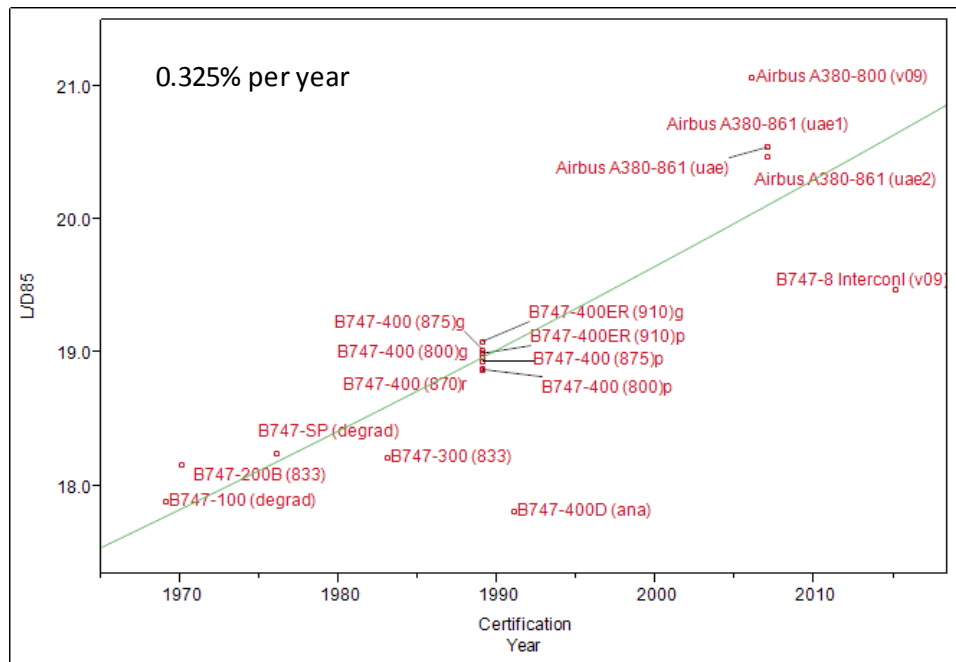


FIGURE 77: L/D vs. CERTIFICATION YEAR FOR LQ

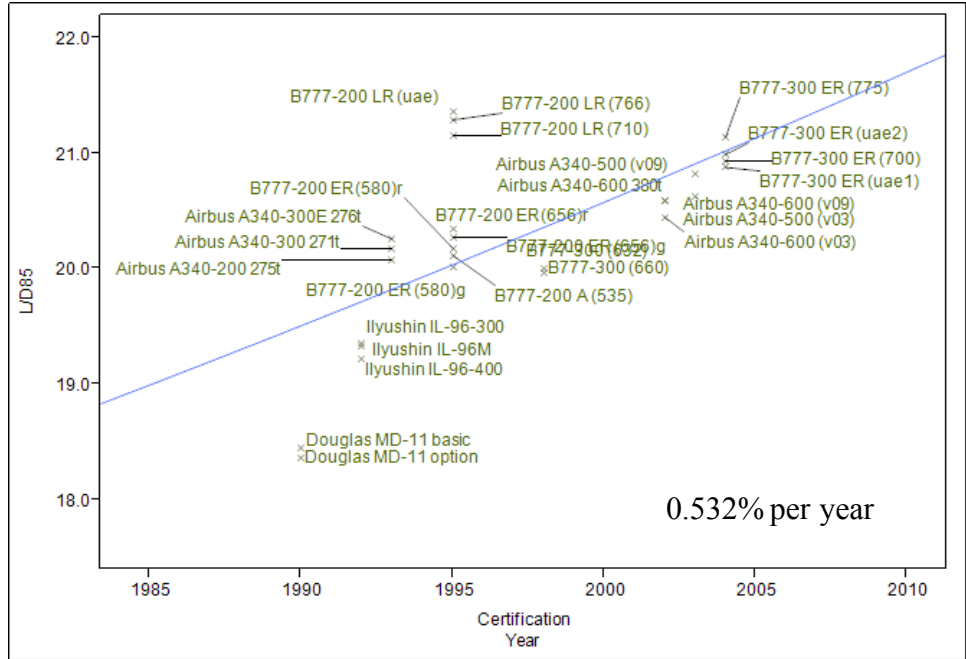


FIGURE 78: L/D vs. CERTIFICATION YEAR FOR LTA

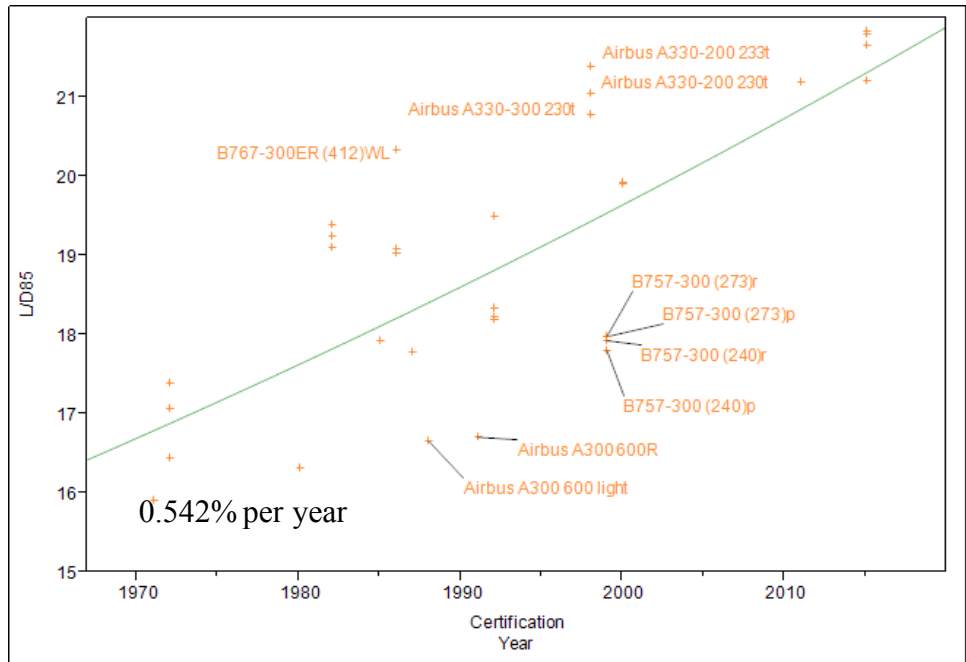
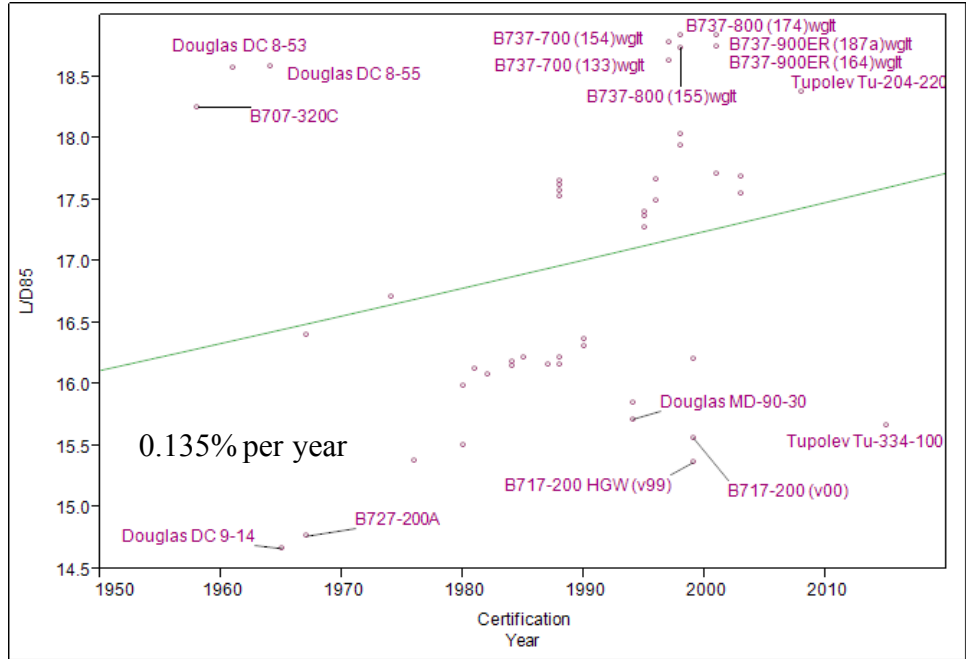
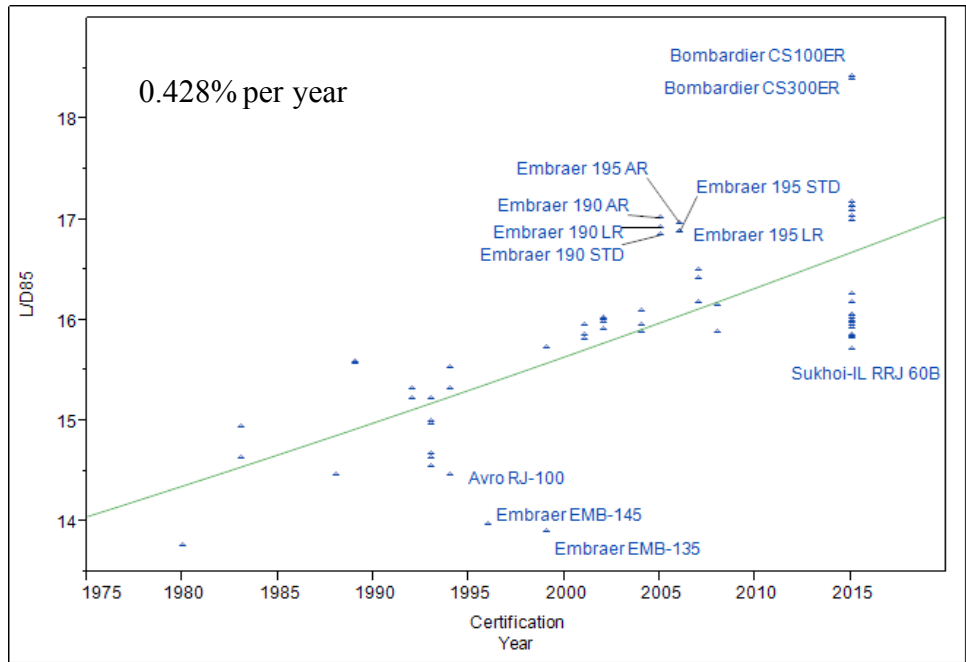


FIGURE 79: L/D vs. CERTIFICATION YEAR FOR STA



**FIGURE 80: L/D vs. CERTIFICATION YEAR FOR SA**



**FIGURE 81: L/D vs. CERTIFICATION YEAR FOR RJ**

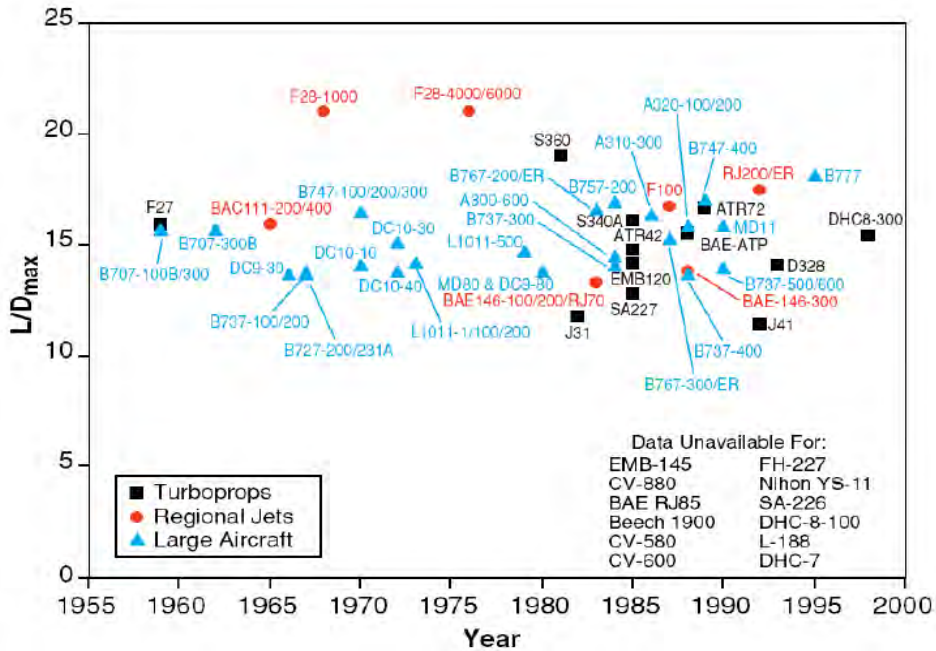


FIGURE 82:  $L/D_{MAX}$  VS. CERTIFICATION YEAR [62]

### Fuel Burn/(Payload \* Range)

The metric fuel burn divided by payload and range is used as an aircraft fuel efficiency metric. The metric is evaluated at two points along the Payload-Range chart. The R1 point is defined as the point along the maximum takeoff gross weight (TOGW) line that intersects with the maximum payload. The R2 point is defined as the point along the maximum TOGW line that intersects with the maximum fuel. The vehicles are first shown for the R1 point, Figure 83-Figure 87. There is a general downward trend for all of the vehicles. This is evident in the percent change values in Table 23 for the LQ, LTA, and SA, the vehicles in which a trend line was able to be fitted. For the STA and the RJ, the vehicles' values had too many outliers which did not allow for a regression; however the downward trend is still evident.

Figure 88-Figure 92 are the 5 vehicles shown for the R2 point. The LQ's efficiency largely increases over time while the other vehicles have slight increases or decreases.

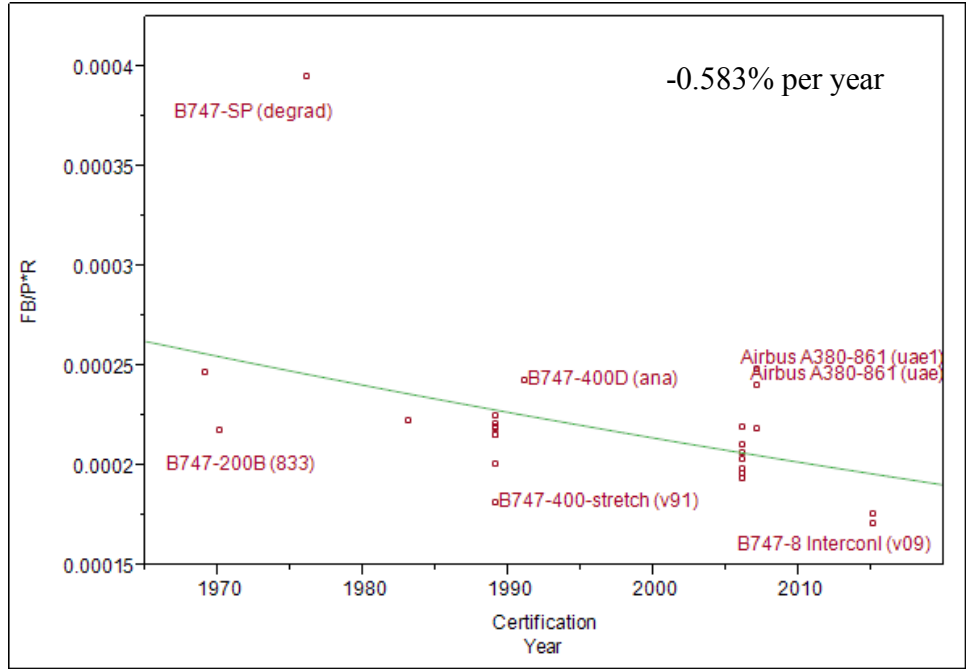


FIGURE 83: FUEL BURN/(PAYLOAD \* RANGE) FOR R1 vs. CERTIFICATION YEAR FOR LQ

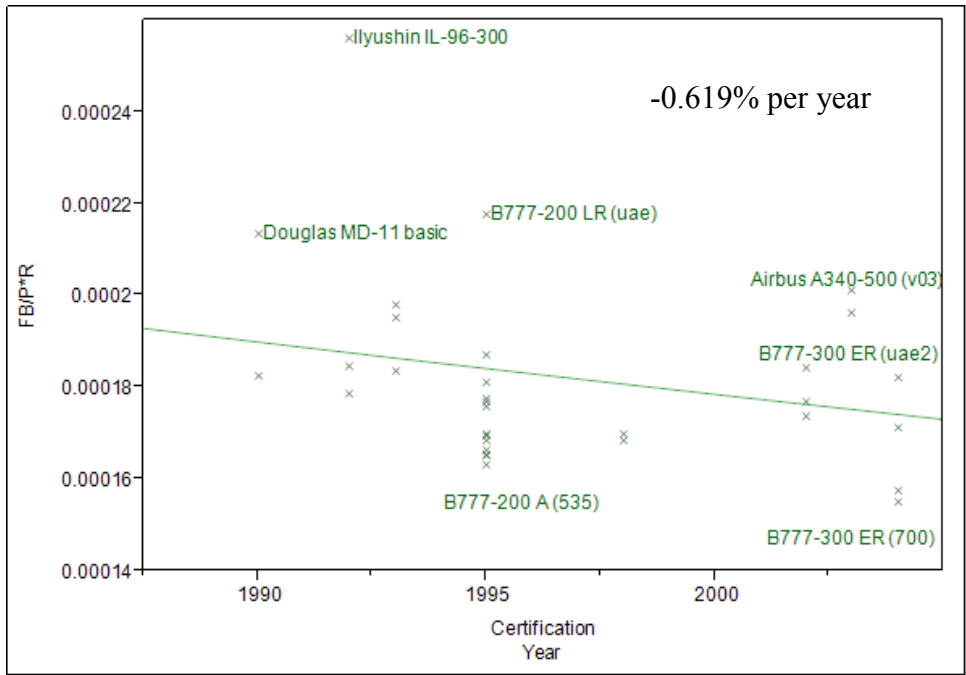
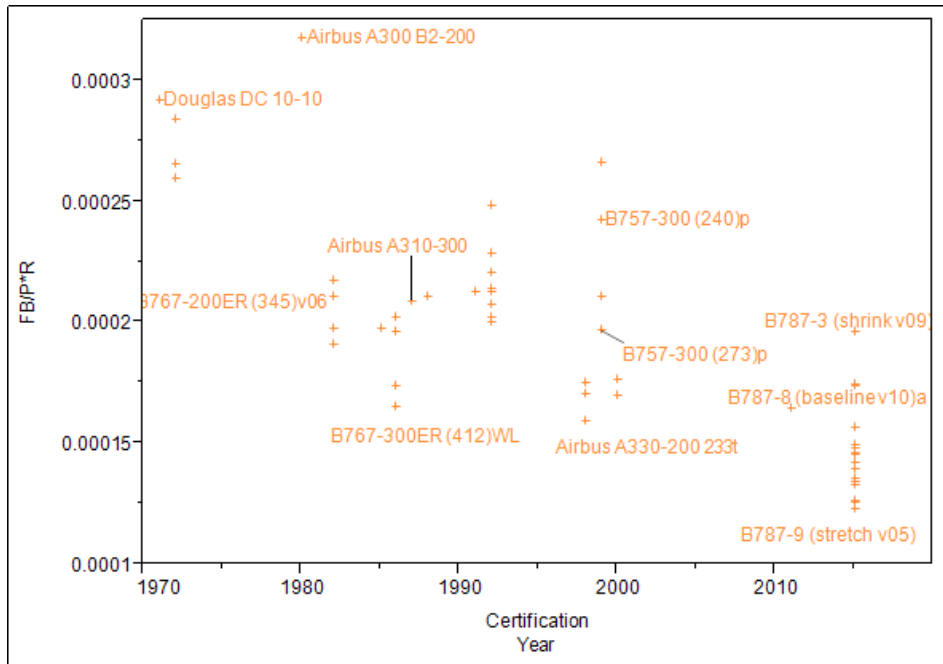
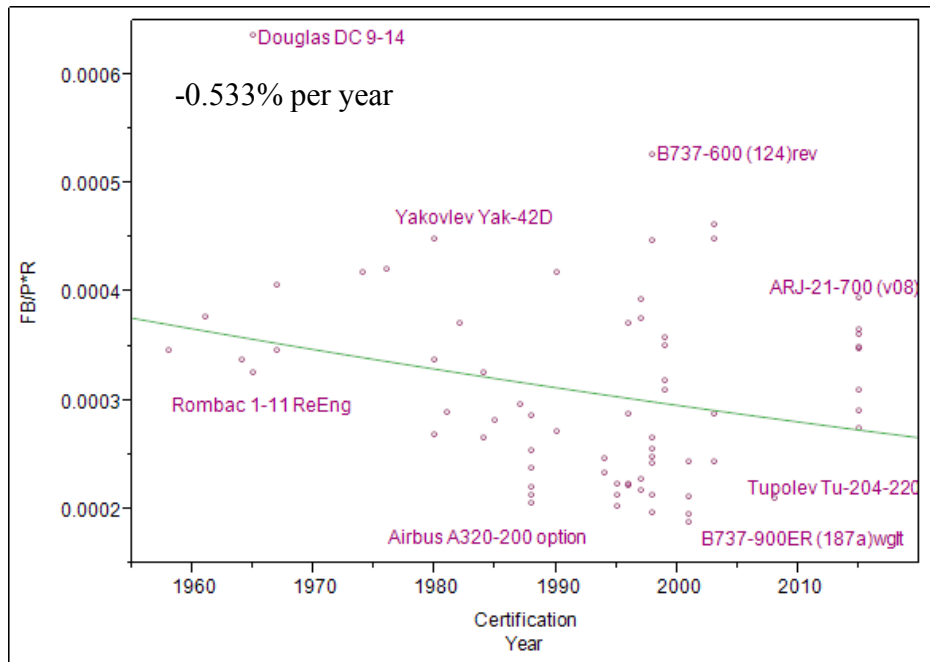


FIGURE 84: FUEL BURN/(PAYLOAD \* RANGE) FOR R1 vs. CERTIFICATION YEAR FOR LTA



**FIGURE 85: FUEL BURN/(PAYLOAD \* RANGE) FOR R1 VS. CERTIFICATION YEAR FOR STA**



**FIGURE 86: FUEL BURN/(PAYLOAD \* RANGE) FOR R1 VS. CERTIFICATION YEAR FOR SA**

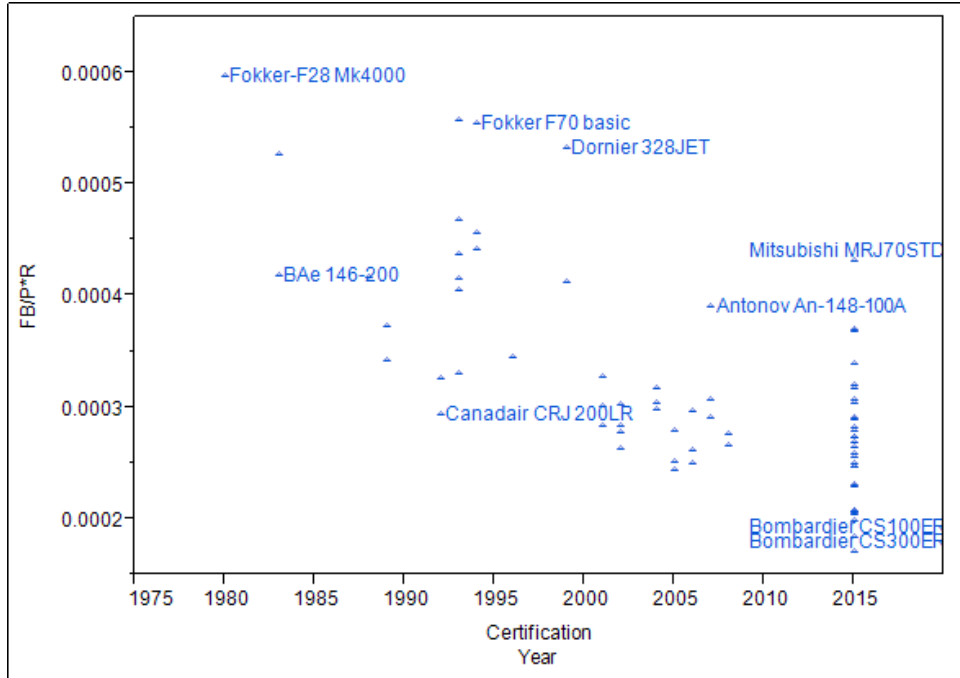


**FIGURE 87: FUEL BURN/(PAYLOAD \* RANGE) FOR R1 vs. CERTIFICATION YEAR FOR R1**

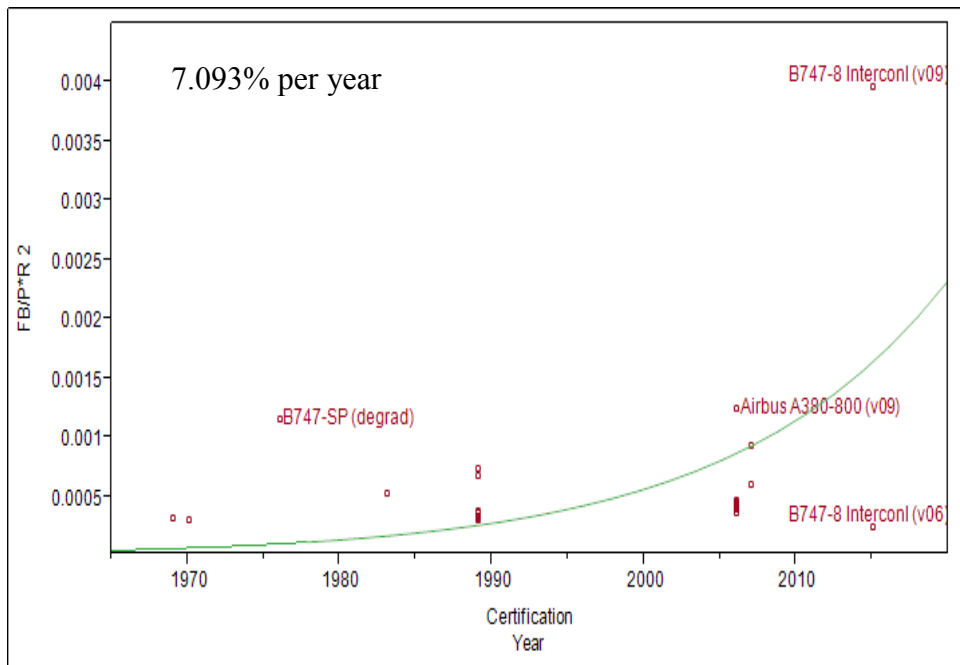


**FIGURE 88: FUEL BURN/(PAYLOAD \* RANGE) FOR R2 vs. CERTIFICATION YEAR FOR LQ**



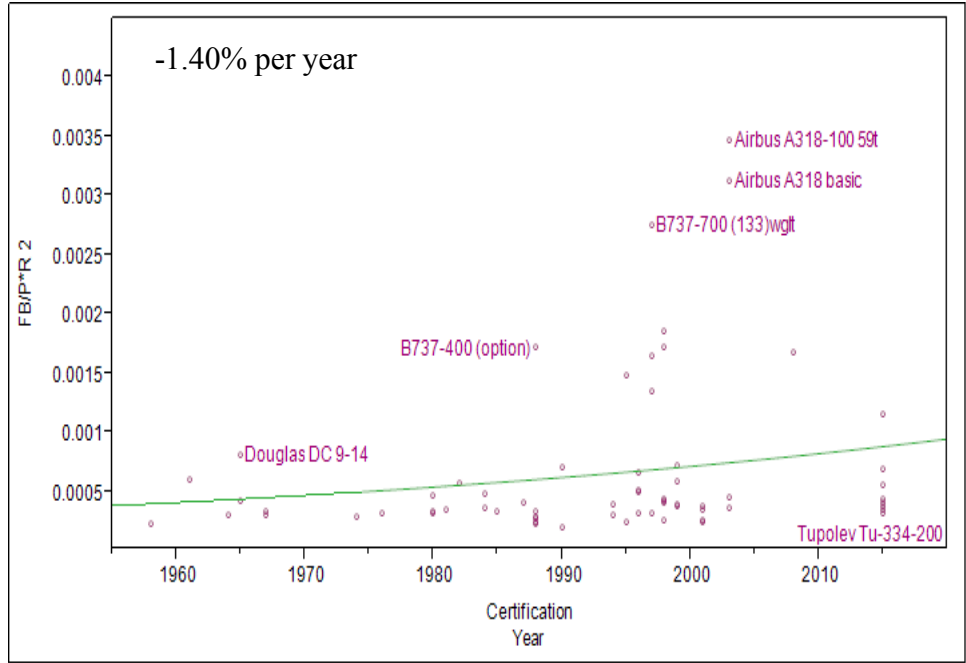


**FIGURE 91: FUEL BURN/(PAYLOAD \* RANGE) FOR R2 vs. CERTIFICATION YEAR FOR SA**

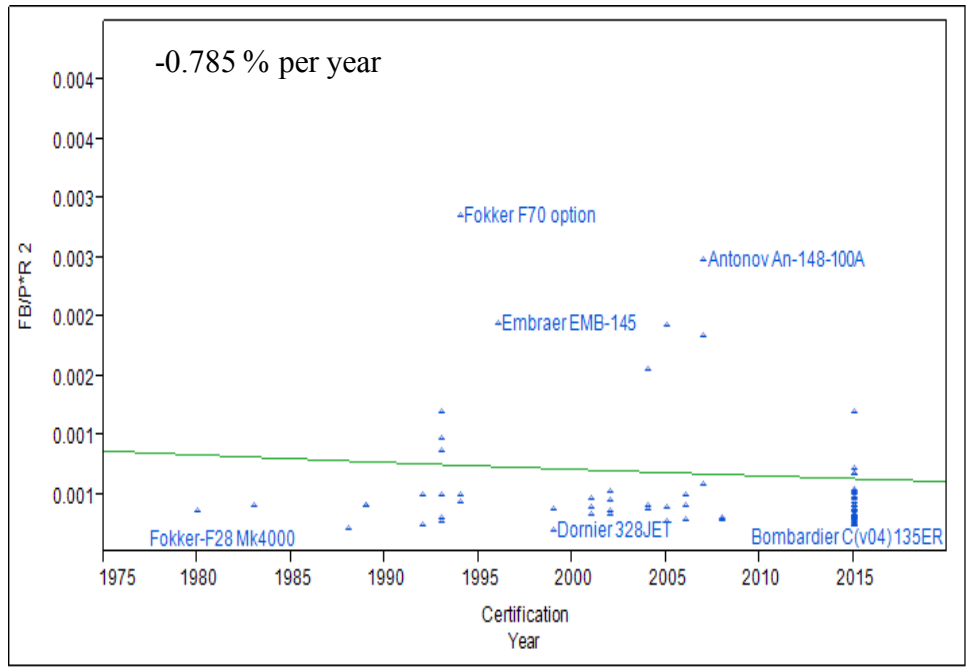


**FIGURE 92: FUEL BURN/(PAYLOAD \* RANGE) FOR R2 vs. CERTIFICATION YEAR FOR RJ**

**Maximum Takeoff Weight (MTOW)**

The MTOW is the maximum weight that the aircraft is allowed to takeoff due to structural or thrust, or takeoff length constraints. Figure 93-Figure 97 depict the increase of MTOW over time

over all classes of vehicles. This compares well to the literature search and Figure 98 found in [62]. The trend and magnitudes match well. The LQ and LTA magnitudes match with the wide body trend, while the SA and RJ fit in the narrow body trend.

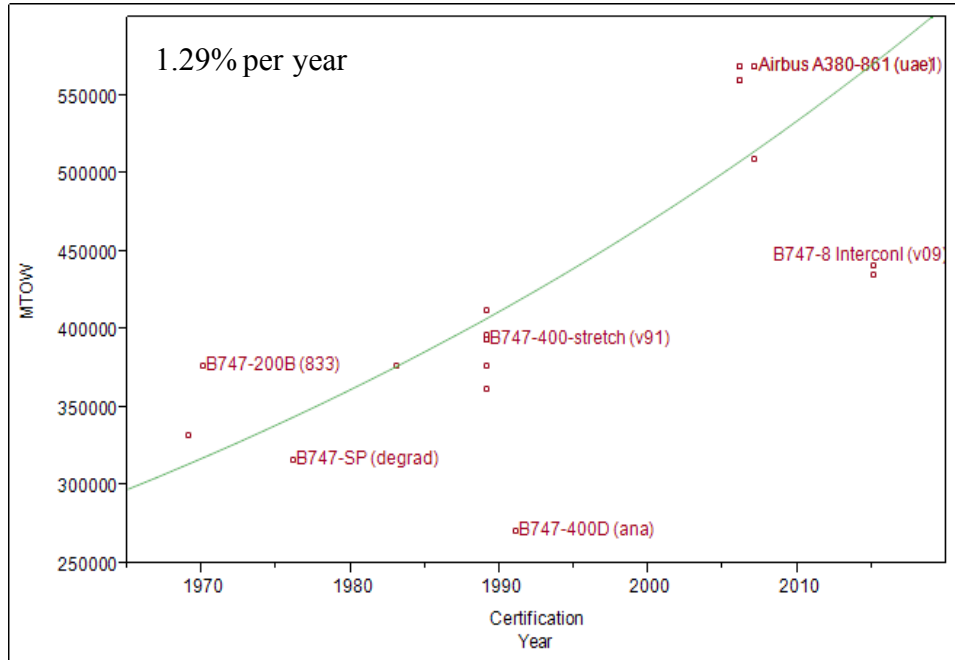


**FIGURE 93: MTOW vs. CERTIFICATION YEAR FOR LQ**

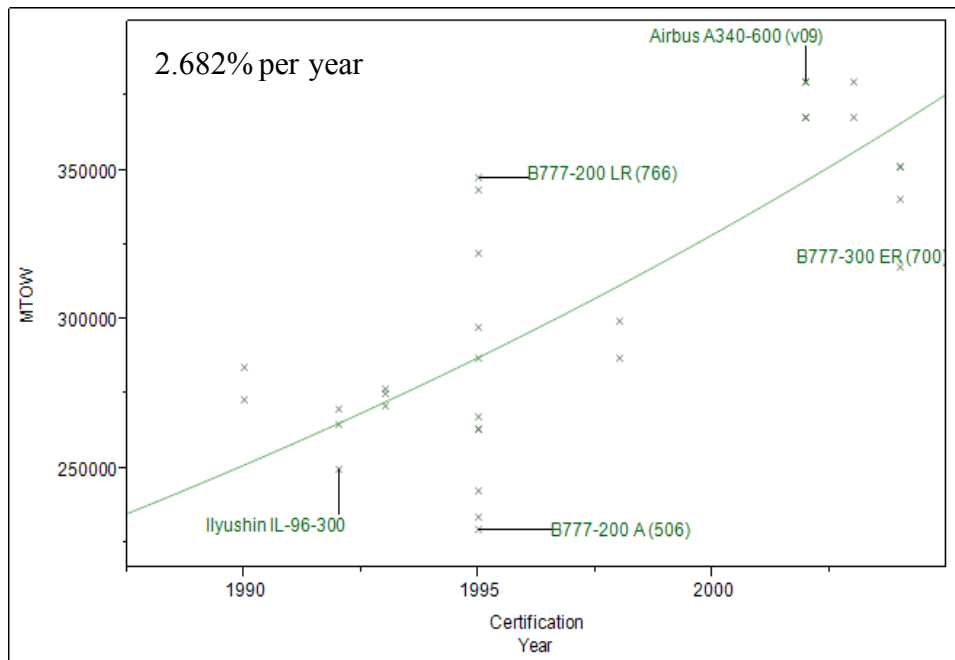


**FIGURE 94: MTOW vs. CERTIFICATION YEAR FOR LTA**

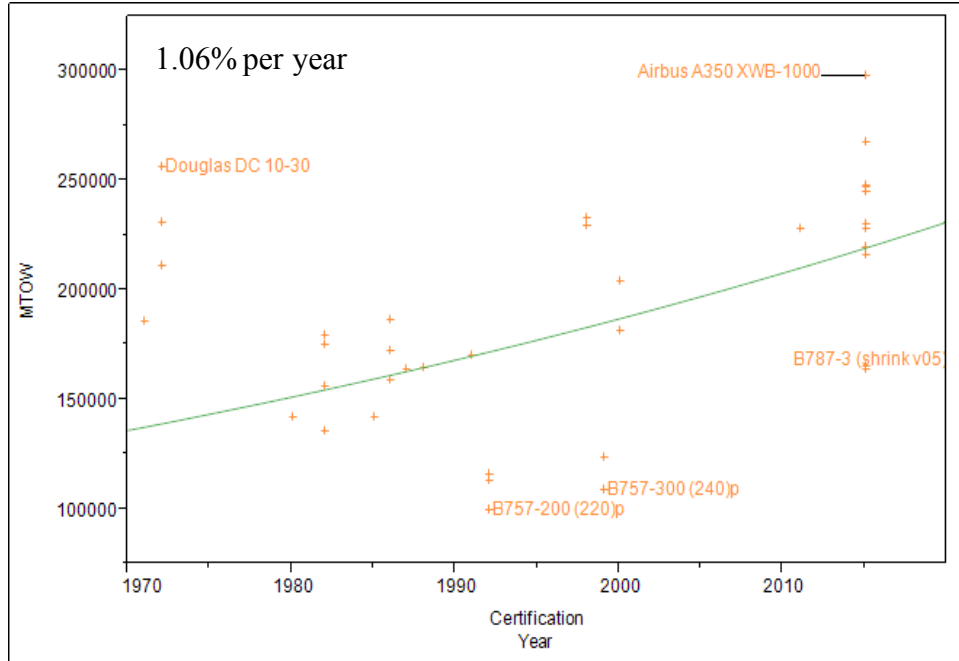


**FIGURE 95: MTOW vs. CERTIFICATION YEAR FOR STA**

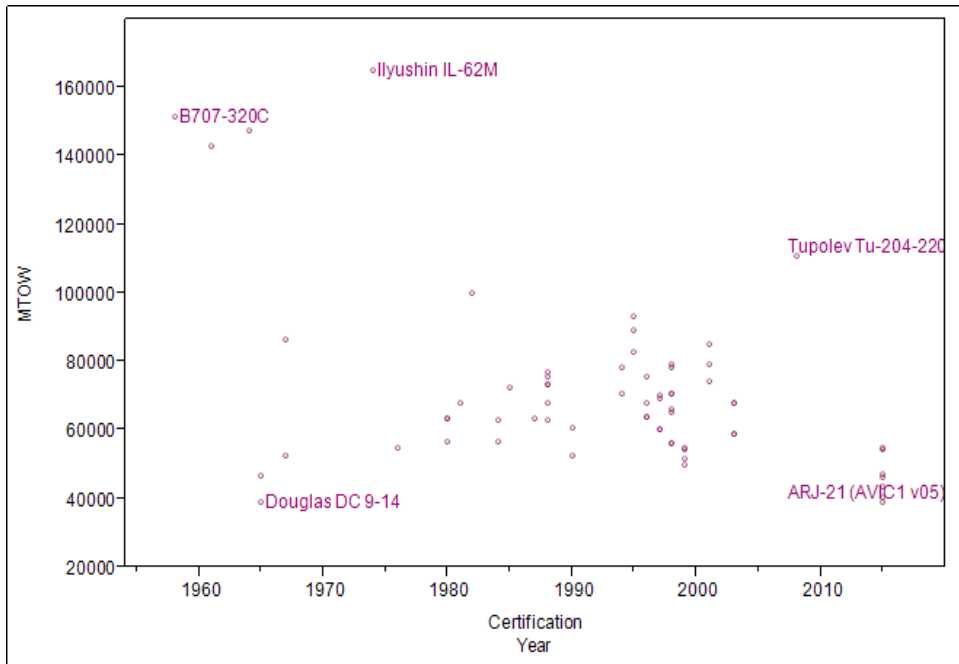


**FIGURE 96: MTOW vs. CERTIFICATION YEAR FOR SA**

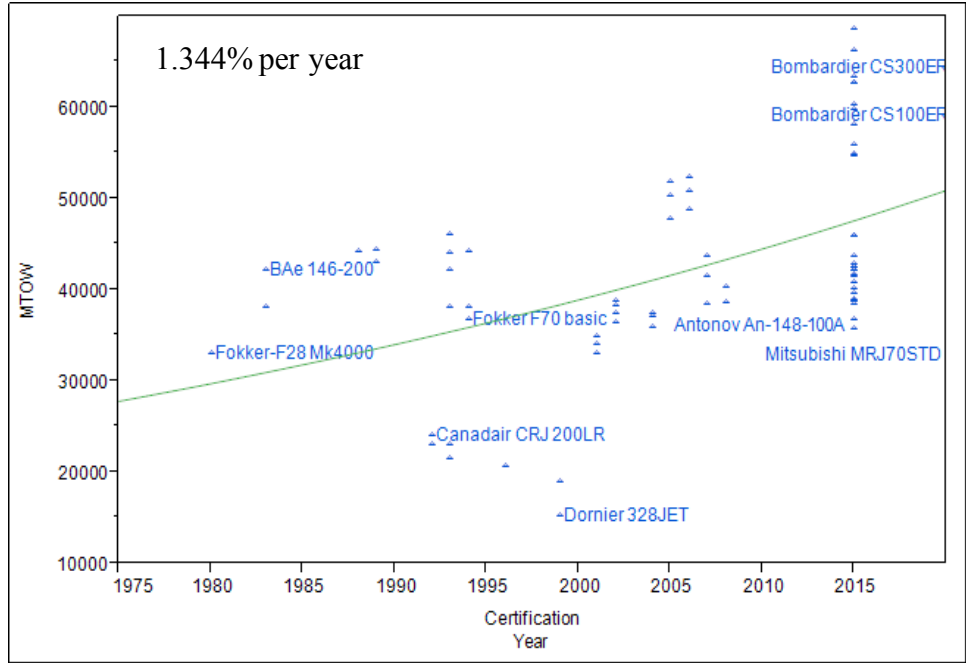


FIGURE 97: MTOW vs. CERTIFICATION YEAR FOR RJ

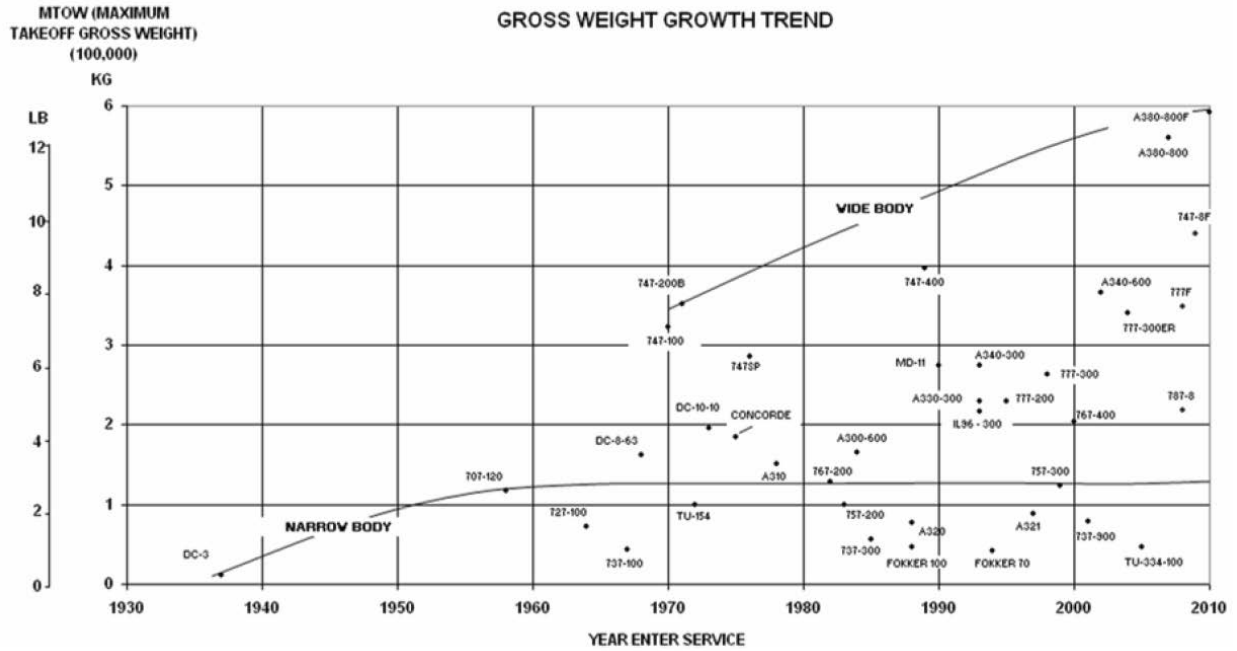
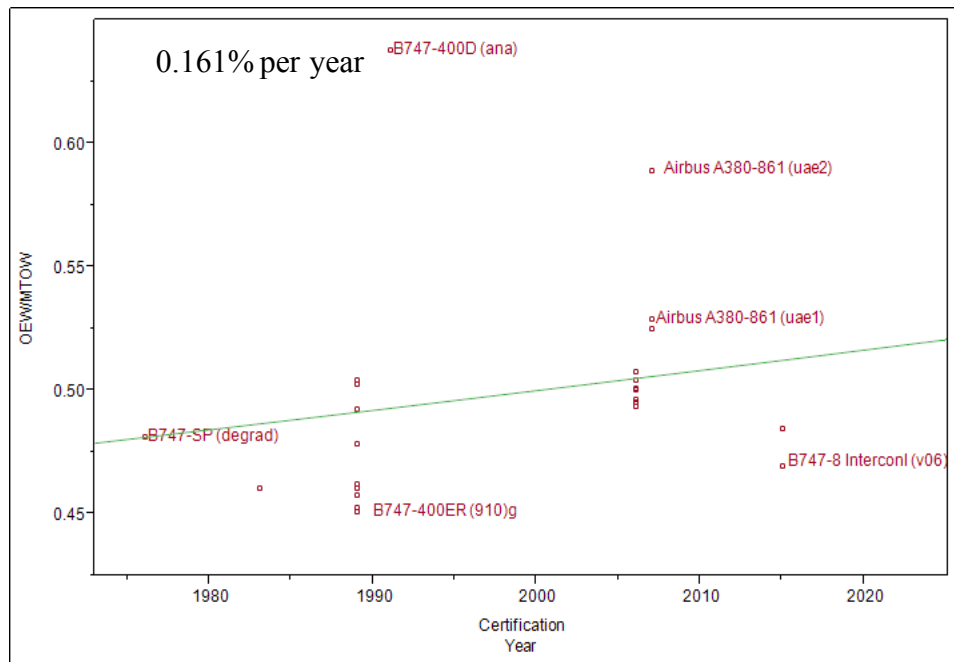


FIGURE 98: MTOW vs. CERTIFICATION YEAR [62]

### Operating Empty Weight (OEW)

The first metric assessed for OEW is OEW/MTOW in Figure 99-Figure 103. This is a measure of how light an airplane can be to lift the same amount of weight, including payload and fuel. The small percent change over time is due to the fact that aircraft are still mainly manufactured from aluminum. Also, as noted later, while bypass ratios increase over time this leads to bigger engine diameter and more weight, offsetting any improvements in aircraft structural weight. Lastly, the increase in range capability over time, leads to an increase in fuel weight. This will also drive up structures weight and cause more of a constant trend for this metric. Figure 104, from a study conducted at the University of Illinois at Urbana-Champaign [63], confirm these findings with a similar plot showing all vehicles over time. The percent change of +/- 0.1% corresponds with the constant trend shown in the graph.

OEW was also used in the metric OEW/Maximum Payload in Figure 105-Figure 109. Maximum payload is the difference between maximum zero-fuel weight and OEW. The slight increase over time is due to the fact the range capability is increasing, seen in the OEW/MTOW metric; however the OEW is increasing at a higher rate than the payload weight due to the increase in structures weight for the increase in fuel.



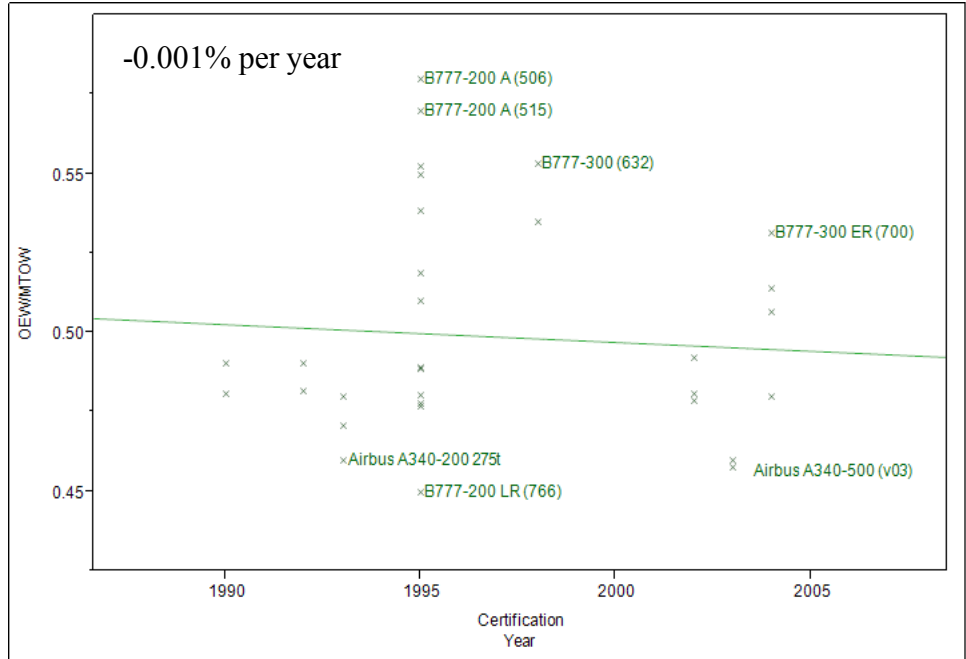


**FIGURE 100: OEW/MTOW vs. CERTIFICATION YEAR FOR LTA**

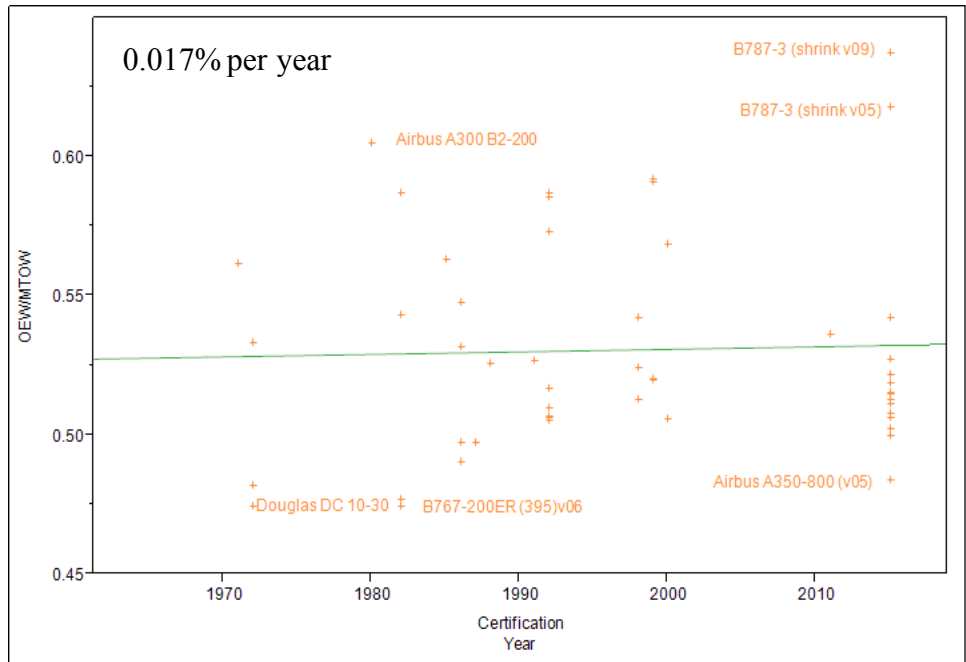


**FIGURE 101: OEW/MTOW vs. CERTIFICATION YEAR FOR STA**

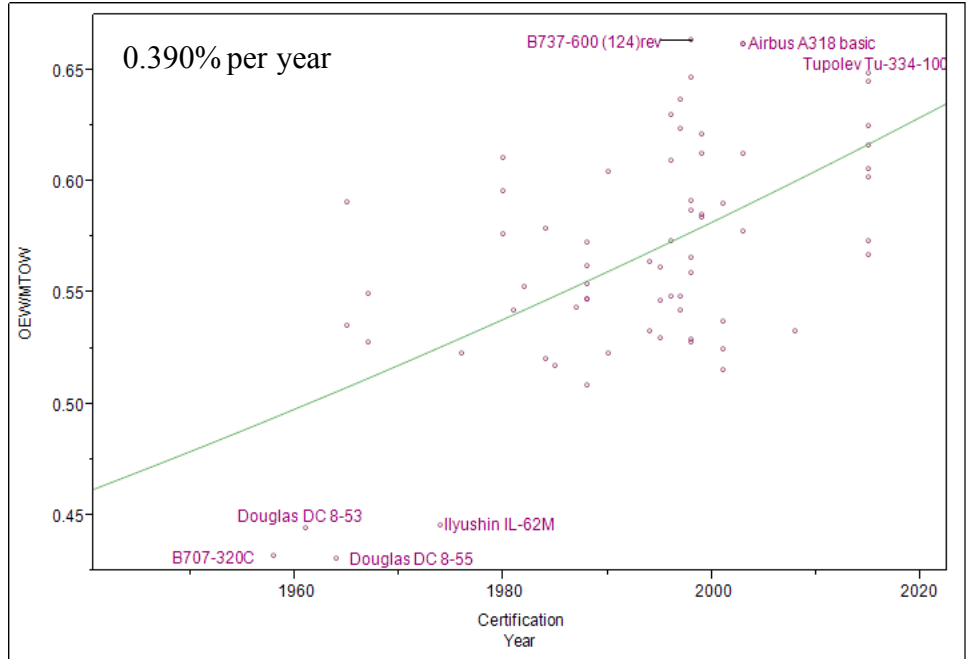


**FIGURE 102: OEWM/TOW vs. CERTIFICATION YEAR FOR SA**

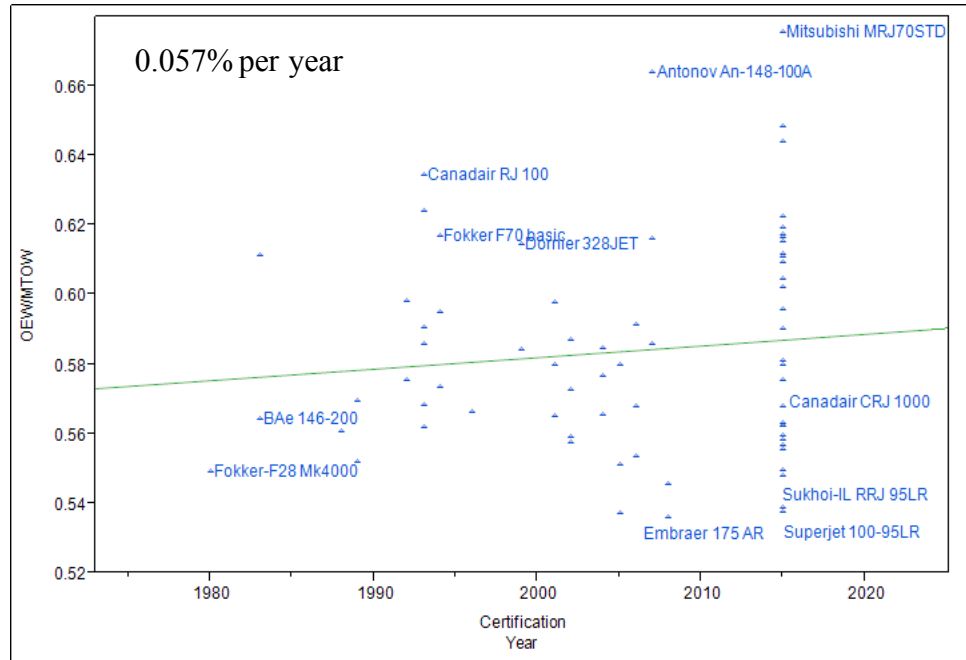


**FIGURE 103: OEWM/TOW vs. CERTIFICATION YEAR FOR RJ**

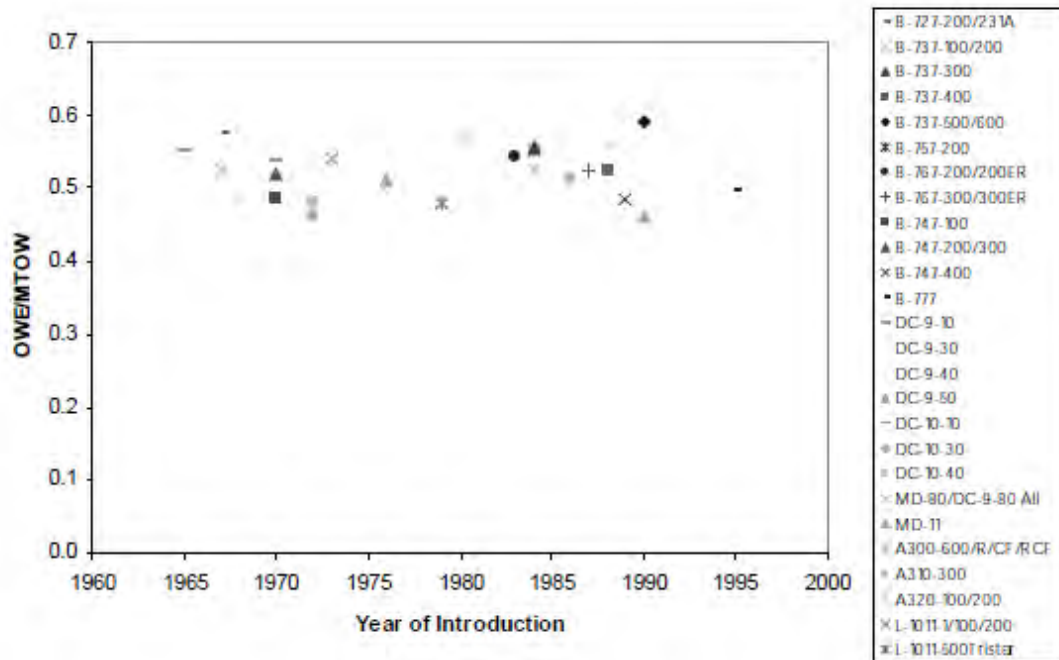


FIGURE 104: OEW/MTOW VS. YEAR OF INTRODUCTION [63]

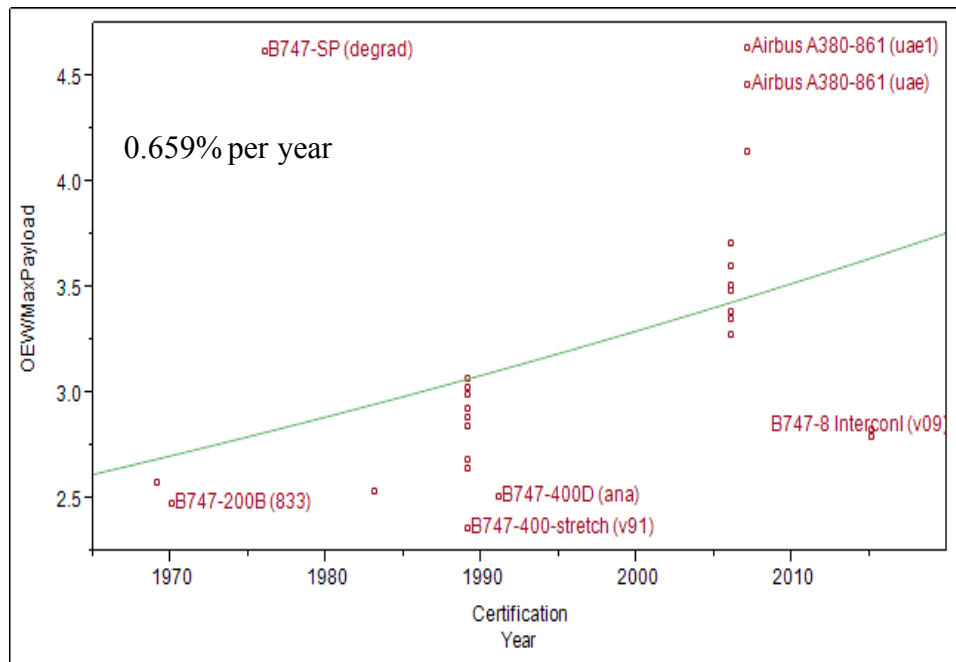
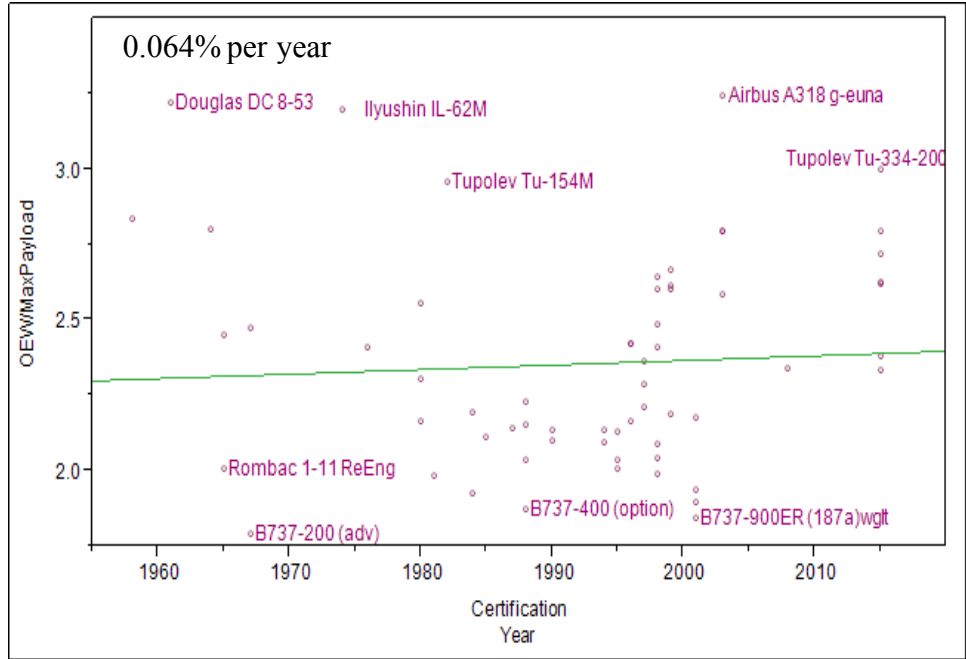
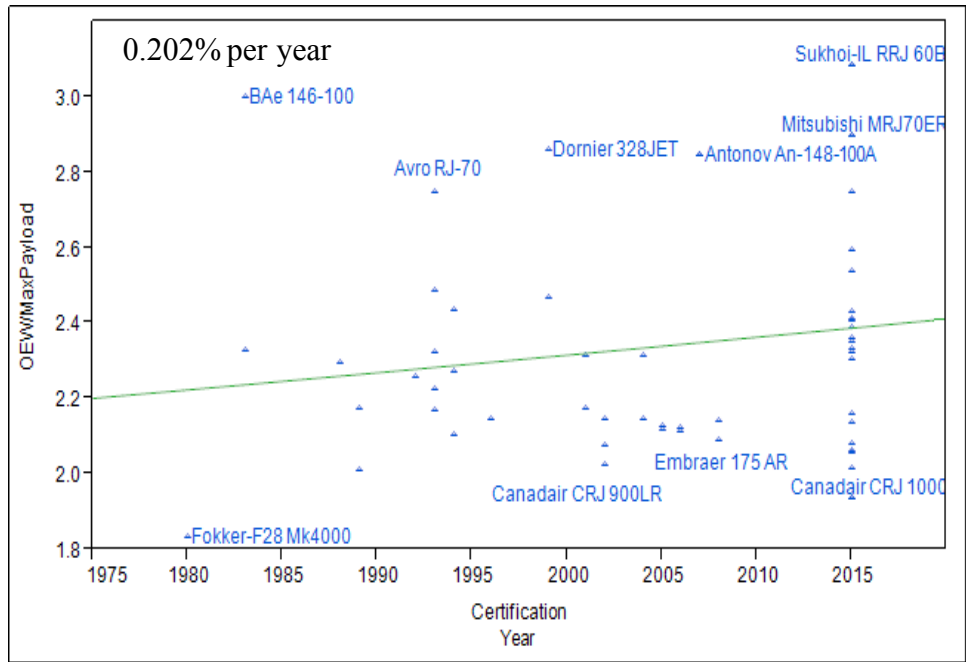


FIGURE 105: OEW/MAX PAYLOAD VS. CERTIFICATION YEAR FOR LQ





**FIGURE 108: OEW/MAX PAYLOAD VS. CERTIFICATION YEAR FOR SA**



**FIGURE 109: OEW/MAX PAYLOAD VS. CERTIFICATION YEAR FOR RJ**

### ***Rated Output***

The rated output of the engine is plotted against time in Figure 110-Figure 114. The rated output in kN increases between 1-2% per year for the larger vehicles (LQ, LTA and STA). However, engines for SA only increase 0.1% per year. Finally, the RJ increases 5.32% per year due to the room for improvement for regional jets.

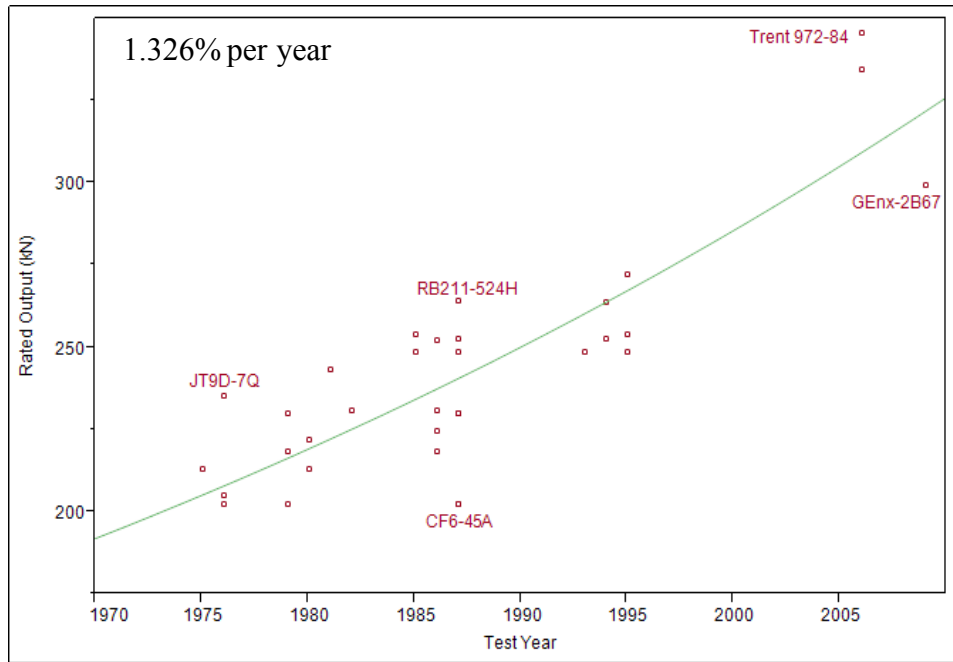


**FIGURE 110: RATED OUTPUT VS. CERTIFICATION YEAR FOR LQ**

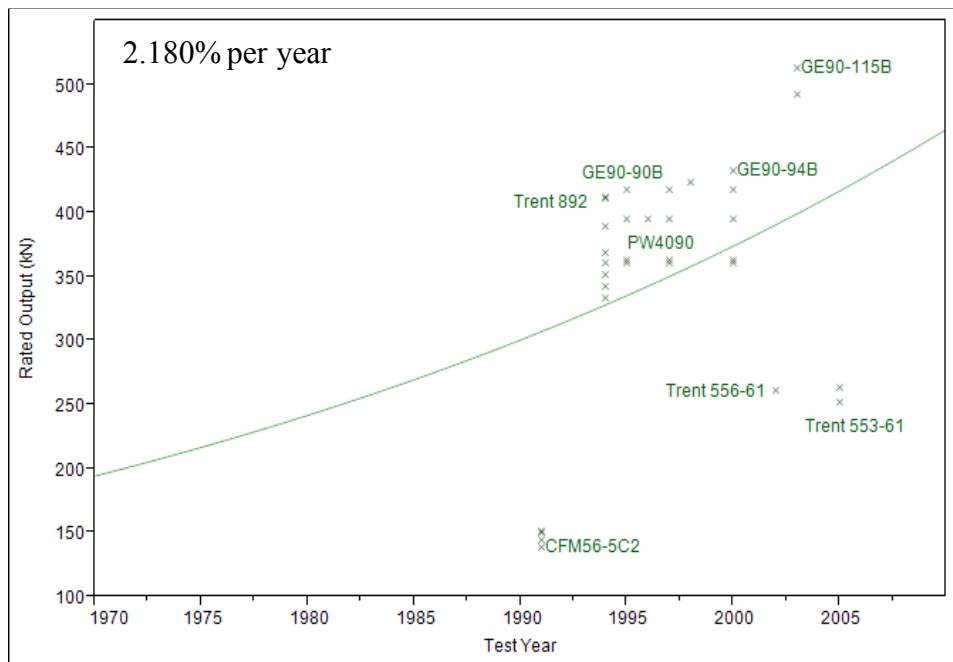


**FIGURE 111: RATED OUTPUT VS. CERTIFICATION YEAR FOR LTA**

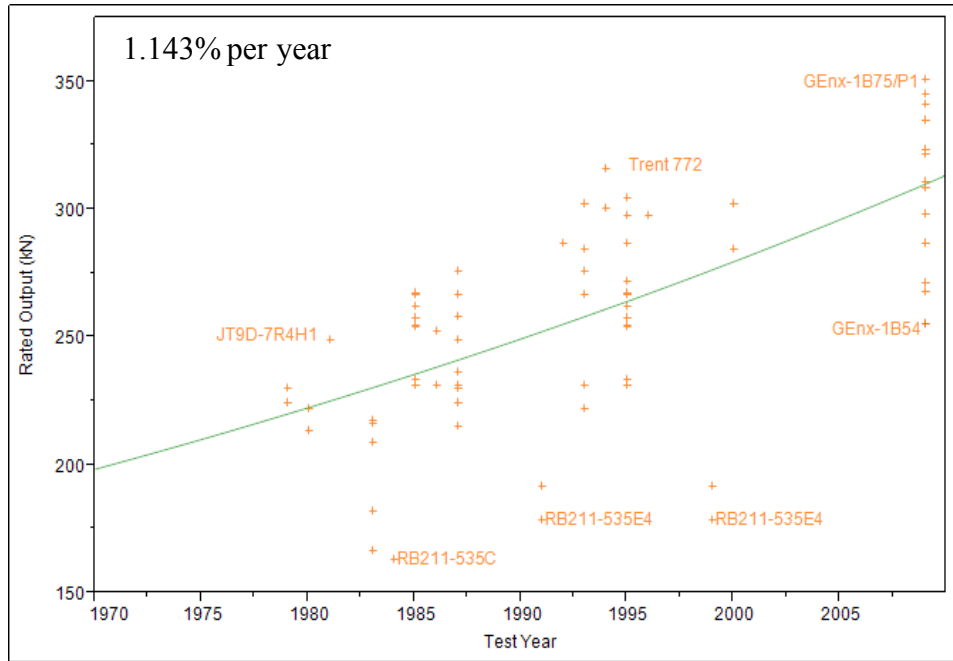


**FIGURE 112: RATED OUTPUT VS. CERTIFICATION YEAR FOR STA**

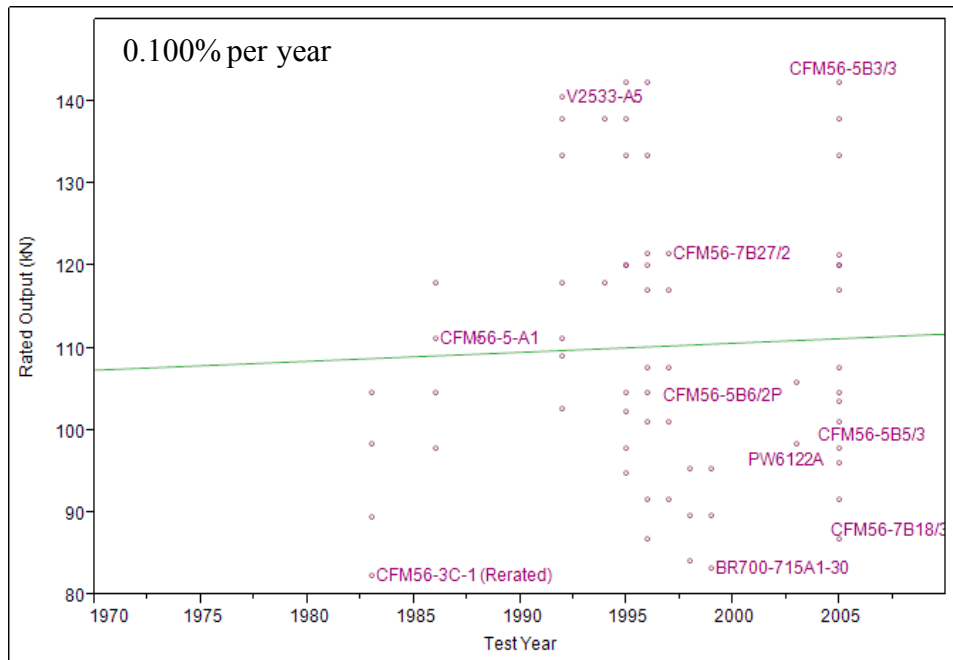


**FIGURE 113: RATED OUTPUT VS. CERTIFICATION YEAR FOR SA**

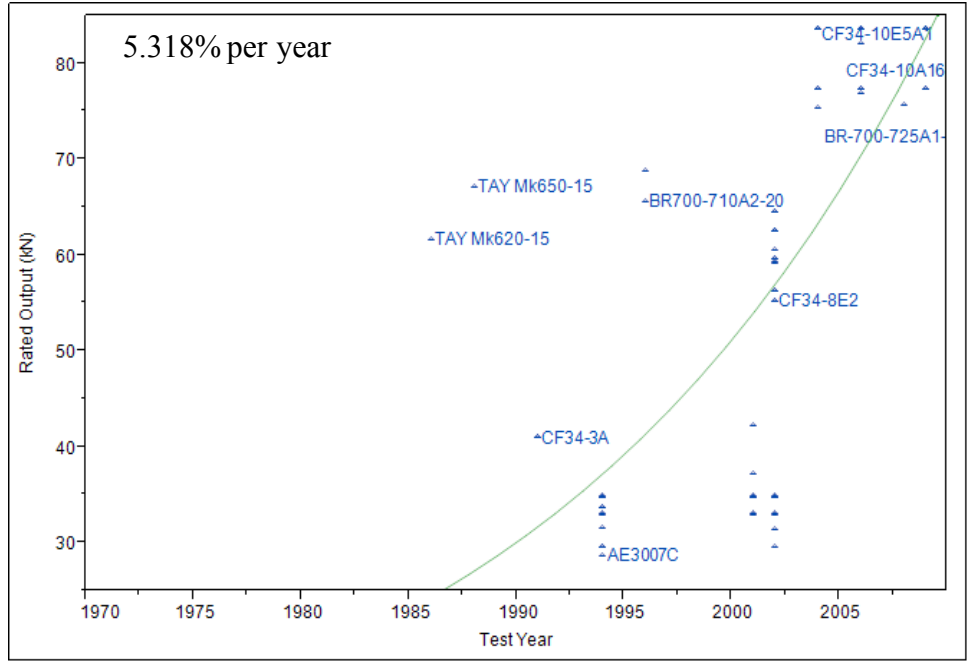


**FIGURE 114: RATED OUTPUT VS. CERTIFICATION YEAR FOR RJ**

***Engine Weight-to-Thrust Ratio***

The engine weight-to-thrust ratio increases slightly over time in Figure 115-Figure 119, meaning the engine’s weight is increasing at a higher rate than the thrust produced. The increase in engine weight can be attributed to the increase in BPR over time. Higher BPR leads to increase in fan size and weight.

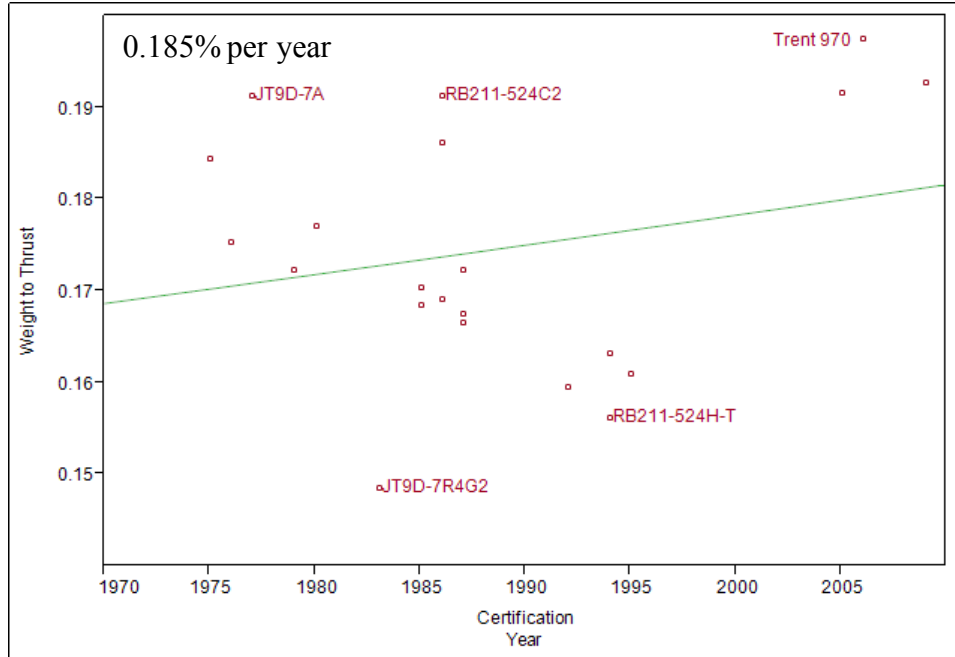
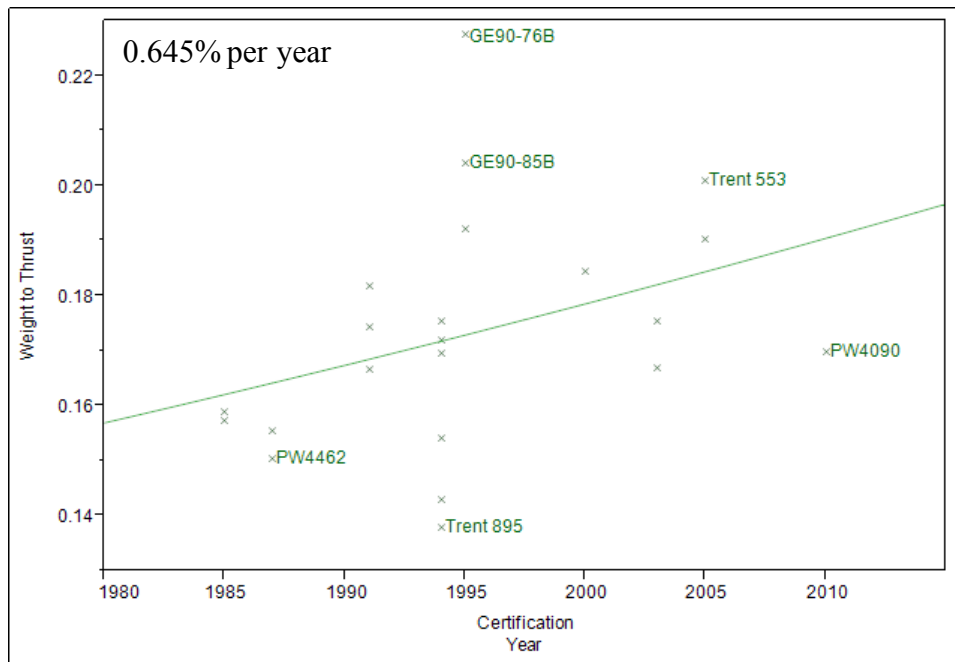
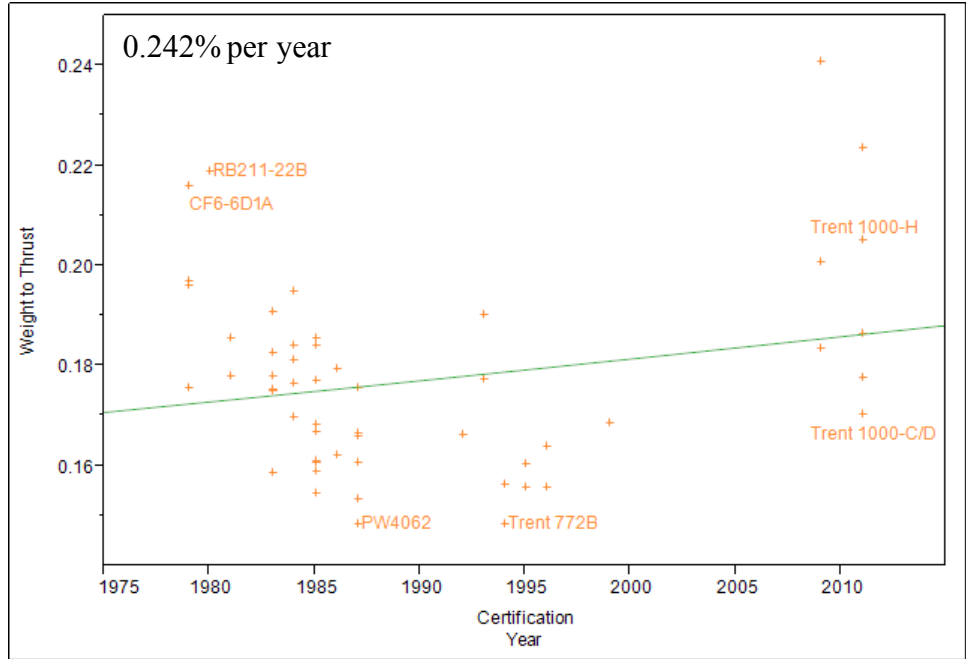
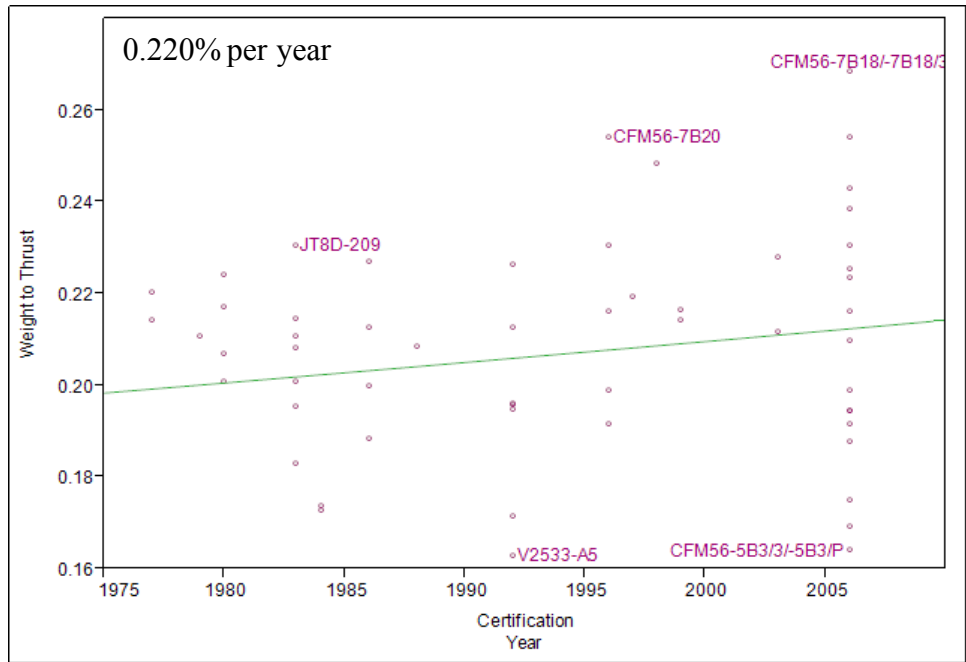


FIGURE 115: ENGINE W/T VS. CERTIFICATION YEAR FOR LQ





**FIGURE 117: ENGINE W/T VS. CERTIFICATION YEAR FOR STA**



**FIGURE 118: ENGINE W/T VS. CERTIFICATION YEAR FOR SA**

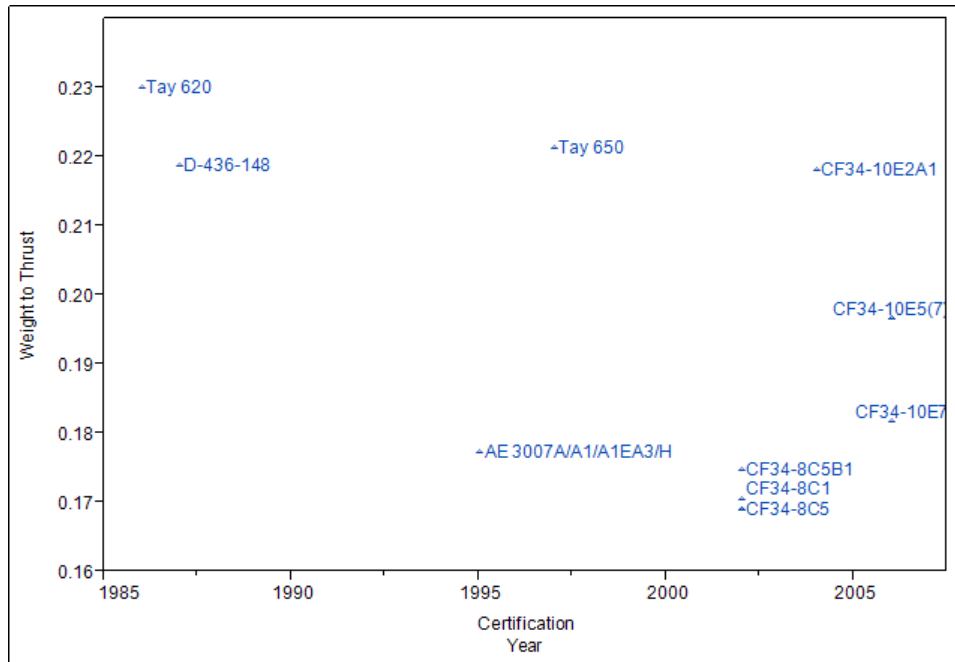


**FIGURE 119: ENGINE W/T VS. CERTIFICATION YEAR FOR RJ**

***Specific Fuel Consumption (SFC)***

The specific fuel consumption describes the fuel efficiency of an engine. For this metric we see a decreasing trend for all vehicles in Figure 120-Figure 124, which is shown through the percent changes in Table 23 for LQ, SA and RJ. One reason for the decreasing SFC is the increasing OPR over time, which is shown in Figure 132-Figure 136. The trends are consistent with the goal to increase in engine efficiency over time. Figure 125 and Figure 126 also show the same downwards trend for uninstalled SFC and TSFC over time, respectively. Both plots credit the decrease in TSFC towards the trend for increasing BPR. The plots show a 50% reduction in TSFC during the past 50 years

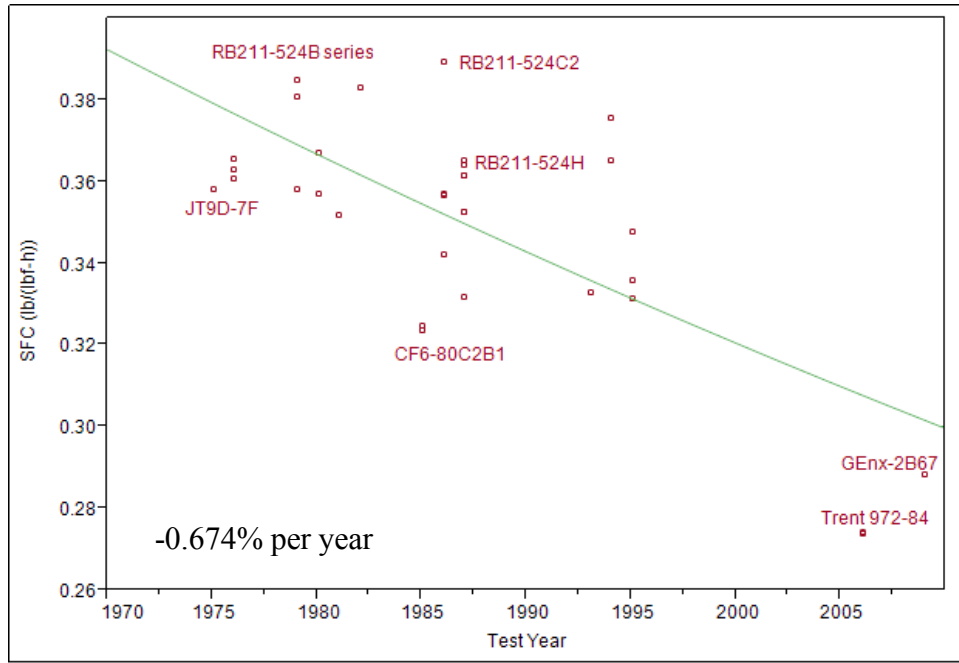


**FIGURE 120: SFC vs. CERTIFICATION YEAR FOR LQ**

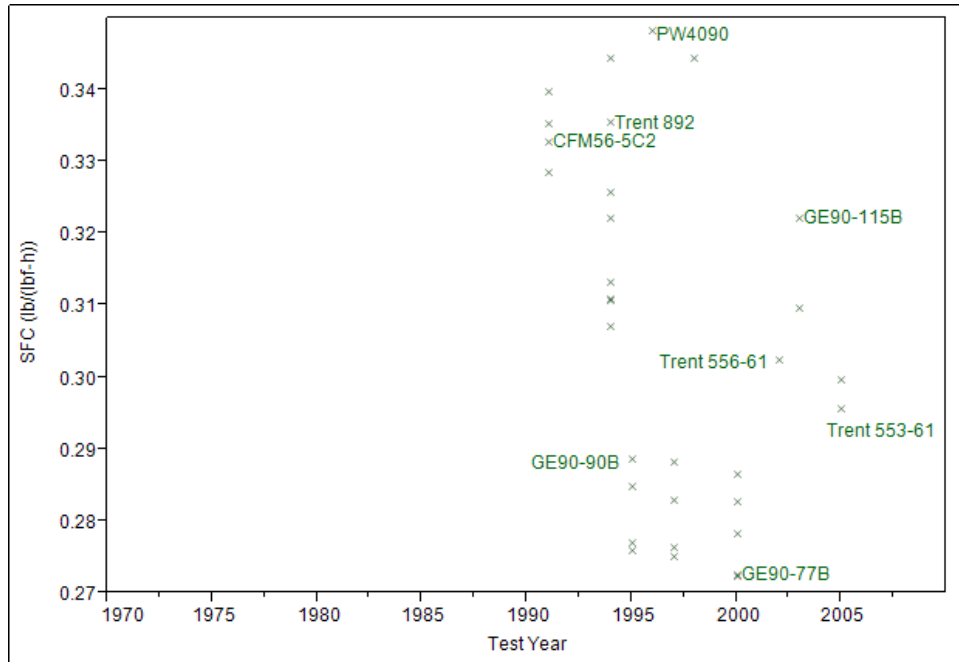


**FIGURE 121: SFC vs. CERTIFICATION YEAR FOR LTA**

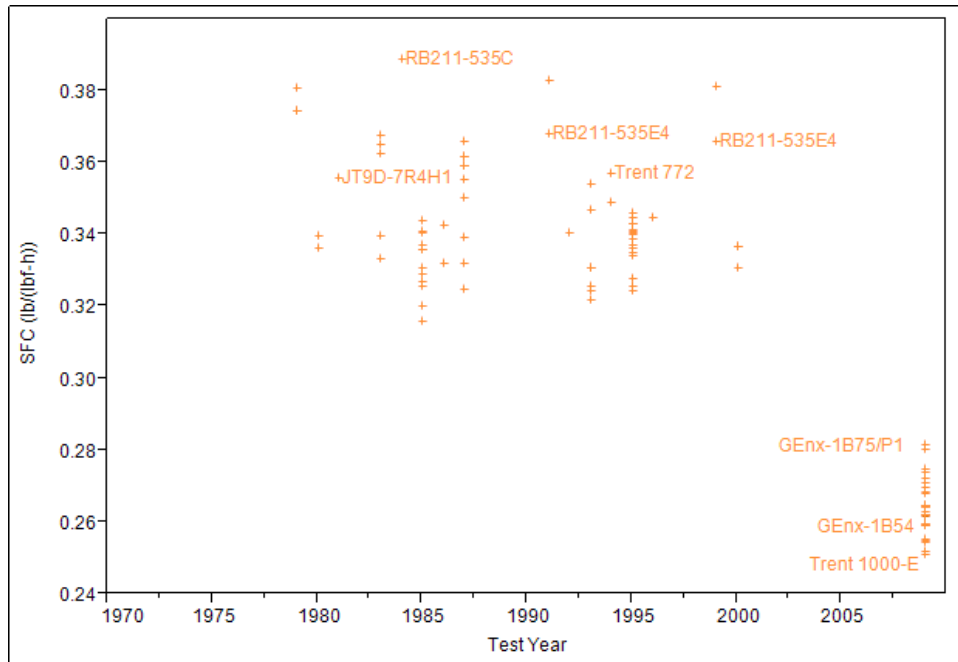


**FIGURE 122: SFC vs. CERTIFICATION YEAR FOR STA**

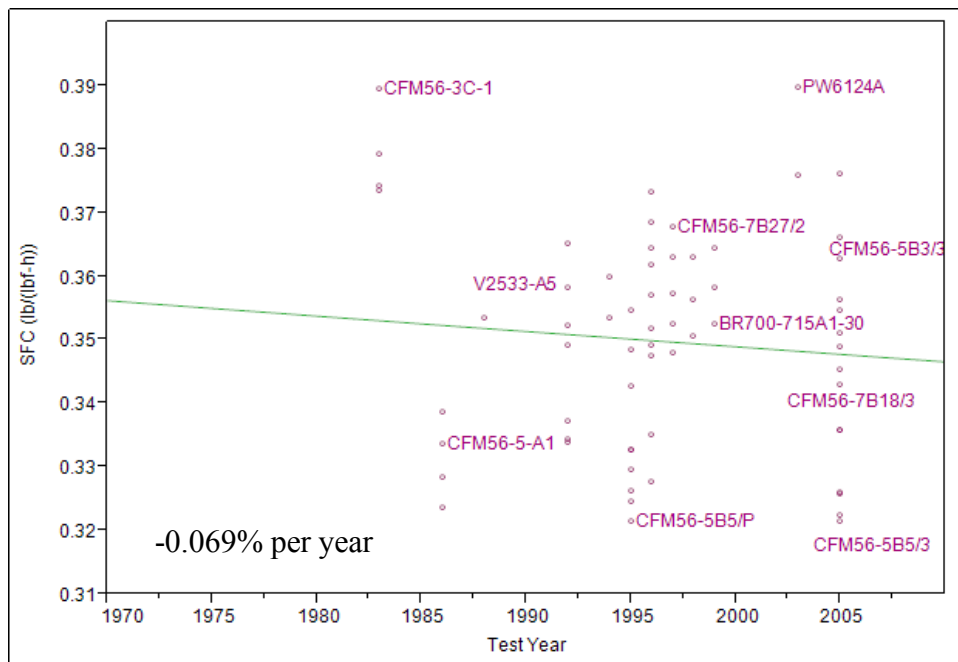


**FIGURE 123: SFC vs. CERTIFICATION YEAR FOR SA**

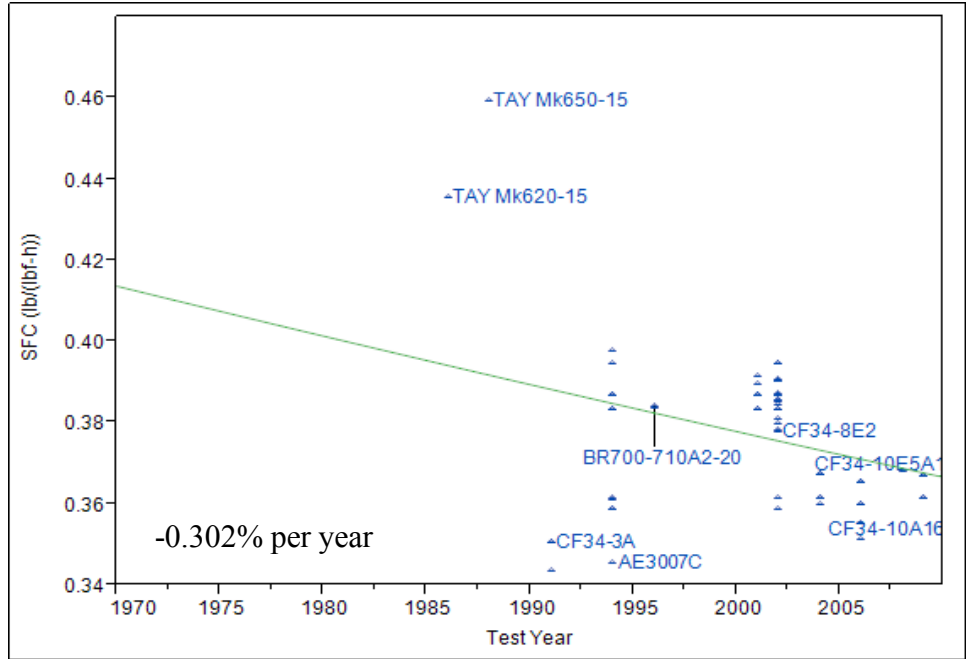


FIGURE 124: SFC VS. CERTIFICATION YEAR FOR RJ

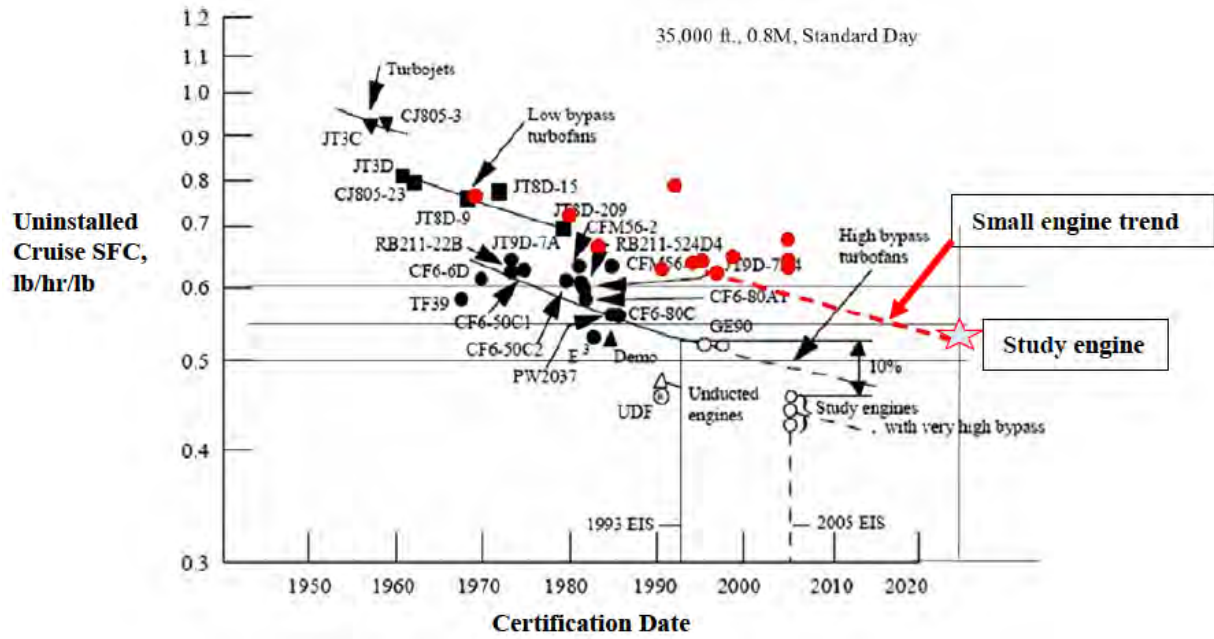


FIGURE 125: UNINSTALLED CRUISE SFC VS. CERTIFICATION YEAR [63]

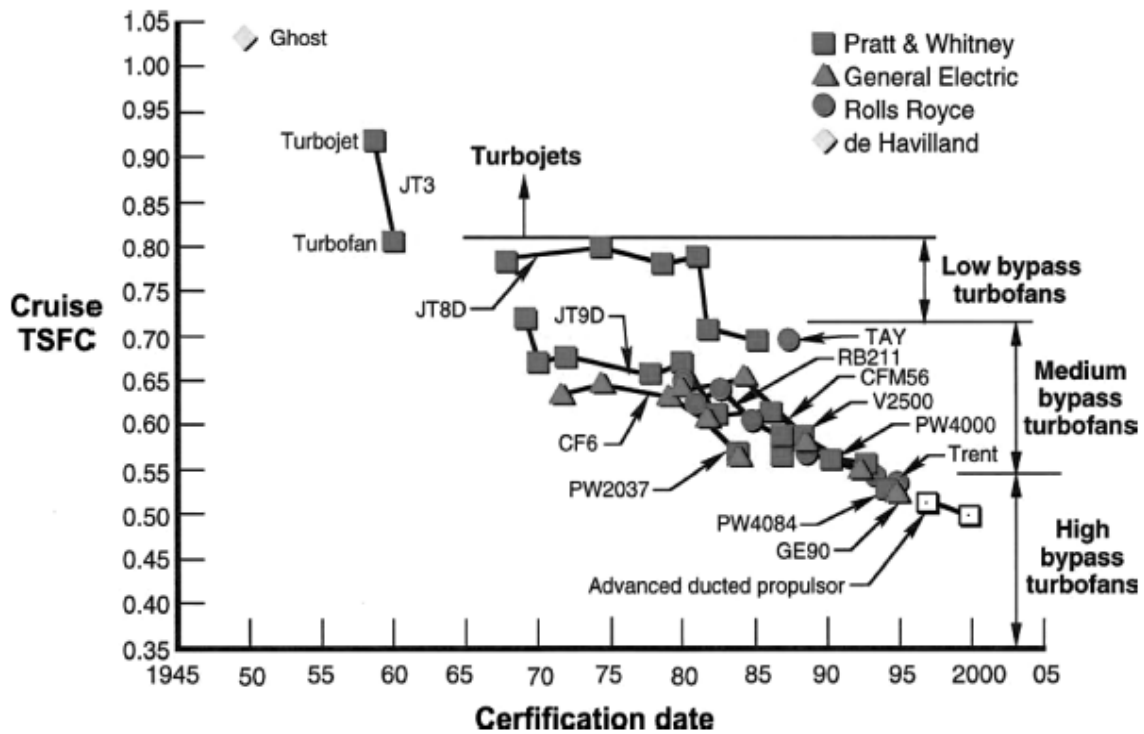
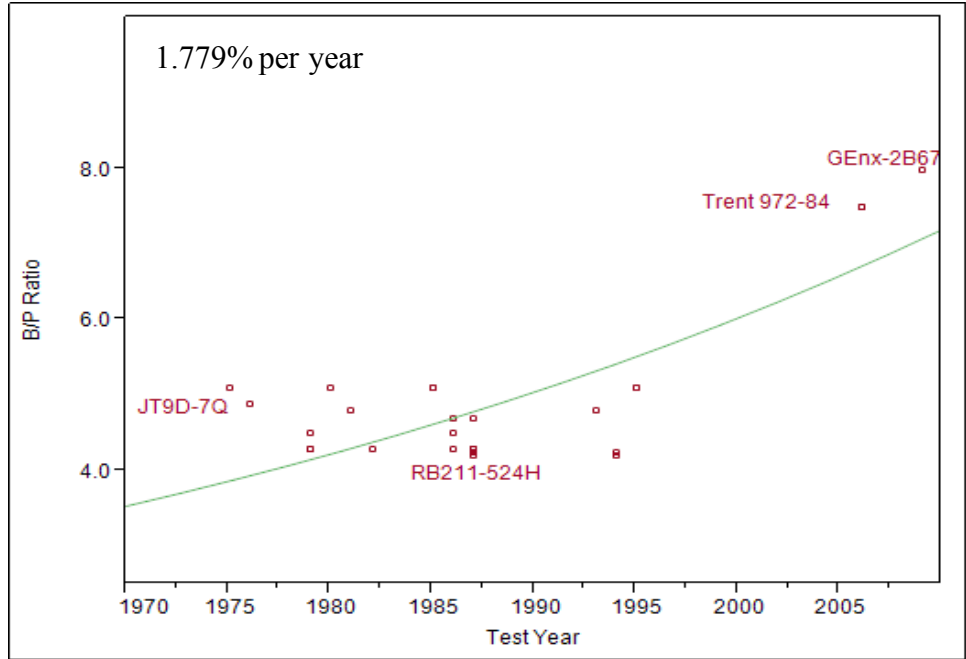


FIGURE 126: CRUISE TSFC VS. CERTIFICATION DATE [64]

### *Bypass Ratio (BPR)*

Bypass Ratio is the ratio between the mass flow rates of air that bypasses the core of the engine and air that passes through the engine core. Figure 127-Figure 131 depict the expected trend of BPR increasing in time. A higher bypass ratio provides lower TSFC and lower noise output. The optimum BPR for lowest fuel consumption is likely to increase with time.



**FIGURE 127: BPR VS. CERTIFICATION YEAR FOR LQ**

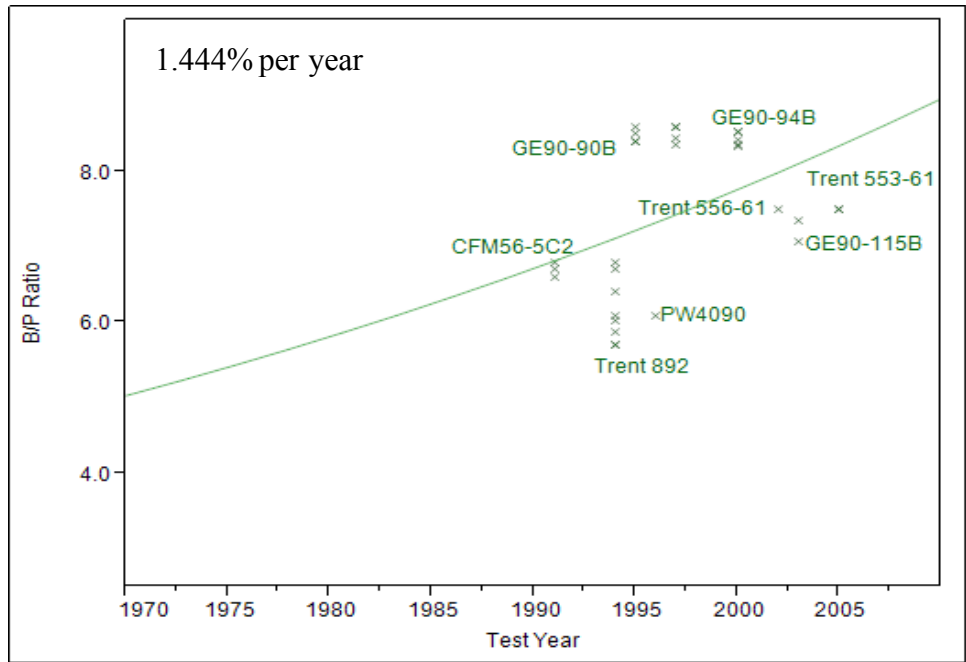


**FIGURE 128: BPR VS. CERTIFICATION YEAR FOR LTA**

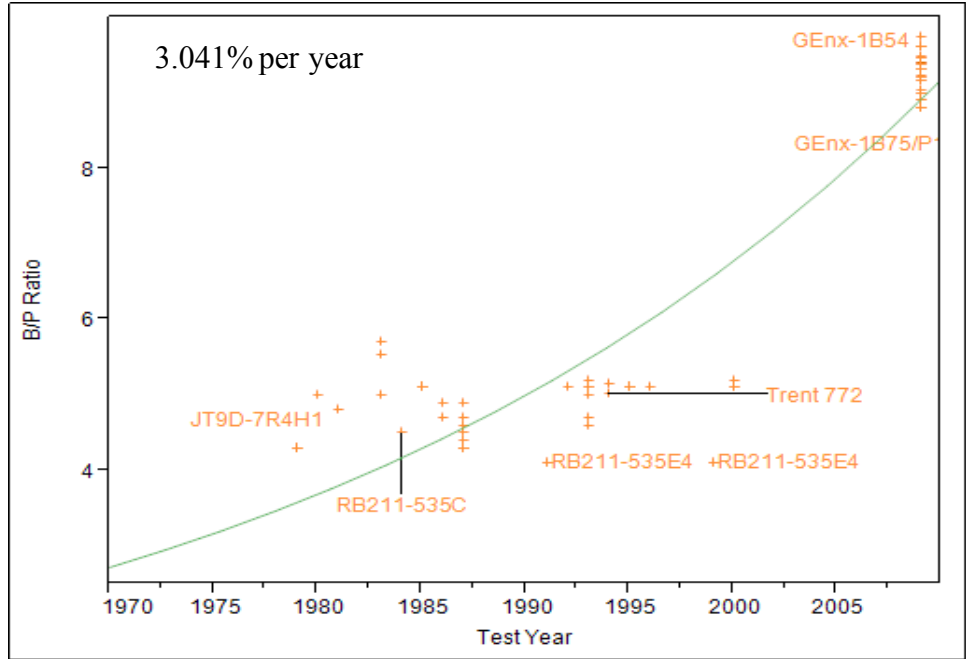


**FIGURE 129: BPR VS. CERTIFICATION YEAR FOR STA**

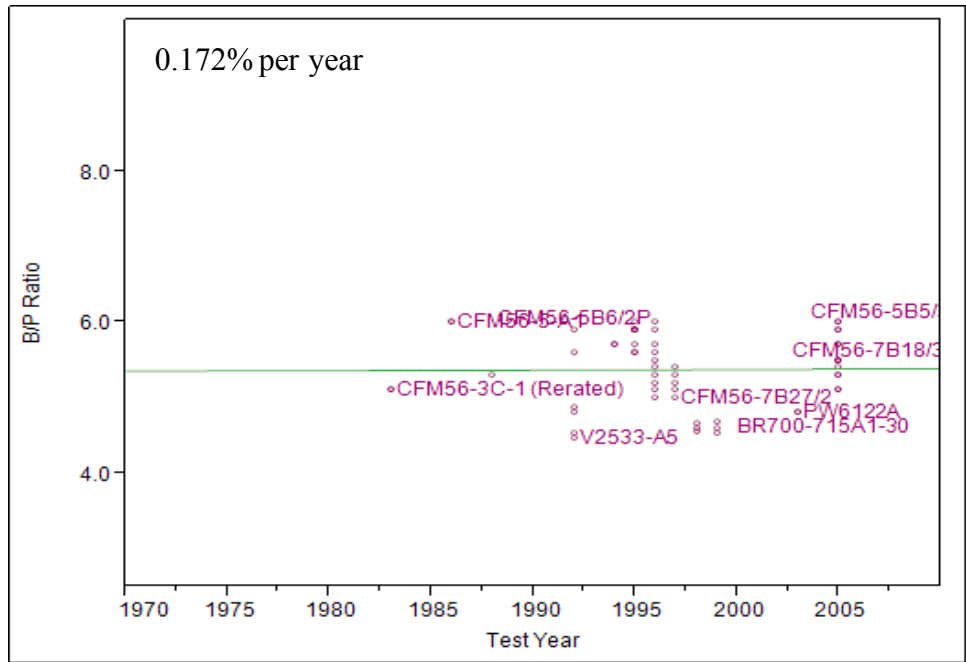


**FIGURE 130: BPR VS. CERTIFICATION YEAR FOR SA**

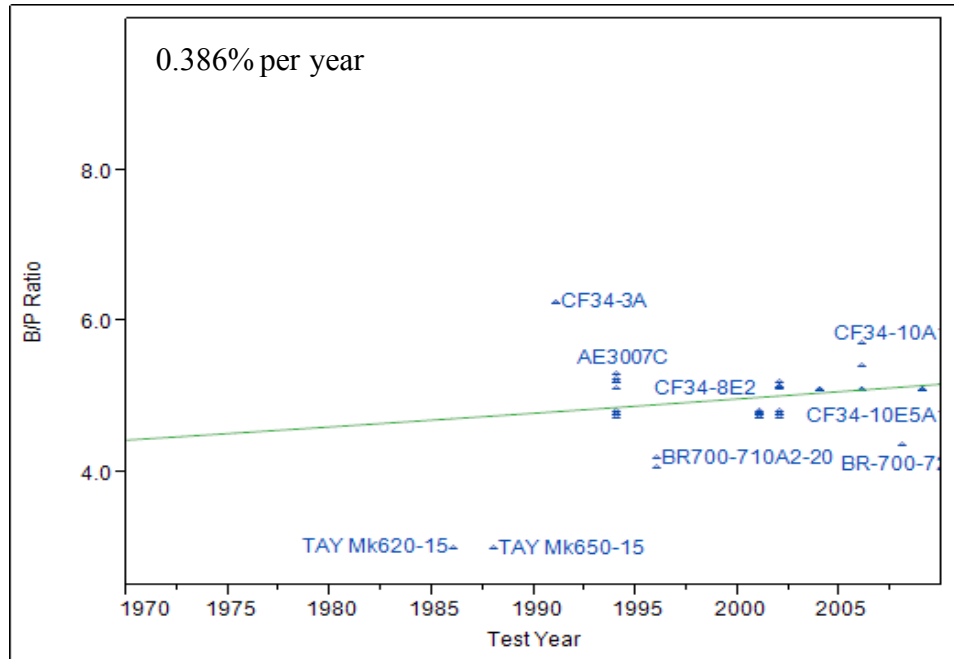


**FIGURE 131: BPR VS. CERTIFICATION YEAR FOR RJ**

***Overall Pressure Ratio***

The OPR is defined as the ratio of the stagnation pressure measured from the front and the rear of the cold section of the turbofan. This includes the fan, high pressure and low pressure compressor. Generally speaking, the OPR will be the multiplication of FPR, LPCPR and HPCPR. Early jet engines had very low OPR due to construction of the compressors; however improvements in materials, compressor blades and the addition of multi-spool engines have led to much higher OPR values seen in Figure 132-Figure 136.

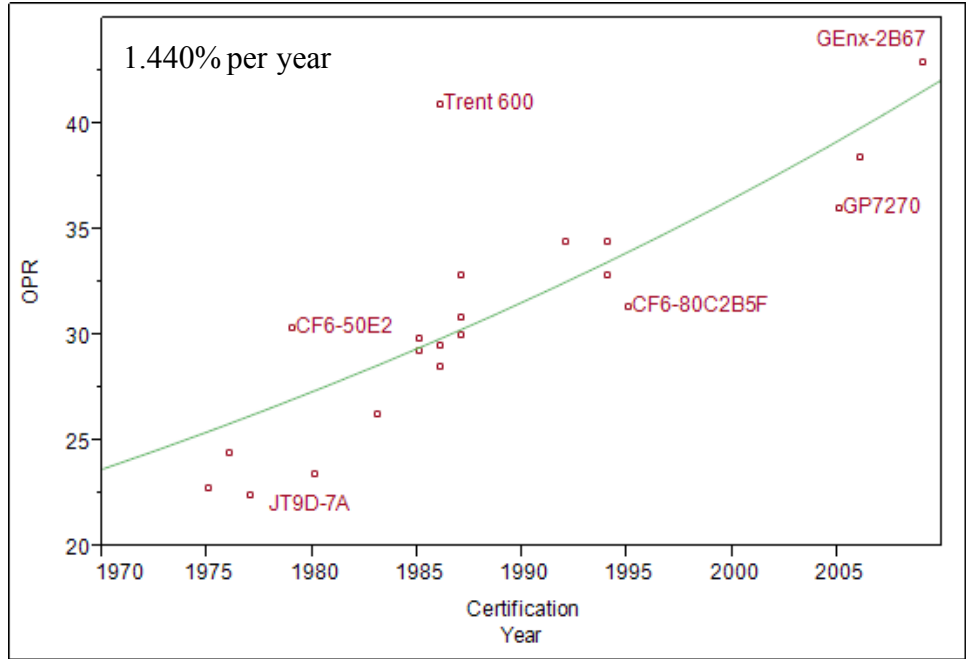


**FIGURE 132: OPR VS. CERTIFICATION YEAR FOR LQ**

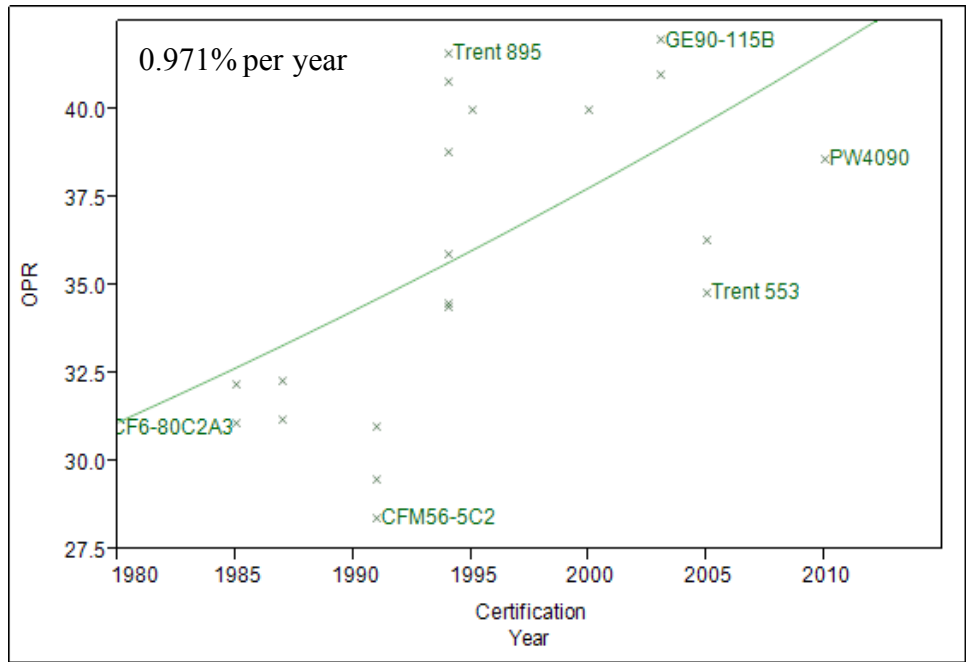


**FIGURE 133: OPR VS. CERTIFICATION YEAR FOR LTA**

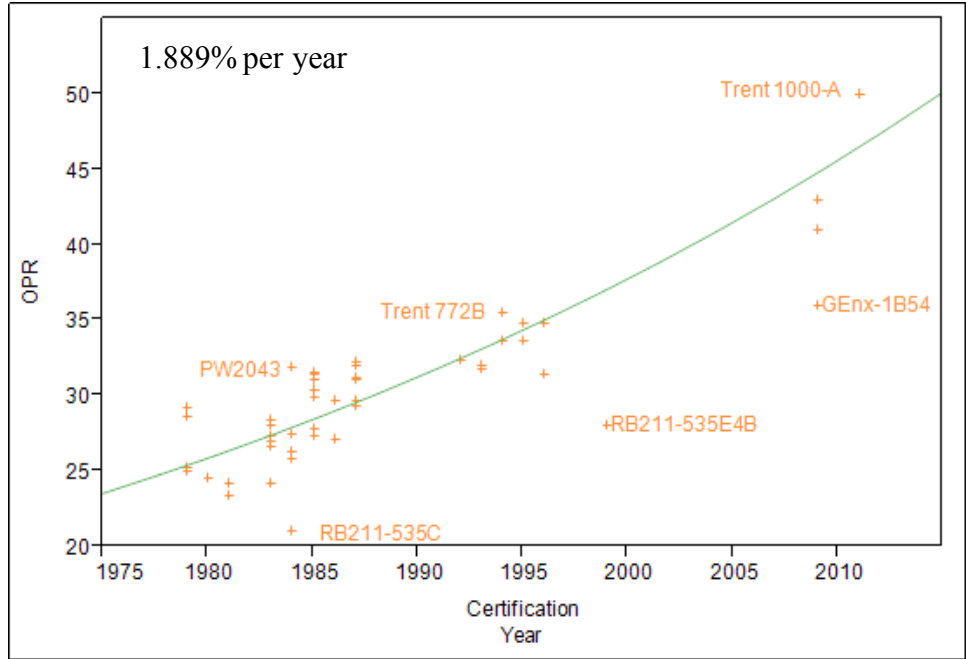


**FIGURE 134: OPR VS. CERTIFICATION YEAR FOR STA**

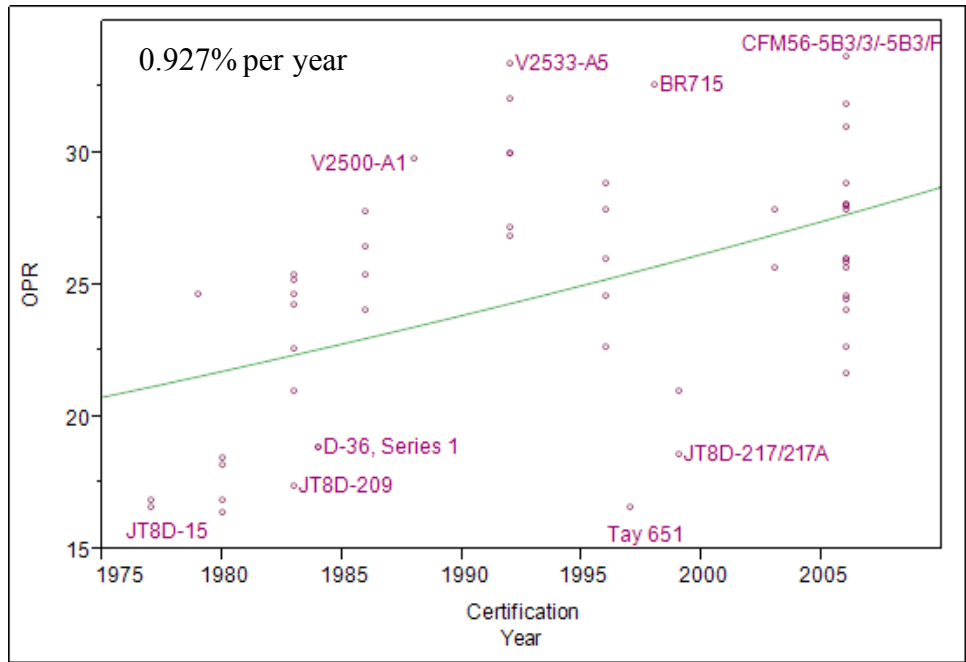


**FIGURE 135: OPR VS. CERTIFICATION YEAR FOR SA**

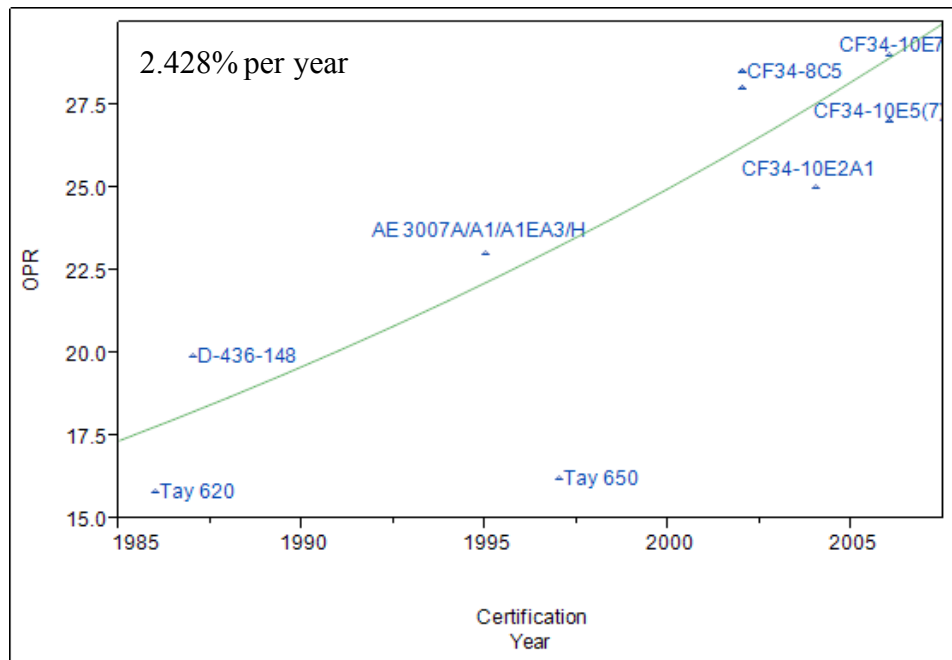


**FIGURE 136: OPR vs. CERTIFICATION YEAR FOR RJ**

### *Cumulative Noise and Noise Margin*

The cumulative noise, or the addition of sideline, cutback and approach noise values, is plotted against time in Figure 137-Figure 141 in terms of EPNdB. The percent changes in Table 23 range from +/- 0.2%. The downward trend for the LQ is confirmed in Figure 148 from [65]. Note opposite trends for the RJ and LTA classes showing increased total noise over time relative to the other sizes (SA, STA, LQ). This requires additional explanation. The LTA (Figure 138) is a relatively new size class. As such, attempting to fit a linear trend over the same timeframe as the other vehicles does not make sense. Furthermore, the scatter in the LTA clearly shows upsized vehicles, such as the 777-330, create more noise due to uprated engine. It is expected that future LTA sized vehicles, with higher bypass ratios, will follow similar noise trends as the STA and LQ. In the RJ class, there has been significant upgauging of RJ sizes with the RJ's approaching the size of the smaller single aisles. As a result, the increase in thrust required increases cumulative noise. Trends are slightly altered when looking at noise margin rather than cumulative noise because the upgauged vehicles are allowed to emit higher levels of noise due to higher takeoff weights.

Lastly, the Noise Margin relative to Chapter 4 is shown in Figure 143-Figure 147 in terms of EPNdB. However, these trends are opposite of what is shown in Figure 148 from [66]. This is because reference's plot shows the noise margin, as opposed to total EPNdB.

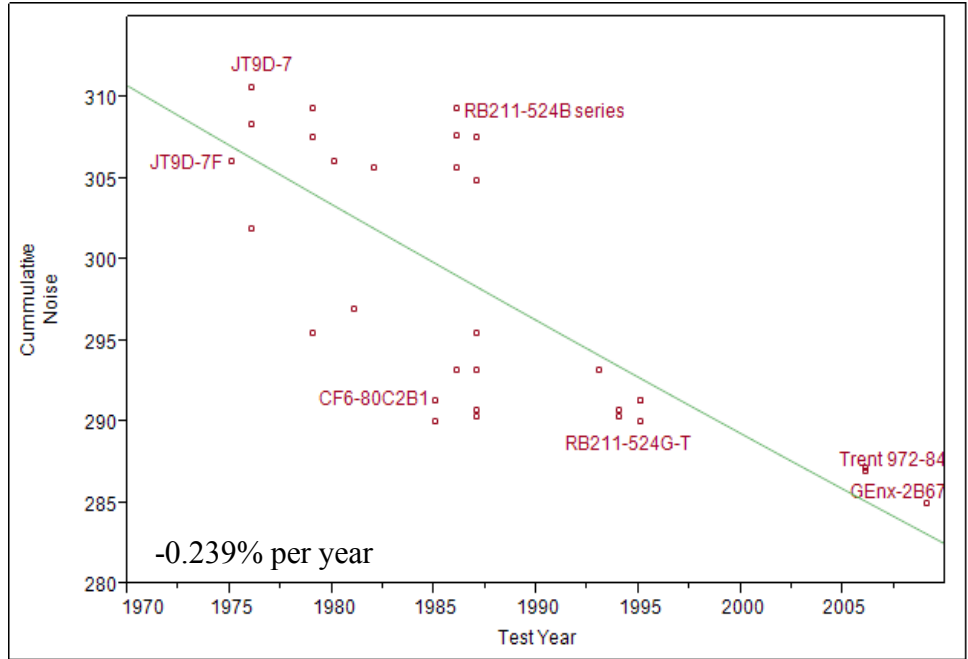


FIGURE 137: CUMULATIVE NOISE (EPNdB) VS. CERTIFICATION YEAR FOR LQ

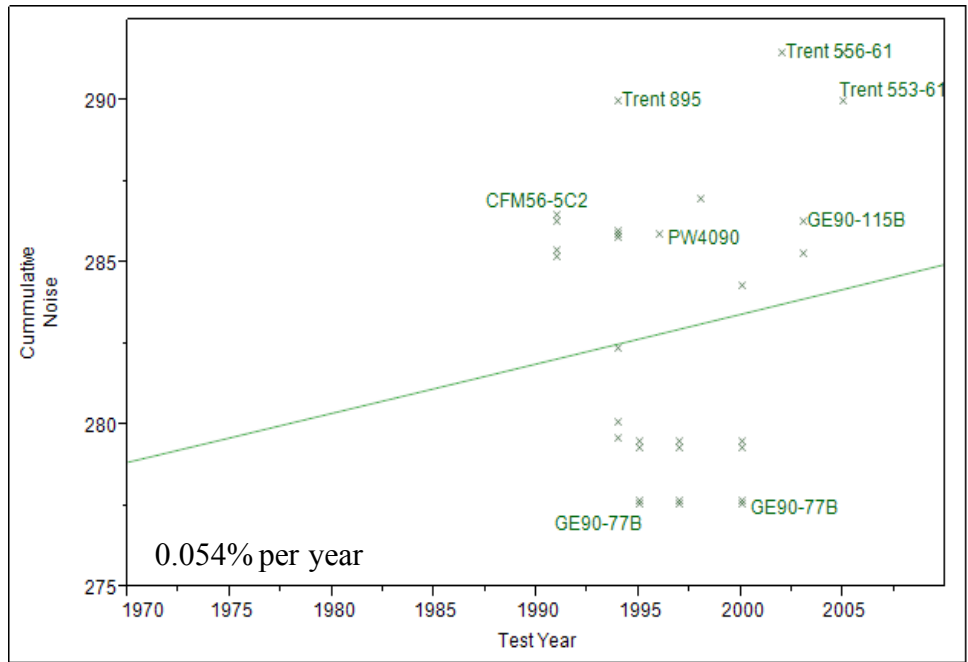
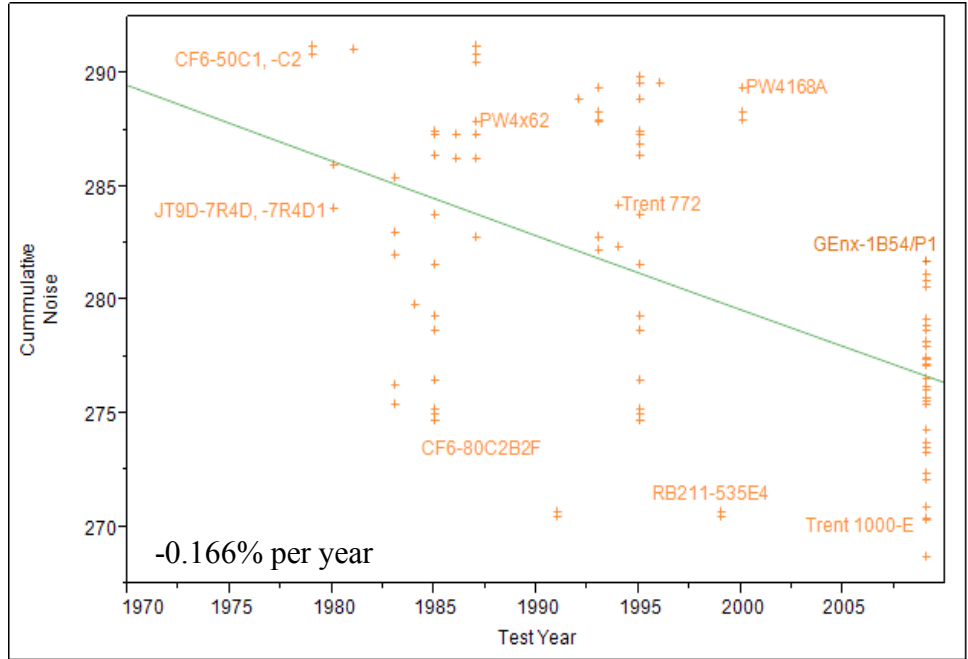
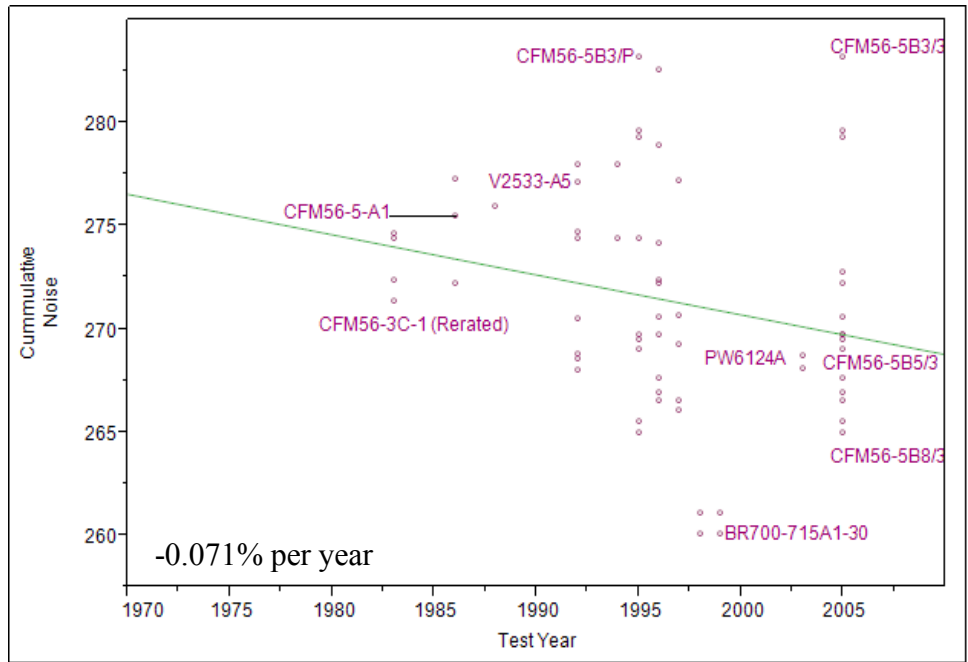


FIGURE 138: CUMULATIVE NOISE (EPNdB) VS. CERTIFICATION YEAR FOR LTA



**FIGURE 139: CUMULATIVE NOISE (EPNdB) VS. CERTIFICATION YEAR FOR STA**



**FIGURE 140: CUMULATIVE NOISE (EPNdB) VS. CERTIFICATION YEAR FOR SA**



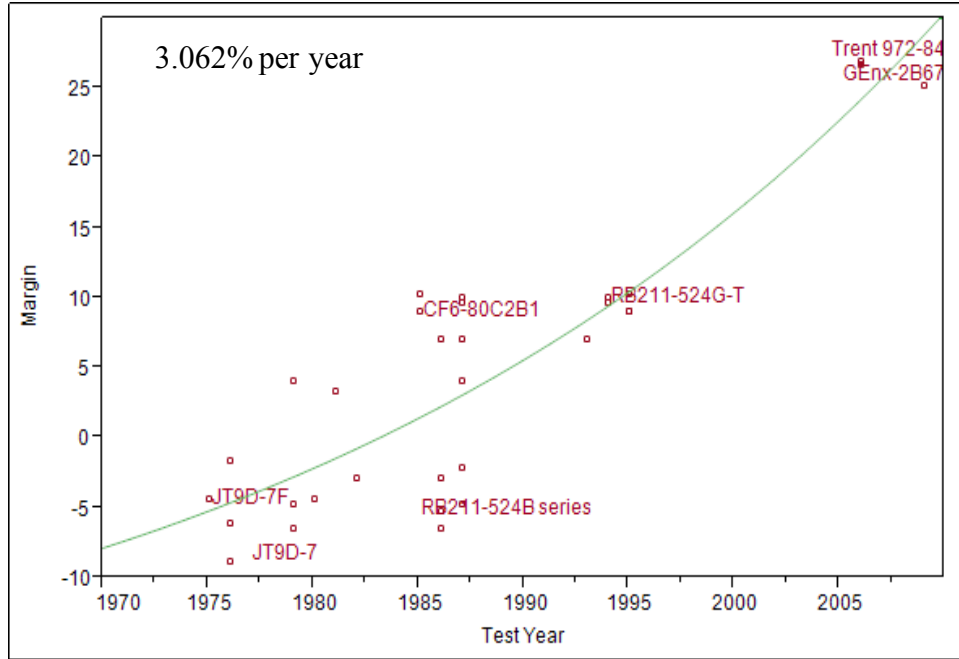


**FIGURE 143: NOISE MARGIN RELATIVE TO CHAPTER 4 (EPNdB) VS. CERTIFICATION YEAR FOR LQ**

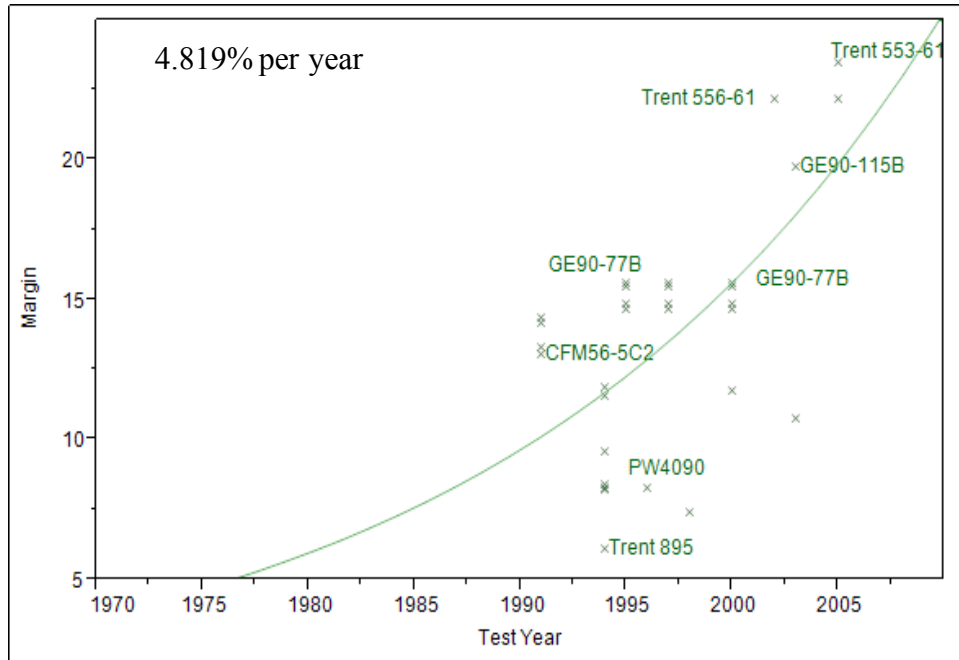


**FIGURE 144: NOISE MARGIN RELATIVE TO CHAPTER 4 (EPNdB) VS. CERTIFICATION YEAR FOR LTA**

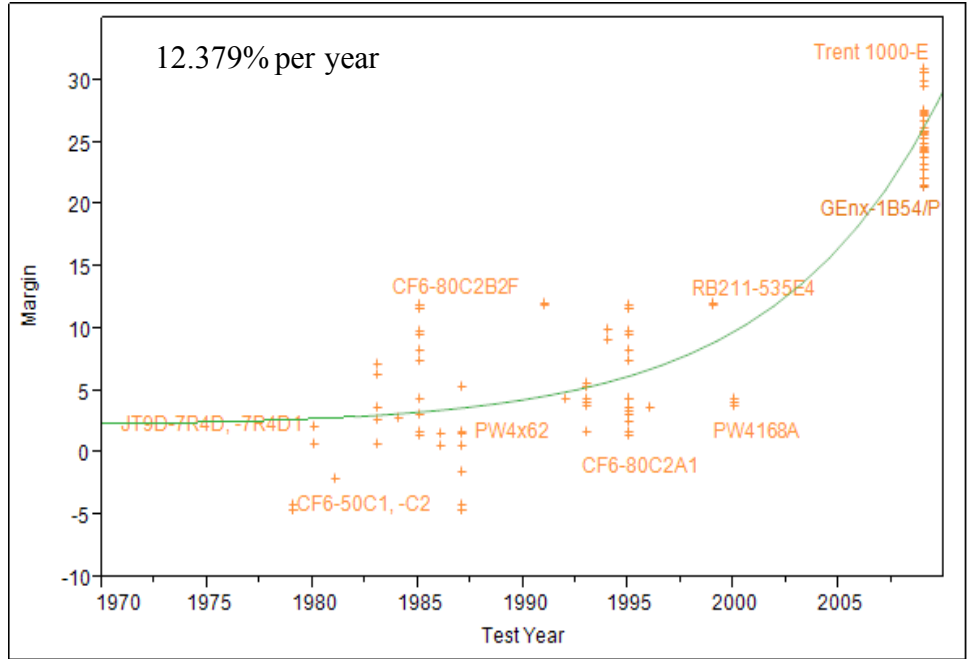


**FIGURE 145: NOISE MARGIN RELATIVE TO CHAPTER 4 (EPNdB) vs. CERTIFICATION YEAR FOR STA**

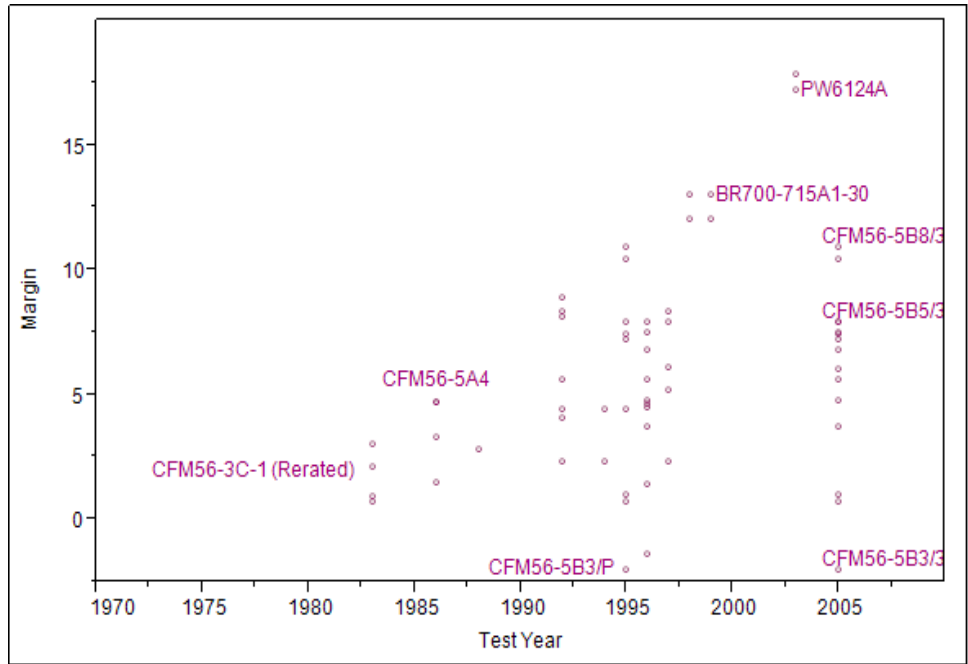


**FIGURE 146: NOISE MARGIN RELATIVE TO CHAPTER 4 (EPNdB) vs. CERTIFICATION YEAR FOR SA**

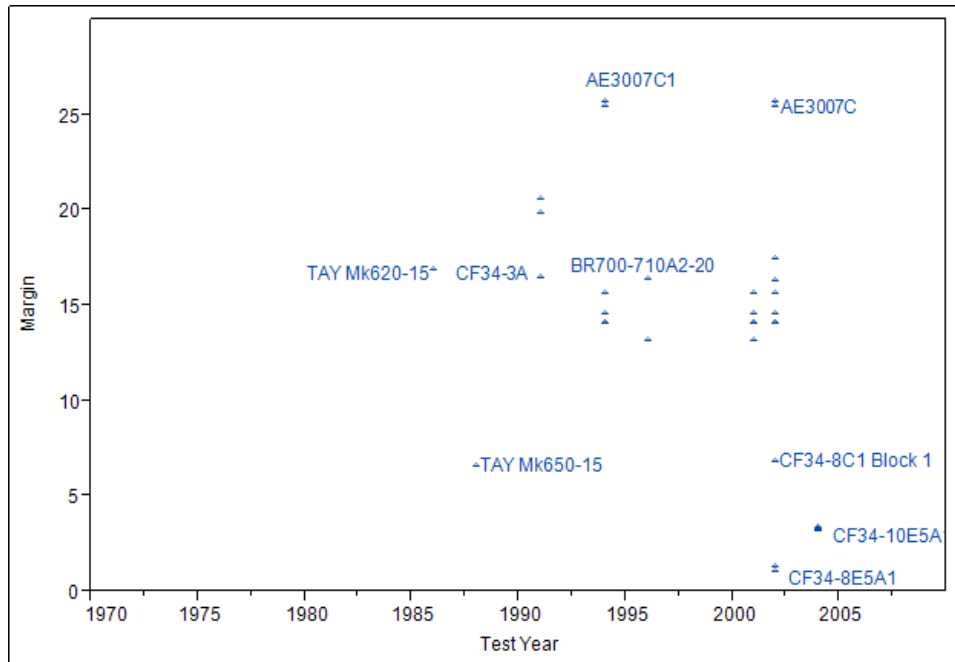


FIGURE 147: NOISE MARGIN RELATIVE TO CHAPTER 4 (EPNDB) VS. CERTIFICATION YEAR FOR RJ

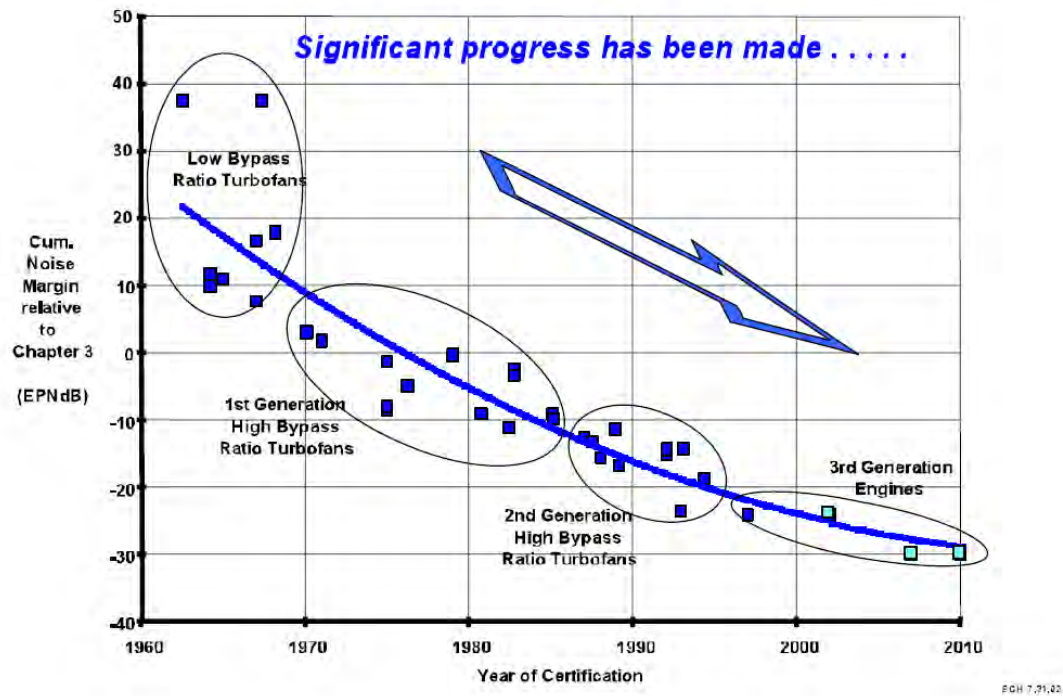


FIGURE 148: CUMULATIVE NOISE MARGIN RELATIVE TO CHAPTER 3 VS. CERTIFICATION YEAR [66]

**TABLE 23: PERCENT CHANGE PER YEAR FOR EACH METRIC AND VEHICLE CLASS**

Metric	LQ	LTA	STA	SA	RJ
L/D	0.325%	0.532%	0.542%	0.135%	0.428%
MTOW	1.29%	2.682%	1.06%	-	1.344%
FB (Payload * Range) for R1	-0.583%	-0.619%	-	-0.533%	-
FB (Payload * Range) for R2	7.093%	0.825%	-0.779%	1.40%	-0.785%
OEW/MTOW	0.161%	-0.001%	0.017%	0.390%	0.057%
OEW/Max Payload	0.659%	0.532%	0.021%	0.064%	0.202%
Rated Output	1.326%	2.180%	1.143%	0.100%	5.318%
Engine W/T	0.185%	0.645%	0.242%	0.220%	-
SFC	-0.674%	-	-	-0.069%	-0.302%
BPR	1.779%	1.444%	3.041%	0.172%	0.386%
OPR	1.440%	0.971%	1.889%	0.927%	2.428%
Cumulative Noise	-0.239%	0.054%	-0.166%	-0.071%	0.258%
Noise Margin	3.062%	4.819%	12.379%	-	-

**Appendix B.D Low Level Trends**

After the data was plotted, a number of other metrics were also of interested, however, the data was not as readily available. A list of “Low Level Metrics” was then created in consultation with the FAA, displayed in Table 24. A literature search was conducted to find a plot of each of these metrics over time within AIAA papers or other journals, for instance *Journal of Propulsion and Power*.

**TABLE 24: LOW LEVEL METRICS FOR HISTORICAL TREND RESEARCH**

Low Level Metrics		
Metal Temperature Capability	Cooling Effectiveness	Turbine Inlet Temperature
Core Engine Power	Compressor Pressure Ratio	Stage Loading
Combustor Exit Temperature	Thermal & Propulsive Efficiency	Materials Usage

***Compressor Pressure Ratio & Stage Loading***

Figure 149 and Figure 150 show the rise of compressor pressure ratio over time. Figure 149 from [64] shows that pressure ratios for subsonic aircraft have increased by a factor of 4 during the

past 50 years. The paper explains that this is because more recent engines are pushing the compressor discharge temperature limit. Figure 150 also shows the compressor pressure ratio increasing with time in the plot on the left. This is due to the introduction of the combined multiple rotor and variable stator features in the 1970s. The plot on the right shows that the number of stages required decreases over time as stage loading increased with an increasing compressor pressure ratio [67].

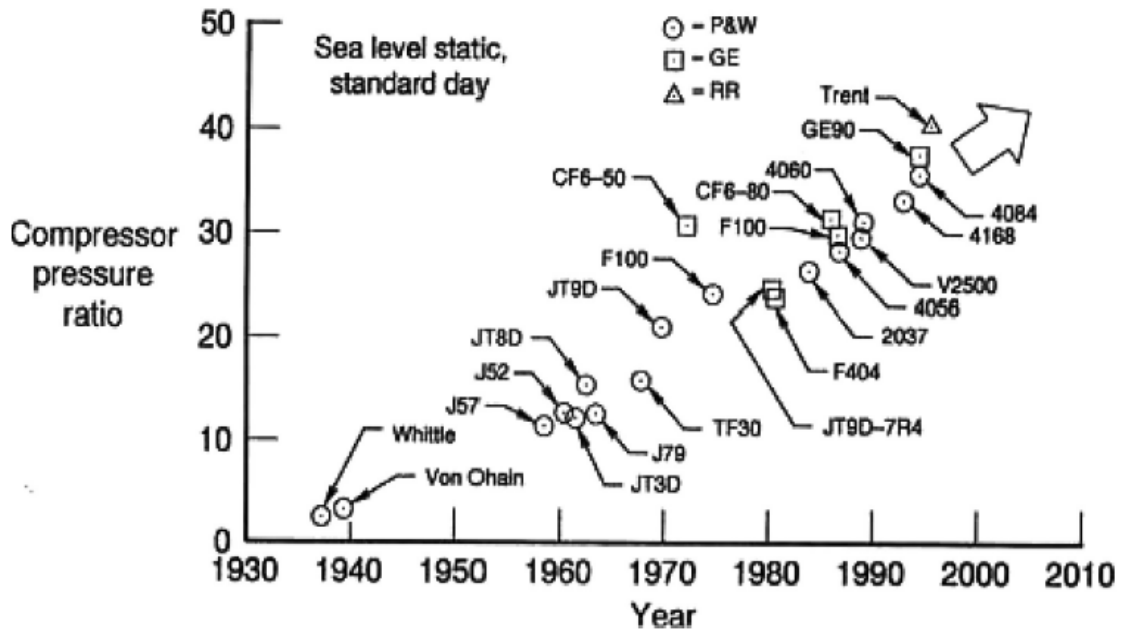
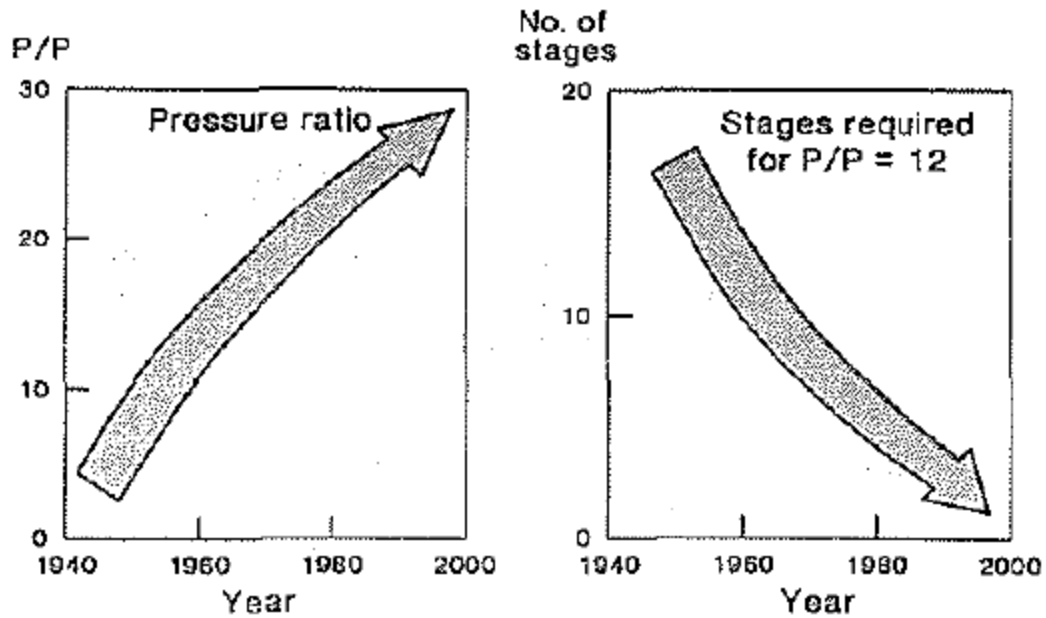


FIGURE 149: COMPRESSOR PRESSURE RATIO VS. CERTIFICATION YEAR [64]



**FIGURE 150: IMPROVEMENTS IN COMPRESSOR PRESSURE RATIO AND STAGE LOADING [67]**

### *Metal Temperature Capability*

Metal temperature capability plotted against the engine's availability date is shown in Figure 151 and Figure 152. Figure 151 from [64] shows an improvement of 500 degrees Fahrenheit for turbine airfoils. This is a result of materials research, processing and manufacturing technology. Research and development for superalloys began in the 1940s. In the 1950s, vacuum induction melting became a breakthrough technology which was able to boost an alloy's capability. Then larger forgings for disks were made possible with the vacuum arc remelting process.

Figure 152 depicts the introduction of thermal barrier coatings for hot section airfoils. Aluminide coatings were first applied during the mid-1970s as the turbine's airfoils began to have a longer lifespan. Ceramic thermal barrier coatings were then applied in the mid-1980s. The plot shows that the material can now reach within 200 degrees of incipient melting with the best alloys [64].

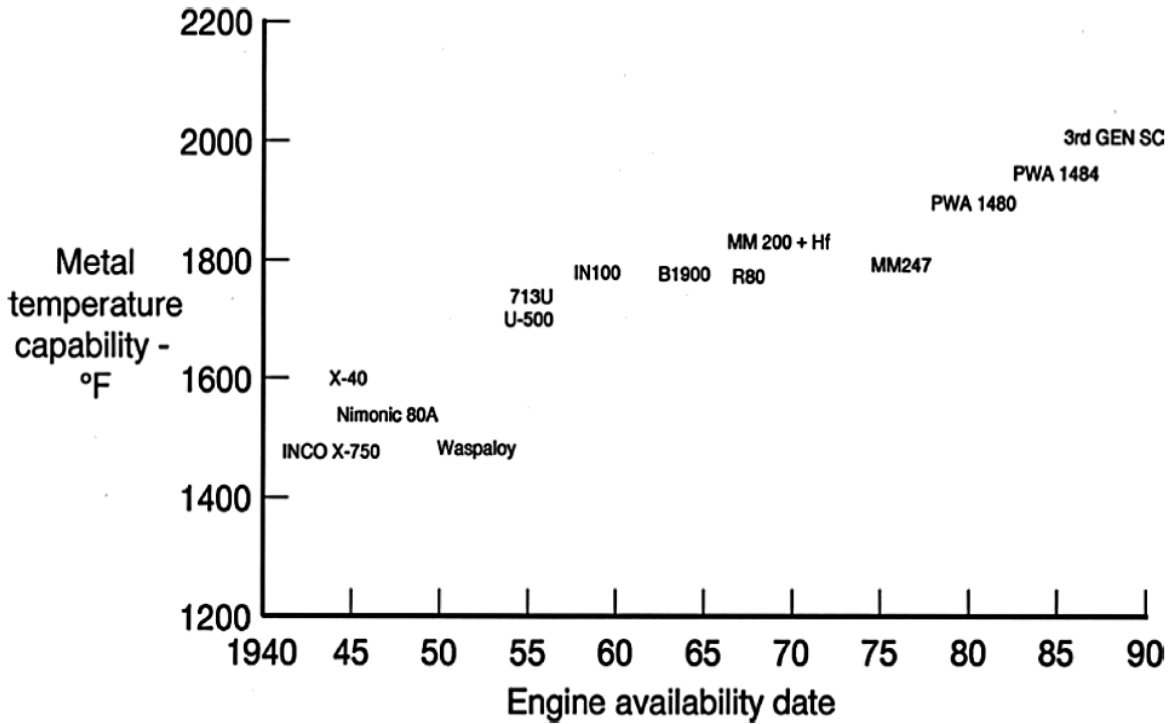


FIGURE 151: METAL TEMPERATURE CAPABILITY VS. ENGINE AVAILABILITY DATE [64]

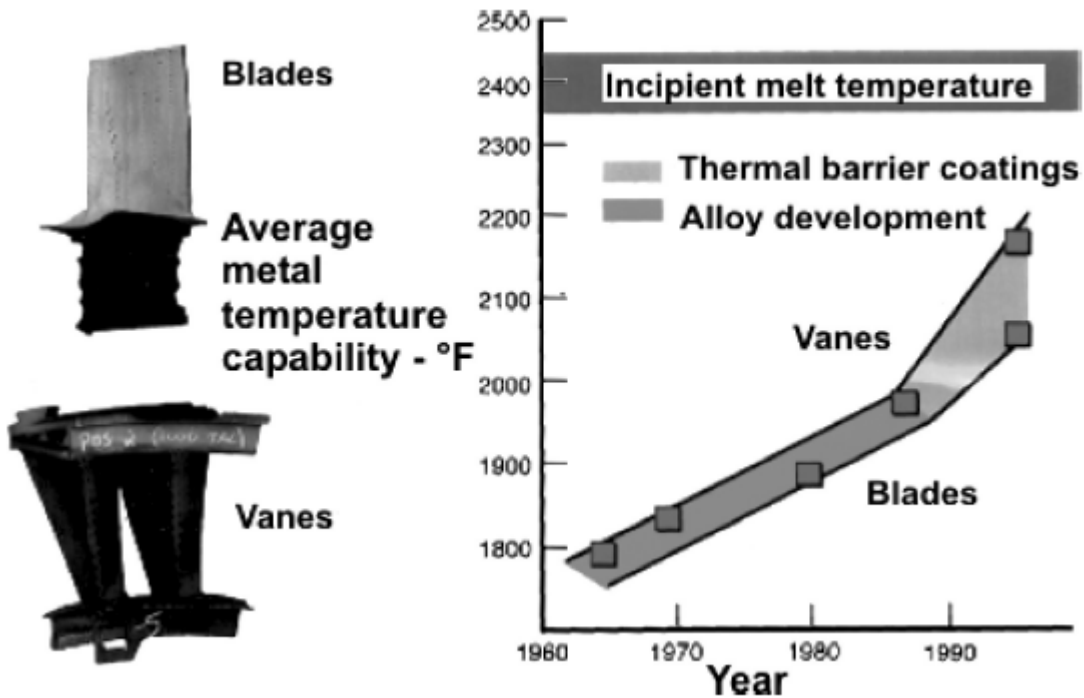
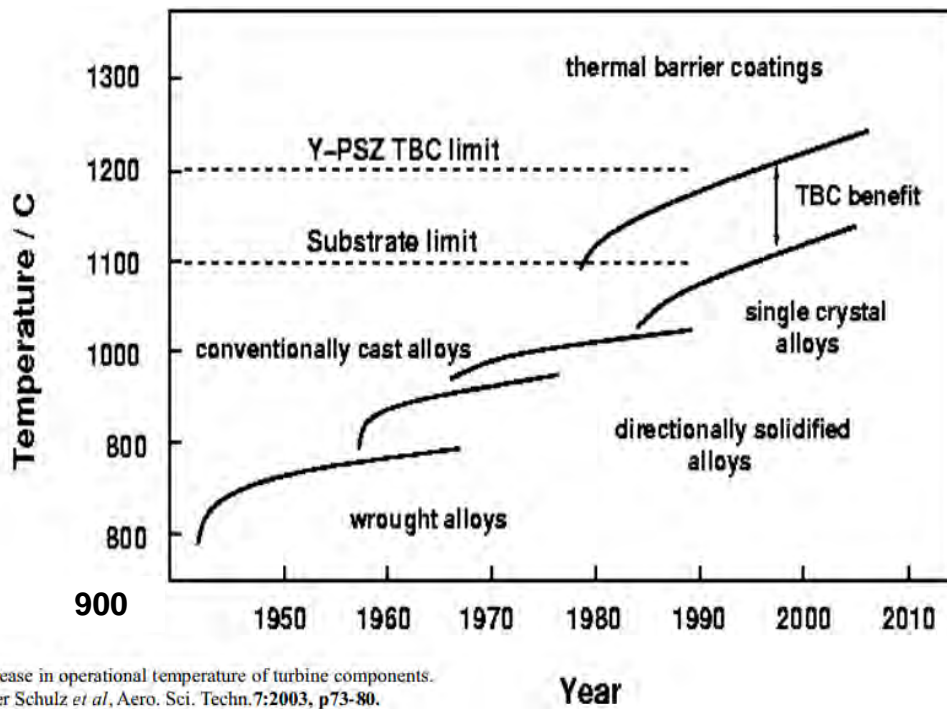


FIGURE 152: AVERAGE METAL TEMPERATURE CAPABILITY VS. YEAR [64]

### ***Turbine Inlet Temperature, Cooling Effectiveness & Specific Core Power***

Figure 153 and Figure 154 illustrate the turbine inlet temperature trend over time. Figure 153 plots the temperature of the metal, or T4, with respect to different materials. This plot illustrates the increase in capabilities of the alloys over time and the addition of thermal barrier coatings (TBC). Figure 154 also shows T4, but instead versus the cooling effectiveness. The cooling effectiveness is the ratio of the airfoil head load to cooling flow. This measures how well the airfoil is cooled. As cooling effectiveness of the rotor increases, T4 is able to increase exponentially. This can also be seen as a chronological evolution. The solid rotor blades refer to the 1950s, by the 1960s, blades progressed to convection cooled blades. By the 1980s, single crystal film/convection cooled blades increased the cooling effectiveness to 0.6+ with a T4 capability 1200 degrees Fahrenheit above the solid uncooled blades [64].



**FIGURE 153: TURBINE INLET TEMPERATURE VS. YEAR [68]**

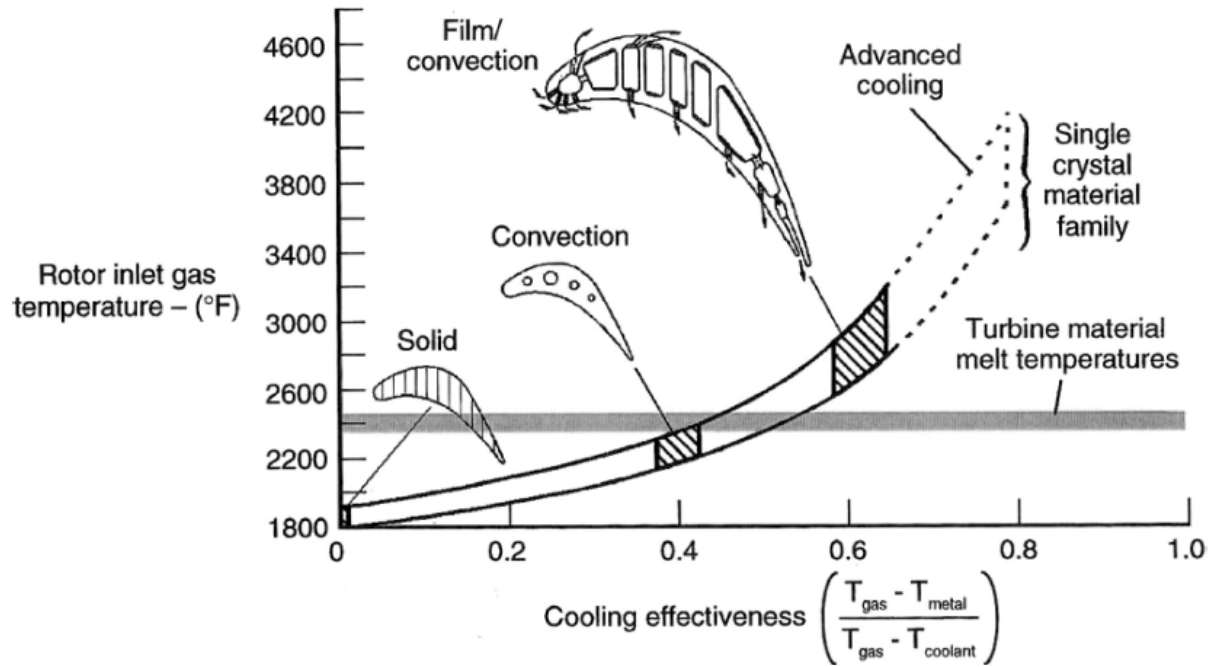


**FIGURE 154: ROTOR INLET GAS TEMPERATURE (T4) VS. COOLING EFFECTIVENESS [64]**

### Core Engine Power

Figure 155 is a comparison of the power of the core engine with the turbine rotor inlet temperature (T41). In this plot the power is normalized by dividing by the mass flow. This eliminates the size effect of each of the engines. The specific core engine power increases steadily with turbine temperature and with time. By the 1990s, the core engine power became 5 times more than the early engines seen in the 1930s [64]. The evolution is largely driven by the introduction of dual spool turbojets or turbofans.

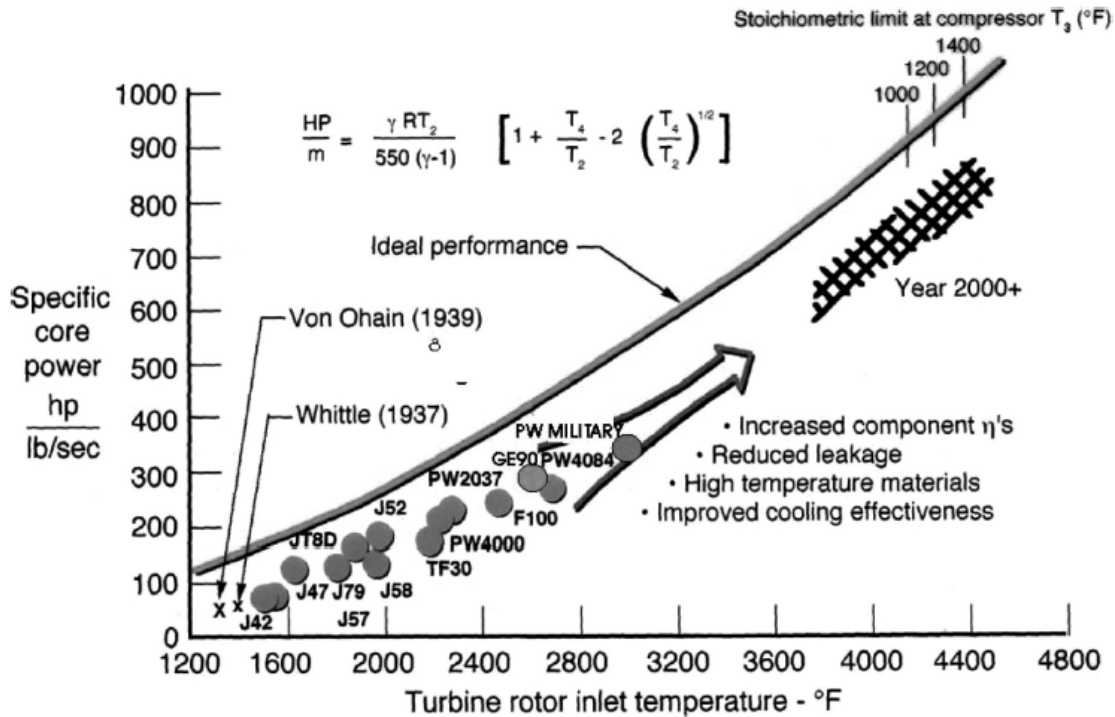


FIGURE 155: CORE ENGINE POWER VS. TURBINE ROTOR INLET TEMPERATURE [64]

### Combustor Exit Temperature

The combustor or burner outlet temperature over time is seen in Figure 156 and Figure 157. Figure 156 depicts this by showing the increase of durability of the combustion liners. With increasing engine life requirements, enclosing the hot gases within the combustor became an issue. The plot shows how the manufacturing process of the liners attributed to the increase in combustor exit temperature. Combustion liners were first manufactured by spot and seam welded louvers. The Machined ring liners provided a 10x life improvement. By the 1970s, the Air Force funded removable liner panels that shielded the outer liner from the hot gases. This, again, provided a 10x life improvement. Figure 157 shows the actual increase in magnitudes of the burner outlet temperature (T3) over time by the types of engines.

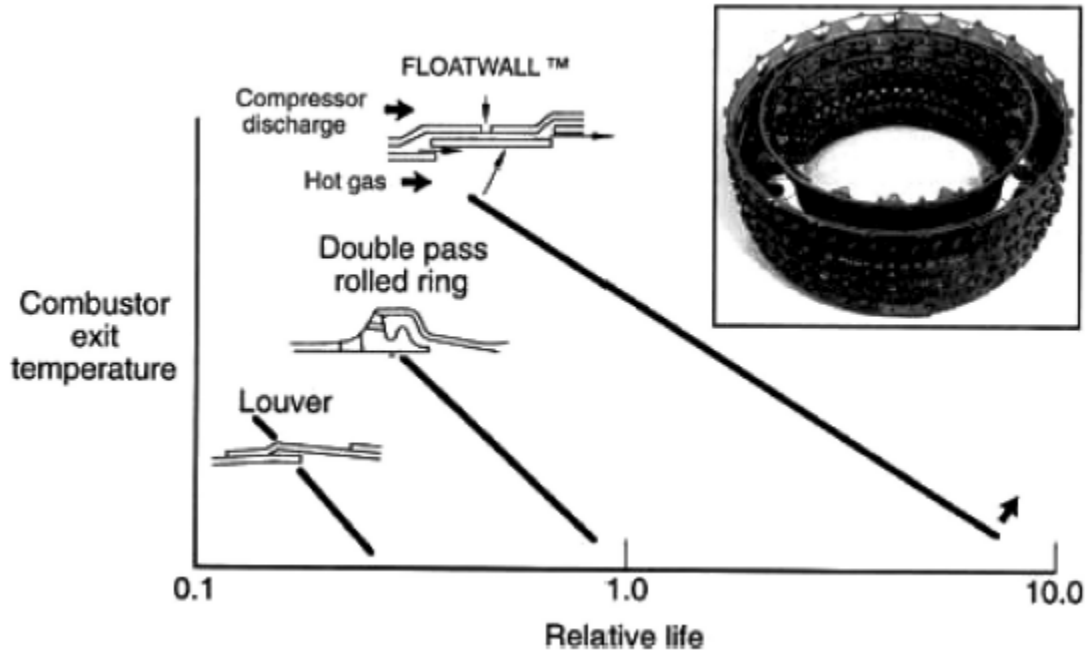


FIGURE 156: COMBUSTOR EXIT TEMPERATURE VS. RELATIVE LIFE [64]

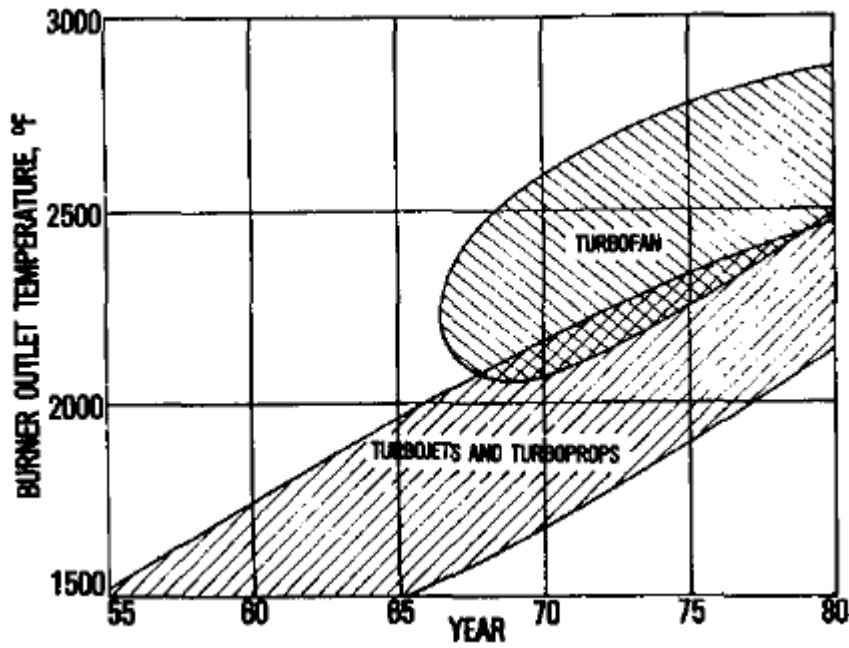
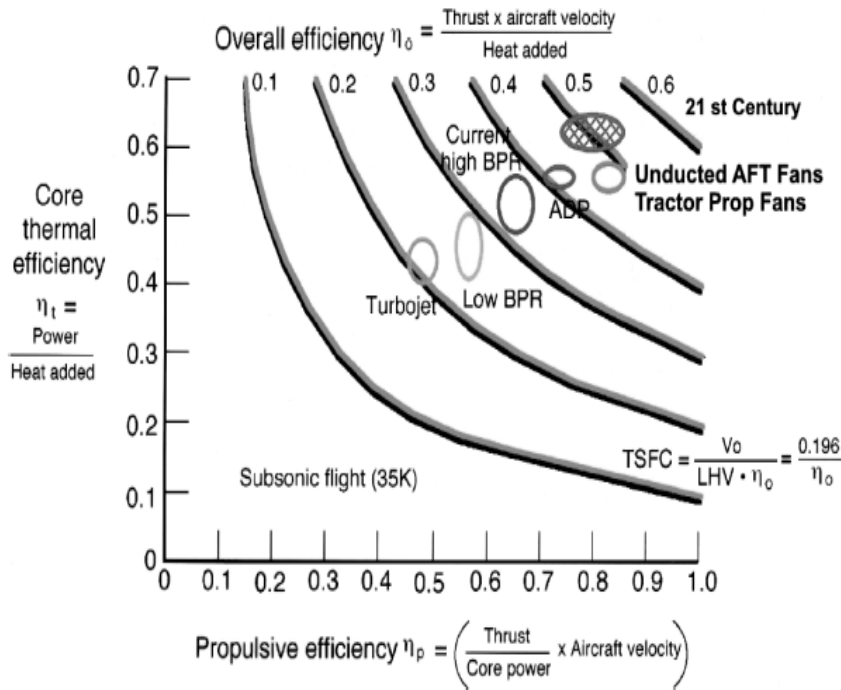


FIGURE 157: BURNER OUTLET TEMPERATURE VS. YEAR BY TYPES OF ENGINES [69]

### Thermal and Propulsive Efficiency

The core engine thermal efficiency and propulsive efficiency relationship will determine the overall engine efficiency. Figure 158 shows the thermal efficiency plotted against the propulsive efficiency. As the overall efficiency increases diagonally up and to the right, this also shows the increase over time. The cross-hatched area in the 50% overall efficiency indicate the final frontier for subsonic flight [64].



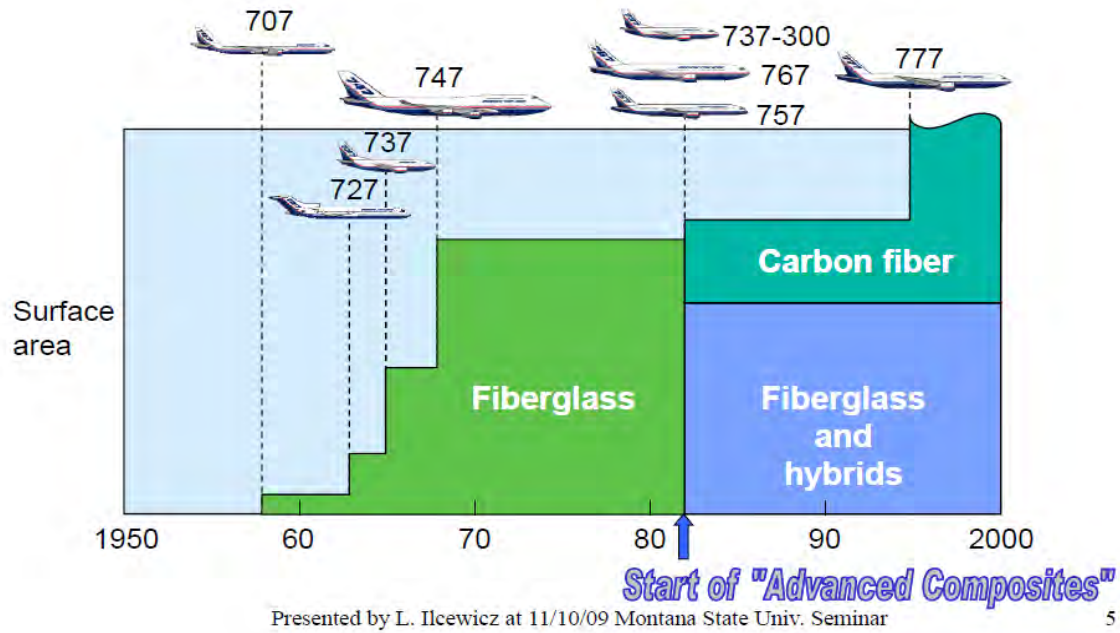
**FIGURE 158: ENGINE THERMAL EFFICIENCY VS. PROPULSIVE EFFICIENCY [64]**

### Materials Usage

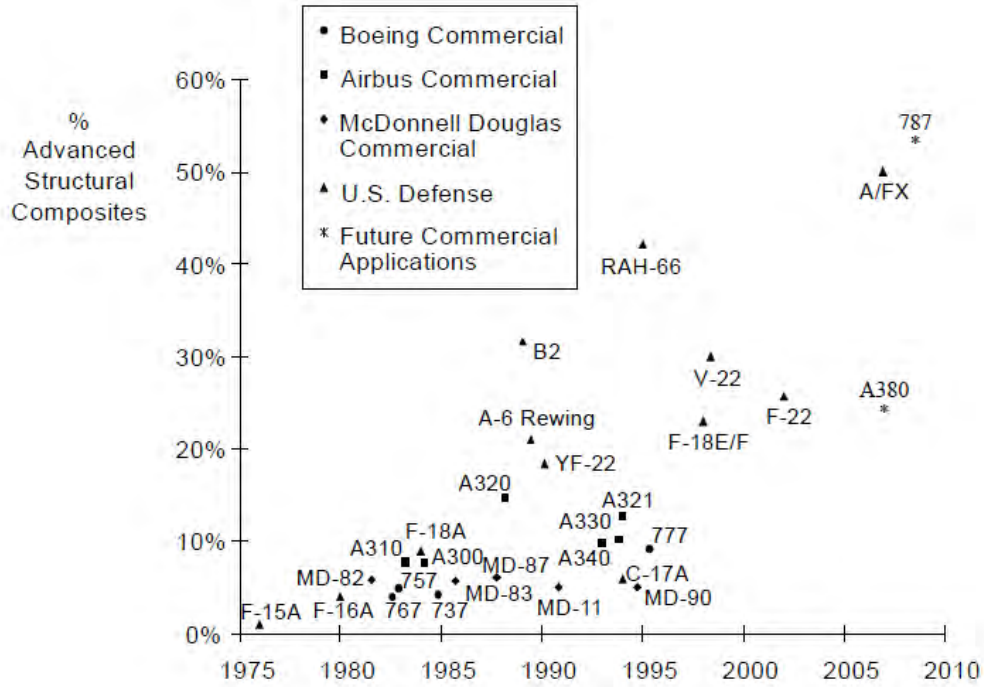
The type of materials used plays a major role in the weight of the aircraft. The following 3 plots, Figure 159-Figure 161 depict the surface area or percentage of material/weight of different materials over time. The increased use of composites in the structures of the aircraft is shown in Figure 159 and Figure 160. Figure 159, a plot about the use of composites in Boeing aircraft, plots the surface area over time, while Figure 160 shows all types of aircraft over time. As expected, the Boeing 787 is shown apart from the rest of the vehicles with over 50% composites in its structures. The benefits of the increase in use of composites include weight reduction, improvement in fatigue resistance, corrosion prevention and fabrication cost advantages [70].

Figure 161 shows the percentage of total airframe material compared to the previous figures with only the percentage of the structural composites. Over time, the percentage of aluminum is decreasing in time while the composites percentage is increasing. This also leads to reduced structural weight. During the 1950s the introduction of high strength aluminum alloys and titanium for high temperature applications offered weight savings. After the 1960s the

development of composite materials showed 30% weight savings potential over aluminum and lead to their increased use [67].



**FIGURE 159: SURFACE AREA OF COMPOSITES VS. YEAR OF INTRODUCTION [70]**



Presented by L. Ilcewicz at 11/10/09 Montana State Univ. Seminar

FIGURE 160: PERCENTAGE OF COMPOSITES VS. YEAR OF INTRODUCTION [70]

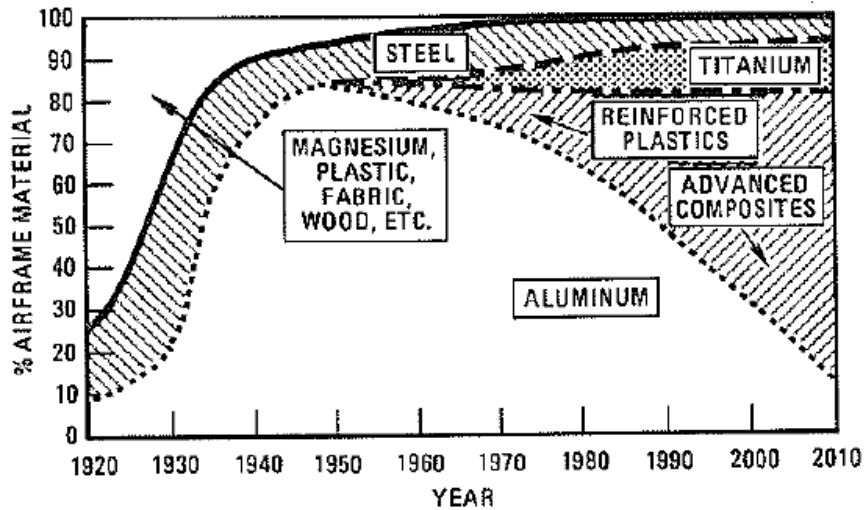


FIGURE 161: PERCENTAGE OF AIRFRAME MATERIAL VS. YEAR [67]

## References

- 1 D. McLean, ""Wingtip Devices: What They Do and How They Do It"," Article 4, Presented at the 2005 Boeing Performance and Flight Operations Engineering Conference.
- 2 Green, J., "Laminar Flow Control – Back to the Future", 38<sup>th</sup> Fluid Dynamic Conference and Exhibit, June 2008, AIAA 2008-3738.
- 3 Feagin, Richard C. and Morrision, William D., Jr: Delta Method, An Empirical Drag Buildup Technique. NASA CR-151971, December 151971
- 4 Perullo, C., Tai, J., Mavris, D., "Effects of Advanced Engine Technology on Open Rotor Cycle Selection and performance," Journal of Engineering for Gas Turbines and Power, Vol. 135, 071204-1 – 071204-9, 2013.
- 5 Perullo, C., Havrilesko, B., Mavris, D., "An Integrated Assessment of an Advanced Open Rotor Configuration Using the Environmental Design Space," 48<sup>th</sup> AIAA/ASME/SAE/ASEE Joint Propulsion Conference & Exhibit, July 2012.
- 6 Kurzke, J., "Fundamental Differences Between Conventional and Geared Turbofans", Proceedings of the ASME Turbo Expo 2009: GT2009-59745
- 7 Tong, M., Scott, J., Haller, W., "Engine Conceptual Designs for a Hybrid Wing Body Aircraft", NASA/TM – 2009-215680
- 8 Chironis, N., "Gear Design and Application", New York: McGraw Hill, 1967.
- 9 Aungier, R., "Turbine Aerodynamics: Axial-flow and Radial-inflow turbine design and analysis", New York : ASME Press, 2006.
- 11 [http://www.newac.eu/uploads/media/Active\\_Core\\_Concept.jpg](http://www.newac.eu/uploads/media/Active_Core_Concept.jpg)
- 12 Boyle, J., Jones, S., "Effects of Precooling Turbine Cooling Air on Engine Performance", Proceedings of the ASME Turbo Expo 2009: GT2009-60120
- 13 Incropera, F., "Fundamentals of Heat and Mass Transfer", New York : Wiley, 1985.
- 14 Shah, Ramesh K., and Dušan P. Sekulić. *Fundamentals of Heat Exchanger Design*. New York: John Wiley & Sons, 2003. Print.
- 15 Car, D., et al., "Analysis of a Highly Loaded, Transonic, Inlet Compressor Stage: Isolated and Multi-stage Performance", AIAA 2000-3206
- 16 Dickens, T., Day, I., "The Design of Highly Loaded Axial Compressors", Proceedings of ththe ASME Turbo Expo 2009: GT2009-59291
- 17 <http://www.grantadesign.com/education/overview.htm>
- 18 Dorfner, C., Nicke, E., Voss, C., Axis-Asymmetric Profiles Endwall Design Using Multiobjective Optimization Linked With 3D RANS-Flow-Simulations, ASME GT2007-27268
- 19 Lu, J., Chu, W., Wu, Y., Effects Of Endwall Profiling On Axial Compressor Stage, ASME GT2009-59418
- 20 Hu, S., Lu, X., Zhang, H., Zhu, J., Xu, Q., Numerical Investigation of a High-subsonic Axial-flow Compressor Rotor with Non-axisymmetric Hub Endwall, Journal of Thermal Science Vol.19, No.1, Springer, 2010
- 21 Reising, S., Schiffer, H., Non-Axisymmetric End Wall Profiling In Transonic Compressors. Part I: Improving The Static Pressure Recovery At Off-Design Conditions By Sequential Hub And Shroud End Wall Profiling, ASME GT2009-59133
- 22 Dorfner, C., Hergt, A., Nicke, E., Moenig, R., Advanced Non-Axisymmetric Endwall Contouring For Axial Compressors By Generating An Aerodynamic Separator – Part I: Principal Cascade Design And Compressor Application, ASME GT2009-59383
- 23 Reising, S., Schiffer, H., Non-Axisymmetric End Wall Profiling In Transonic Compressors. Part II: Design Study Of A Transonic Compressor Rotor Using Non-Axisymmetric Walls – Optimization Strategies And Performance, ASME GT2009-59134
- 24 Zorumski, W.E.: "Aircraft Noise Prediction Program Theoretical Manual," NASA TM-83199, 1981, Parts 1 and 2
- 25 Molin, Nicolas, Piet, Jean-Francois, et al, Prediction of Low Noise Aircraft Landing Gears and Comparison with Test Results, AIAA 2006-2623
- 26 Molin, Nicolas, Piet, Jean-Francois, et al, Prediction of Low Noise Aircraft Landing Gears and Comparison with Test Results, AIAA 2006-2623
- 27 Guo, Y., On Noise Reduction by Flap Side Edge Fences, Vol. 277, Journal of Sound and Vibration, 2004

- 28 Slooff, J. W., de Wolf, W. B., et al, Aerodynamic and Aero-acoustic Effects of Flap Tip Fences, AIAA-2002-0848
- 29 Saiyed, N.H.; Mikkelsen, K.L.; and Bridges, J.E.: Acoustics and Thrust of Separate-Flow Exhaust Nozzles with Mixing Devices for High-Bypass-Ratio Engines. NASA Glenn Research Center and Aero Systems Engineering Report. AIAA-2000-1961, 2000.
- 30 Montgomery, S., "Engine noise reduction programme: Making aircraft engines better neighbours.", Airbus circular, accessed 12/8/2010
- 31 Yu, J., Chein, E., "Folding Cavity Acoustic Liner for Combustion Noise Reduction", AIAA 2006-2681
- 32 Mabe, J., "Variable Area Jet Nozzle for Noise Reduction Using Shape Memory Alloy Actuators"
- 33 Mercer, C., Haller, W., Tong, M., "Adaptive Engine Technologies for Aviation CO2 Emissions Reduction", 42<sup>nd</sup> AIAA/ASME/SAE/ASEE Joint Propulsion Conference & Exhibit, July 2006, AIAA 2006-5105.
- 34 Woodward, R., Elliot, D., Hughes, C., Berton, J., Benefits of Swept-and-Leaned Stators for Fan Noise Reduction, Journal Of Aircraft Vol. 38 No. 6, 2001, AIAA
- 35 Cooper, A., Peake, N., Rotor Stator Interactions Noise in Swirling Flow: Stator Sweep and Lean Effects, AIAA Journal Vol. 44 No.5, 2006
- 36 Gazziniga, J., Performance Of Advanced Fan Exit Guide Vane Concepts For High Speed Fans, AIAA 2002-0377
- 37 Hanson, D., Theory for Broadband Noise of Rotor and Stator Cascades With Inhomogeneous Inflow Turbulence Including Effects of Lean and Sweep, NASA CR 2001-210762
- 38 Jones, M.G., et al., "Assessment of Soft Vane and Metal Foam Engine Noise Reduction Concepts", 15<sup>th</sup> AIAA/CEAS Aeroacoustics Conference, May 2009, AIAA 2009-3412.
- 39 Wolter, J., "Drag Measurements of Porous Plate Acoustic Liners", 43<sup>rd</sup> AIAA Aerospace Sciences Meeting and Exhibit, January 2005, AIAA 2005-803
- 40 Onat, E. and Klees, G. W., "A Method to Estimate Weight and Dimensions of Large and Small Gas Turbine Engines," NASA CR-159481, Cleveland, OH, 1979.
- 41 Lawrence, R.L., "Afterbody Flow Fields and Skin Friction on Short Duct Fan Nacelles", AIAA Journal of Aircraft, Vol 2, No 4.
- 42 Kors, Eugene, SILENCE(R) programme presentation, Snecma, [http://www.calm-network.com/cc07\\_17.pdf](http://www.calm-network.com/cc07_17.pdf), cited in July 2010
- 43 Gantie, F., Batard, H., "Zero Splice Intake Technology and Acoustic Benefits", AIAA 2006-2455
- 44 Gauntner, J.W., "Algorithm for Calculating Turbine Cooling Flow and the Resulting Decrease in Turbine Efficiency", NASA TM 81453, Feb. 1980
- 45 Young, J.B., Wilcock, R.C., "Modeling the Air-Cooled Gas Turbine: Part 2—Coolant Flows and Losses", ASME Journal of Turbomachinery, Vol. 124, pp. 214-221, Apr. 2002
- 46 Onat, E. and Klees, G. W., "A Method to Estimate Weight and Dimensions of Large and Small Gas Turbine Engines," NASA CR-159481, Cleveland, OH, 1979.
- 47 Mamaev, B.I., Petukhovskiy, M.M., "Gas Temperature Profile Attenuation Through a Multistage Axial-Flow Turbine", Proceedings of the ASME Turbo Expo 2009: GT2009-59033
- 48 Casey, M., Robinson, C., "A Method to Estimate the Performance Map of a Centrifugal Compressor Stage", Proceedings of the ASME Turbo Expo 2011: GT2011-45502
- 49 NATO Research and Technology Organization, "Performance Prediction and Simulation of Gas Turbine Engine Operation for Aircraft, Marine, Vehicular, and Power Generation." February 2007.  
<<http://ftp.rta.nato.int/public//PubFullText/RTO/TR/RTO-TR-AVT-036//TR-AVT-036-ANN-B.pdf>>
- 50 Mavris, D., Kirby, M., "Project 14: Environmental Design Space: 17<sup>th</sup> Semiannual PARTNER Technical Status Report," May 2012.
- 51 Kirby, M.R., Becker, K., Isley, S., Burdette, G., and Mavris, D., "Development of an Interactive Capability to Trade Off new Technologies and Future Aircraft to Reduce Aviation Environmental Impacts," Georgia Institute of Technology Aerospace System Design Laboratory, 27<sup>th</sup> International Congress of the Aeronautical Sciences, 2010.
- 52 Isley, Steven, "Forecasting Generic World Wide Fleet Operations Using a Modified Fleet and Operations Module Approach," Georgia Tech School of Aerospace Engineering, April 30 2010.
- 53 Becker, K., Nam, T., Kirby, M., Mavris, D., "A Process for Future Aviation Environmental Impacts: A Surrogate Fleet Analysis Approach for NextGen," 9<sup>th</sup> AIAA Aviation Technology, Integration, and Operations Conference, Hilton Head, 2009, AIAA-2009-6934.

- 54 LeVine, M., Wilson, A., Kirby, M., Mavris, D., "Development of Generic Vehicles for Fleet-Level Analysis of Noise and Emissions Tradeoffs," AIAA Aviation, Atlanta, 2014, AIAA-2014-2731.
- 55 C. Johnson and J. Schutte, "Basic Regression Analysis for Integrated Neural networks Documentation, Version 2.4"
- 56 M. D. Guynn, J. J. Berton, K. L. Fisher, W. J. Haller, M. T. Tong and D. R. Thurman, "Refined Exploration of Turbofan Design Options for an Advanced Single-Aisle Transport," NASA TM-2011-216883, Jan. 2011.
- 57 J. J. Berton and M. D. Guynn, "Multi-Objective Optimization of a Turbofan Design Parameters for an Advanced, Single-Aisle Transport," AIAA-2010-9168.
- 58 J. J. Berton and M. D. Guynn, "Multi-Objective Optimization of a Turbofan for an Advanced, Single-Aisle Transport," Journal of Aircraft, vol. 48, no. 5, Sept-Oct 2011.
- 59 M. D. Guynn, J. J. Berton, K. L. Fisher, W. J. Haller, M. T. Tong and D. R. Thurman, "Engine Concept Study for an Advanced Single-Aisle Transport," NASATM-2009-215784, August 2009.
- 60 M. D. Guynn, J. J. Berton, K. L. Fisher, W. J. Haller, M. T. Tong and D. R. Thurman, "Analysis of Turbofan Design Options for an Advanced Single-Aisle Transport Aircraft," in AIAA Paper 2009-6942, Sept 2009.
- 61 J. J. Berton, E. Envia and C. Burkley, "An Analytical Assessment of NASA's N+1 Subsonic Fixed Wing Project Noise Goal," in AIAA Paper 2009-3144, May 2009.
- 62 F. I. Romli, "Preliminary Study of Emissions Regulation Effects on Future Commercial Aircraft Designs," International Journal of Environmental Science and Development, vol. 4, 2013.
- 63 J. J. Lee, "Historical and Future Trends in Aircraft Performance, Cost, and Emissions," University of Illinois at Urbana-Champaign, 2000.
- 64 B. L. Koff, "Gas Turbine Technology Evolution: A Designer's Perspective," Journal of Propulsion and Power, vol. 20, 2004.
- 65 I. A. Waitz, "Military Aviation and the Environment: Historical Trends and Comparison to Civil Aviation".
- 66 International Industry Working Group, "Commercial Aircraft Design Characteristics Trends and Growth Projections," 2007.
- 67 "Evolution of Aircraft/Aerospace Structures and Materials," Dayton-Cincinnati Section AIAA, 1985.
- 68 J. Heimann, "Improving Engine Efficiency through Core Developments," AIAA Aero Sciences meeting, 2011.
- 69 K. N. Hopkins, "turbopropulsion Combustion - Trends and Challenges," AIAA-80-1199.
- 70 Ilcewicz, "Past Experiences and Future Trends for Composite Aircraft Structure," 2009.